AN AGENT-BASED MODEL FOR FLOOD RISK MAPPING: INTEGRATION OF URBANIZATION AND CLIMATE CHANGE IMPACTS

A THESIS SUBMITTED TO
THE GRADUATE SCHOOL OF NATURAL AND APPLIED SCIENCES
OF
MIDDLE EAST TECHNICAL UNIVERSITY

BY

MURAT YEĞİN

IN PARTIAL FULFILLMENT OF THE REQUIREMENTS
FOR
THE DEGREE OF DOCTOR OF PHILOSOPHY
IN
CIVIL ENGINEERING

July 2024

Approval of the thesis:

AN AGENT-BASED MODEL FOR FLOOD RISK MAPPING: INTEGRATION OF URBANIZATION AND CLIMATE CHANGE IMPACTS

submitted by **MURAT YEĞİN** in partial fulfillment of the requirements for the degree of **Doctor of Philosophy** i**n Civil Engineering, Middle East Technical University** by,

Prof. Dr. Naci Emre Altun
Dean, **Graduate School of Natural and Applied Sciences** _____

Prof. Dr. Erdem Canbay
Head of the Department, **Civil Engineering** _____

Prof. Dr. Elçin Kentel
Supervisor, **Civil Engineering, METU** _____

Assoc. Prof. Dr. Gülşah Karakaya
Co-Supervisor, **Business Administration**, **METU** _____

Examining Committee Members:

Prof. Dr. İsmail Yücel
Civil Engineering, METU _____

Prof. Dr. Elçin Kentel
Civil Engineering, METU _____

Prof. Dr. Ceylan Talu Yozgatlıgil
Statistics, METU _____

Prof. Dr. Holger Schüttrumpf
Civil Engineering, RWTH Aachen University _____

Prof. Dr. Cevza Melek Kazezyılmaz Alhan
Civil Engineering, İstanbul University - Cerrahpaşa _____

Date: 01.07.2024

I hereby declare that all information in this document has been obtained and presented in accordance with academic rules and ethical conduct. I also declare that, as required by these rules and conduct, I have fully cited and referenced all material and results that are not original to this work.

Name Last name : Murat Yeğin

Signature :

ABSTRACT

AN AGENT-BASED MODEL FOR FLOOD RISK MAPPING: INTEGRATION OF URBANIZATION AND CLIMATE CHANGE IMPACTS

Yeğin, Murat
Doctor of Philosophy, Civil Engineering
Supervisor: Prof. Dr. Elçin Kentel
Co-Supervisor: Assoc. Prof. Dr. Gülşah Karakaya

July 2024, 247 pages

The frequencies and the magnitudes of flood events are changing along with climate change (CC). In addition to CC, land use/land cover (LULC) also affects flood events. Thus, flood risks cannot be managed with traditional methods. Accordingly, this study combines a hydrological model (HM), a 1D/2D combined hydraulic model (CHM), and an agent-based model (ABM) to assess the impacts of CC and LULC on flood risks. Initially, the HM is calibrated and validated for the study area and then run using 17 regional climate models (RCM) outputs. The flood hydrographs are generated for different return periods using the best RCM. Concurrently, the historical satellite images are analyzed to quantify LULC. The flood hydrographs are used in the CHM, and flood inundation maps (FIMs) are obtained. FIMs are generated for both stationary and nonstationary conditions. Finally, the ABM is developed to assess the effects of the public and government agents in flood risk

management (FRM) based on 100 realizations of 11 scenarios. The calculated peak discharges with the historical observations are approximately 52% greater than those of the RCM outputs. Economic damage for the scenario with 113% increased urbanized area is 59% greater than that of the stationary scenario with the historical records. A proactive management strategy decreases the economic damage by 52% compared to a reactive management strategy. When public and government agents are included in the FRM, the economic damages become the lowest; thus, integrating agents' behavior in FRM through ABM is crucial.

Keywords: Stationarity Analysis, Hydrological Model, Combined 1D/2D Hydraulic Model, Agent-Based Model, Flood Risk

ÖZ

TAŞKIN RİSK HARİTALAMASI İÇİN AKTÖR-TABANLI BİR MODEL: KENTLEŞME VE İKLİM DEĞİŞİKLİĞİ ETKİLERİNİN ENTEGRASYONU

Yeğin, Murat
Doktora, İnşaat Mühendisliği
Tez Yöneticisi: Prof. Dr. Elçin Kentel
Ortak Tez Yöneticisi: Doç. Dr. Gülşah Karakaya

Temmuz 2024, 247 sayfa

Değişen iklim koşulları ile birlikte taşkın olaylarının da frekansları ve şiddeti değişmektedir. İklim değişikliğine ek olarak arazi kullanımı / arazi örtüsü de taşkın olaylarını etkilemektedir. Bu yüzden taşkın riskleri geleneksel yöntemler ile yönetilememektedir. Dolayısıyla, bu çalışma hidrolojik model, bütünleşik 1D/2D hidrolik model ve aktör-tabanlı model kullanılarak iklim değişikliği ve kentleşmenin taşkın riskleri üzerindeki etkilerini değerlendirmektedir. Birinci olarak, çalışma sahasının hidrolojik modelinin başarılı bir şekilde kalibrasyon ve doğrulaması yapıldıktan sonra, 17 bölgesel iklim modeli verisi hidrolojik modelde çalıştırılmış ve en iyi bölgesel iklim modeli seçilmiştir. Taşkın hidrografları farklı dönüş periyotları için en iyi bölgesel iklim modeli kullanılarak hesaplanmıştır. Aynı zamanda, çalışma sahasının arazi kullanımı / arazi örtüsü indirilen tarihi uydu görüntüleri kullanılarak analiz edilmiştir. Bütünleşik 1D/2D hidrolik model ve taşkın hidrografları kullanılarak taşkın yayılım haritaları elde edilmiştir. Taşkın yayılım alanları hem

durağan olma hem de durağan olmama koşulları düşünülerek elde edilmiştir. Son olarak, halk ve hükümet aktörlerinin taşkın risk yönetimi üzerindeki etkilerini görebilmek adına aktör-tabanlı model kurulmuştur. Bu etkiler 11 farklı model ve 100 farklı set çalıştırılarak analiz edilmiştir. Tarihi debiler kullanılarak hesaplanan pik debiler, en iyi bölgesel iklim modeli kullanılarak hesaplanan pik debilerden yaklaşık olarak %52 daha azdır. Ekonomik zarar değeri, kentleşmenin %113 artırıldığı senaryoda durağan senaryoya göre %59 daha fazla hesaplanmıştır. Proaktif yönetim stratejisi ekonomik zararı yaklaşık olarak %52 azaltmaktadır. Ekonomik zarar hem halk hem de hükümetin birlikte önlem aldığı koşullarda en düşük seviyeye inmektedir. Bu yüzden aktörlerin taşkın risk yönetimine entegre edilmesi çok önemlidir.

Anahtar Kelimeler: Durağanlık Analizi, Hidrolojik Model, Bütünleşik 1D/2D Hidrolik Model, Aktör-Tabanlı Model, Taşkın Riski

To the various storms

ACKNOWLEDGMENTS

I would like to thank my supervisor, Prof. Dr. Elçin Kentel Erdoğan, for her unwavering support, guidance, and motivation throughout my Ph.D. journey. Her mentorship has profoundly shaped my academic and personal growth, and I am fortunate to have been her student.

I also would like to express my deepest gratitude to my co-supervisor Assoc. Prof. Gülşah Karakaya's invaluable guidance and positive energy broadened my perspectives during the research.

I am deeply thankful to Prof. Dr. Holger Schüttrumpf for his assistance, valuable recommendations, and the opportunity to conduct research at Aachen RWTH University. I am also grateful to Shima Nabinejad for her guidance during my studies in Aachen.

I deeply appreciate Prof. Dr. Ceylan Yozgatlıgil and Prof. Dr. İsmail Yücel for their constructive feedback and help throughout the study. I am also thankful to Prof. Dr. Cevza Melek Kazezyılmaz Alhan for her recommendations during the defense.

I am grateful to Prof. Dr. Melih Yanmaz and Prof. Dr. Zuhal Akyürek for their continuous support and encouragement.

I thank the Scientific and Technological Research Council of Türkiye for supporting this thesis under project number TUBITAK 220N054.

I sincerely thank my family, Seyhan Yeğin and Mustafa Yeğin, for doing their best over the years; Arzu Çelik, for being my second mother; and Ayça Yeğin, to whom words cannot express my feelings enough. I always feel how much they love, support, and trust me.

I want to thank G-team members Sıla Gülgeç, Bilgenur Erol, and Hüseyin Erol for their tremendous friendships and all the things we have done and shared. I am also grateful to Yasemin Yılmaz for being an incredible friend and supporting me under all circumstances. I also want to thank Eray Ercan, Burak Akgün, Eren Düzenli, the TEİAŞ group, and Çelik Family for supporting me during my study.

TABLE OF CONTENTS

LIST OF TABLES

TABLES

LIST OF FIGURES

FIGURES

LIST OF ABBREVIATIONS

ABBREVIATIONS

1D	One-Dimensional
2D	Two-Dimensional
ABM	Agent-Based Model
AHP	Analytical Hierarchy Process
AIC	Akaike Information Criterion
AL	Agricultural Land
AMFS	Annual Maximum Flow Series
BL	Bare Land
CC	Climate Change
CORDEX	Coordinated Regional Climate Downscaling Experiment
CORINE	Coordination of Information on the Environment
Corr	Correlation Coefficient
DEM	Digital Elevation Model
F	Forest
FAO	Food and Agriculture Organization of the United Nations
FRM	Flood Risk Management
Ga	Gamma Distribution
GAMLSS	Generalized Additive Model for Location, Scale and Shape parameters
GCM	General Circulation Model
GEV	Generalized Extreme Value
GHG	Greenhouse Gas

GLO	Generalized Logistic
Gu	Gumbel Distribution
HBV	Hydrologiska Byrans Vattenbalansavdelning
HEC-HMS	Hydrologic Engineering Center – The Hydrologic Modeling System
HEC-RAS	The Hydrologic Engineering Center River Analysis System
HEC-SSP	Hydrologic Engineering Center's Statistical Software Package
IPCC	Intergovernmental Panel on Climate Change
KC	Kappa Coefficient
LiDAR	Light Detection and Ranging
Lo	Logistic Distribution
LogNo	Log-normal Distributions
LULC	Land Use/Land Cover
M	Marshes
MLC	Maximum Likelihood Classification
MLE	Maximum Likelihood Estimation
MOS	Meteorological Observation Station
MP	Annual Maximum Precipitation
NDVI	Normalized Difference Vegetation Index
No	Normal Distribution
NS	Nonstationary
NSE	Nash Sutcliffe Efficiency
OA	Overall Accuracy

PA	Producer's Accuracy
PBIAS	Percent Bias
PMT	Protection Motivation Theory
Pop	Population
ProGo100	The proactive government takes action to mitigate the consequences of a 100-year return period flood event
ProGo50	The proactive government takes action to mitigate the consequences of a 50-year return period flood event
PubRand	Risk and coping perceptions are randomly assigned to public agent
PubSur	Risk and coping perceptions are assigned to the public agent according to the survey results
PubSur – ProGo100	PubSur and ProGo100 together
PubSur – ProGo50	PubSur and ProGo50 together
PubSur – ReGo100	PubSur and ReGo100 together
PubSur – ReGo50	PubSur and ReGo50 together
Q_2	Peak discharge of a 2-year flood event
Q_5	Peak discharge of a 5-year flood event
Q_{10}	Peak discharge of a 10-year flood event
Q_{25}	Peak discharge of a 25-year flood event
Q_{50}	Peak discharge of a 50-year flood event

Q_{100}	Peak discharge of a 100-year flood event
Q_{500}	Peak discharge of a 500-year flood event
R^2	Coefficient of Determination
RCM	Regional Climate Model
RCP	Representative Concentration Pathway
ReGo100	The reactive government agent takes action to mitigate a 100-year return period flood event after a 100- or 500-year return period flood event is experienced.
ReGo50	The reactive government agent takes action to mitigate a 50-year return period flood event after a 50-, 100- or 500-year return period flood event is experienced.
RI	Reservoir Index
RMSE	Root Mean Square Error
RSR	Root Mean Squared Error-Observations Standard Deviation Ratio
S0	Scenario 0 for flood mapping studies
S1	Scenario 1 for flood mapping studies
S2	Scenario 2 for flood mapping studies
S3	Scenario 3 for flood mapping studies
S4	Scenario 4 for flood mapping studies
Sc1	Scenario 1 for ABM
Sc2	Scenario 2 for ABM

Sc3	Scenario 3 for ABM
Sc4	Scenario 4 for ABM
Sc5	Scenario 5 for ABM
Sc6	Scenario 6 for ABM
Sc7	Scenario 7 for ABM
Sc8	Scenario 8 for ABM
Sc9	Scenario 9 for ABM
Sc10	Scenario 10 for ABM
Sc11	Scenario 11 for ABM
SCS	Soil Conservation Service
SG	Stream Gage
SHW	State Hydraulic Works
SWAT	Soil and Water Assessment Tool
Temp	Annual Average Temperature
TP	Annual Total Precipitation
UA	User’s Accuracy
UrA	Urbanized Area
WB	Water Bodies

CHAPTER 1

INTRODUCTION

Floods rank among the most devastating natural hazards, and characteristics of floods, such as rates of occurrences of different magnitude floods, change over time. Climate Change (CC) and Land Use/Land Cover (LULC) change are among the most important reasons for the changes in flood risk characteristics (Chang & Franczyk, 2008). Accurate results cannot be obtained if climate and LULC changes are not embedded in flood models.

Traditional flood models are developed, assuming flood events are stationary. However, flood characteristics change over time. For this reason, realistic results may not be obtained with stationarity assumption in flood models. The non-stationarity of flood events should be analyzed and integrated into the flood models.

Another significant challenge in current Flood Risk Management (FRM) studies is to include human-flood interaction in the modeling approach to investigate how stakeholders/agents respond to flooding and how their involvement affects the development of more effective FRM strategies. In addition, traditional flood risk analysis assume static conditions in which humans and their surrounding environment are inactive and their vulnerability is constant. Under such assumptions, time-dependent features such as human interactions, individual adaptations, and technology innovation cannot be incorporated in current models, and there is a lack of modeling approaches to include social aspects of human behavior in FRM. The behaviors of the stakeholders/agents and their changes over time are integrated into FRM via the Agent-Based Model (ABM) to develop effective and sustainable flood mitigation measures and adaptation strategies.

The main purpose of this study is to combine the impacts of CC, LULC, and behaviors of the agents through a flood risk assessment framework. Moreover,

nonstationarity in flood discharges are investigated. Three different models (i.e., a hydrological model, a 1D/2D combined hydraulic model, and an agent-based model) are developed to combine the impacts of CC, LULC, and the agents' behavior. Due to the meetings with the State Hydraulic Works staff, the study area is selected as the Göksu River, Silifke. This region has experienced many destructive flood events in the past.

Hydrological model is developed to convert rainfall values to runoff values. Three different periods are considered in the development of the hydrological model. 17 different regional climate models (RCM) are downloaded to include CC impacts in the study. The outputs of these RCMs are entered into the calibrated and validated hydrological model. The best RCM is selected using some statistical measures based on the observed discharges and the calculated discharges from the hydrological model with RCM data. After selecting the best RCM, the hydrological model is run using the outputs of the best RCM for the future. Finally, the flood hydrographs, which will be the inputs of a combined 1D/2D hydraulic model, are generated for different return periods considering the stationary and nonstationary conditions.

LULC analysis is conducted for the study area to include LULC changes during the development of the hydrological model. Historical satellite images are downloaded and analyzed to show how LULC changed in the past, and the change in the future is tried to be estimated.

The second model is the combined 1D/2D hydraulic model, and it is developed to generate flood inundation maps. Flood inundation maps are generated considering the different scenarios. These scenarios are generated to analyze the impacts of CC and LULC both separately and together. Furthermore, stationary and nonstationary models are used in these scenarios. The combined 1D/2D hydraulic model is run using the flood hydrographs for different return periods and all scenarios. Economic damage values are calculated and compared.

Finally, an ABM is developed to include the behaviors of the agents. In this study, two different agents are considered: the public agent (i.e., people living in the study

area) and the government agent. The behaviors of the public are represented by risk perception and coping perception values. A survey is conducted in the study area to calculate these values. On the other hand, for the government agent, two different policies are considered: reactive and proactive. 11 different scenarios are generated to investigate the impacts of the agents on flood risks. In ABM, the results of the hydrological model with the best RCM are used. 100 different realizations are also generated due to the uncertainty of the flood events, and all scenarios are run for these realizations.

The study results showed that i) The peak discharges that are calculated using the outputs of the hydrological model with the best RCM are less than the peak discharges calculated with historical records, ii) The urbanized area is increasing in the region, iii) The performance of the nonstationary models are better than the stationary models for all probability distributions. In addition, LULC-related covariates are identified to be more important than CC-related covariates in the study area, iv) Calculated economic damages showed the importance of urban planning. If the new urbanized areas are not planned considering flood inundation maps, the results of the floods might be devastating for the region, v) ABM results showed the importance of integrating the agents into FRM. The economic damage is calculated as the lowest for the scenarios with both public and government agents.

The following organization is adopted within this study. Chapter 2 presents literature review of climate models, CC analysis in Türkiye, CC impacts on floods, LULC change and LULC analysis, nonstationarity analysis, ABM, and risk and coping perceptions. Chapter 3 provided information and photographs from the study area. In Chapter 4, the detailed methodology of the study is provided. In addition to CC and LULC analyses, detailed information about the hydrological modeling, the combined 1D/2D hydraulic model, and the ABM are given. Chapter 5 presents the results and the discussions of the study. The limitations of the study are also given in this chapter. Finally, Chapter 6 concludes the study by highlighting the major findings and making suggestions for future researches and applications.

CHAPTER 2

LITERATURE REVIEW

As mentioned before, the main purpose of this study is to combine various models and approaches under flood risk assessment. A detailed literature review of these topics is conducted under the related chapters.

2.1 Climate modeling and global / regional climate models

Climate change, as defined by the Intergovernmental Panel on Climate Change (IPCC), encompasses alterations in the climate system resulting from either natural internal processes or external factors like persistent anthropogenic changes in atmospheric composition or land use (IPCC, 2014). These changes, notably in precipitation and temperature patterns, deviate significantly from current conditions or those of the pre-industrial era, profoundly impacting natural systems (Easterling et al., 2000; Giorgi & Lionello, 2008; IPCC, 2014; IPCC, 2018; Mahmood et al., 2019; Mariotti et al., 2011). One of the most prevalent consequences of climate change is the shift in the frequencies and intensities of extreme weather events such as floods and droughts. These events, in turn, indirectly degrade the quantity and quality of freshwater ecosystems on a global scale (Bucak et al., 2018; Dudgeon et al., 2006; Walther et al., 2002; IPCC, 2018; IPCC, 2014; Butchart et al., 2010).

Scientists worldwide have been developing adaptation and mitigation strategies to prevent possible adverse outcomes as climate change is causing irreversible impacts on all aspects of Earth's ecosystems. In this context, future climatic conditions are evaluated using the general circulation models (GCMs) and regional climate models (RCMs). These tools are used to generate future climate projections under different socioeconomic development scenarios. Outputs of GCMs are widely used in the global assessment of climate change (Rivera & Arnould, 2020). GCMs are

developed based on the mathematical expressions of physical phenomena such as fluid dynamics, heat, and radiation transfer to simulate changes in hydrometeorological parameters such as air temperature, precipitation, and evaporation on a global scale (Sato et al., 2012). Hence, GCMs are based on describing current atmospheric processes through mathematically formulated physical laws to obtain future climate projections emanating from predefined Greenhouse Gas (GHG) emission scenarios.

GCM outputs are not convenient to use in catchment scale analysis (e.g., drought, flood risk analysis) due to restrictions in the resolution of GCM outputs. The low resolution of GCMs poses limitations on accurate simulation of orographic precipitation and conventional and local scale hydrological processes (Fujihara et al., 2008). The state-of-the-art GCMs are developed to simulate with an approximate 111 km horizontal resolution (i.e., 1° mesh size for the ocean and 1°-2° for the atmosphere typically) (Flato et al., 2013). The vertical resolution is adjusted to work on 30-40 layers in the atmosphere and 30-60 layers in the ocean (Flato et al., 2013). However, they are insufficient for analyzing local-scale hydrological processes, especially for regions with complex topographic and land cover properties (Jaw et al., 2015). Inaccurate results may be obtained locally in the case of direct use of course scale GCMs (Jaw et al., 2015; Sharma et al., 2007; Piani et al., 2010).

Regional climate projections are obtained using downscaling methods considering GCM data as boundary conditions since GCMs cannot provide high-resolution data for spatial scales (Jaw et al., 2015; Kara & Yücel, 2015; WCRP CORDEX, n.d.; Fujihara et al., 2008). Statistic and dynamic downscaling approaches are standard methodologies for obtaining higher-resolution simulation results from the GCMs. The dynamical downscaling method uses GCM outputs as the initial and boundary conditions of RCMs to generate regional simulations (Fujihara et al., 2008). RCMs enable high-resolution simulations of hydrometeorological parameters (Kara & Yücel, 2015) suitable for catchment-scale hydrological studies with up to 0.11° (~12.5 km) horizontal resolution. The higher resolution of RCMs enables better simulation of spatial and temporal variability of climate and extreme events (Giorgi

& Gutowski Jr, 2015). For this reason, the outputs of RCM simulations are used for climate change assessment studies.

2.2 Climate change analysis in Türkiye

Negative impacts of CC in the Mediterranean Region are emphasized in IPCC's 5th and 6th assessment reports (IPCC, 2014; IPCC, 2021). Many studies identified this region as a hot spot concerning climate change impacts (Giorgi, 2006; Giorgi & Lionello, 2008; Spinoni et al., 2020). These findings have been verified by the studies that focus on the impacts of climate change in the Eastern Mediterranean and/or Türkiye through the analysis of historical data (Kostopoulou & Jones, 2005; Kuglitsch et al., 2010) and GCM/RCM analysis (Aziz et al., 2020; Kentel et al., 2021; Mesta et al., 2022).

Research examining the effects of climate change on surface air temperature by analyzing historical temperature trends has revealed a notable increase in warming, especially in the southern and inland regions of Türkiye (Tayanç et al., 2009; Toros, 2012; Unal et al., 2013; Erlat et al., 2021).

Conversely, the study by Yucel et al. (2015) indicated no statistically significant change in the historical precipitation records in eastern Türkiye. Sensoy et al. (2013) analyzed the trends in the climate indices for 109 stations across Türkiye between 1960 and 2010. The analysis revealed interregional variability in the changing trends in total annual precipitation, with an increase in the north and a decrease in the south and west of Türkiye. In contrast, trends relating to high precipitation events indicated an increase in the number of heavy precipitation days (i.e., 17 days in 100 years), particularly in west and southeast Türkiye, and in the intensity of heavy precipitation in the entire country, except for the east (Sensoy et al., 2013).

Several studies assess the impacts of climate change in Türkiye by the use of projections from climate models considering ecosystem dynamics, energy, management of extreme events, forestry, reservoir planning, hydropower generation,

crop yield, and tourism activities (Fujihara et al., 2008; Özdoğan, 2011; Deidda et al., 2013; Kara & Yücel, 2015; Öztürk et al., 2015; Yilmaz, 2015; Mehr & Kahya, 2017; Bucak et al., 2018; Dino & Akgül, 2019; Kentel et al., 2021).

A few researchers have studied the impact of climate change on extreme storm events in Türkiye. Yilmaz (2015) investigated the potential increase in flood risk in Antalya. In this study, historical rainfall records and future climate projections are analyzed. He found that extreme rainfall increases statistically significant based on historical data. Balov (2020) analyzed projections of NorESM1-M GCM under the Representative Concentration Pathways (RCP) 4.5 and 8.5 scenarios to assess change in flood risk due to climate change in Bursa, Türkiye. The study revealed that despite the statistically non-significant change in the mean annual precipitation, the frequency of intense precipitation is projected to increase.

2.3 Climate change impacts on floods

In recent years, studies on the impact of CC on different types of floods have emerged in the literature. Radojevic et al. (2010) conducted an assessment of the impact of global change on flood regimes in Lyon, France. They selected the 1970s and 1990s as reference periods to examine the effects of CC on rainfall and flood regimes and simulate urban development's impact on flood regimes in 2025. The study found that urban development has the effect of reducing the 10-year flood to a 1-year flood. Hallegatte et al. (2010) conducted a study on flood risks in Mumbai, highlighting the impacts of CC and the benefits of adaptation strategies. The researchers estimated the economic loss for a 100-year flood event under five scenarios: the present day, an unchanged city with the high-end scenario in the 2080s, more resilient properties in the 2080s, improved outflow using Hydrologic Engineering Center - The Hydrologic Modeling System (HEC-HMS), and the impacts of climate change and urbanization are planned to be investigated through a scenario-based analysis.

Harada et al. (2020) studied flood frequency analysis and impact assessment for CC in Japan. One climate model was used, and flood runoff analysis was performed using the storage function method. Finally, they concluded that the peak flood flow was expected to increase at most 33% in the future. Oubennaceur et al. (2021) investigated the flood risk under CC for 2050 and 2080 in Quebec. They used two different RCPs and one climate model. They concluded that flood peaks and flood damages show a minor decrease in the future. In a more recent study, Rincon et al. (2022) studied the flood risk under CC in Toronto. They considered future rainfall based on different RCPs drainage systems that can handle 50-year rainfall events in the 2080s and more resilient properties with an improved drainage system. They found that economic loss is the least in the scenario of more resilient properties with improved drainage systems. Hirabayashi et al. (2013) worked on global flood risk under CC in a similar study. They presented global flood risk based on the outputs of 11 climate models. They calculated the peak discharge of the 100-year return period for the 20th century, estimated the return period of this discharge in the 21st century, and compared them. They found a large increase in flood frequency in Southeast Asia, Peninsular India, eastern Africa, and the northern half of the Andes. In another study, Dutta et al. (2013) studied flood vulnerability assessment under CC conditions for two selected coastal zones in Australia and Japan. Four water inundation parameters, three water-quality parameters, and twenty-two key issues were determined by experts from Australia and Japan as well as international experts within the context of the project. A questionnaire was prepared to obtain participants' views on how different levels of coastal inundation affect key issues and assets. They concluded that synthetic response functions were beneficial where historical quantitative data on flood hazard impacts on key issues are not available and the proposed methodology could be used to manage flood risk in coastal zones in any region. In this project, similar to those in the literature 17 of CORDEX (Coordinated Regional Climate Downscaling Experiment) RCMs are used to carry out CC analysis. In a more recent study, the impacts of CC on river floods at the global scale were investigated by Arnell and Gosling (2016). The researchers employed the

results of 21 climate models in their study. The magnitude, return period of the flood peaks, flood-prone population, and flood-prone cropland for the 100-year flood event in 2050 were selected as indicators, and flood hazard was calculated based on these indicators. The study's results demonstrated the variations in flood risk under different climate models, and the primary reason for this variation was identified as the precipitation projections of the climate models.

Xu et al. (2019) evaluated the impacts of CC on fluvial flood risk in a mixed-used watershed. They used the Soil and Water Assessment Tool (SWAT) to estimate daily flows. They used five different climate models. They found a decrease in flood risk if the precipitation increase is less than 10%. In a more recent study, Cabrera and Lee (2018) worked on the impacts of CC on flood-vulnerable areas in the Philippines. They used 39 general circulation models to obtain the rainfall projections and conducted flood risk analysis using the Analytical Hierarchy Process (AHP) for 2015, 2030, 2050, and 2100. Flood risk indicators were selected: rainfall, slope, elevation, drainage density, soil type, distance to the main channel, and population density. They concluded that there would be no dramatic change in the future.

Garijo and Mediero (2018) conducted a study about the impact of CC on flood magnitude and seasonality in Spain using 24 global climate models under two RCPs. The hydrological behavior of the catchment was modelled by using Hydrologiska Byrans Vattenbalansavdelning (HBV) rainfall-runoff model. The magnitude of extreme floods decreased for most of the climate projections while it increased for the remaining projections. In a similar study, Robi et al. (2018) conducted a flood hazard mapping study in Ethiopia under a CC scenario using SWAT for the hydrological model and MIKE FLOOD for the hydraulic model. They generated flood hazard maps of 100-year return period floods for 2005, 2030, and 2060. They found that CC causes an increase in peak discharge of the 100-year flood hydrograph.

Bangalore et al. (2019) studied exposure to floods, CC, and poverty in Vietnam. They studied coastal, fluvial, and pluvial floods together. They did not cover the impacts of CC in precipitation events or river discharges. They assumed 30 cm sea

level rise for coastal flooding. They finally concluded that more people will be affected from floods due to CC in the future.

Bai et al. (2019) conducted a study to assess the impact of CC on flood events. One general circulation model and three emission scenarios were used in their study. The comparison of 10, 25, 50, and 100-year precipitation and streamflow for low, medium, and high emission scenarios showed that calculated values were higher than the historical records. In this project, the hydrological modeling of the study basin is carried out for different periods using different global climate models. They found that the rainfall intensities are likely to increase. Hence, it increases flood risk in Toronto.

In a similar study, Chen et al. (2022) assessed flood risk maps under CC RCP8.5 scenarios in Taiwan. They generated flood risk maps for 2075-2099. They downscaled the MRI-JMA-AGCM Model and used it as a climate model. Finally, they investigated the areas where hazard indicators increase and those with higher vulnerability levels. They also suggested some adaptation measures and strategies.

The results of many studies showed that CC impacts on flood risk differ from region to region. CC caused and was estimated to cause an increase or decrease in flood risks in some regions, while it did not and was estimated not to affect flood risks in others. For this reason, CC analysis is very important for the assessment of flood risks in the future. In this study, outputs of different RCMs (17 RCMs) will be used in the HEC-HMS hydrological model, and flood hydrographs for different return periods will be calculated. These hydrographs will be used in the hydrodynamic model to determine flood-inundated areas.

2.4 Land use / land cover (LULC) change

LULC change might be one factor that increases the severity of flood consequences. There are numerous studies demonstrating the impact of LULC changes on floods. In their 2004 study, Dezso and colleagues examined LULC change in the Carpathian Region. It was stated that several severe flood events had occurred in the region and

that the only reason for these events could not be attributed to heavy precipitation events. Consequently, they conducted an analysis of the LULC change in the study area and discovered that the forest area had decreased in the region. The authors concluded that the reduction in forest area may be a contributing factor to the occurrence of severe flood events in the region.

Petchprayoon et al. (2010) conducted a study about the hydrological impacts of land use/land cover change in a large river basin in central-northern Thailand. They compared the peak discharges and urban areas in 1990 and 2006. They also analyzed the precipitation trends but could not find a significant trend except for one station. Small increase was found in the peak flows, while urban areas increased by 132%. They concluded that the increase in peak discharges was the result of the expansion of urbanized areas.

Brody et al. (2015) examined the impact of LULC change on floods from a different point of view. The study analyzed the impacts of LULC changes on flood losses in the Gulf of Mexico between 1999 and 2009. The findings indicated that an increase in wetland areas was associated with a reduction in flood losses. Furthermore, the study indicated that an increase in impervious surface area and a reduction in vegetation generally results in an increase in flood losses.

In a different study, Szwagrzyk et al. (2018) studied the impacts of LULC changes on flood risk in Poland. They used three LULC change scenarios in their research. Hydrological simulations were conducted considering the current state. They found that peak discharges decreased in some areas while they increased in the remaining regions. Hence, flood-related monetary losses are projected to increase in the areas where peak discharges increase. In a similar study, Guzha et al. (2018) conducted research about the impacts of LULC on surface runoff, discharge, and low flows in East Africa. The findings of the study indicated that annual discharges and surface runoff increase with the loss of forest cover. Additionally, the researchers observed a weak correlation between forest cover and surface runoff, mean discharge, and peak discharge.

In a more recent study, Costache et al. (2020) studied the correlation between LULC changes and flash-flood potential in Romania. They carried out the analysis for 1989 and 2019. They found a high correlation between LULC change and flash-flood potential change. In a similar study, Feng et al. (2021) conducted research about the impact of urbanization on flood risks in Canada. Six distinct land use scenarios were employed as input in coupled hydrological and hydraulic models. The study revealed that flood-prone areas are expanding as a consequence of urbanization. Furthermore, the study revealed that discharge rates increase while times to peak decrease due to urbanization. Azizi et al. (2021) studied the impacts of land use change on flood hydrograph by using HEC-HMS hydrological model. The analysis was conducted for 1985, 2000, and 2015. They determined LULC classes by using satellite images and they used these classes to calculate weighted curve number that is used in HEC-HMS hydrological model. They found that urbanized area increased while grasslands and agricultural lands decreased. They also found that peak discharge volume increased between the studied dates.

It can be demonstrated that LULC changes have a significant impact on flood risk. Consequently, it is of paramount importance to integrate LULC changes into flood risk assessment studies. Literature review reveals that there are few studies in Türkiye that evaluate the impacts of LULC changes on floods. The urbanization trends are analyzed using historical satellite images, with the results subsequently utilized as an input for both the hydrological model and the hydrodynamic model.

There are also many studies that investigate the effects of CC and LULC together or separately. Beckers et al. (2013) carried out a study about contribution of land use changes to future flood damage (2100) for 100-year flood event. Nine urbanization scenarios under two climate scenarios were developed. The results showed that urbanization scenarios contribute more flood damages in dry climate scenario while they are not very effective in wet climate scenario. In wet climate scenario, CC impacts cause increases in flood damages much more than LULC change scenarios.

In a different study, Akter et al. (2018) investigated the impact of CC and land use change on flood risk in Belgium in 2100. The findings indicated that climate change is a more significant driver of peak flows than land use change.

In a more recent study, Avand et al. (2021) investigated the impacts of CC and land use on flood probability in Iran. They predicted the land use in 2020 - 2040 based on the land use change between 1990 and 2019. They used RCP2.6 and RCP8.5 scenarios in their study. They found that rainfall is likely to increase under both scenarios while urbanized area and forests are likely to decrease. They concluded that these changes would increase flood probabilities in downstream of the study area.

In a study published in 2018, Igarashi and colleagues examined the impact of land use and climate change on flood discharge. The authors underscored the significance of land use change on flood risk in developing countries. A total of 14 scenarios for land use change (based on changes in forest cover) were generated and compared to average daily discharges from 3.3 and 10-year return period rainfall. The study concluded that climate change would result in a reduction in the average daily flood discharge in the future. Nevertheless, they posited that the 10-year return period discharge would be greater due to a reduction in forest area.

For more studies on CC and urbanization impacts on flood risk, please see: Dankers & Feyen, 2008; Wilby et al., 2008; Feyen et al., 2009; Klijn et al., 2012; Poelmans et al., 2011; Feyen et al., 2012; Alfieri et al., 2015; Mahmoud & Gan, 2018; Haer et al., 2020.

In most studies, flood risks have been found to increase even when future rainfall projections decrease. The most significant contributing factor to this increase is the expansion of urbanized areas. To assess future flood risk, it is of the utmost importance to analyze the effects of components both separately and together. This will enhance the efficacy of flood-related initiatives in the region.

After reviewing the literature, it is realized that no study covers the impact of the LULC change of Silifke on river flow and floods. Table 2.1 summarizes the literature review of the LULC change studies conducted for the areas in the vicinity of Silifke.

Table 2.1 Literature review of LULC change around the study area

Reference	Date	Study Area	Period	BE	AL	Forest	PG	FCM
Alphan	2003	Adana	1984-2000	107.58	-22.99	-33.99		
Seyran	2009	Lower Seyhan Basin	1967-2007	465.53	-39.99	-17.85		
Derse and Alphan	2012	Erdemli District	1984-2006	550.97	21.48	-7.79		
Sönmez	2012	Adana	1990-2010	8.73 to 9.00	34.40 to 35.66	12.98 to 9.31		
Tübitak MAM Çevre Enstitüsü	2013	Dogu Akdeniz Basin	2012-2040				20.84	
TÜİK	2018	Adana, Hatay, Mersin, Osmaniye, Türkiye	2018-2025				3.89, 6.96, 7.43, 8.49, 8.52	
TÜİK	2018	Türkiye	2018-2069				31.51	
Zadbagher et al.	2018	Seyhan Basin	2016-2036	50	8	-5		
Göksel and Balçık	2019	Akdeniz District	2006-2014	-6.41	60.11	-57.54		
DSİ Strateji Geliştirme Dairesi Başkanlığı	2020	Mersin and Hatay	2019					FCMs are applied

BE: Built Environment, AL: Agricultural Land, PG: Population Growth, FCM: Flood Control Measures

2.5 Analysis of land use / land cover change

Image classification has been used to analyze LULC classification by many researchers. Güler et al. (2007) used Landsat images to determine LULC change in Samsun, Türkiye. They used three images and six LULC classes in their study. They found an increase in the urbanized area during the studied time period. In a similar study, Manandhar et al. (2009) used Landsat images for LULC classification, and they also used post-classification enhancement to improve the classification accuracy in Australia. They used three Landsat images, and according to their results,

the method successfully improved the accuracy of the classification. In another study, Tan et al. (2010) used Landsat images to evaluate urban expansion and LULC change in Malaysia. They used different supervised classification techniques and compared the results. Their study used two images and seven LULC classes and found that the highly built-up area increased dramatically. In a similar study, Otukei and Blaschke (2010) used different algorithms to analyze land cover change in Uganda. They used two images (Landsat 5 and Landsat 7) and eight different LULC classes and obtained satisfactory results for their algorithms.

Yin et al. (2011) conducted a study to detect urban expansion and LULC change in Shanghai between 1979 and 2009. They used four different Landsat images and five LULC classes in their study. They found that urbanized areas increased drastically in the study area. El Kawy et al. (2011) studied to detect LULC change in the Western Nile Delta of Egypt. Four satellite images and five LULC classes were used in their study. Barren land changed into agricultural areas according to the results of their study. In a similar study, Hassan et al. (2016) studied the dynamics of LULC change in Pakistan. They compared 1992 and 2012, and five LULC classes were used in their classification. They found that agricultural areas, urbanized areas, and water bodies increased while forests and barren areas decreased during the studied time period. In a more recent study, Deng et al. (2019) used Landsat 8 images to classify LULC of a heavily urbanized area. They did not detect LULC change in the study area where seven different LULC classes were considered.

In a different study, Kafy et al. (2020) studied the impacts of LULC change on land surface temperature in Bangladesh. They used three different Landsat images in LULC classification. In a similar study, Alam et al. (2020) used Landsat images to assess LULC change in Kashmir Valley. They used three different images and five different LULC classes. They found the maximum increase in urbanized areas while the maximum decrease in pasture class. Many studies can be found in the literature about LULC change detection using satellite images. For more references, please see Muttitanon & Tripathi, 2005; Fan et al., 2007; Fu & Weng, 2016; Zaidi et al., 2017;

Allam et al., 2019; Mukherjee & Singh, 2020; Chen et al., 2020; Alawamy et al., 2020; Aik et al., 2020.

2.6 Nonstationarity analysis

It is generally assumed that extreme events are stationary in the design of hydraulic structures where probabilistic methods are applied (Salas & Obeysekera, 2014; Read & Vogel, 2015). However, nonstationarity exists in nature. Human interventions in the river basin, LULC changes, and CC are the major causes of nonstationarity. For this reason, the concepts such as risk and return period should also be assessed considering nonstationarity. There are various studies that try to investigate the impacts of nonstationarity on extreme hydrological events such as floods, droughts, etc. Madsen et al. (2014) reviewed the trend analysis and CC projections of extreme precipitation and floods in Europe. They found that some evidence exists that shows the increase in extreme precipitation, while extreme streamflow does not show a significant increase. They also found that many areas are affected both positively and negatively by the hydrological projections of peak flows. Condon et al. (2015) studied non-stationary flood risk for the upper Truckee River basin. Variable Infiltration Capacity model and non-stationary Generalized Extreme Value (GEV) models were used in the study. Nonstationary models were generated using historical monthly total precipitation and average temperature. They found that flood risk increases significantly from 1950 through 2099. They also highlighted that the traditional methods underestimate flood risk. Sraj et al. (2016) investigated the influence of non-stationarity in extreme hydrological events on flood frequency estimation. They used the GEV distribution, and time and annual precipitation were used as the covariates. They selected two stream gauges from Slovenia. They found that the stationary model tends to underestimate flood quantiles.

The year after, Debele et al. (2017) compared three approaches, namely maximum likelihood, two-stage and generalized additive model for location, scale, and shape parameters (GAMLSS), to non-stationary flood frequency analysis. They found that

GAMLSS gave the best results. In the same year, Gao et al. (2017) investigated the risk of extreme precipitation under nonstationary conditions in the Southeastern Coastal Region of China. They analyzed the trend of the extreme precipitation series using the Mann-Kendall test. The climate change index and human activity index were used as the covariates in the study. They generated nonstationary models using GAMLSS. They found a significant positive correlation between CC and human activities and the mean/variance of extreme precipitation. Gu et al. (2017) evaluated nonstationary flood risk in the Pearl River basin. They used the GEV model and time as the only covariate. They found that peak flood flow increases in some parts while decreasing in others. Furthermore, they found that the return period under stationary and nonstationary assumptions differs for periods longer than 50 years. They also stated that the failure risk of flood control infrastructure is higher for the nonstationary case. In the same year, Razmi et al. (2017) studied non-stationary frequency analysis of extreme water levels in a coastal part of New York City. The trend and stationarity of the series were checked using some statistical tests. They generated non-stationary models using the GEV and Generalized Pareto Distributions. They found that extreme water levels were significantly different under stationary and non-stationary assumptions.

Luca and Galasso (2018) analyzed extreme rainfall time series under stationary and non-stationary conditions in Southern Italy. Two-Component Extreme Value probability distribution was used in the study, and they found that generating non-stationary models is not essential. They also found no significant trend in historical data, which supports the study's previous finding. In the same year, Sun et al. (2018) evaluated food frequency and flood risk in the Huai River basin under non-stationary conditions. They analyzed monthly streamflow data of nine gauging stations. They did not find a significant change for the three stations, while they found a significant change for the rest. Another finding of the study was that flood flows of three stations were non-stationary, while the others were stationary. They also tried different probability distributions and found that the Weibull distribution was the best among the others.

Yan et al. (2019) analyzed flood hazard under nonstationary conditions. They considered the impacts of climate change and population growth on flood hazard by using rainfall and population as the covariates. They also generated nonstationary models using time as the covariate. They found that population and rainfall covariates provided more reasonable estimates than time covariate. Lu et al. (2020) studied the impacts of climate and reservoirs on extreme floods. They used the GEV distribution in the study. Time, climate indices, and climate-reservoir index were considered as the covariates. The performance of the nonstationary model with climate-reservoir index was better than the others. Oruc et al. (2022) studied the effect of climate change on extreme precipitation in Ankara. They used nonstationary GEV models, and they found a decreasing extreme trend. Barbhuiya et al. (2023) reviewed the methods and models in nonstationary flood frequency analysis. They discussed many methods, such as GAMLLS, probability-based approaches, time-varying moments, etc. They also included the challenges associated with nonstationary hydrological frequency analysis. The most important inference of the study is that incorporating nonstationarity in flood risk assessment is needed.

2.7 Agent-based modeling (ABM) and flood risk management

One of the significant challenges in current FRM studies is to include human-flood interaction in the modeling approach to investigate how stakeholders/agents respond to flooding and how their involvement results in a more effective FRM. In addition, these studies assume static conditions in which humans and their surrounding environment are inactive and their vulnerability is constant. Under such assumptions, time-dependent features such as human interactions, individual adaptations, and technology innovation cannot be incorporated in current models, and there is a lack of modeling approaches to include social aspects of human behavior in FRM. To fill these knowledge gaps, interdisciplinary approaches, which allow the formulation of dynamic individual decision-making under uncertainty, are in demand. More specifically, there is a need for a technique to model social processes and

complexities of stakeholders' behaviors over time through a bottom-up approach and in combination with engineering practices. We incorporate the behaviors of the stakeholders/agents and their changes over time into FRM via ABM to develop effective and sustainable flood mitigation measures and adaptation strategies.

Not many studies incorporate ABM into FRM, but it is becoming popular, and integrating agent behaviors into FRM is gaining importance. Dawson et al. (2011) estimated the vulnerability of people to flood under different storm surge conditions, defense scenarios, evacuation strategies, and flood warning times by coupling ABM with a hydrodynamic model in the coastal town of Towyn in the United Kingdom. Their study determined agent behaviors based on age, sex, employment, and household size. They used the same distribution of these parameters that census generated and randomly located in the study area. Hassani-Mahmooei and Parris (2012) studied internal migration patterns under climate change. Their main goal was to study the migration dynamics due to climate change in Bangladesh. Migrants were the main agents, and decision rules were determined based on various parameters. They generated scenarios considering the combined effects of droughts, floods, sea level rise, and cyclones. They believed that the study's results could be used to prepare and manage the future migration flow while increasing the country's adaptation to CC.

An ABM was developed to focus mainly on the role of flood insurance by Dubbelboer et al. (2017) in Camden, United Kingdom. They covered the interaction between homeowners, insurers, local government, developers, and banks. They highlighted how socioeconomic development can worsen surface water flood risk in the study area. They also found that the implementation of different adaptation measures was successful in reducing surface water flood risk. However, average surface water flood risk increased over time, even with implemented adaptation measures. Haer et al. (2017) integrated household risk mitigation behavior into FRM in Heijplaat, Rotterdam. They analyzed household behavior under three different economic decision models. They showed that future flood risk may be underestimated if human behavior is neglected in FRM. Jenkins et al. (2017)

generated different scenarios using the adaptation options used in the study of Dubbelboer et al. (2016) for the same study area in 2017. They analyzed the effects of different adaptation options on surface water flood risk, individually and in combination. They calculated the average water surface flood risk under the effect of CC. Their study highlighted that surface water flood risk decreases with sustainable urban drainage systems and property-level flood protection. Tonn and Guikema (2018) developed an agent model that analyzes the impacts of community policies and individual decisions on community flood risk. Individual decisions of people were determined based on risk perception and coping perception values. They calculated those values based on parameters such as the number of flood experiences, the number of near-miss flood experiences, individual mitigation, etc. They explored that community mitigation decreases future flood damage. They also found that individual action significantly impacts community flood risk.

Abebe et al. (2019) combined ABM and flood model to manage flood risk in Sint Maarten. Households and government were the main agents in their study. Three institutions represented the government agent. Three compliance rate values, one for each institution, were assigned to each agent using uniform random distribution. Households took actions based on these values. They used MIKE FLOOD as the hydraulic model. Haer et al. (2020) developed an ABM to study flood risk under CC in the European Union. Government and households were the main agents. They generated scenarios based on the different behavior types of the agents. The government agent can be proactive or reactive, while the households can be boundedly rational or rational. They found that the effects of extreme flood events are more significant when governments provide high protection levels in large metropolitan areas. In the same year, Tonn et al. (2020) investigated the behavioral impacts on community flood risk under CC. Their previous study (Tonn & Guikema, 2018) solely included the CC impacts. Their study used one historic climate scenario and three future climate scenarios. They found that actions taken by both the community and individuals decrease the flood damage over time.

Zhuo and Han (2020) conducted a detailed literature review of ABM and FRM. They identified three topics that ABM was used, and different research challenges were addressed. These topics are real-time flood emergency management, long-term flood adaptation planning, and flood hydrological planning. They emphasized the potential contribution of ABM to future flood risk management. They also discussed the limitations of ABM. Taillandier et al. (2021) studied the inhabitants' behavior during a flood event. They provided a new ABM called SiFlo, and they tried to answer the challenges that could not be answered by the previous studies.

2.8 Risk perception and coping perception

The risk-reducing behavior of individuals against natural hazards is interpreted using the Protection Motivation Theory (PMT) introduced by Rogers (1975) and has become very popular nowadays. Risk perception and coping perception are the two main cognitive processes of PMT.

Hunter (2002) defined risk perception as identifying and evaluating risk associated with hazardous events. Several recent studies investigated how to evaluate people's risk perception regarding floods. Liu et al. (2022) studied flood risk perception and effecting factors in Jiaozuo City, China. They prepared a questionnaire and asked four questions in this survey. They assessed demographic factors, residential conditions, and other factors such as flood experience, adaptation measures, etc., and found the most influencing factors. In the same year, Ridha et al. (2022) investigated the impacts of CC on infrastructure in coastal urban areas. They determined the relationship between flood risk perception and assessment of water infrastructure through a survey. Results of the study showed that flood risk perception influences public evaluation of water infrastructure conditions. Buchenrieder et al. (2021) investigated the flood risk perception in a developing country. They also investigated the risk perception influencing factors such as religion, location, sex, age, etc. They found that location is one of the most critical factors influencing flood risk perception.

In 2020, Netzel et al. (2021) analyzed the importance of public risk perception for efficiently managing pluvial floods in urban areas. They selected two case study sites in Western Germany. They conducted a questionnaire-based telephone survey. Their study revealed that personal and global risk perceptions should be distinguished. They also found that global risk perception was high while personal risk perception was relatively low among the participants. They also analyzed the impacts of some parameters on risk perception and found that personal risk perception, education, housing conditions, and knowledge influence people's behavior in terms of mitigation. Liu et al. (2018) studied the flood risk perception of rural households in China. They used eight influencing factors based on the existing literature. They stated that the study's results can help the local government, and households may use them to improve their FRM. Adelekan and Asiyanbi (2016) assessed flood risk perception in flood-affected communities in Lagos, Nigeria. They designed a questionnaire, and 1,000 residents answered the questions. They examined the relationship between socio-demographic attributes of the households and flood risk perception.

Bubeck et al. (2012) examined if flood risk perception contributed to FRM. They selected central Vietnam as a case study and stated that its results provide significant input to the existing literature on flood risk perception in developed countries. Botzen et al. (2009) investigated how geographical and socioeconomic characteristics, flood experience, flood threat knowledge, and risk attitude influence flood risk perception in the Netherlands. They found that flood risk perception is generally low. They also stated that flood risk awareness may be increased by educating people about the causes of floods.

Many studies investigate risk perception, while coping perception is rarely studied. Coping perception is an essential parameter in terms of protective behavior. Bubeck et al. (2012) and Bubeck et al. (2018) stated that coping perception better predicts protective behavior than risk perception. Holley et al. (2022) investigated the roles of place attachment, emotions, and location on coping perception. They stated that coping perception could be used to predict discrete behavioral intentions. Laudan

(2019) analyzed the damage-driving factors of Germany's flash floods and river floods. Furthermore, he assessed the psychological impacts on the coping capacity of flood-affected households. He found that damage-driving factors are different for flash floods and river floods; flood types weakly influence the coping perception of people.

Bormudoi and Nagai (2017) assessed risk perception and coping capacity in Jiadhal Basin, India. They prepared a questionnaire and asked the questions to understand the respondents' perceptions about the primary cause of the disaster. They found that if a respondent's perception of the causes of the disaster is high, coping with them is better. Richert et al. (2017) analyzed the factors that affect households' flood mitigation decisions in France. Their study highlighted that risk perception influences mitigation decisions. Bubeck et al. (2013) studied the impacts of coping perception on mitigation behavior. They analyzed four different flood mitigation behaviors and highlighted the significance of coping perception on flood mitigation behavior. Zaalberg et al. (2009) investigated the flooding experiences in the Netherlands. They wondered if flood experience motivates residents to cope with future flooding. They found that the people who had flood experience reported strong emotions. They also worry more about future flooding and think they are more vulnerable to future floods.

Risk and coping perceptions are effective indicators of people's decisions on whether to take action or not. Thus, these two factors are included in the FRM framework through ABM.

CHAPTER 3

STUDY AREA

Göksu River, which is approximately 271 km, is one of the longest rivers in Türkiye. It runs through Silifke and discharges to the Mediterranean Sea. Silifke, a district of Mersin located at the downstream part of Göksu River, has been selected as the study area because, in the meeting with the State Hydraulic Works staff, they stated that there are not many flood studies in this region. In addition to this, flood events occur frequently in this region (Buldur et al., 2007; İhlas Haber Ajansı, 2017). The population of Silifke in 2023 was around 137,047 (Turkish Statistical Institute, 2024). Lidar point cloud data of the study area with 1 m resolution was obtained from the Ministry of Environment, Urbanization, and Climate Change. It covers approximately 500 km^2, and its resolution is 1 m. The location of buildings is also taken from the same institution. There are approximately 29,000 buildings in the study area. On the other hand, the bathymetry of Göksu River is obtained from the State Hydraulic Works, and the resolution of bathymetry data is 1 m as well. The bathymetry data covers the river section between the point where Göksu River discharges to sea and 8 km upstream of Silifke District Center. A digital elevation model is generated using lidar point cloud data and the bathymetry of the Göksu River. The location of the study area is given in Figure 3.1.

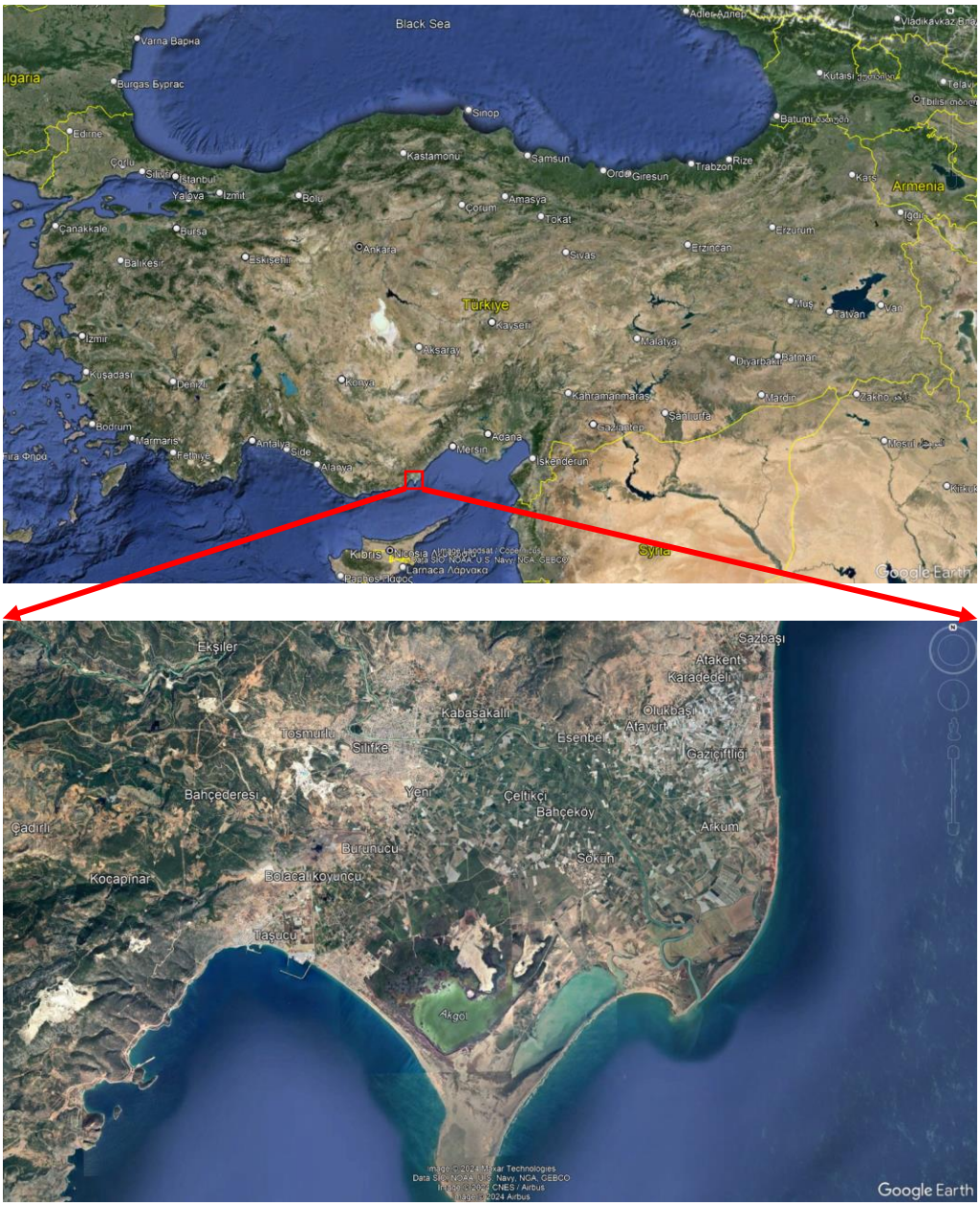

Figure 3.1. Location of the study area (Source: Google Earth)

The study area was visited on the 29th of January, 2024. The photographs from the Göksu River, the center of Silifke, the Göksu Delta, wetlands, and beaches around the Göksu River are given in Figure 3.2. Figure 3.2 (a) and Figure 3.2 (b) show the wetlands around the Göksu River. These areas are near where the Göksu River discharges to the Mediterranean Sea. Figure 3.2 (c) and Figure 3.2 (d) show the

photographs taken from the Göksu River. These photographs are taken from the downstream part of the river. It can be seen that the width of the river is quite wide in this region. Figures 3.2 (e), 3.2 (f), 3.2 (g), and 3.2 (h) show the Göksu River passing through the center of Silifke. It can be seen that there are many bridges on the Göksu River (Figure 3.2 (e) and Figure 3.2 (h)). The Göksu River meanders in Silifke, and it can be seen that the left and right sides of the Göksu River are highly urbanized. Figure 3.2 (i) shows the beaches near the Göksu River and the Mediterranean River, and finally, Figure 3.2 (j) shows the Göksu Delta.

(a) Wetland around Göksu River

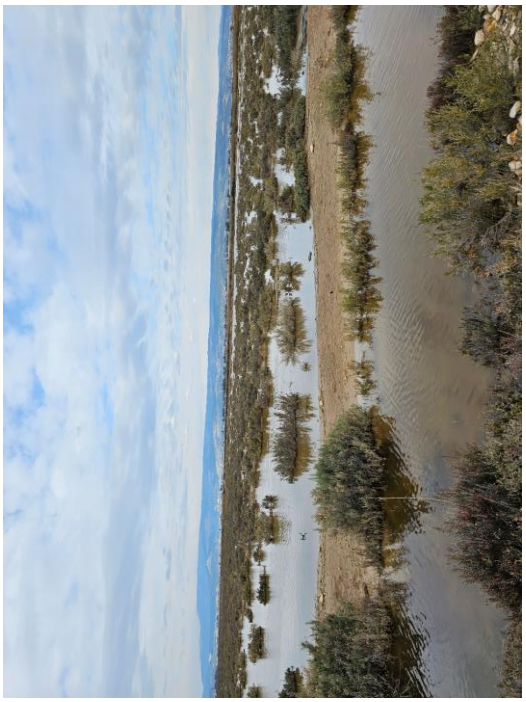

(b) Wetland around Göksu River

Figure 3.2. The photographs from the study area: (a) and (b) Wetland around Göksu River (c) and (d) Göksu River (e) Göksu River passes through the center of Silifke (f) and (g) Meandering part of Göksu River (h) Bridges on Göksu River (i) Beaches around the Göksu River and the Mediterranean Sea (j) Göksu Delta

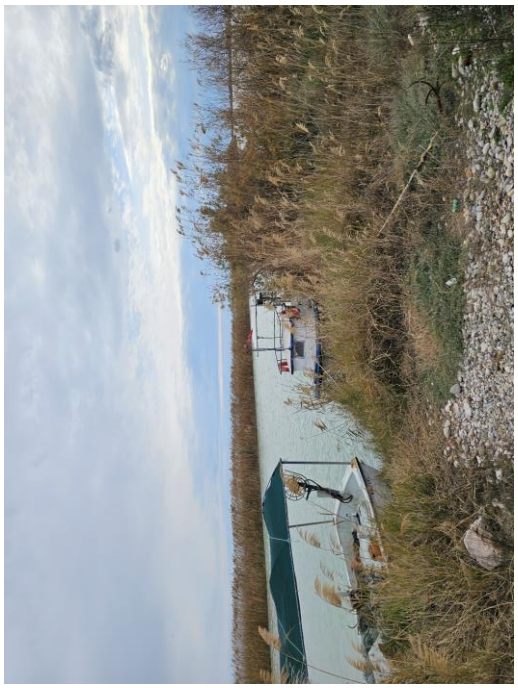

(c) Göksu River

(d) Göksu River

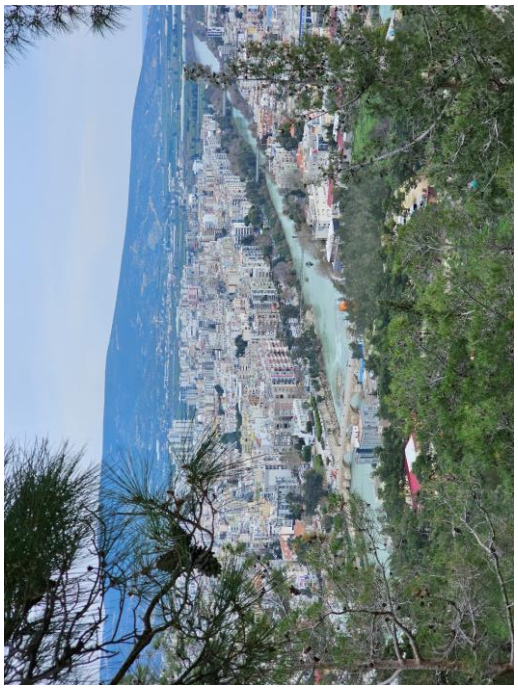

(e) Göksu River passes through the center of Silifke

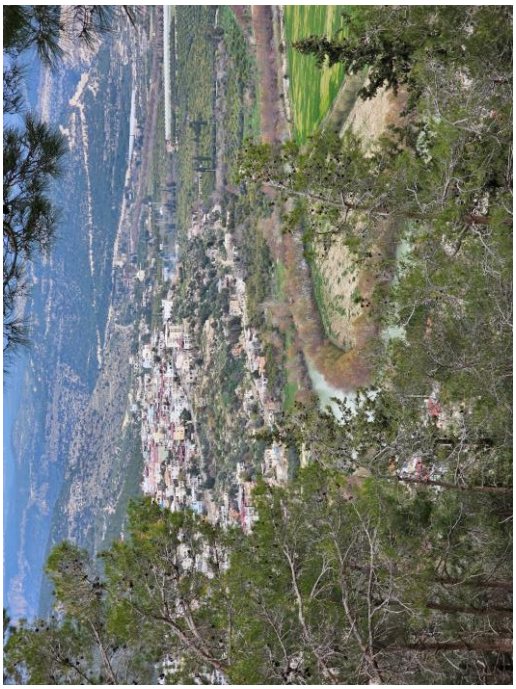

(f) Meandering part of Göksu River

Figure 3.2. (cont'd)

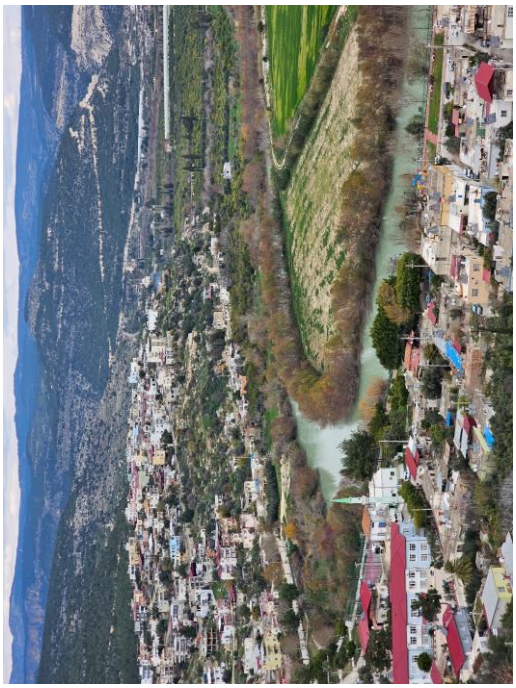

(g) Meandering part of Göksu River

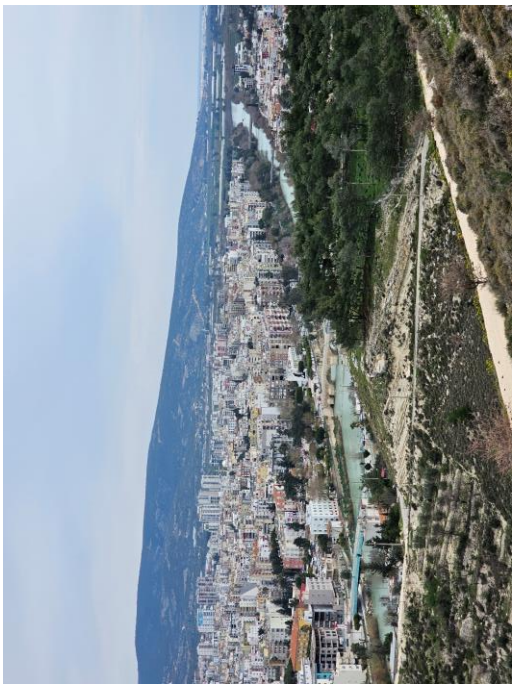

(h) Bridges on Göksu River

(i) Beaches around the Göksu River and the Mediterranean Sea

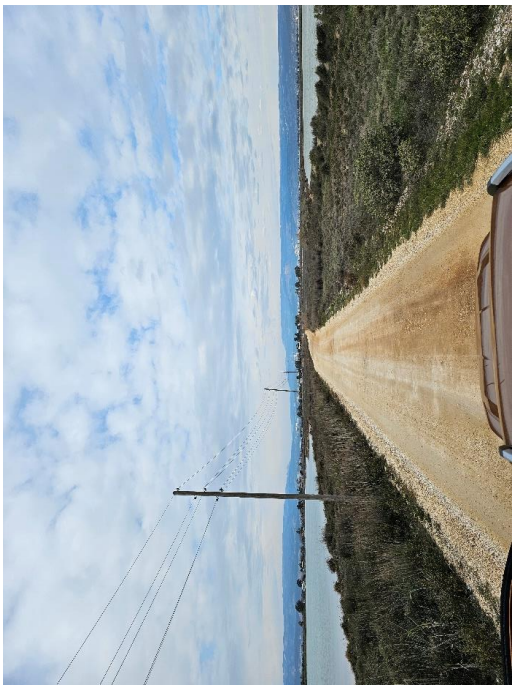

(j) Göksu Delta

Figure 3.2. (cont'd)

A meeting with the State Hydraulic Works (SHW) Silifke Branch was conducted on the 29th of January. In this meeting, the historical floods, the problems of the Göksu River, and the studies about the Göksu River were discussed. The combined 1D/2D hydraulic model is validated based on the information taken in this meeting. It is stated that the historical flood in 2004 hit Silifke from Democracy Park, and the flood water left Silifke after the fourth bridge on the Göksu River. They also stated that the Göksu River can pass safely 800 m^3/s discharge. They also stated that there are expropriation problems around the Göksu River, and because of that, in some parts of the river, it is not possible to regulate the river bed. Figure 3.3 shows the hydraulic structures, meteorological stations, and stream gauges in the basin.

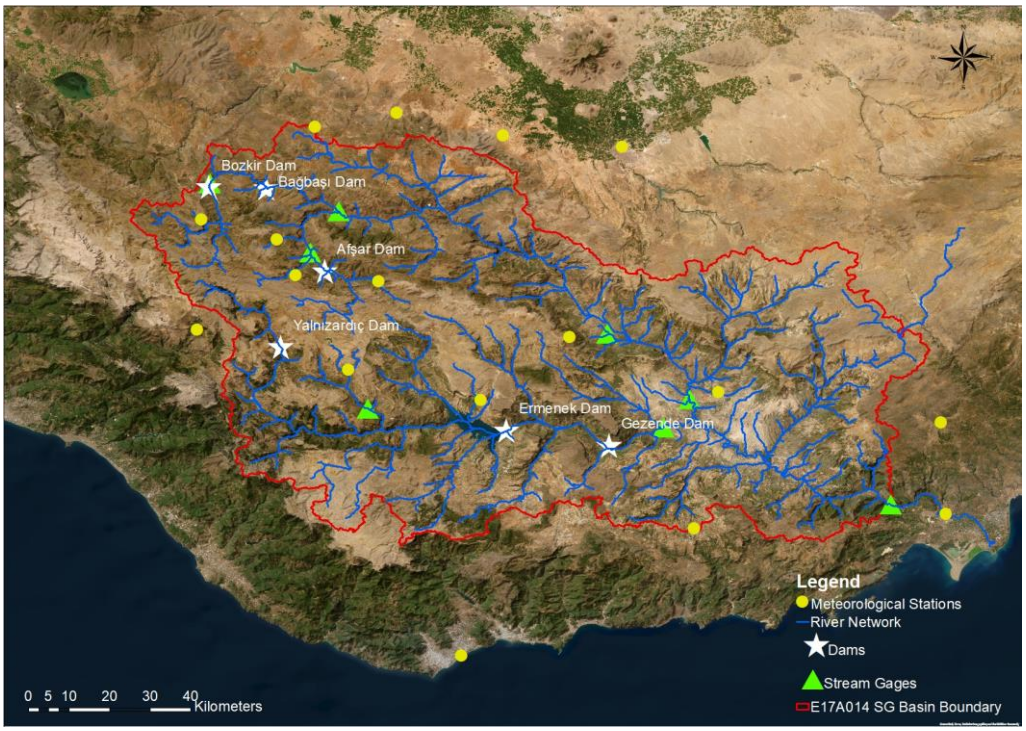

Figure 3.3. Meteorological stations, stream gages, and dams in the basin (Basemap source: Esri, Maxar, Earthstar Geographics, and the GIS User Community)

The hypsometric curve of the basin is given in Figure 3.4. It can be seen that the elevation is greater than 1500 m for approximately 62% of the basin. These areas can be considered as snow storage locations. Flood events caused by snow melting

are a problem for the study area. The latest historical flood event supports this implication (Buldur et al., 2007).

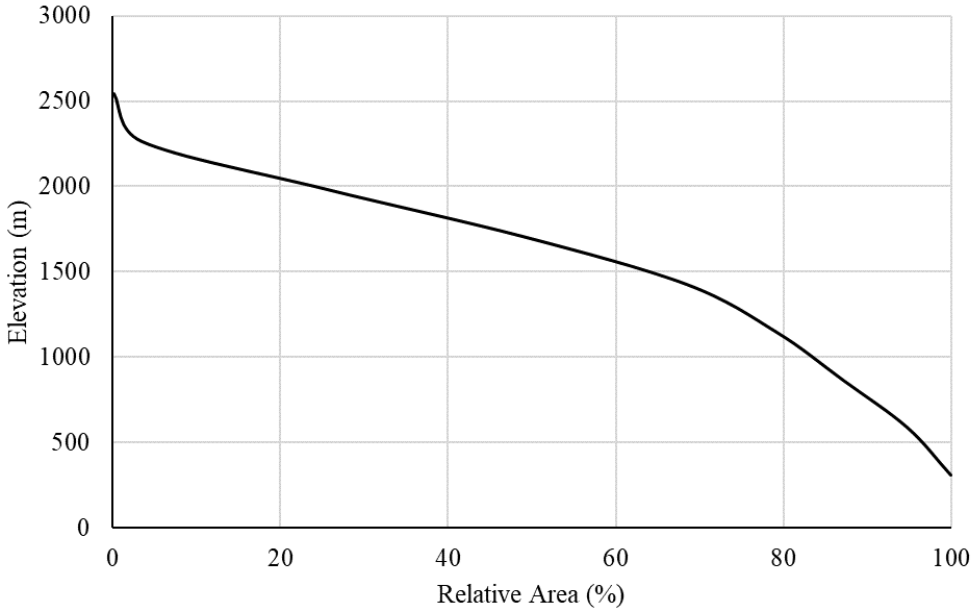

Figure 3.4. Hypsometric curve of the basin

The information about the stream gages is given in Table 3.1, while the information about the meteorological stations is given in Table 3.2.

Table 3.1 The information about the stream gages in the basin

	Basin area (km^2)	Minimum (m^3/s)	Average (m^3/s)	Maximum (m^3/s)	Observation Period
D17A016	3163.5	0.5	33.1	591.0	1964-…
D17A017	364.0	-	5.1	238.0	1967-…
D17A033	588.4	-	6.2	245.0	1985-…
D17A035	491.0	-	5.9	225.0	1985-…
E17A014	10065.2	-	100.6	1996.0	1961-…
E17A020	4304.0	-	38.9	698.0	1965-…
E17A025	203.0	0.1	3.7	333.0	1989-…

Table 3.2 The information about the meteorological stations in the basin

Station No	Minimum Temperature (°C)	Average Temperature (°C)	Maximum Temperature (°C)	Maximum Precipitation (mm)	Observation Period
17246	-28.0	12.1	40.4	68	1951-…
17320	-28.0	19.5	44.2	168.6	1950-…
17330	-5.0	19.6	42.4	139.5	1951-…
17928	-19.6	9.9	36.4	80.9	1960-…
17956	-10.1	17.6	46.7	71.9	1959-…
18059	-10.2	14.2	38.4	124.0	2012-…
18062	-11.8	13.7	36.5	93.3	2012-…
18210	-14.0	12.5	36.7	68.5	2012-…
18484	-20.1	12.9	39.1	45.3	2014-…
18485	-16.6	10.3	33.8	65.9	2014-…
18495	-17.6	12.7	38.0	108.7	2014-…
18498	-17.1	10.0	33.4	70.2	2014-…
18592	-15.4	10.6	33.7	37.5	2014-…
18611	-14.0	11.3	33.7	139.2	2014-…
18655	-14.4	10.0	33.5	63.7	2015-…
18681	-18.1	10.7	34.5	52.7	2015-…
18758	-15.8	10.8	36	36.9	2015-…

CHAPTER 4

METHODOLOGY

The general flowchart of the study is given in Figure 4.1. The study mainly comprises two branches: i) stationary series and ii) non-stationary series. Flood studies are conducted using the traditional approach in the stationary series part. CC, LULC, and the effect of the agents are not considered for this branch. On the other hand, for the non-stationary series part, CC, LULC, and the effects of the agents are integrated into the flood modeling using the ABM. Several RCMs are downloaded and analyzed to include CC effects in flood studies. For the LULC change analysis, satellite images of the study area are used. Finally, for the ABM, a survey is conducted by Infakto Research Workshop in the study area, and the collected information is used to represent the behavior of the agents (i.e., people living in the study area). The main components of the study are explained in the following sections (see Figure 4.1).

4.1 Climate change analysis

CC directly affects floods and their consequences. In this study, effects of CC are represented through the use of RCM projections of precipitation and temperature for the future.

This study assesses the potential impacts of CC by analyzing 17 CORDEX-RCMs for RCP8.5 scenario. The CORDEX RCMs in this study are selected by the following considerations:

- CORDEX-RCMs with the daily simulation results for the EURO-11 domain and publicly available in the ESFG portal are used after being downloaded from the relevant website (https://esgf-node.llnl.gov/search/esgf-llnl/).

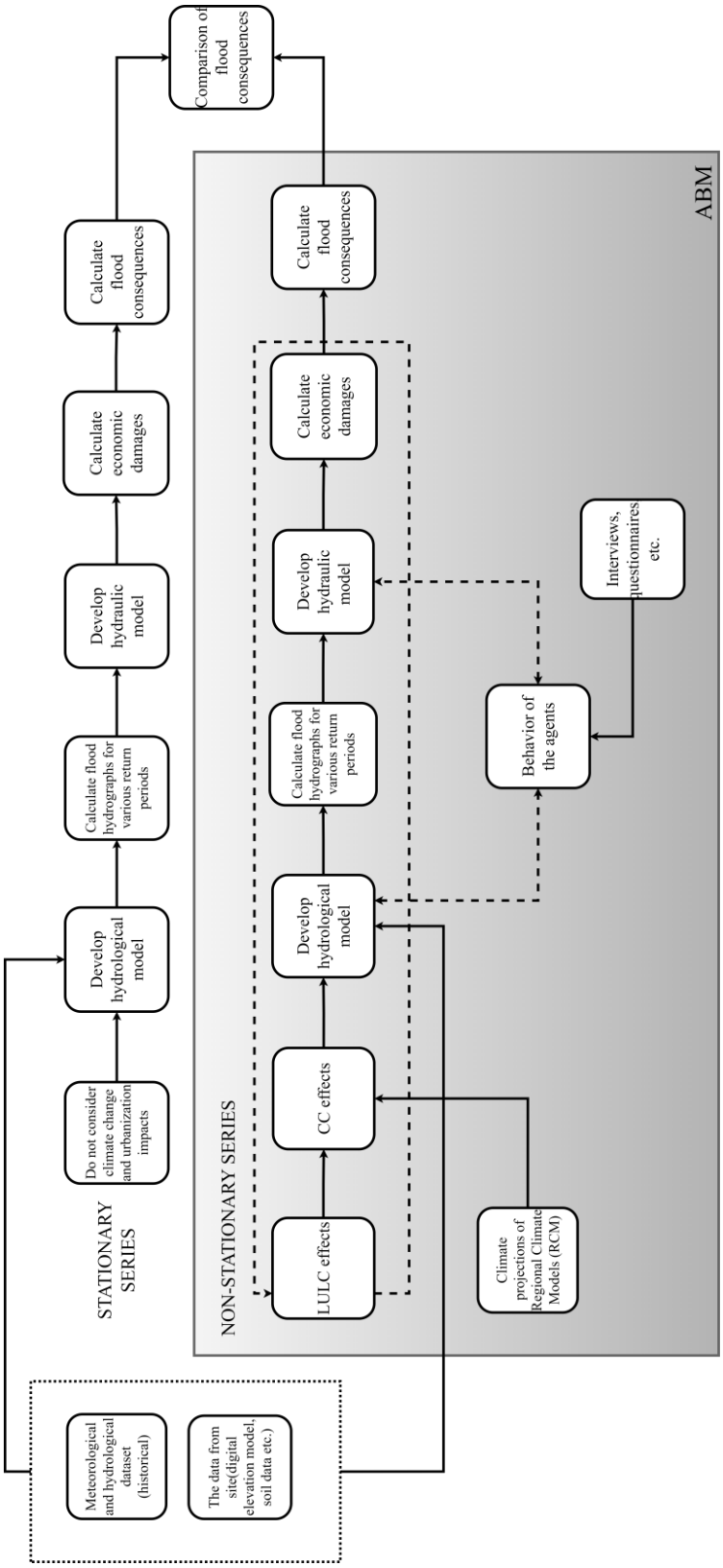

Figure 4.1. Flowchart of the study

- The CORDEX-RCMs that have historical and future climate simulations for the RCP8.5 scenario are employed for the analysis to achieve a comparative assessment of the medium and no GHG mitigation conditions.
- CORDEX-RCMs that were used in recent studies (e.g., Kentel et al. (2021) and Aziz et al. (2020)) on climate change impact assessment in Türkiye are considered as candidate models in this study. The findings from these studies, particularly those pertaining to the simulation skills of the models, have been taken into consideration in the selection of models.
- In order to evaluate the CORDEX-RCMs, it is necessary to consider the CORDEX Errata page (EURO-CORDEX, 2021). Models that have been identified as having potential issues that may be significantly relevant to the scope and objectives of this study are excluded from the final climate model list.

The final list of RCMs that is used is given in Table 4.1. The selected RCMs data to be used is downloaded and processed. Historic precipitation and temperature data of these models are entered into the hydrological model, and the best RCM is determined based on comparison of estimated and observed streamflow values using Correlation Coefficient (Corr), Root Mean Square Error (RMSE), Percent Bias (PBIAS), and Nash Sutcliffe Efficiency (NSE). These measures are calculated for both sorted and unsorted streamflow.

4.2 Land use / land cover change analysis

LULC is another important parameter that affects flood magnitude. Landsat images that are the products of U.S. Geological Survey are used as historical satellite images. Historical satellite images are classified, and urbanization trends are evaluated using these results. Information about satellite images that are used in the analysis is provided in Table 4.2.

Table 4.1 Timeframes of the simulation outputs of climate models used in this study

Climate Model (RCM/GCM)			Output Period	
Model ID[+]	Driving GCM	RCM	Historic	Future (Scenarios)
M1*	CNRM-CM5	CCLM4-8-17	1950-2005	2006-2100 (RCP4.5, RCP8.5)
M2*	CNRM-CM5	ALADIN63	1951-2005	2006-2100 (RCP4.5, RCP8.5)
M3*	CNRM-CM5	RCA4	1970-2005	2006-2100 (RCP4.5, RCP8.5)
M4*	EC-EARTH	HIRHAM5	1951-2005	2006-2100 (RCP4.5, RCP8.5)
M5*	EC-EARTH	CCLM4-8-17	1949-2005	2006-2100 (RCP4.5, RCP8.5)
M6*	EC-EARTH	RACMO22E	1950-2005	2006-2100 (RCP4.5, RCP8.5)
M7*	EC-EARTH	RCA4	1970-2005	2006-2100 (RCP4.5, RCP8.5)
M8*	CM5A-MR	WRF331F	1951-2005	2006-2100 (RCP4.5, RCP8.5)
M9*	CM5A-MR	WRF381P	1951-2005	2006-2100 (RCP4.5, RCP8.5)
M10*	CM5A-MR	RCA4	1970-2005	2006-2100 (RCP4.5, RCP8.5)
M11*	HadGEM2-ES	CCLM4-8-17	1949-2005	2006-2100 (RCP4.5, RCP8.5)
M12*	HadGEM2-ES	RACMO22E	1950-2005	2006-2100 (RCP4.5, RCP8.5)
M13*	HadGEM2-ES	RCA4	1970-2005	2006-2100 (RCP4.5, RCP8.5)
M14*	MPI-ESM-LR	CCLM4-8-17	1949-2005	2006-2100 (RCP4.5, RCP8.5)
M15*	MPI-ESM-LR	REMO2009(r1i1p1)	1950-2005	2006-2100 (RCP4.5, RCP8.5)
M16*	MPI-ESM-LR	REMO2009(r2i1p1)	1950-2005	2006-2100 (RCP4.5, RCP8.5)
M17*	NorESM1-M	HIRHAM5	1951-2005	2006-2100 (RCP4.5, RCP8.5)

[+] Model ID's used in this study

* Models from the CORDEX Database: ESGF, Earth System Grid Federation website, https://esgf-node.llnl.gov/search/esgf-llnl/, (CoG version v4.0.0b2, ESGF P2P Version v4.0.4)

Table 4.2 Satellite images used in LULC classification (Landsat-5 image courtesy of the U.S. Geological Survey and Landsat-8 image courtesy of the U.S. Geological Survey)

Satellite	Access Date	Data
Landsat 8	25.08.2021	LC08_L2SP_176035_20210825_20210901_02_T1
Landsat 8	10.05.2017	LC08_L2SP_176035_20170510_20200904_02_T1
Landsat 8	22.10.2013	LC08_L2SP_176035_20131022_20200912_02_T1
Landsat 5	19.09.2004	LT05_L2SP_176035_20040826_20200903_02_T1
Landsat 5	23.09.1985	LT05_L2SP_176035_19850923_20200918_02_T1

Landsat 5 and Landsat 8 images are employed in the LULC classification process. Landsat 7 images are not utilized due to a scan line corrector failure. Image classification is conducted utilizing the "Image Classification" tool of ArcGIS. The dates of the downloaded images are selected with consideration of both cloud cover and Google Earth image dates, as training polygons and the validation of the classified images are conducted using Google Earth.

The literature review revealed a correlation between urbanization and deforestation. This is a crucial finding in the context of hydrological studies, as it suggests that an increase in urbanization may lead to a greater risk of flooding (see Section 2.4). Conversely, a reduction in forest areas could potentially result in an increase in peak discharges and flood events, which in turn could increase the risk of flooding. Consequently, the analysis of LULC change incorporates the classification of satellite images to identify trends in LULC change within the study area.

Satellite images are classified using the Image Classification tool of ArcGIS, and the classification procedure is given in Figure 4.2. After downloading the Landsat images, they are clipped considering the study area in Figure 4.3.

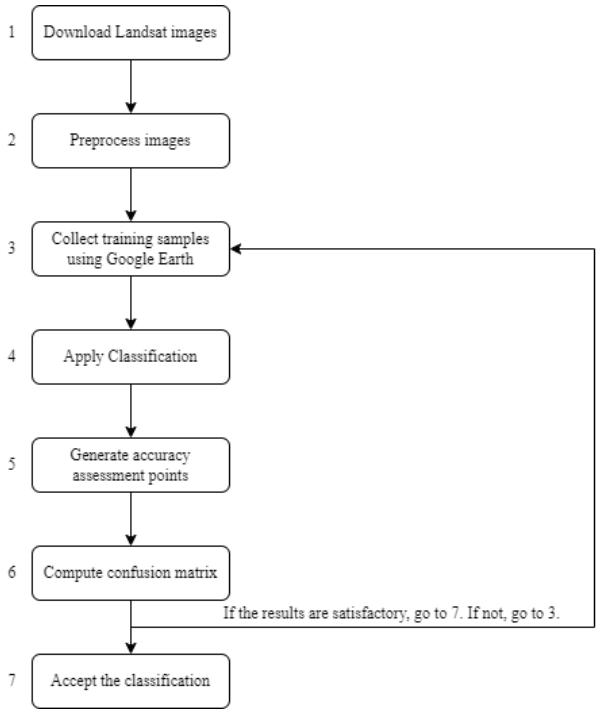

Figure 4.2. Image classification flowchart

Figure 4.3. Image classification of the study area (Basemap source: Esri, Maxar, Earthstar Geographics, and the GIS User Community)

Training samples are collected using Google Earth images. In accordance with the literature, a variety of LULC classes are employed within the context of the study, including agricultural land, forests, urbanized areas, bare land, water bodies, and marshes. Following the collection of training samples, a LULC map is generated using the Maximum Likelihood Classification (MLC) tool of ArcGIS. The MLC tool employs two fundamental principles: i) normally distributed cells in each class sample and ii) Bayes' theorem of decision-making.

The means and variances of each LULC class are considered when assigning an LULC class to a cell. The MLC tool calculates the probabilities of each LULC class and the LULC class with the highest probability is assigned to each cell.

Following classification, accuracy assessment points are generated randomly, considering the boundaries of the training samples, to evaluate the accuracy of LULC classification. The image classification algorithm uses training samples to identify LULC classes. The LULC classes are then assigned to the generated accuracy assessment points using the generated LULC map. Approximately 500 accuracy assessment points are used, and a confusion matrix is calculated based on these points. In order to ensure fairness, the accuracy assessment points are generated so that they do not overlap with the training samples.

Four different parameters can be obtained using the confusion matrix. These are $User's\ Accuracy\ (UA)$, $Producer's\ Accuracy (PA)$, $Overall\ Accuracy\ (OA)$ and *KHAT statistics* or $Kappa\ Coefficient\ (KC)$. UA (Equation 4-1) can be calculated by dividing the number of correctly classified samples of a category by the total number of samples that are classified in that category. It can be used to indicate how well the classified map represents ground truth. On the other hand, PA (Equation 4-2) is calculated by dividing the number of correctly classified samples of a category by the total number of reference samples of that category. It indicates how well a specific area can be correctly mapped. Furthermore, OA (Equation 4-3) can be calculated by dividing the total number of correctly classified samples by the total number of samples. It represents the accuracy of the entire product (Story &

Congalton, 1986). Finally, KC can be calculated using Equation 4-4 and it shows the strength of agreement between two sets.

$$User's\ Accuracy = \frac{x_{ii}}{x_{i+}} \tag{4-1}$$

$$Producer's\ Accuracy = \frac{x_{ii}}{x_{+i}} \tag{4-2}$$

$$Overall\ Accuracy = \frac{\sum_{i=1}^{r} x_{ii}}{N} \tag{4-3}$$

$$Kappa\ Coefficient = \frac{N \times \sum_{i=1}^{r} x_{ii} - \sum_{i=1}^{r} x_{i+} \times x_{+i}}{N^2 - \sum_{i=1}^{r} x_{i+} \times x_{+i}} \tag{4-4}$$

where N is the total number of samples, r is the total number of LULC classes, i is the index for the LULC class number, x_{ii} is the total number of correctly classified samples belonging to LULC class i, x_{i+} and x_{+i} are the marginal totals of row i and column i of the confusion matrix (Congalton, 1991).

4.3 Development of the hydrological model

HEC-HMS is employed to simulate the rainfall-runoff relationships of the stream gauges within the study basin. HEC-HMS is a conceptual modeling software developed by the US Army Corps of Engineers Hydrologic Engineering Center (U.S. Army Corps of Engineers, 2000). It facilitates the analysis of hydrological processes in dendritic watershed systems. The system diagram depicting the runoff process at a local scale is presented in Figure 4.4 (U.S. Army Corps of Engineers, 2000).

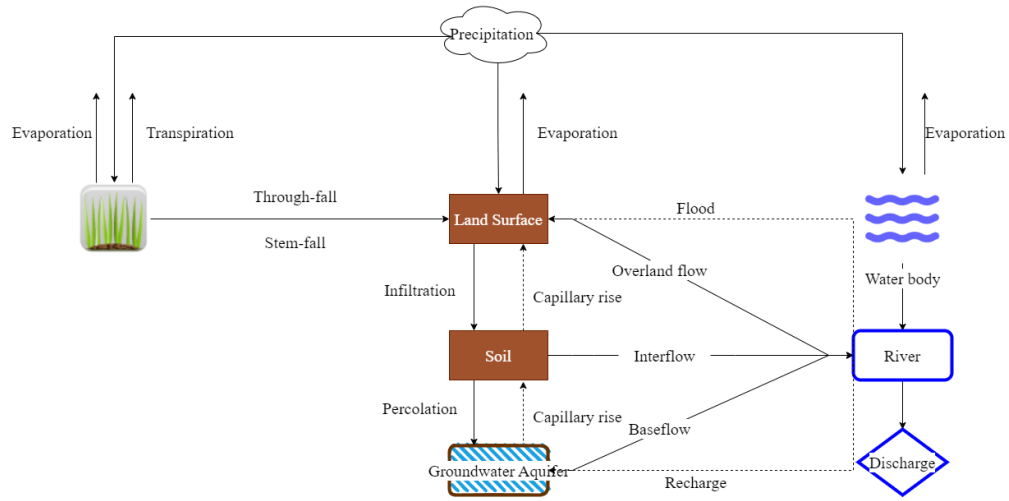

Figure 4.4. System diagram of the runoff process (U.S. Army Corps of Engineers, 2000)

For the hydrological processes where a detailed accounting is not required (e.g., calculation of the peak discharge), the simpler version can be employed. Figure 4.5 illustrates the simplified representation of the watershed runoff process (U.S. Army Corps of Engineers, 2000).

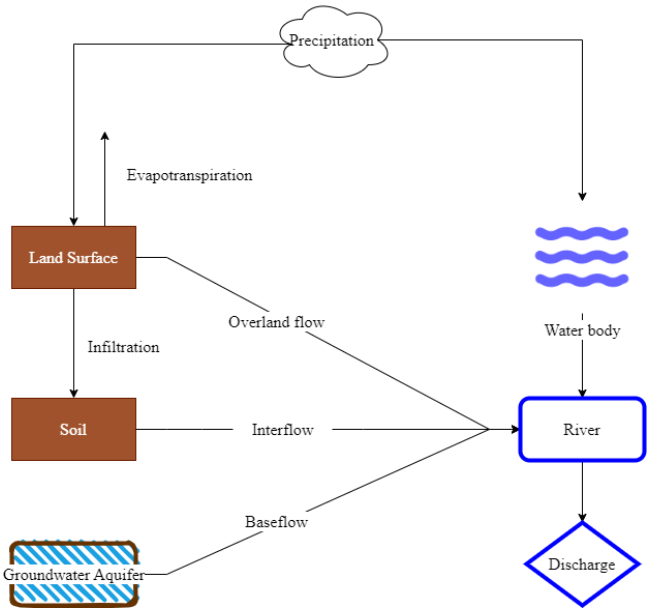

Figure 4.5. Typical representation of the runoff process (U.S. Army Corps of Engineers, 2000)

The development of the rainfall-runoff model comprises six primary model components: basin model, meteorologic model, control specifications, time-series data, paired data, and terrain data. The basin model's primary objective is to translate atmospheric conditions into streamflow at specified locations. The meteorologic model is utilized to define meteorological boundary conditions for the sub-basins. Control specifications serve to set the simulation start and end times, encompassing calibration and validation dates/times. Time-series data component is utilized for inputting various datasets such as precipitation, temperature, discharge, and sunshine hour data. Paired data, such as elevation-area or elevation-storage relationships, can be incorporated in functional form within HEC-HMS. Terrain data aids in watershed delineation and provides surface elevation information. A flowchart illustrating the hydrological modeling process using HEC-HMS is depicted in Figure 4.6.

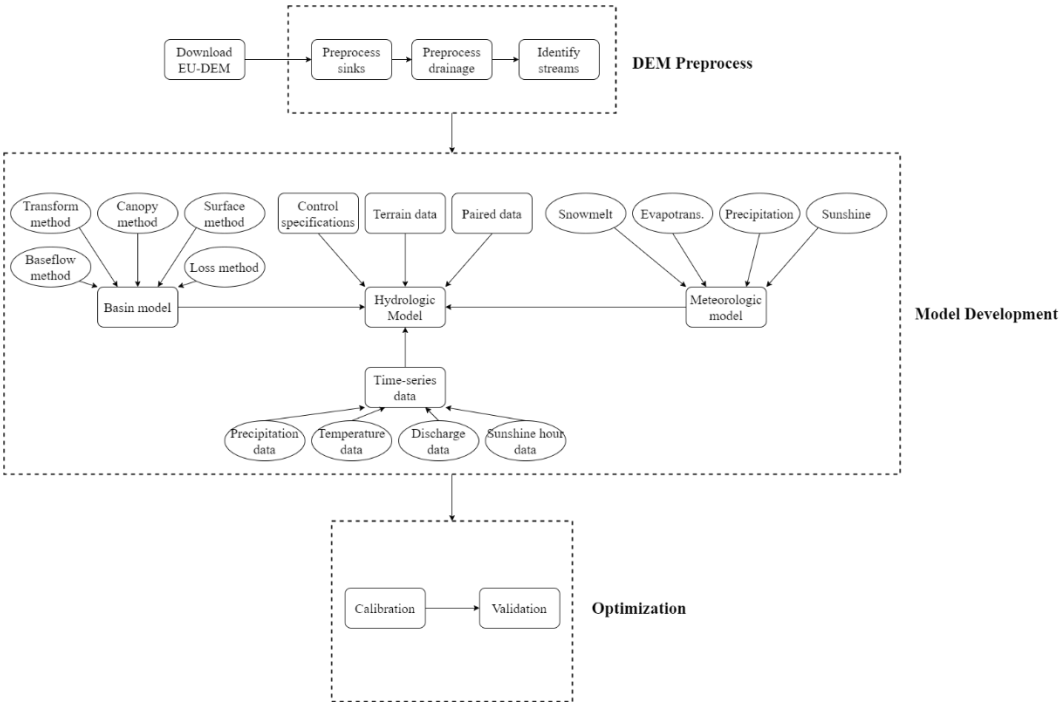

Figure 4.6. The flowchart of the hydrological model

There are several methods under the basin model in HEC-HMS. These methods are used to calculate the outflow and the methods should be chosen considering the simulation type. There are two types of simulation: event-based simulation and

continuous simulation. For flood events, event-based simulations are generally preferred. However, firstly, the continuous simulation is performed to understand the rainfall-runoff relationship of the basin. Moreover, hourly or smaller than daily streamflow data for the stream gages of the basin could not be obtained from State Hydraulic Works; thus, event-based simulations are not possible. Thus, continuous simulation is used in this study, and methods are chosen according to the HEC- HMS User's Manual (U.S. Army Corps of Engineers, 2024). The canopy method is used to represent the presence of plants in the landscape. The selection of the canopy method is optional but it is suggested to be used for continuous simulation (U.S. Army Corps of Engineers, 2024). Thus, simple canopy is selected as the canopy method. Selection of surface method is also optional. The ground surface where water may accumulate in surface depression storage can be represented by the surface method. It is generally used for continuous simulation and in the modeling studies, simple surface method is selected as the surface method (U.S. Army Corps of Engineers, 2024). Moreover, the loss method should be selected according to the simulation type. The Loss method calculates actual infiltration and all options under the loss method conserve mass. Deficit and constant method is selected, which is suitable for continuous simulation. Furthermore, the transform method is used to perform surface runoff calculations and the Soil Conservation Service (SCS) unit hydrograph method is selected. Finally, subsurface calculations are carried out by using the baseflow method. Simulation type is again important in the selection of the baseflow method. The monthly constant baseflow method is used for the baseflow calculations.

There are several methods under the meteorological model component. These methods are used to calculate the outflow in HEC-HMS. Evapotranspiration is the combination of evaporation from the ground surface and transpiration from the plants. The evapotranspiration method is not important for short events but it is important for continuous simulation (U.S. Army Corps of Engineers, 2024). In this study, Priestley Taylor method is employed to represent evapotranspiration. This method requires the use of the shortwave and temperature methods. The shortwave

radiation method is used to represent the incoming radiation from the sun and it is suggested to be used when energy-balance evapotranspiration methods, namely, Penman Monteith and Priestley Taylor methods, are used in the hydrological model (U.S. Army Corps of Engineers, 2024). In this study, the Food and Agriculture Organization of the United Nations (FAO) 56 is selected as the shortwave radiation method. The longwave radiation method is not preferred in the modeling studies because the selected evapotranspiration method does not require using the longwave radiation method (U.S. Army Corps of Engineers, 2024). The precipitation method is used to determine the amount of water falling to the land surface. The gauge weights are assigned using the Thiessen polygons method. Moreover, the temperature method is used to represent the heat intensity of air over the land surface. Specified thermograph is selected as the temperature method. Windspeed, pressure, and dewpoint methods are not used in the hydrological model because the selected evapotranspiration method does not require them. Lastly, the temperature index method is selected as the snowmelt method that is used to represent snow melting. Selected methods for basin and meteorology models are summarized in Table 4.3.

Table 4.3 Hydrological model specifications

Basin Model Methods		Meteorologic Model Methods	
Canopy Method	Simple Canopy	Shortwave Method	FAO56
Surface Method	Simple Surface	Longwave Method	-
Loss Method	Deficit and Constant	Precipitation Method	Gage Weights
Transform Method	SCS Unit Hydrograph	Temperature Method	Specified Thermograph
Baseflow Method	Recession	Windspeed Method	-
		Pressure Method	-
		Dew Point Method	-
		Evapotranspiration Method	Priestly Taylor
		Snowmelt Method	Temperature Index

Coefficient of Determination (R^2), Nash Sutcliffe Efficiency (NSE), Root Mean Squared Error- Observations Standard Deviation Ratio (RSR), Percent Bias ($PBIAS$), the observed peak, the observed volume, and time to peak are measures that are employed to evaluate the results of the hydrological model.

$$R^2 = 1 - \frac{\sum_{i=1}^{n}(y_i - \hat{y}_i)^2}{\sum_{i=1}^{n}(y_i - \bar{y})^2} \quad (4\text{-}5)$$

$$NSE = 1 - \frac{\sum_{i=1}^{n}(y_i - y_i^{sim})^2}{\sum_{i=1}^{n}(y_i - \bar{y})^2} \quad (4\text{-}6)$$

$$RSR = \frac{\sqrt{\sum_{i=1}^{n}(y_i - y_i^{sim})^2}}{\sqrt{\sum_{i=1}^{n}(y_i - \bar{y})^2}} \quad (4\text{-}7)$$

$$PBIAS = \frac{\sum_{i=1}^{n}(y_i - y_i^{sim}) * 100}{\sum_{i=1}^{n} y_i} \quad (4\text{-}8)$$

where y_i is the i^{th} observation, $\hat{y}_i$ is the corresponding predicted value of y_i, $\bar{y}$ is the mean of observed data, y_i^{sim} is i^{th} simulated value of y_i and n is the total number of observations. Performance evaluation criteria for these measures are defined by Moriasi et al. (2015) as shown in Table 4.4.

Table 4.4 Performance evaluation criteria for the selected measures (Moriasi et al., 2015)

Measure	Performance Evaluation Criteria			
	Very Good	Good	Satisfactory	Not Satisfactory
R^2	$R^2 > 0.85$	$0.75 < R^2 \leq 0.85$	$0.60 < R^2 \leq 0.75$	$R^2 \leq 0.60$
NSE	$NSE > 0.80$	$0.70 < NSE \leq 0.80$	$0.50 < NSE \leq 0.70$	$NSE \leq 0.50$
$PBIAS$ (%)	$PBIAS < \pm 5$	$\pm 5 \leq PBIAS < \pm 10$	$\pm 10 \leq PBIAS < \pm 15$	$PBIAS \geq \pm 15$
RSR*	$0.00 \leq RSR \leq 0.50$	$0.50 < RSR \leq 0.60$	$0.60 < RSR \leq 0.70$	$RSR > 0.70$

* It is taken from (Moriasi, et al., 2007)

Hydrologic Engineering Centre (HEC-HMS, 2023) proposes to check the observed peak, the observed volume, and time to peak values. It also states that ± 10% difference between the observed and simulated values is acceptable, and the time to

peak of the simulations should be within ± 12 hours range of the observed time to peak value.

The basin boundary for E17A014 Stream Gage (SG) is given in Figure 4.7. A prominent challenge associated with this basin pertains to the presence of numerous hydraulic structures. This is problematic because the operation strategies of these hydraulic structures are not available on a daily time scale. Developing a hydrological model becomes particularly arduous in the absence of such operational strategies.

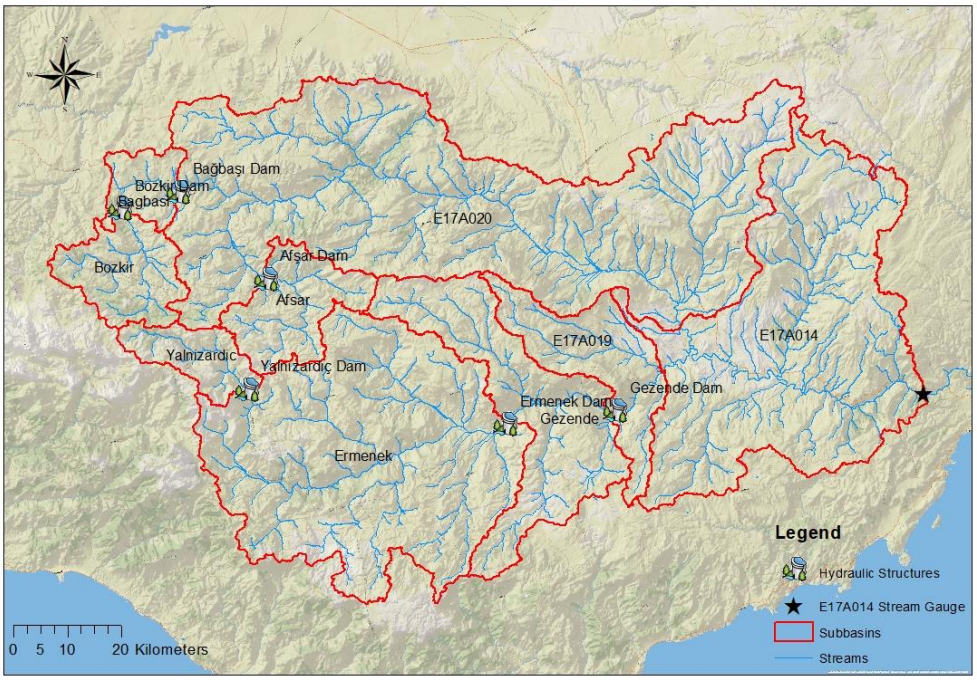

Figure 4.7. E17A014 SG basin and major hydraulic structures (Basemap source: National Geographic World Map)

The hydrological model is developed firstly for the period before the major hydraulic structures are built in the basin. The hydraulic structures with storages of more than 20 hm^3 are assumed to be the major structures. The names and the characteristics of these structures are given in Table 4.5 (Doğu Akdeniz Basin Master Plan Report, 2017). The locations of these structures and the SGs are given in Figure 4.7.

Table 4.5 Characteristics of the major hydraulic structures in E17A014 Basin (obtained from Doğu Akdeniz Basin Master Plan Report, 2017)

Hydraulic Structure	Purpose	Drainage Area (km^2)	Total Volume (hm^3)	Operation Start Date
Bozkır Dam	E + D	370.0	360.7	2020
Bağbaşı Dam	D + I	539.0	204.9	2015
Afşar Dam	D + I	384.0	363.7	2021
Yalnızardıç Dam	E	261.9	109.5	2015
Ermenek Dam	I + E	2304.0	4582.6	2010
Gezende Dam	E	3158.5	95.0	1994

E: Energy D: Diversion I: Irrigation

E17A014 SG basin is divided into nine sub-basins considering the locations of the major hydraulic structures and two other stream gages, E17A019 and E17A020. These nine sub-basins are also shown in Figure 4.7. Gezende Dam is the first major structure of the basin which was built in 1994 (see Table 4.5). Table 4.6 shows the meteorological observation stations (MOS) used in developing the hydrological model.

These MOSs are manual stations and the representation percentages of the MOSs and the areas of the sub-basins are also given in Table 4.6. The representation percentages are calculated using the Thiessen Polygons Method. These MOSs have continuous data till 1986, thus, the hydrologic model is developed for the period between 1965 and 1986. The calibration period is selected between October 1, 1965, and October 1, 1978, and the validation period is selected between August 1, 1981 and August 1, 1986.

After developing and successfully calibrating the hydrological model that represents the basin's natural response, hydraulic structures are entered into the hydrological model since these structures affect the rainfall-runoff relationship of the basin for the present times' conditions (i.e., with major hydraulic structures).

Table 4.6 The MOSs used in the hydrological model

Station No	Latitude	Longitude	Elevation (m)	Representation Percentage (%)				
				Afsar	Bagbasi	Bozkir	Ermenek	E17A014
17246	37.1932	33.2202	1018					
17320	36.0686	32.8649	2				30.4	
17330	36.3824	33.9373	10					20.7
17928	36.9893	32.4557	1552	100	100	100	60	
17956	36.6514	33.4339	340				9.6	79.3
Area (km^2)				383	168	355	2192	2181

Station No	Latitude	Longitude	Elevation (m)	Representation Percentage (%)			
				E17A019	E17A020	Gezende	Yalnizardic
17246	37.1932	33.2202	1018		19.8		
17320	36.0686	32.8649	2			17.8	
17330	36.3824	33.9373	10				
17928	36.9893	32.4557	1552		40.7	16.1	100
17956	36.6514	33.4339	340	100	39.5	66.1	
Area (km^2)				495	3425	893	220

There are different options to represent routing in HEC-HMS. The outflow curve, specified release, and outflow structures are the methods to define the routing process in the model. Each routing method has different storage methods and initial condition options. Hydraulic structures should be integrated into the model considering the available data. Storage-outflow relationships are used by the outflow curve routing method to represent reservoirs. The outlet structures cannot be used with this method. The specified release routing method can be used if the specified release from the reservoir is known. On the other hand, the outflow structures routing method can be used if the information about outlet structures is known (U.S. Army Corps of Engineers, 2024). The outflow curve routing method is selected as the routing method due to the limited data. The elevation-storage-discharge method is used as the storage method, while the elevation is selected as the initial condition.

The hydrological model is tested between August 31, 2016, and August 31, 2020. Bağbaşı Dam, Ermenek Dam, Gezende Dam, and Yalnızardıç Dam are in operation in the test period, while Afşar Dam and Bozkır Dam are not active in the test period. Thus, the active hydraulic structures are entered into the hydrologic model. In the hydrological model, the following points are taken into consideration when entering these hydraulic structures into the model:

- One of the main purposes of Bağbaşı Dam is to transfer water from Doğu Akdeniz Basin to the Konya Closed Basin. The diversion tool of HEC-HMS is used to input the transferred water to the hydrologic model.
- There are many irrigation projects in the basin. The amount of water diverted from related reservoirs for irrigation purposes is entered into the hydrologic model.
- Evaporated water from the reservoirs is also diverted from the related reservoirs.
- Initial water elevation of the reservoirs is calibrated according to the performance of the statistical parameters.

All necessary data is taken from the Doğu Akdeniz Basin Master Plan Report (Yüksel Proje, 2017).

The MOSs used in the test period differ from the calibration and validation periods because automatic MOSs were established around 2010. The representation percentages of the MOSs and the areas of the divided subbasins are given in Table 4.7. The representation percentages are calculated using the Thiessen Polygons Method.

Table 4.7 The MOSs used in the test period

Station No	Latitude	Longitude	Elevation (m)	Representation Percentage (%)				
				Afsar	Bagbasi	Bozkir	Ermenek	E17A014
17330	36.3824	33.9373	10					8
17928	36.9893	32.4557	1552		16	10		
17956	36.6514	33.4339	340					40
18059	36.3495	33.3797	1013					26
18062	36.5839	33.9267	1204					25
18210	36.6336	32.9075	1415				37	
18484	37.2186	32.9564	1070					
18485	36.7011	32.6139	1655	13			53	
18495	37.268	32.7208	1190					
18498	36.9093	32.4976	1679	37				
18592	36.8969	32.6817	1590	50			3	
18611	36.7886	32.2792	1672			3	7	
18655	36.7731	33.1039	1659					1
18681	37.0331	32.2886	1592		69	87		
18758	37.2378	32.5408	1496		15			
Area (km^2)				383	168	355	2192	2181

Station No	Latitude	Longitude	Elevation (m)	Representation Percentage (%)			
				E17A019	E17A020	Gezende	Yalnizardic
17330	36.3824	33.9373	10				
17928	36.9893	32.4557	1552		9		
17956	36.6514	33.4339	340	21	27		
18059	36.3495	33.3797	1013	19		7	
18062	36.5839	33.9267	1204				
18210	36.6336	32.9075	1415			69	
18484	37.2186	32.9564	1070		10		
18485	36.7011	32.6139	1655				2
18495	37.268	32.7208	1190		6		
18498	36.9093	32.4976	1679		4		34

Table 4.7 (cont'd)

Station No	Latitude	Longitude	Elevation (m)	Representation Percentage (%)			
				E17A019	E17A020	Gezende	Yalnizardic
18592	36.8969	32.6817	1590		15	7	
18611	36.7886	32.2792	1672				63
18655	36.7731	33.1039	1659	60	23	17	
18681	37.0331	32.2886	1592				1
18758	37.2378	32.5408	1496		6		
Area (km^2)				495	3425	893	220

4.4 Development of combined 1D/2D hydrodynamic model

The Hydrologic Engineering Center River Analysis System (HEC-RAS) is employed to develop a coupled One-Dimensional/Two-Dimensional (1D/2D) combined hydrodynamic model. Hydraulic models might be 1D, 2D, or combined 1D/2D. The most important factor to consider is the model's purpose when selecting the model type. 1D models can be used to model the rivers with regular flow. If the river passes through a non-urbanized area and flood events happen never or rarely, 1D models are good options. 2D models can be used to model the rivers that do not have structures on them. There are some approaches to enter these structures in 2D models, but they are not straightforward. The combined 1D/2D model is a good option for rivers with many structures and urbanized areas (Betsholtz & Nordlöf, 2017).

Geometry and flow data are the most important parameters of the hydraulic models. High-resolution geometry data will lead to more accurate results. For this reason, high-resolution geometry data is needed for accurate flood inundation maps. Terrain data of the study area and location of the buildings are obtained from the Ministry of Environment, Urbanization, and Climate Change. The study area's digital elevation model (DEM) is generated using the LiDAR (Light Detection and Ranging) data,

and the point space is 1 m. A 3-dimensional view of the study area is given in Figure 4.8.

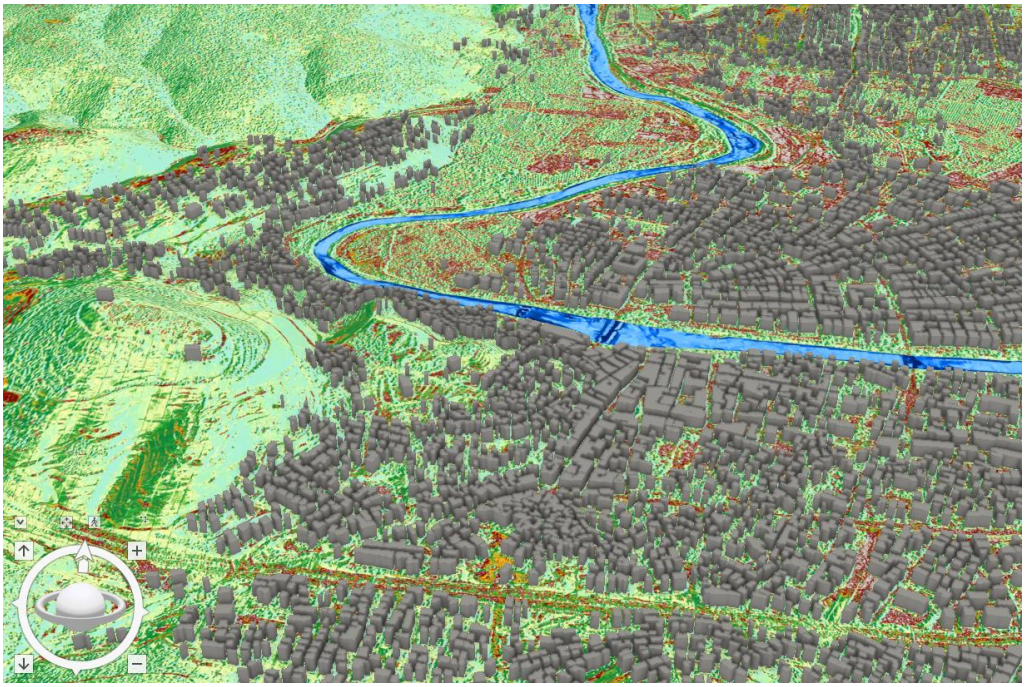

Figure 4.8. 3-dimensional view of the study area

Bathymetry data of the river is needed to model the river bed, which was obtained from the SHW. Firstly, river center line and bank lines are generated using this data. River cross-sections are generated by considering bank lines, and some examples are given in Figure 4.9. The distance between each cross-section is approximately 25 m, and a total number of 1024 cross-sections are generated.

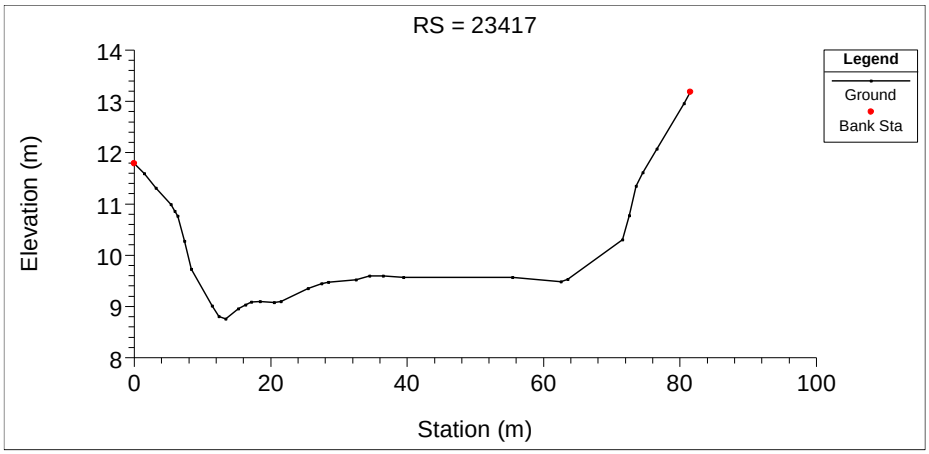

(a) River Station = 23417

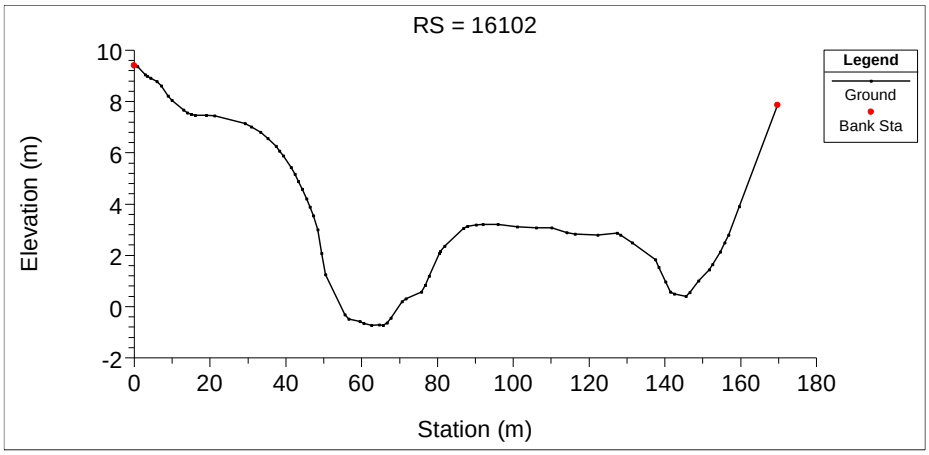

(b) River Station = 16102

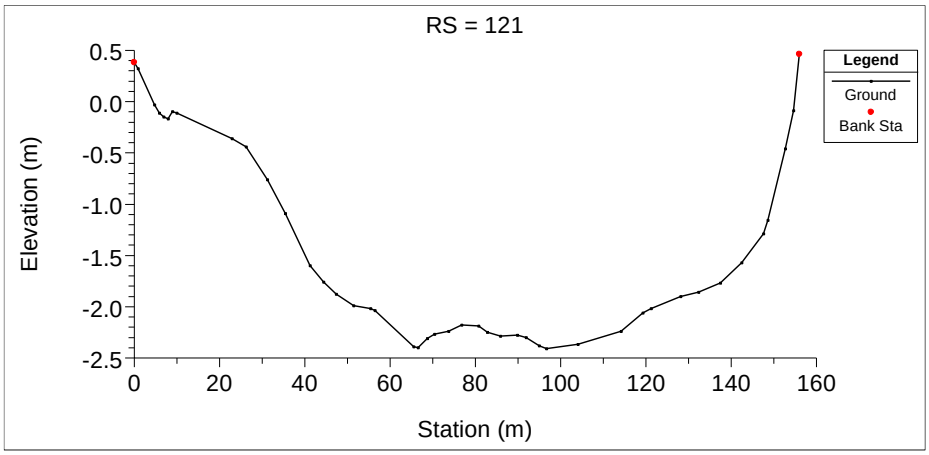

(c) River Station = 121

Figure 4.9. Cross-section examples from Göksu River: (a) River Station = 23417 (b) River Station = 16102 (c) River Station = 121

Manning’s Roughness Coefficient value is another important parameter for the hydraulic models. Manning’s Roughness Coefficient values are selected based on the study of Papaioannou et al. (2018) and Coordination of Information on the Environment (CORINE) Land Cover data. The Land use / land cover and Manning’s roughness coefficient map of the study area is given in Figure 4.10. Manning’s roughness coefficient is selected as 0.06 for the 1D domain.

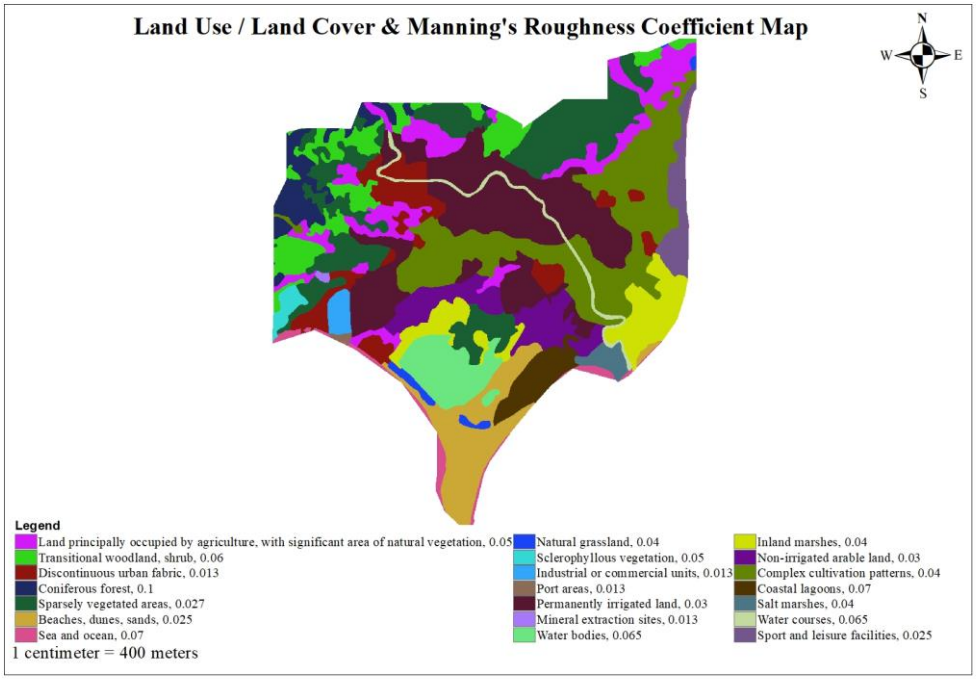

Figure 4.10. Land use / land cover & Manning’s roughness coefficient map

Another important parameter for 1D/2D Coupled Hydraulic Modelling is the cell size of the 2D domain. It should be selected as small as possible to get accurate results. However, small cell sizes may increase computation times significantly. For this reason, computation time should also be considered while selecting the cell size of the 2D domain. The total area of the study region is around 237 km^2. The total number of cells varies with different cell sizes given as in Table 4.8.

Table 4.8 Change of the total number of cells with changing cell size

Cell size (m)	Total number of cells	Cell size (m)	Total number of cells	Cell size (m)	Total number of cells
1	236947616	6	6581879	15	1053101
2	59236904	7	4835666	20	592370
3	26327513	8	3702307	25	379117
4	14809226	9	2925280	30	263276
5	9477905	10	2369477		

Table 4.8 shows that if the cell size is lower than 15 m, the total number of cells is greater than one million. It significantly prolongs the computational time. On the other hand, 15 m cell size is not good enough for urbanized areas to get accurate results. For this reason, two different cell sizes are used in this study. 100 m buffer zone is created around the Göksu River. For this buffer zone and urbanized areas, 6 m cell size is used, while 30 m cell size is used for the remaining part of the study area of the hydraulic model. On the other hand, the computation interval is selected as 1 second.

After the geometry data, the flow data is prepared. Two different boundary conditions should be entered into the model for unsteady flow computations. The upstream boundary condition is entered as the "flow hydrograph," while the downstream boundary condition is selected as the "normal depth." In addition to upstream and downstream boundary conditions, the external boundary condition is entered to represent the seaside. This boundary condition is also selected as the "normal depth." After entering geometry and flow data, the model is run considering flood hydrographs with different return periods.

The validation of the combined 1D/2D hydraulic models is of paramount importance. However, in Türkiye, the validation of hydraulic models is challenging due to limited data availability. The model is validated based on the information obtained at the SHW staff meeting, during which insights were provided regarding a significant

flood event that occurred in Silifke between the 5th and 7th of March 2004. The locations at which floodwater enters and leaves Silifke from the left bank of the Göksu River were shown by the SHW staff (see Figure 4.11) and they are validated using the developed combined 1D/2D hydraulic model. Furthermore, it was stated that the Göksu River can pass a discharge of approximately 800 m^3/s without significant adverse effects. Our model corroborates this assertion, indicating that the river can handle this discharge with minimal amount of overflow. This overflow may be attributed to the inexact dimensions of the bridges. Finally, the inundated neighborhoods of Silifke as a result of the flood event in 2004 are stated in the study of Buldur et al. (2007). These neighborhoods (Gazi, Göksu, Sayağzı, Sarıcalar, Atik, Bucaklı, Çeltikç, Arkum etc.) are also inundated when the developed hydraulic model is run for a similar flood event.

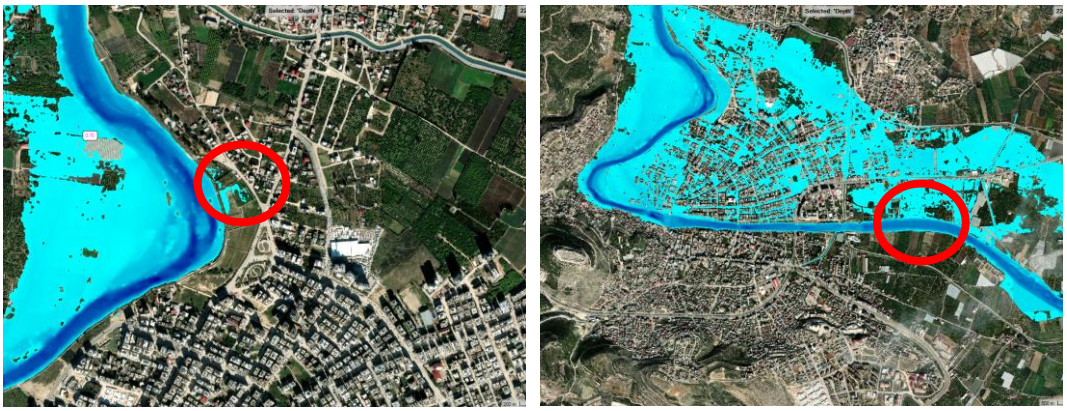

(a) The location where flood water entered the center of Silifke

(b) The location where flood water left the center of Silifke

Figure 4.11. The combined 1D/2D hydraulic model results: (a) The location where flood water entered the city (b) The location where flood water left the city (Basemap source: ArcGIS World Imagery)

4.5 Economic damage calculations

Total economic damage for the study area is calculated using depth-damage curves for Europe given by Huizinga et al. (2017) because depth-damage curves for Türkiye

are not available. On the other hand, the costs of the government's actions are calculated based on the study of Haer et al. (2020), where € is used as the currency unit. Thus, calculated economic damage values bear a certain degree of error; however, relative comparisons of the outcomes of the scenarios evaluated in this study provide useful information.

4.6 Agent-based model

ABM is an approach to model complex social dynamics. Actors in the model are represented as autonomous agents. The rules are assigned to the actors to model their behaviors. ABM is used in many areas, such as biology, social sciences, economics and finance, land use, anthropology, etc. (Hammond R., 2015). ABM in this study is developed using NetLogo, which was created by Uri Wilensky (1999).

NetLogo is used to simulate social and natural phenomena. There are four types of agents in NetLogo: i) patches, ii) turtles, iii) links, and iv) the observer. Patches are stationary and organized in a grid pattern. Turtles can move over the patches, and the turtles can be connected using the links. The observer oversees all activities and handles tasks that the turtles, patches, and links cannot perform independently. In this study, land parcels are the patches, while the public (i.e., people living in the study area) and the government agents are the turtles. In this study, the movement is not assigned to the turtles. Figure 4.12 shows the turtles and patches in this study.

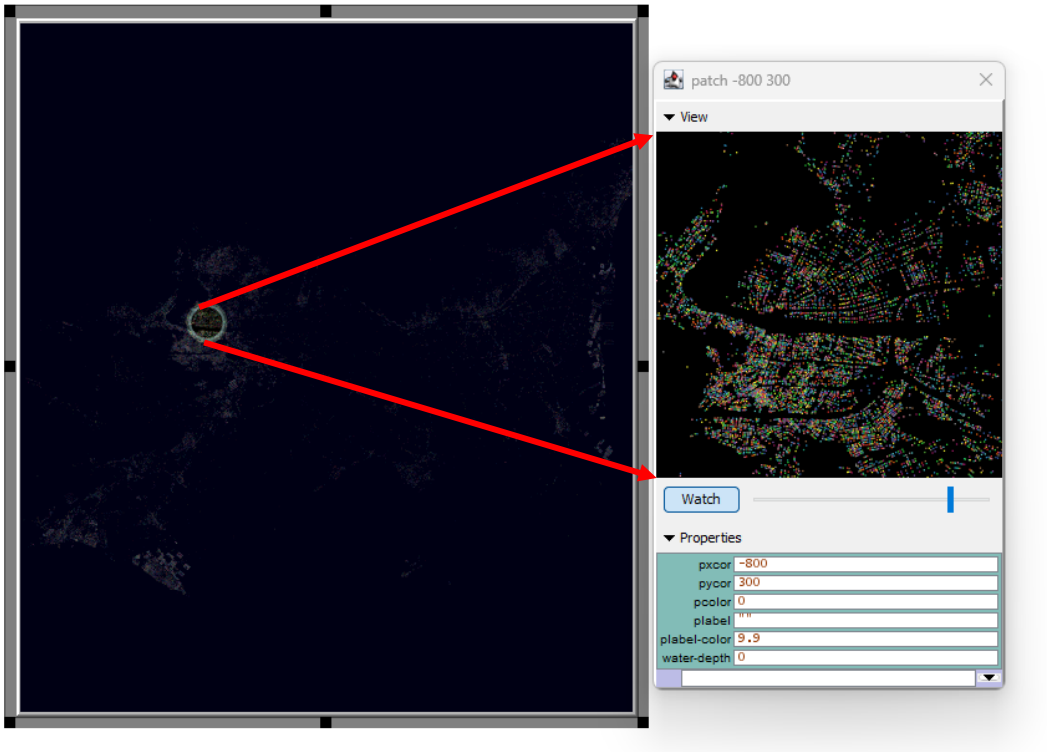

Figure 4.12. Study area at NetLogo's interface

NetLogo consists of three tabs, which are the interface, the info, and the code tabs. The interface tab is used to edit, delete, and create items in the model. The info tab includes the information and explanations about the model, while the code tab stores the code for the model. A piece of the code developed in this study is shown in the code tab in Figure 4.13.

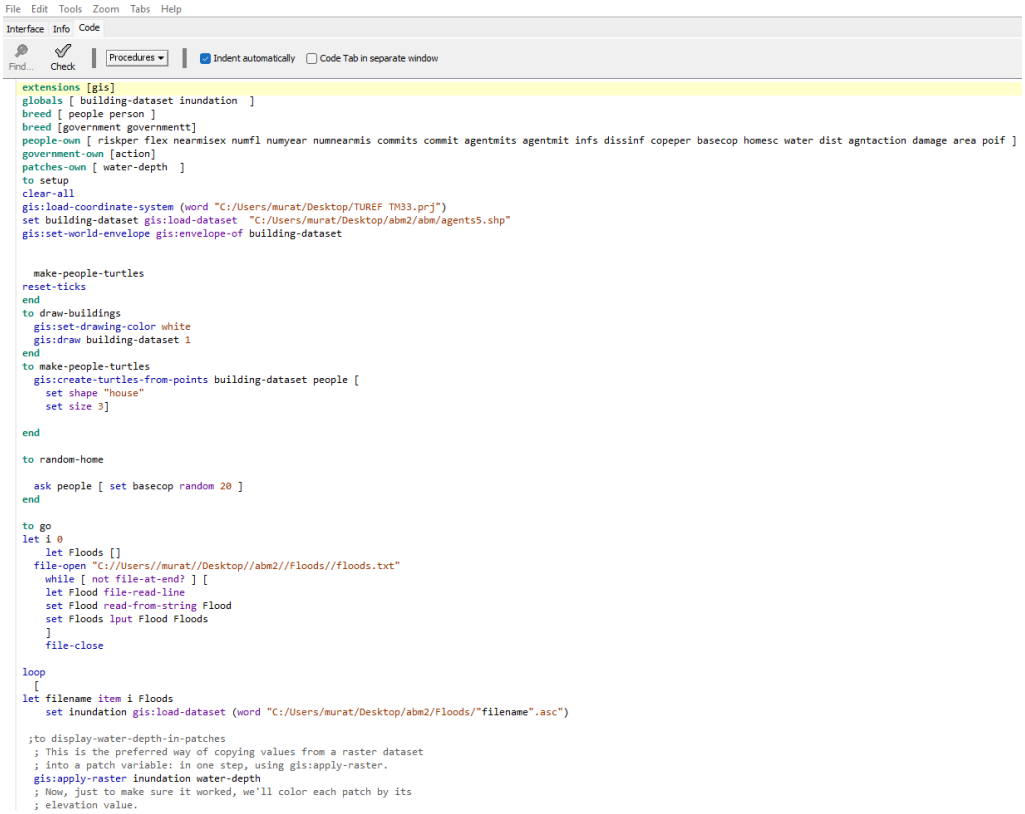

Figure 4.13. A piece of the code developed in this study is shown in the code tab of NetLogo

Two different agents are included in this study. The first one is the public agent, which represents the people who live in the study area, and the second one is the government agent. The public agents' behaviors are functions of the coping and risk perception values. In other words, the public agent decides to take action based on those values. The original equations can be found in the study of Tonn and Guikema (2018). Threshold values are selected as 30 for both risk and coping perceptions (see Figure 4.14). These values are determined based on a sensitivity analysis. The details can be found in Appendix A. On the other hand, two different management strategies are selected for the government agent: proactive management and reactive management. Eleven scenarios are generated to analyze the impacts of the public agent, the government agent, and both. These scenarios and explanations are given in Table 4.9. Sc1 is the base scenario that is used traditionally in FRM studies. Sc2 and Sc3 are the scenarios where only the public agent is considered. In Sc2, coping

perception and risk perception values are calculated based on random values like most of the studies given in the literature (Tonn & Guikema, 2018; Abebe et al., 2019), while in Sc3, these parameters are calculated based on the survey results. Sc4 – Sc7 scenarios include only the government agent. In two of these scenarios, reactive management strategy is implemented, while in the others, proactive management strategy is used. In this study, government actions are defined as taking mitigation measures against a 50-year flood or 100-year flood. The government's action is represented as the construction of a dike that prevents the inundation of a 50-year or a 100-year flood. In scenarios Sc8 - Sc11, both the public and the government agents are considered.

In this study, the simulation period is from 2025 to 2100; and 1-year time step is used. Moreover, 2-, 5-, 10-, 25-, 50-, 100-, and 500-year floods are considered. However, it is unknown if a flood will occur in each year of the simulation and it is also unknown if a flood occurs, what will be its magnitude (i.e., which return period flood event will occur?). Thus, the following approach is used to assign flood events to each year of the simulation period (i.e., 2025-2100): A random number between zero and one is generated for each year for each potential magnitude (i.e., 2-, 5-, 10-, 25-, 50-, 100- and 500-year floods). If the generated number is less than the exceedance probability of the flood event, that event is presumed to happen in that year. If multiple flood events are projected to occur in a year, the flood event with the highest return period is assumed to occur in that year. This will result in one possible realization of flood events in the simulation period (hereafter will be referred to as "Realization"). An example calculation is given in Table 4.10.

To handle the uncertainties arising from the procedure of assigning flood events to the simulation period, 100 different Realizations are generated and used in flood risk analysis. Each scenario is run considering these 100 different Realizations, and economic damage values are calculated for each realization. In addition to the economic damage values, the costs of the actions (for the scenarios with the government agent) are calculated as well, and a cost-benefit analysis is conducted

for each realization and scenario. The flowchart of the ABM is given in Figure 4.14. This flowchart is run once for each realization.

Table 4.9 The scenarios designed to analyze the impacts of the agents on flood risks

Scenario Number	Scenario Name	Agent[1]	Survey[2]	Explanations
Sc1	Base	None	No	No agents
Sc2	PubRand	Public	No	Risk and coping perceptions are randomly assigned to public agent.
Sc3	PubSur	Public	Yes	Risk and coping perceptions are assigned to the public agent according to the survey results.
Sc4	ProGo50	Government	-	The proactive government takes action against a 50-year return period flood event.
Sc5	ProGo100	Government	-	The proactive government takes action against a 100-year return period flood event.
Sc6	ReGo50	Government	-	The reactive government agent takes action to mitigate a 50-year return period flood event after a 50-, 100- or 500-year return period flood event is experienced.
Sc7	ReGo100	Government	-	The reactive government agent takes action to mitigate a 100-year return period flood event after a 100- or 500-year return period flood event is experienced.
Sc8	PubSur – ReGo50	Public & Government	Yes	PubSur and ReGo50 together.
Sc9	PubSur – ReGo100	Public & Government	Yes	PubSur and ReGo100 together.
Sc10	PubSur – ProGo50	Public & Government	Yes	PubSur and ProGo50 together.
Sc11	PubSur – ProGo100	Public & Government	Yes	PubSur and ProGo100 together.

[1] The government, the public, or both are used as agents in this study.
[2] When survey results are used in assigning risk and coping perceptions to people, “Yes” is used in this column; when risk and coping perceptions are randomly assigned to people, “No” is used in this column; if public agent is not considered, “-“ is used

Table 4.10 An example realization

	Flood events							Selected Flood Event
	2	5	10	25	50	100	500	
2025	0.81	0.15	0.96	0.40	0.02	0.47	0.81	50
2026	0.59	0.49	0.29	0.39	0.94	0.85	0.59	-
.								
.								
2100	0.28	0.24	0.57	1.00	0.64	0.77	0.001	500

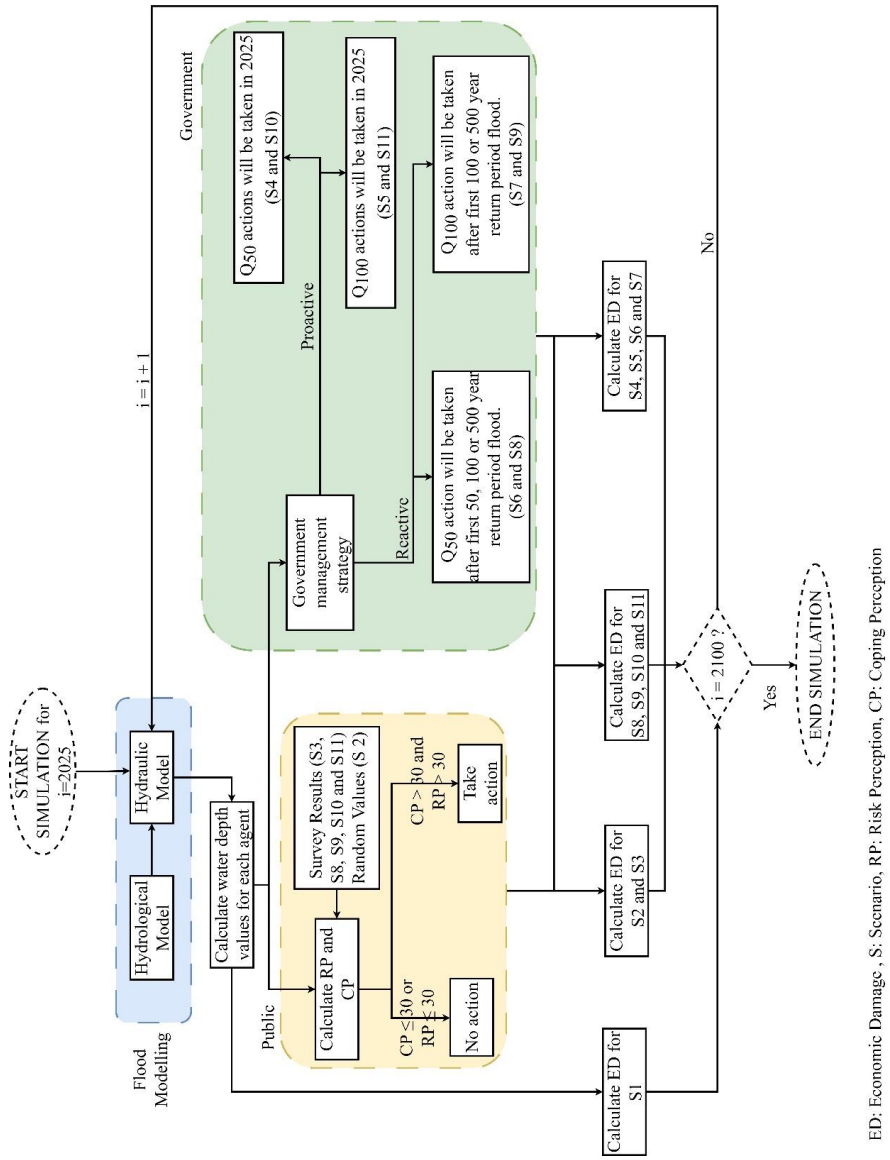

Figure 4.14. The flowchart of the ABM

4.7 Survey

A survey is prepared in order to understand people's perception of flood hazards. It is designed to collect information about the risk perception and coping perception of the people in the study area about flood risks. It is conducted by Infakto Research Workshop. It is really important to conduct surveys and use the results to reflect the people's real behaviors in the ABM. The questions are selected based on the literature review. The survey consists of open-ended questions, multiple choice questions and yes/no type questions. Some questions are asked to collect information on the demography of the people in the study area while the others are asked to be used in the analysis of the risk perception and the coping perception of the people. The questions are asked to 180 participants and they are selected randomly from the entire study area to reduce bias. The answers are analyzed and distributed to whole study area. Survey questions and what kind of analysis that they are used for are given in Table 4.11 and the participants of the survey are shown in Figure 4.15.

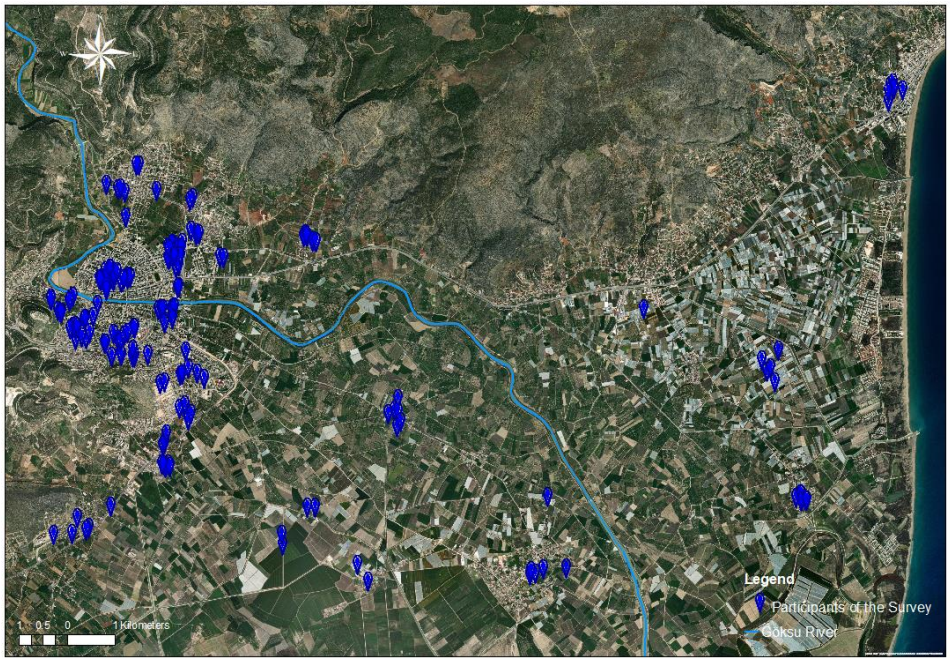

Figure 4.15. Participants of the survey (Basemap source: Esri, Maxar, Earthstar Geographics, and the GIS User Community)

Table 4.11 Survey questions

Question	Analysis Type
Age	D
Gender	D
Education level	D
Household income (monthly)	D
Owner / renter / lodgment / parent's home	D
Number of households	D
How many of the household need care?	D
Residence / commercial	D
Employment status	D
How many floods have you experienced in this house in previous years? *	RP
How many near-miss flood events have you experienced in this house in previous years? *	RP
Have one of the governmental institutions taken measures against floods? If yes, what type of mitigation measures were implemented? *	RP
Have you previously taken measures against floods? *	RP, CP
Do you believe that you are well-informed about flood hazard in Silifke by the authorities? *	RP, CP
How many of your neighbors in Silifke have experienced flood in previous years?	RP
How many of your neighbors in Silifke have experienced near-miss flood event in previous years?	RP
How many of your neighbors in Silifke have taken measures against floods?	CP

The questions with * are used to calculate risk perception and coping perception values in this study, D: Demographic, RP: Risk Perception, CP: Coping Perception

The equation of risk and coping perceptions can be found in Appendix B.

CHAPTER 5

RESULTS AND DISCUSSIONS

In this section, the results of RCM selection, LULC analysis, nonstationarity analysis of annual maximum flow series (AMFS), hydrological model, combined 1D/2D hydraulic model, and ABM are given. Furthermore, the limitations of the study are summarized at the end of this chapter.

5.1 Selection of the best regional climate model

To select the best RCM Corr (R^2), $RMSE$, $PBIAS$, and NSE are used. The calibrated hydrological model is run using the outputs of RCM for the calibration, validation, and test periods. The hydrological model is calibrated (01.10.1965 – 01.10.1978) and validated (01.08.1981 – 01.08.1986) considering the natural response of the basin. After the calibration and validation, the model is tested (31.08.2016 – 31.08.2020) by including the major hydraulic structures. The performances of the original outputs and the sorted outputs are evaluated. The statistical measures calculated for the daily discharge values are given in Table 5.1, Table 5.2, and Table 5.3 for the calibration, validation, and test periods. The best RCMs for each period are shown with bold characters.

Table 5.1 Calculated statistical measures for the calibration period

	Calibration - Original									
	Corr	Rank	RMSE	Rank	PBIAS	Rank	NSE	Rank	Total	Final Rank
M1	0.52	13	103.36	4	-15.13	13	0.00	14	26	14
M2	0.26	17	148.63	1	-37.87	4	-1.07	17	7	17
M3	0.66	9	81.95	13	20.88	11	0.37	5	46	5
M4	0.66	8	81.64	14	22.04	9	0.37	4	47	4
M5	0.59	12	93.47	6	0.12	17	0.18	12	35	9
M6	0.65	10	81.56	15	20.39	12	0.38	3	50	3

Table 5.1 (cont'd)

Calibration - Original										
	Corr	Rank	RMSE	Rank	PBIAS	Rank	NSE	Rank	Total	Final Rank
M7	0.68	6	81.21	16	23.44	7	0.38	2	51	2
M8	0.33	16	114.46	2	-2.27	16	-0.23	16	22	16
M9	0.73	1	88.98	7	38.43	1	0.26	9	34	10
M10	0.71	4	82.63	11	29.51	5	0.36	7	41	7
M11	0.51	14	106.00	3	-11.82	14	-0.05	15	24	15
M12	0.48	15	94.65	5	7.60	15	0.16	13	28	13
M13	0.65	11	82.87	10	21.49	10	0.36	8	37	8
M14	0.73	1	88.98	7	38.43	1	0.26	9	34	10
M15	0.73	1	88.98	7	38.43	1	0.26	9	34	10
M16	0.69	5	82.20	12	24.81	6	0.37	6	43	6
M17	**0.67**	**7**	**81.12**	**17**	**23.20**	**8**	**0.38**	**1**	**53**	**1**
Calibration - Sorted										
	Corr	Rank	RMSE	Rank	PBIAS	Rank	NSE	Rank	Total	Final Rank
M1	0.97	10	31.15	15	-15.13	13	0.91	3	51	4
M2	0.99	3	52.92	9	-37.88	4	0.74	9	37	9
M3	0.97	9	55.39	7	20.88	11	0.71	11	34	10
M4	0.98	6	50.01	11	22.03	9	0.77	7	43	7
M5	**0.99**	**1**	**10.61**	**17**	**0.12**	**17**	**0.99**	**1**	**68**	**1**
M6	0.99	5	45.81	12	20.39	12	0.80	6	49	5
M7	0.98	8	53.65	8	23.44	7	0.73	10	33	11
M8	0.95	14	31.52	13	-2.29	16	0.91	5	46	6
M9	0.94	15	76.94	1	38.43	1	0.44	15	8	15
M10	0.97	12	64.09	4	29.51	5	0.61	14	19	14
M11	0.99	2	19.67	16	-11.85	14	0.96	2	62	2
M12	0.99	4	31.37	14	7.60	15	0.91	4	57	3
M13	0.96	13	56.45	6	21.48	10	0.70	12	27	12
M14	0.94	15	76.94	1	38.43	1	0.44	15	8	15
M15	0.94	15	76.94	1	38.43	1	0.44	15	8	15
M16	0.97	11	60.61	5	24.81	6	0.66	13	23	13
M17	0.98	7	52.39	10	23.20	8	0.74	8	39	8

Table 5.2 Calculated statistical measures for the validation period

Validation - Original										
	Corr	Rank	RMSE	Rank	PBIAS	Rank	NSE	Rank	Total	Final Rank
M1	0.43	13	111.40	4	-10.25	15	-0.06	14	28	13
M2	0.23	16	144.22	1	-26.36	11	-0.77	17	15	17
M3	0.56	9	95.49	13	27.67	8	0.59	1	47	5
M4	**0.56**	**10**	**94.62**	**17**	**24.25**	**12**	**0.24**	**2**	**53**	**1**
M5	0.50	12	101.87	9	10.67	14	0.12	9	38	7
M6	0.50	11	99.20	10	26.72	10	0.16	8	37	9
M7	0.58	5	94.63	16	28.51	6	0.24	3	50	2
M8	0.22	17	129.07	2	-2.39	16	-0.42	16	21	16
M9	0.60	1	102.23	6	41.71	1	0.11	10	32	10
M10	0.58	6	95.96	12	30.27	4	0.21	6	40	6
M11	0.39	15	115.87	3	0.59	17	-0.14	15	26	15
M12	0.41	14	104.73	5	17.44	13	0.06	13	27	14
M13	0.57	8	94.90	15	26.84	9	0.23	4	48	3
M14	0.60	1	102.23	6	41.71	1	0.11	10	32	10
M15	0.60	1	102.23	6	41.71	1	0.11	10	32	10
M16	0.59	4	94.97	14	28.24	7	0.23	5	48	3
M17	0.57	7	96.13	11	29.79	5	0.21	7	38	7
Validation - Sorted										
	Corr	Rank	RMSE	Rank	PBIAS	Rank	NSE	Rank	Total	Final Rank
M1	0.97	5	31.19	14	-10.25	15	0.92	4	56	4
M2	0.99	1	36.48	13	-26.36	11	0.89	5	54	5
M3	0.95	9	65.75	7	27.67	8	0.81	6	36	8
M4	0.96	8	57.63	11	1827.00	12	0.72	8	43	7
M5	0.98	3	28.23	15	10.67	14	0.93	3	59	3
M6	0.95	11	61.37	10	26.72	10	0.68	9	36	8
M7	0.96	6	63.57	9	28.51	6	0.66	10	35	10
M8	**0.99**	**2**	**19.69**	**17**	**-2.39**	**16**	**0.97**	**1**	**66**	**1**
M9	0.90	15	87.21	1	41.71	1	0.35	15	8	15
M10	0.94	12	70.97	6	30.27	4	0.57	12	22	12
M11	0.97	4	25.68	16	0.59	17	0.94	2	63	2
M12	0.96	7	48.25	12	17.44	13	0.80	7	47	6
M13	0.95	10	63.90	8	26.84	9	0.65	11	32	11
M14	0.90	15	87.21	1	41.71	1	0.35	15	8	15
M15	0.90	15	87.21	1	41.71	1	0.35	15	8	15
M16	0.92	14	73.33	4	28.24	7	0.54	14	19	14
M17	0.93	13	71.86	5	29.79	5	0.56	13	20	13

Table 5.3 Calculated statistical measures for the test period

Test - Original										
	Corr	Rank	RMSE	Rank	PBIAS	Rank	NSE	Rank	Total	Final Rank
M1	0.48	7	61.63	9	12.67	10	0.02	11	37	10
M2	0.12	17	124.53	1	-41.98	1	-3.02	17	4	17
M3	0.47	8	59.36	12	14.91	6	0.09	6	40	8
M4	0.49	4	59.12	14	18.47	3	0.09	5	44	6
M5	0.50	1	61.35	10	5.77	15	0.03	10	50	2
M6	0.43	11	62.21	8	11.54	11	0.00	12	32	12
M7	0.46	10	60.00	11	13.98	8	0.07	7	38	9
M8	0.27	15	81.65	4	-8.50	12	-0.73	15	22	15
M9	0.35	13	73.26	5	-6.34	14	-0.39	13	29	13
M10	0.49	5	58.80	15	16.79	5	0.10	4	47	4
M11	0.23	16	101.44	2	-13.80	9	-1.49	16	15	16
M12	0.42	12	62.51	6	8.33	13	0.05	9	34	11
M13	0.47	9	59.30	13	14.11	7	0.15	3	44	6
M14	0.49	6	62.51	7	3.05	16	0.05	8	45	5
M15	0.31	14	84.09	3	-1.90	17	-0.71	14	28	14
M16	**0.50**	**3**	**58.32**	**17**	**16.95**	**4**	**0.18**	**1**	**53**	**1**
M17	0.50	2	58.79	16	18.79	2	0.16	2	50	2
Test - Sorted										
	Corr	Rank	RMSE	Rank	PBIAS	Rank	NSE	Rank	Total	Final Rank
M1	0.99	6	17.21	13	12.67	10	0.92	5	48	5
M2	0.99	3	63.09	1	-41.98	1	-0.03	17	18	14
M3	0.98	11	25.04	8	14.91	6	0.84	10	29	11
M4	0.97	15	29.23	4	18.47	3	0.78	14	14	16
M5	0.99	1	8.74	16	5.77	15	0.98	2	64	2
M6	0.99	5	18.48	11	11.54	11	0.91	7	46	6
M7	0.98	10	23.51	10	13.98	8	0.86	8	36	8
M8	0.98	8	17.46	12	-8.50	12	0.92	6	46	6
M9	0.98	7	13.52	15	-6.34	14	0.95	3	55	3
M10	0.97	13	27.48	7	16.79	5	0.80	11	24	12
M11	0.97	12	39.74	2	-13.80	9	0.59	16	19	13
M12	0.99	4	15.54	14	8.33	13	0.94	4	55	3
M13	0.98	9	23.88	9	14.11	7	0.85	9	34	9
M14	0.99	2	7.77	17	3.05	16	0.98	1	66	1
M15	0.95	17	27.70	6	-1.90	17	0.80	12	30	10
M16	0.97	14	27.92	5	16.95	4	0.80	13	18	14
M17	0.96	16	30.04	3	18.79	2	0.77	15	10	17

The ranks of RCMs for each period are summed and given in Table 5.4. The lower the value means the better the RCM. It can be seen that M5 is the best RCM, and for the CC analysis, the outputs of M5 are used.

Table 5.4 Final scores of RCMs

RCM	Final Score	RCM	Final Score	RCM	Final Score
M1	50	M7	42	M13	49
M2	79	M8	60	M14	56
M3	47	M9	66	M15	74
M4	41	M10	55	M16	51
M5	**24**	M11	63	M17	48
M6	43	M12	50		

5.2 Land use / land cover change analysis results

The satellite images of 1985, 2004, 2013, 2017, and 2021 are classified, and LULC maps are generated. The generated maps are given in Figure 5.1. LULC analysis is conducted considering the years that have clear satellite and Google Earth images.

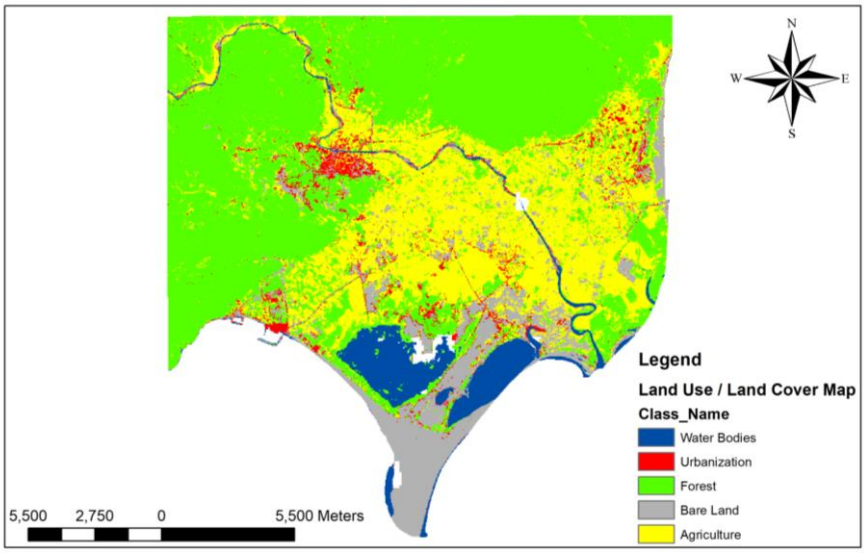

(a) LULC Map of 1985

Figure 5.1. LULC Maps of the study area: (a) LULC map of 1985 (b) LULC map of 2004 (c) LULC map of 2013 (d) LULC map of 2017 (e) LULC map of 2021

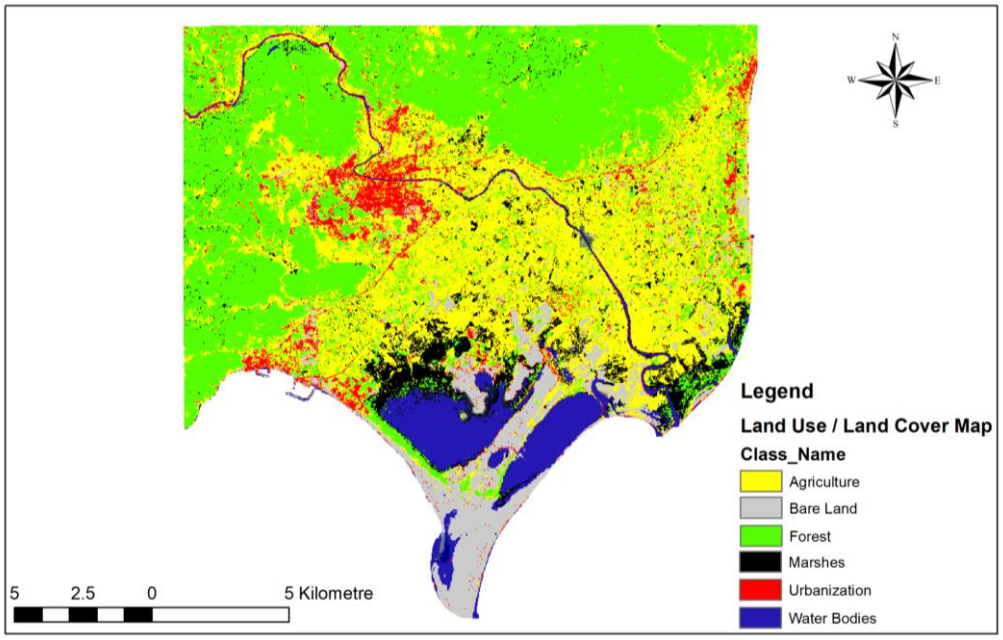

(b) LULC Map of 2004

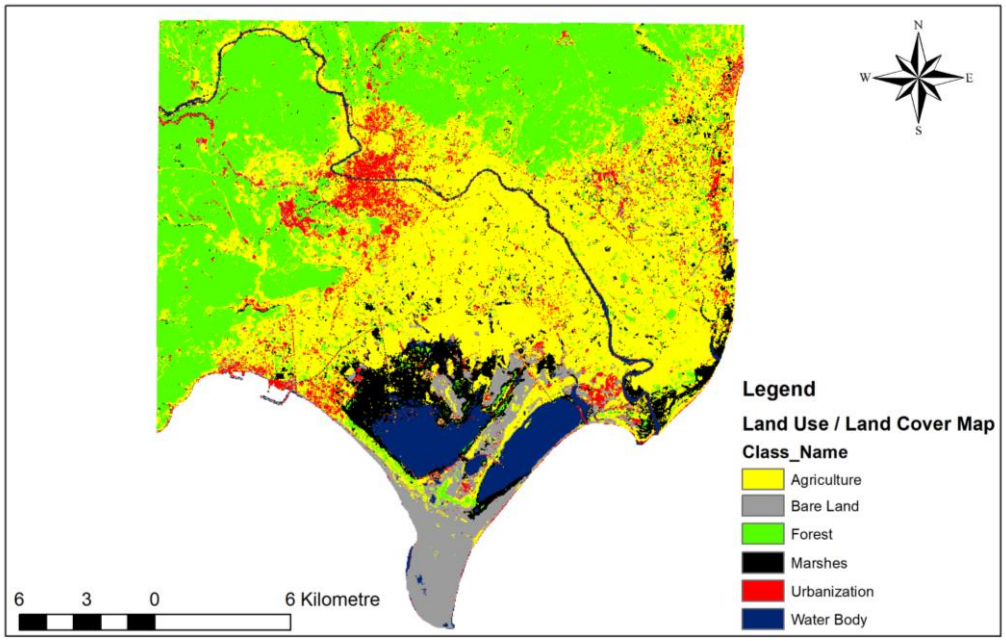

(c) LULC Map of 2013

Figure 5.1. (cont'd)

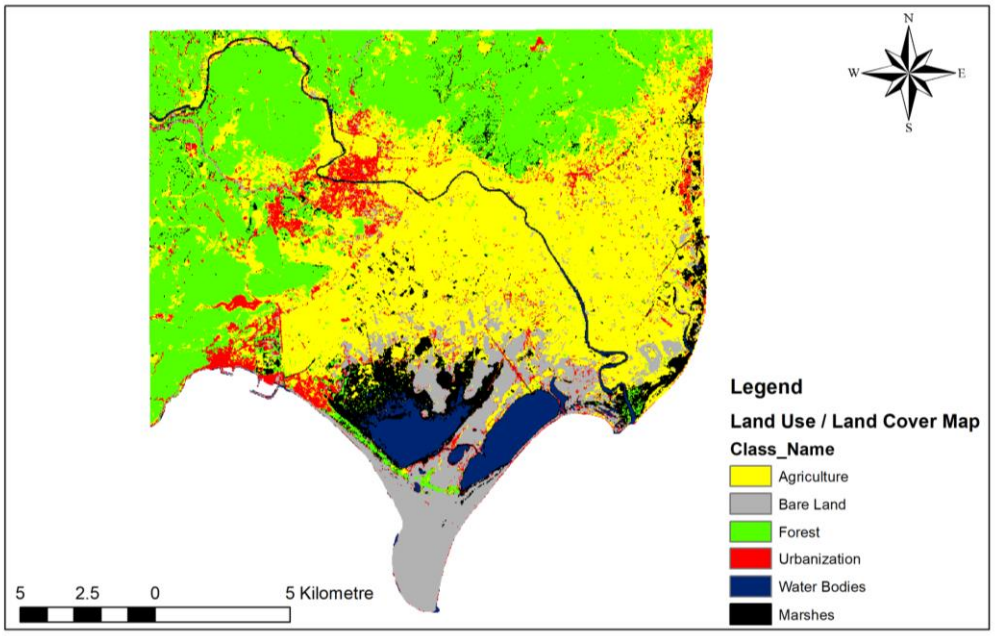

(d) LULC Map of 2017

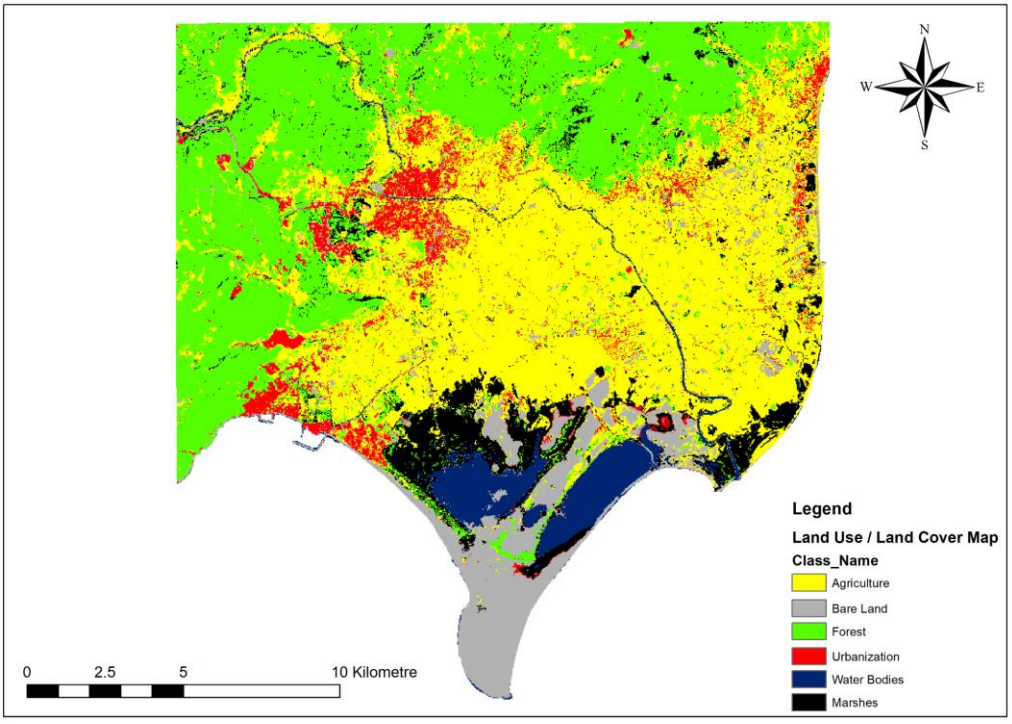

(e) LULC Map of 2021

Figure 5.1. (cont'd)

The confusion matrices are calculated to determine if the classification is satisfactory. The confusion matrix for 1985 could not be calculated because the classified image could not be validated due to the lack of the Google Earth image of 1985. For this reason, the results of the 1985 LULC map are not used in this study. According to Landis & Koch (1977), the strength of agreement of the calculated KC is "substantial" for 2004 and 2013 (Table 5.5 and Table 5.6), while it is "almost perfect" for 2017 and 2021 (Table 5.7 and Table 5.8). Furthermore, the calculated OA values are greater than 0.80 for all years. According to the confusion matrices, the classifications of forests and water bodies are the most accurate. The classification of marshes is not very accurate, but it is within the desired ranges. In this study, the aim is to detect the urbanized areas. Therefore, the most critical objective is to correctly identify the urbanized areas. According to the confusion matrices, the classification of the urbanized areas is satisfactory (Landis & Koch, 1977).

Table 5.5 Confusion matrix of LULC map for 2004

LULC Class	F	AL	UrA	WB	BL	M	Total	UA	KC
F	163	24	0	0	1	7	195	0.84	
AL	10	155	1	0	5	3	174	0.89	
UrA	1	0	19	0	4	0	24	0.79	
WB	0	0	0	31	0	0	31	1.00	
BL	0	7	2	0	32	0	41	0.78	
M	2	8	0	0	0	17	27	0.63	
Total	176	194	22	31	42	27	492		
PA	0.93	0.80	0.86	1.00	0.76	0.63		$\boldsymbol{OA}$ **= 0.85**	
KC									**0.78**

F: Forest, AL: Agricultural Land, UrA: Urbanized Area, WB: Water Bodies, BL: Bare Land, M: Marshes, UA: User's Accuracy, PA: Producer's Accuracy, OA: Overall Accuracy, KC: Kappa Coefficient

Table 5.6 Confusion matrix of LULC map for 2013

LULC Class	F	BL	AL	UrA	M	WB	Total	UA	KC
F	145	1	16	0	3	0	165	0.88	
AL	11	11	165	18	5	1	211	0.78	
UrA	0	5	4	17	0	0	26	0.65	
WB	0	0	0	1	2	22	25	0.88	
BL	1	32	1	0	1	0	35	0.91	
M	5	2	5	1	24	0	37	0.65	
Total	162	51	191	37	35	23	499		
PA	0.90	0.63	0.86	0.46	0.69	0.96		$\boldsymbol{OA}$ **= 0.81**	
KC									**0.74**

Table 5.7 Confusion matrix of LULC map for 2017

LULC Class	AL	UrA	BL	F	WB	M	Total	UA	KC
F	7	0	0	154	0	0	161	0.96	
AL	183	4	6	4	0	1	198	0.92	
UrA	6	41	5	0	1	0	53	0.77	
WB	0	0	0	0	21	0	21	1.00	
BL	6	2	36	2	0	0	46	0.78	
M	5	1	1	2	3	27	39	0.69	
Total	207	48	48	162	25	28	518		
PA	0.88	0.85	0.75	0.95	0.84	0.96		$\boldsymbol{OA}$ **= 0.89**	
KC									**0.85**

Table 5.8 Confusion matrix of LULC map for 2021

LULC Class	AL	UrA	BL	F	WB	M	Total	UA	KC
F	17	2	0	145	0	2	166	0.87	
AL	187	3	6	2	1	3	202	0.93	
UrA	2	23	1	1	0	0	27	0.85	
WB	0	0	0	0	21	0	21	1.00	
BL	2	2	42	0	0	0	46	0.91	
M	3	0	0	10	0	25	38	0.66	
Total	211	30	49	158	22	30	500		
PA	0.89	0.77	0.86	0.92	0.95	0.83		$\boldsymbol{OA}$ **= 0.89**	
KC									**0.84**

The change in LULC classes is shown in Table 5.9. As can be seen from this table, the urbanized area has increased from 2004 to 2021 and, based on the general trend, this is expected to continue in the future.

Table 5.9 Percent change of LULC classes

	Percent change in the range		
	2004-2013	2013-2017	2017-2021
Forest	-16.23	0.30	-0.21
Agricultural Land	24.86	-7.53	-0.32
Urbanized Area	12.29	8.56	10.61
Water Bodies	-16.80	-21.03	-0.71
Bare Land	-19.14	51.44	-8.37
Marshes	6.01	7.86	21.46

The results of the previous studies conducted in the vicinity of Silifke and this study area are given in Figure 5.2. The graph shows the urbanized area increased in the vicinity of Silifke and the results of this study for Silifke. It can be seen that the increase for Silifke is approximately 32%. If the results of the 1985 LULC Map are considered, the increase in urbanized area for Silifke is almost 100%.

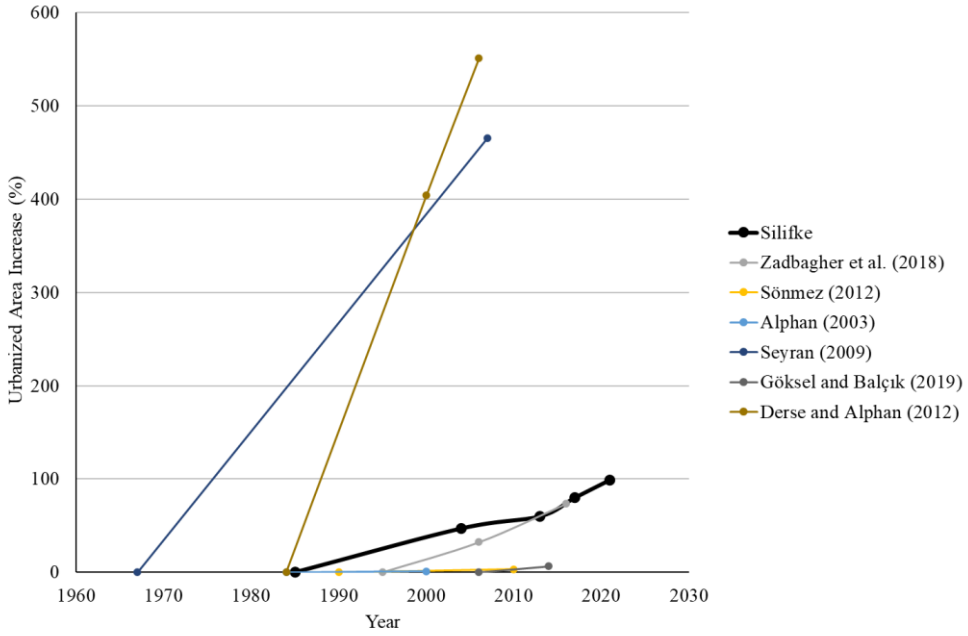

Figure 5.2. Urbanized area increases in the vicinity of Silifke

Based on these results, future scenarios are generated, and these scenarios and the results are given under Chapter 5.4.

5.3 Hydrological model results

Table 5.10 presents the performances of the statistical parameters, while Figure 5.3 and Figure 5.4 show the simulated and observed hydrographs during the calibration and validation periods, respectively. Table 5.10 shows that most of the measures have satisfactory performance. Notably, while the date/time of peak discharge exhibits poor performance, the overall hydrological model performance remains satisfactory.

Table 5.10 Performance of the hydrological model

Measure	Performance Evaluation Criteria			Calibration Period (1965 - 1978)	Validation Period (1981 - 1986)
	Very Good	Good	Satisfactory		
RSR	[0.0,0.5]	(0.5,0.6]	(0.6,0.7]	0.53	0.54
NSE	(0.8,1.0]	(0.7,0.8]	(0.5,0.7]	0.72	0.71
$PBIAS$	(-5,5)	(-10,-5] & [5,10)	(-15,-10] & [10,15)	-3.26	1.04
R^2	(0.85,1.00]	(0.75,0.85]	(0.60,0.75]	0.74	0.72
Peak Discharge (m^3/s)	± 10% of observed value			*1074 – 782	*1090 - 981
Discharge Volume (mm)	± 10% of observed value			*5105.36 – 4939.39	*1835.47 – 1854.52
Date / Time of Peak Discharge	± 12 hours range of observed value			*22.01.1969 – 14.03.1968	*28.12.1981 – 10.11.1985

* The first value represents the observed value while the second one represents the calculated value

Color code that shows the performance evaluation criteria

Very Good	Good	Satisfactory	Not Satisfactory

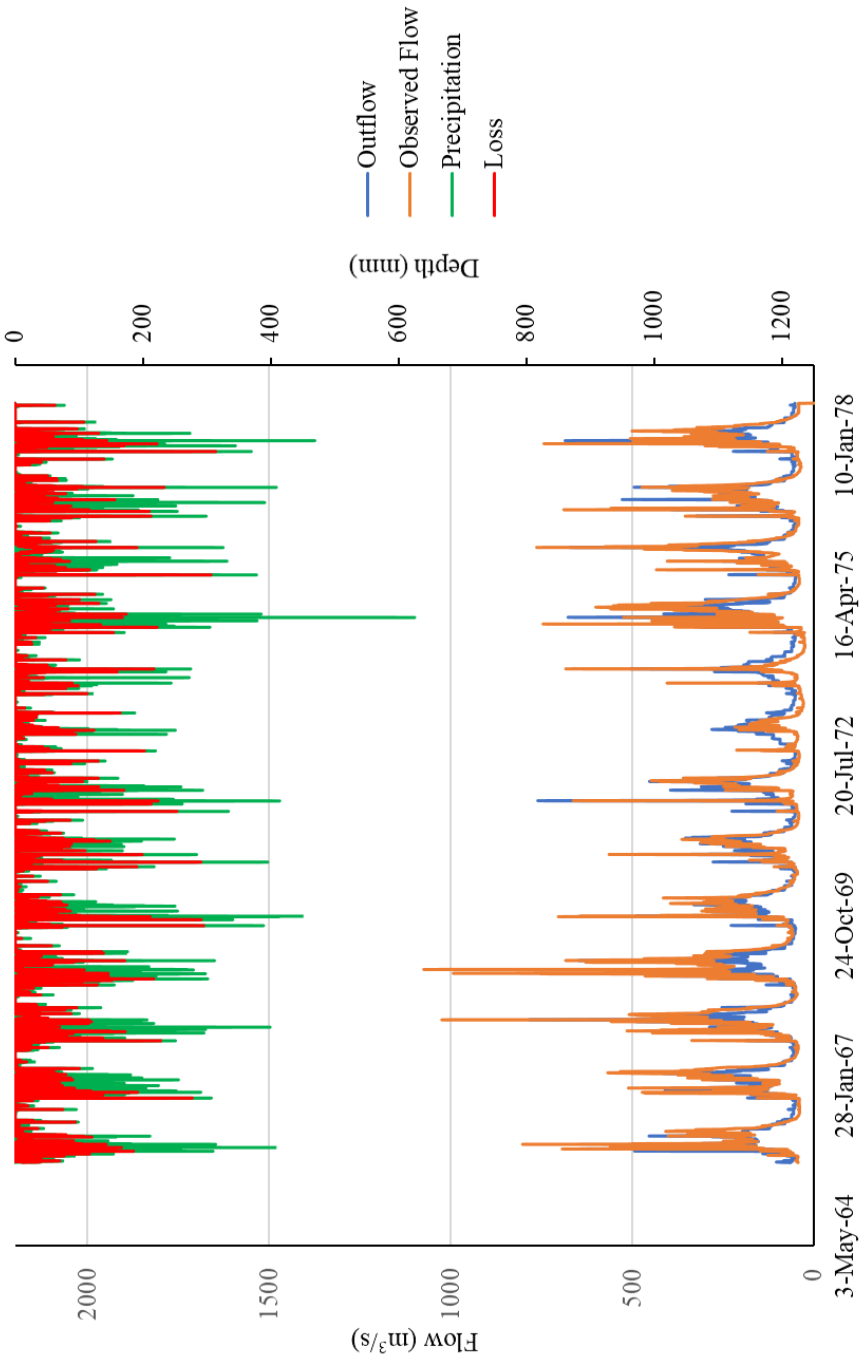

Figure 5.3. Performance of the hydrological model for the calibration period

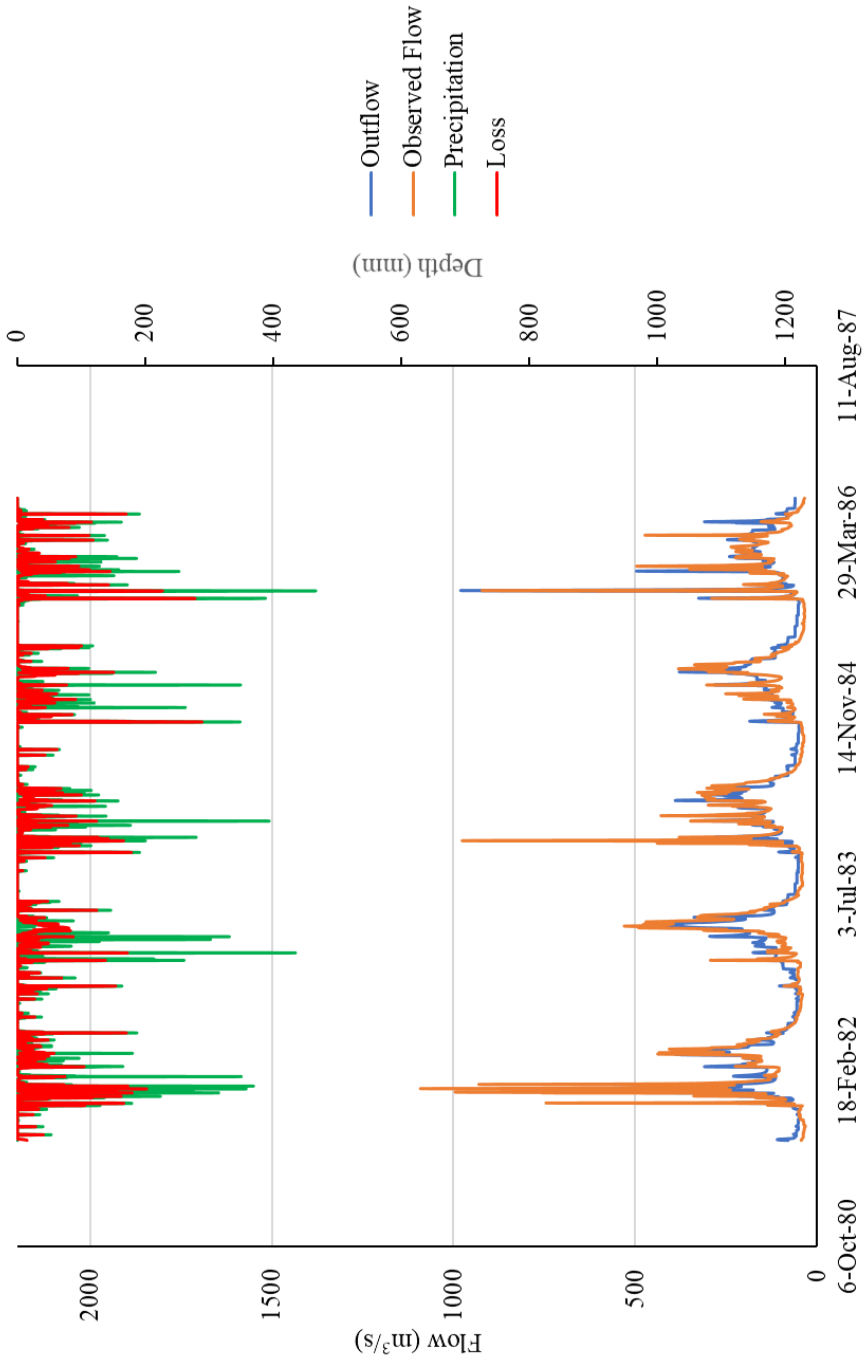

Figure 5.4. Performance of the hydrological model for the validation period

The simulated and observed hydrographs for the test period are given in Figure 5.5. Furthermore, the performances of the statistical measures are given in Table 5.11. Table 5.11 demonstrates that the performances of the statistical parameters are

satisfactory. Thus, this hydrological model is used in determining the peak discharges that input to the hydraulic model.

Table 5.11 Performance of the hydrological model for the test period

Measure	Performance Evaluation Criteria			Test Period (2016 - 2020)
	Very Good	Good	Satisfactory	
RSR	[0.0,0.5]	(0.5,0.6]	(0.6,0.7]	0.52
NSE	(0.8,1.0]	(0.7,0.8]	(0.5,0.7]	0.73
$PBIAS$	(-5,5)	(-10,-5] & [5,10)	(-15,-10] & [10,15)	-12.01
R^2	(0.85,1.00]	(0.75,0.85]	(0.60,0.75]	0.78
Peak Discharge (m^3/s)	± 10% of observed value			*535 – 557.7
Discharge Volume (mm)	± 10% of observed value			*1267.99 – 1115.90
Date / Time of Peak Discharge	± 12 hours range of observed value			*13.03.2017 – 13.03.2017

* The first value represents the observed value while the second one represents the calculated value

Color code that shows the performance evaluation criteria

Very Good	Good	Satisfactory	Not Satisfactory

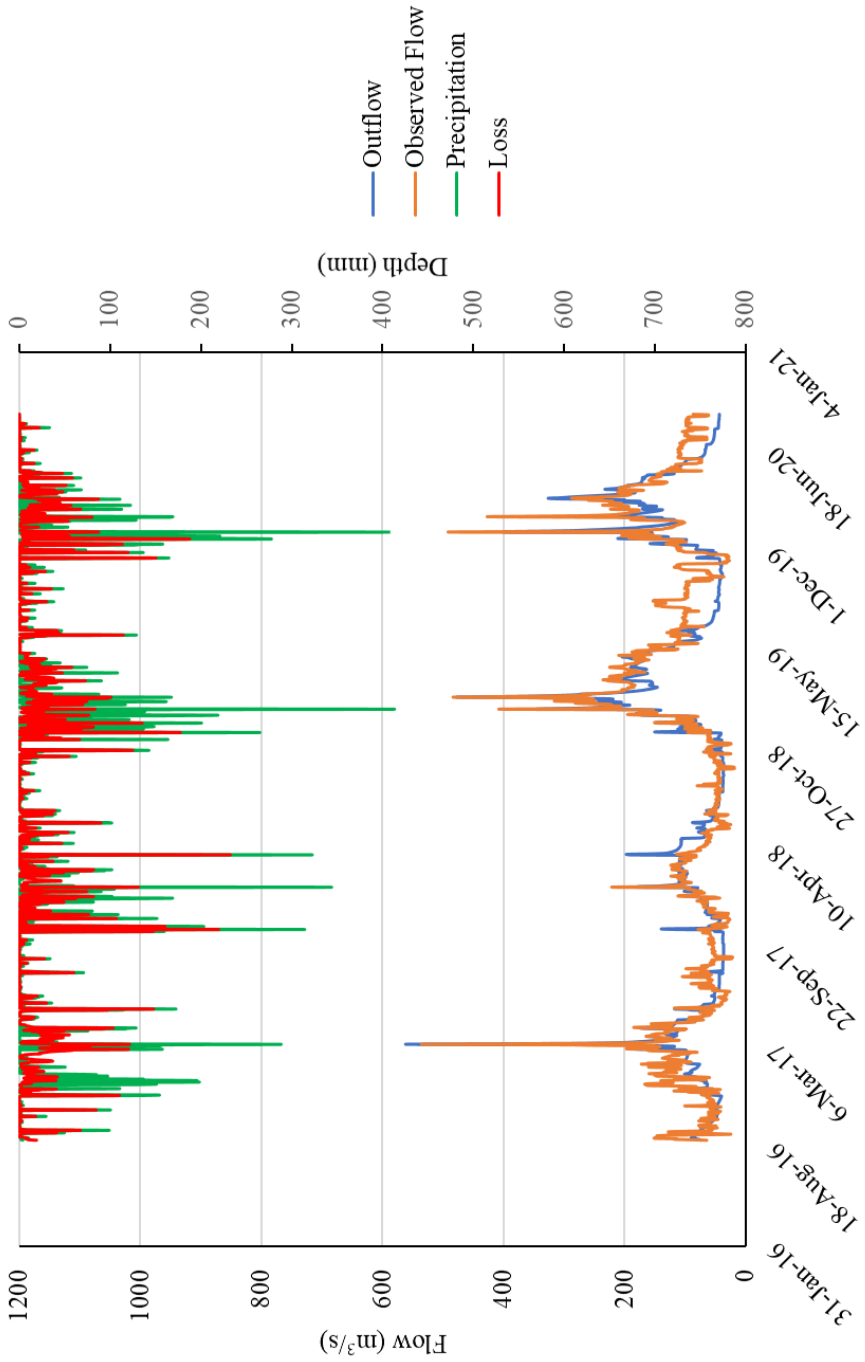

Figure 5.5. Performance of the hydrological model for the test period

5.3.1 Determination of peak discharges and hydrographs with stationarity assumption

Peak discharges are calculated considering two cases: i) the annual maximum discharge time series is stationary, and ii) the annual maximum discharge time series is nonstationary. Here, the peak discharges for different return periods are determined with the stationarity assumption.

The probability distribution that fits the best to the data is determined before calculating peak discharges for different return period events. The annual maximum discharge series of E17A014 SG is tested for different distributions. The Chi-Square Test is used to evaluate the suitability of different probability distributions for annual maximum discharge time series. the Hydrologic Engineering Center's Statistical Software Package (HEC-SSP) (Hydrologic Engineering Center, 2023) is used to calculate the parameters of various probability distributions and Chi-Square Test values. Chi-Square Test results of different distributions are provided in Table 5.12. The calculated values are compared with the critical Chi-square value at a significance level of 5%. The best-fitted probability distribution for the annual maximum discharge series of E17A014 is the Gamma distribution with Maximum Likelihood Estimation (MLE) (see Table 5.12). Thus, peak discharges of different return periods are calculated using the Gamma distribution. Peak discharge values are calculated using the Gamma Distribution. Calculated peak discharge values for various return periods are given in Table 5.13.

Table 5.12 Chi-square test results for annual maximum discharge series

Probability Distribution	Chi-square score
Gamma	3.038
GEV	4.170
Gumbel	4.170
Logistic	5.302
Normal	6.811
Generalized Logistic (GLO)	9.075
Log-normal	12.472

Table 5.13 Calculated peak discharge values for E17A014 SG

Return Period	Peak Discharge (m^3/s)
2	598.0
5	908.4
10	1108.6
25	1355.4
50	1535.1
100	1711.6
500	2116.3

Flow hydrographs are required for unsteady flow analysis, and they are generated using the Snyder Unit Hydrograph Model (Snyder, 1938). Basic concepts and equations are given in the following paragraphs.

In this method, as explained in the study of Snyder (1938); the basin lag, t_p, peak discharge per unit area, q_p, and total time are selected as the critical characteristics of a unit hydrograph. Equation 5-1 is used to calculate unit hydrograph lag:

$$t_p = C \times C_t \times (L \times L_c)^{0.3} \quad (5\text{-}1)$$

where C is a conversion constant (0.75 for SI), C_t is basin coefficient, L is the length of the main stream from SG to the divide and L_c is the length of the main stream from SG to the point nearest basin centroid. Rainfall duration, t_r, is related to the basin lag, t_p :

$$t_r = \frac{t_p}{5.5} \quad (5\text{-}2)$$

On the other hand, adjusted lag time, t_{PR}, can be calculated using Equation 5-3:

$$t_{PR} = t_P + 0.25 \times (t_R - t_r) \quad (5\text{-}3)$$

where t_R is the desired unit duration. After calculation of these parameters, unit peak discharge, q_{pr} can be calculated using Equation 5-4:

$$q_{PR} = 2760 \times \frac{C_p}{t_{PR}} \quad (5\text{-}4)$$

where C_p is the peaking coefficient. If this value is multiplied by drainage area, peak discharge can be calculated. Figure 5.6 shows the flow hydrographs for different return periods.

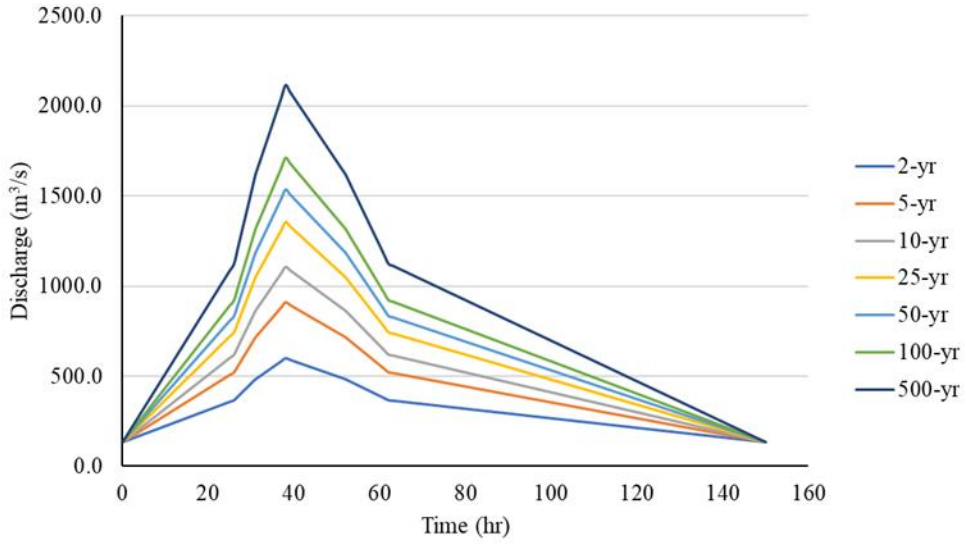

Figure 5.6. Flow hydrographs for different return periods for the stationary case

5.3.2 Determination of peak discharges and hydrographs with nonstationarity assumption

For the nonstationary case, a set of potential covariates are tested with different probability distributions (Normal (No), Log-normal (LogNo), Gamma (Ga), GEV, Gumbel (Gu) and Logistic (Lo)). Covariates used in this study are selected based on literature review as explained in Section 2.6 and are time, reservoir index (RI), annual maximum precipitation (MP), annual total precipitation (TP), annual average temperature (Temp), population (Pop), and Normalized Difference Vegetation Index (NDVI). Since parsimony, obtaining the simplest model that explains the data's variation as much as possible, is the basic principle in identifying the best model (Coles, 2001), the nonstationary (NS) models are limited to two covariates. That is,

maximum two covariates are used for location and scale, and a total of 840 NS models are generated considering all possible combinations of the selected covariates. NS models are generated using extRemes package (Gilleland & Katz, 2016) and GAMLSS (Rigby & Stasinopoulos, 2005) package are used to generated NS models. The parameters are estimated using MLE. Akaike Information Criterion (AIC) (Akaike, 1974) scores are used to evaluate the performance of each model.

$$AIC = (-2)\log_e L + 2K \tag{5-5}$$

where K is the number of adjusted parameters in the model, and L is the model's maximum likelihood. A model with a lower AIC score is considered a better model. Table 5.14 demonstrates the AIC scores of the best 20 models and the stationary model for each probability distribution. This process yields a set comprising 55 NS models, indicating that a substantial proportion of covariate combinations perform relatively well regardless of the distribution. Bold values show the best model for each probability distribution and pink highlighted values belong to the best 20 models for each probability distribution.

Table 5.14 Best 20 NS models for each probability distribution

Combination	LogNo	No	Lo	Ga	GEV	Gu
RI+Pop--NDVI+	**488.63**	500.85	496.14	491.67	488.38	488.55
RI+Pop--Time+NDVI	489.39	499.97	497.97	**490.24**	487.43	489.97
RI+Pop--TP+NDVI	489.44	502.3	496.97	491.27	488.81	488.87
RI+Pop--Pop+NDVI	489.56	502.48	498.06	492.14	490.34	490.3
RI+Pop--RI+NDVI	489.88	500.42	496.46	492.26	487.85	488.18
RI+Pop--Temp+NDVI	490.23	494.7	493.95	493.2	490.37	489.92
RI+Pop--MP+NDVI	490.57	502.64	497.7	493.62	486.85	488.75
RI+Pop--TP+	490.62	513.13	502.87	492.46	497.89	497.24
RI+Pop--TP+Temp	491.56	502.11	497.6	492.8	499.85	498.42
RI+Pop--+	491.76	511.29	500.91	494.81	495.87	495.22
RI+Pop--Time+TP	492.21	514.79	502.8	494.34	487.45	492.65
RI+Pop--TP+Pop	492.24	512.32	504.45	494.01	498.79	498.22
RI+--NDVI+	492.46	506.37	500.98	495.73	492.85	492.63
RI+Pop--MP+TP	492.47	513.27	504.87	494.43	496.71	498.13

Table 5.14 (cont'd)

Combination	LogNo	No	Lo	Ga	GEV	Gu
RI+Pop--RI+TP	492.54	508.21	501.33	494.25	490.54	493.08
RI+TP--NDVI+	492.65	507.92	502.22	496.98	493.05	493.28
RI+Pop--Temp+	492.81	500.21	495.61	495.75	497.85	496.44
RI+--+	492.96	511.81	502.22	495.82	495.8	495.67
RI+TP--+	493.06	513.3	503.05	496.96	493.29	495.12
Time+RI--NDVI+	493.12	504.43	498.63	495.18	493.77	493.08
RI+--RI+Temp	496.56	**493.41**	**491.54**	499.14	487.35	**486.96**
RI+Pop--RI+Temp	494.46	493.79	492.01	497.01	489.49	488.67
Time+RI--RI+Temp	498.21	494.15	492.47	500.76	489.53	488.89
RI+Temp--RI+Temp	495.9	494.96	493.49	496.65	489.45	489.01
RI+TP--RI+Temp	496.16	495.28	493.25	499.88	489.06	488.4
RI+MP--RI+Temp	498.46	495.37	493.5	501.02	489.3	488.9
RI+NDVI--RI+Temp	497.64	495.39	493.54	499.49	488.75	488.39
RI+Pop--Time+Temp	494.49	497.16	494.56	497.75	487.6	489.17
Time+RI--Temp+NDVI	494.99	497.99	495.74	496.79	495.81	494.66
Time+RI--Time+Temp	497.55	498.15	494.74	500.57	488.01	489.78
Time+RI--RI+NDVI	494.78	498.46	494.63	496.89	486.13	487.15
Time+TP--Temp+NDVI	496.83	498.86	497.64	500.54	498.4	496.74
RI+--Time+Temp	496.42	498.98	496.84	499.14	490.54	491.92
RI+--Temp+NDVI	494.28	499.42	497.78	497.3	494.85	494.1
RI+TP--Temp+NDVI	494.09	499.57	498.2	498.25	494.74	494.05
RI+TP--Time+Temp	496.24	499.68	497.57	499.83	492.13	493.07
RI+NDVI--Time+Temp	496.5	500.39	498	498.62	487.01	491.04
RI+Pop--MP+Temp	494.8	501.83	497.25	497.39	496.96	496.79
RI+NDVI--RI+NDVI	495.53	500.8	497.43	497.33	486.66	488.61
Time+RI--Pop+NDVI	494.49	505.82	500.35	494.07	495.76	494.92
RI+Temp--Temp+	494.47	502.95	499.12	495.34	499.03	498.42
RI+NDVI--NDVI+	493.72	506.6	501.28	495.59	494.38	494.07
RI+NDVI--Time+	495.28	513.73	502.15	497.44	**484.7**	492.15
RI+NDVI--Time+RI	497.28	508.6	500.86	499.39	485.13	491.2
RI+Pop--Time+	493.61	513.02	500.82	496.81	485.71	490.78
RI+NDVI--Time+NDVI	495.7	507.93	503.03	497.36	485.79	493.63
Time+RI--Time+RI	498.33	510.26	500.88	501.52	485.81	491.4
RI+Pop--Time+MP	495.51	512.16	502.82	498.27	486.14	492.52
RI+NDVI--Time+MP	497.27	514.6	504.12	499.38	486.14	493.9

Table 5.14 (cont'd)

Combination	LogNo	No	Lo	Ga	GEV	Gu
Time+RI--Time+	496.34	515.28	501.36	499.52	486.47	492.05
RI+NDVI--Time+TP	496.11	515.69	503.73	498.01	486.66	493.59
RI+NDVI--Time+Pop	496.28	513.09	503.65	498.01	486.66	494.08
RI+--RI+	494.96	507.44	499.28	497.82	486.79	490.07
Time+RI--Time+MP	498.27	515.59	503.35	501.23	487.08	493.84
RI+--RI+NDVI	494.47	502.49	498.32	497.72	487.84	489.26
+--+	508.9	520.61	515.06	508.95	510.99	509.44

LogNo: Log-normal, No: Normal, Lo: Logistic, Ga: Gamma, Gu: Gumbel

"--" separates location and scale parameters and "+--+" represents stationary model.
Bold values show the best model for each probability distribution and pink highlighted values belong to the best 20 models for each probability distribution.

Performances of the NS models are better than the stationary model for all probability distributions (see Table 5.14). The number of appearances of each covariate in the best 20 models for each probability distribution are shown in Table 5.15. RI appeared in the location parameter of 54 out of 55 NS models. Furthermore, NDVI, which is used for the first time in NS analysis, appeared 20 times in the scale parameter.

Table 5.15 Total number of the candidate covariates appearance in the best models (i.e., the models in Table 5.14)

Covariate	Location Parameter	Scale Parameter
Time	10	18
RI	54	15
MP	1	6
TP	6	8
Pop	20	4
Temp	2	21
NDVI	10	20

NS models are kept as simple as possible since including several covariates might bring overfitting risk to the NS models. The covariates other than time cause more uncertainty for future forecasts. For example, for the GEV distribution, the AIC score

of the NS model with time covariate is 507.3, while the AIC score of the stationary model is 511.0. The performance of the NS model with time covariate is greater than the stationary model. For this reason, time is selected as the only covariate in the NS modeling of the annual maximum discharge series. The continuation of the studies on NS frequency analysis is presented in our article titled " Nonstationary Frequency Analysis of Annual Maximum Flow Series: Climate Change versus Land Use / Land Cover Change" which is presented in Appendix A.

As mentioned in Chapter 4.1 “Climate change analysis”, 17 RCMs are downloaded and analyzed. According to the analysis, M5 is selected as the best RCM. The outputs of M5 are entered into the hydrological model and the annual maximum discharge series for 2025 - 2100 are obtained. In NS modeling, six distributions are compared based on their Chi-square scores and the GEV distribution is the winner; hence, peak discharges are calculated using the GEV distribution for different return periods. These values are given in Table 5.16 while the flow hydrographs are provided in Figure 5.7.

Table 5.16 Calculated peak discharge values for different return periods – NS case

Return Period	Peak Discharge (m^3/s)
2	257.5
5	352.6
10	426.5
25	534.3
50	626.2
100	728.9
500	1018.2

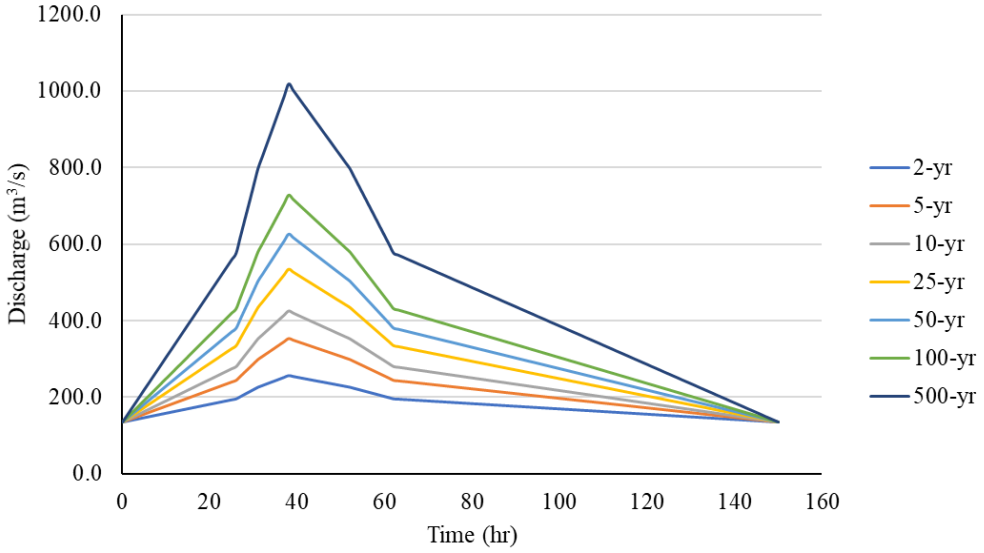

Figure 5.7. Flow hydrographs for different return periods for nonstationary case

5.4 Combined 1D/2D hydrodynamic model results

The validation of the combined 1D/2D hydraulic models is vital. However, in Türkiye, it is difficult to validate the models because of the limited data. The model is validated based on the information received from SHW staff in the meeting conducted on the 29th of January, 2024. Insight was provided regarding a massive flood event that occurred in Silifke between the 5th and 7th of March, 2004. They shared the details about the locations where the flood water entered and left Silifke from the left bank of Göksu River. These locations are marked in Figure 5.8. The developed combined 1D/2D hydraulic model is run for the flood hydrograph estimated for the 2004 event and these locations are validated with the results of it. Moreover, it was learned from the SHW staff that Göksu River can pass around 800 m^3/s safely, and our model in general confirms this as well. Our model projects minor overflowing for discharges over 800 m^3/s and this might be due to the inexact bridge dimensions obtained from SWH.

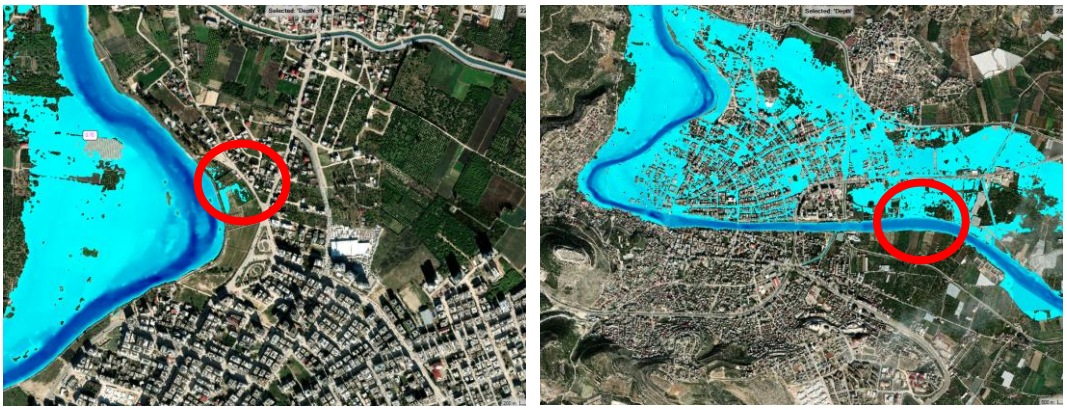

(a) (b)

Figure 5.8. The combined 1D/2D hydraulic model results: (a) The location where flood water entered the center of Silifke (b) The location where flood water left the center of Silifke (Basemap source: ArcGIS World Imagery)

5.4.1 Scenarios used to assess effects of climate change and land use / land cover change

The combined 1D/2D hydraulic model is run using the flood hydrographs which are generated under stationary and nonstationary conditions. Five scenarios are generated to assess the effects of CC and LULC. Scenario 0 (S0) is the scenario in which the traditional methods are used. In this scenario, flood peak discharges are calculated considering the observed historical AMFS. Scenario 1 (S1) is generated to assess the effects of CC and nonstationarity. In this scenario, the flood peak discharges are calculated using the results of the hydrological model obtained using M5 RCM projections as inputs. In addition to this, Time is used as the covariate. Scenario 2 (S2) is generated to see the effects of full reservoir conditions (i.e., all major reservoirs in the basin are assumed to be at their maximum levels). This scenario is developed to represent a worst-case situation where flood mitigation performances of the major dams are neglected. In Scenario 3 (S3), the outputs of the hydrological model with M5 RCM are modeled under stationary conditions. Finally, in Scenario 4 (S4), the urbanized area is adjusted according to the future projections as explained in Section 5.2 to evaluate the effects of LULC change. In this scenario,

CC and nonstationarity effects are investigated as well by using M5 RCM's climate projections and time as the covariate. The explanations are given in Table 5.17.

The peak discharges that are used for each scenario and each return period is given in Table 5.18. It can be seen that when the hydraulic structures are in full condition, Q_{500} is the largest. On the other hand, peak discharges of the NS model are the lowest. If peak discharges of S0 and S3 are compared, it can be seen that peak discharges tend to decrease if M5 outputs are used in the hydrological model. Below, the flood inundation maps are provided for all scenarios.

Table 5.17 Scenarios that are generated for the combined 1D/2D hydraulic model

Scenario	Explanations
Scenario 0 (S0)	Stationary model (historical observed outputs)
Scenario 1 (S1)	Nonstationary model (M5 RCM + Time as the covariate)
Scenario 2 (S2)	Nonstationary model (M5 RCM + Time as the covariate + Hydraulic structures are ignored)
Scenario 3 (S3)	Stationary model (M5 RCM)
Scenario 4 (S4)	Nonstationary model (M5 RCM + Time as the covariate + Increased urbanized area)

Table 5.18 The peak discharges for each scenario and each return period

Return Period	Q (m^3/s)				
	S0	S1	S2	S3	S4
2	637.6	257.5	434.7	307.7	257.5
5	968.5	352.6	600.3	408.2	352.6
10	1181.9	426.5	748.5	490.4	426.5
25	1445.0	534.3	995.8	589.2	534.3
50	1636.6	626.2	1235.4	760.4	626.2
100	1824.8	728.9	1534.3	934.8	728.9
500	2256.2	1018.2	2550.0	1589.9	1018.2

The inundated areas that are calculated as a result of each scenario and each return period are given in Table 5.19. In the case of comparison of S1 and S4, it can be seen that the inundated areas are greater for S4 due to the increased urbanized area.

Table 5.19 The inundated areas as a result of each scenario and each return period

Return Period	Area (km^2)				
	S0	S1	S2	S3	S4
2	58.6	12.2	33.0	21.0	12.2
5	78.4	22.1	58.6	33.0	24.5
10	85.4	33.0	67.4	44.3	35.7
25	91.0	37.4	79.6	55.1	40.5
50	95.7	58.6	88.9	67.4	62.2
100	101.8	67.4	97.8	77.3	71.6
500	117.1	79.6	123.8	97.8	84.5

Total economic damage values are given in Table 5.20. In the case of comparison of S1 and S4, it can be seen that the total economic damage values are greater for S4 due to the inundation of the synthetically generated urbanized areas. It should be

noted that these values are not realistic for Türkiye. However, they can be compared and give an idea about the consequences of floods.

Table 5.20 The economic damages as a result of each scenario and each return period

Return Period	Economic Damage (€)				
	S0	S1	S2	S3	S4
2	409963	73386	266544	205762	73386
5	1337110	262253	405277	316220	307154
10	2142024	327742	486388	356465	423355
25	3048391	377431	1457160	396773	527569
50	3823298	407034	2282370	489636	692187
100	4538085	454218	3350413	1167096	808447
500	6084402	1832446	7630792	3583662	14646553

5.4.2 Flood inundation maps under stationary condition (S0)

Flood inundation maps under stationary conditions are given in Figure 5.9 and Figure 5.10Figure 5.10. Flood inundation maps under stationary conditions (S0) (a) 2-year flood (b) 5-year flood (c) 10-year flood (d) 25-year flood (e) 50-year flood (f) 100-year flood (g) 500-year flood. When 500-year flood occurs, the flood-inundated area doubles compared to that of Q_2. On the other hand, the total economic damage increases by a factor of 1507.

Q_{500} inundation map of the study area is provided in Figure 5.9. The economic damage occurring at the city center is the major contribution of the total economic damage. Thus, flood inundation maps of the city center, which is shown with a red rectangle in Figure 5.9, are shown for better demonstration for the rest of the scenarios.

As can be seen from 5.10 (a), Figure 5.10 (b) and Figure 5.10 (c), water from the Göksu River overflows from the left bank and inundates the left part of the Silifke Center for Q_2, Q_5, and Q_{10} flood events. In case of other flood events, water starts to

overflow from both the left and right banks of the Göksu River. The elevation difference between the right part of the Silifke Center and the Göksu River is higher compared to the difference between the left part of the Silifke Center and the Göksu River. This situation can be seen in Figure 3.2. For this reason, water initially starts to overflow from the left bank.

Figure 5.9. Q_{500} flood inundation map under stationary conditions (S0) (Basemap source: ArcGIS World Imagery)

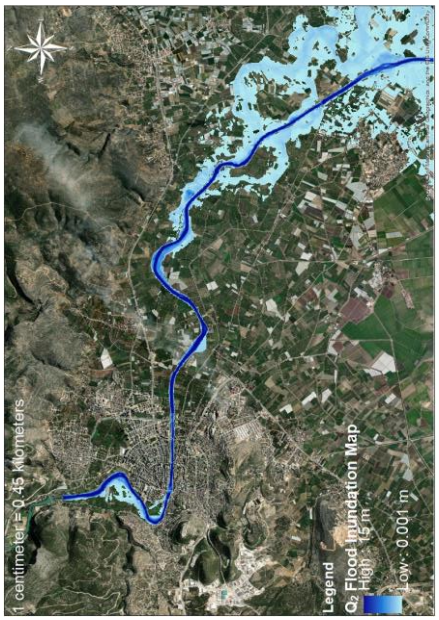

(a) 2-year flood

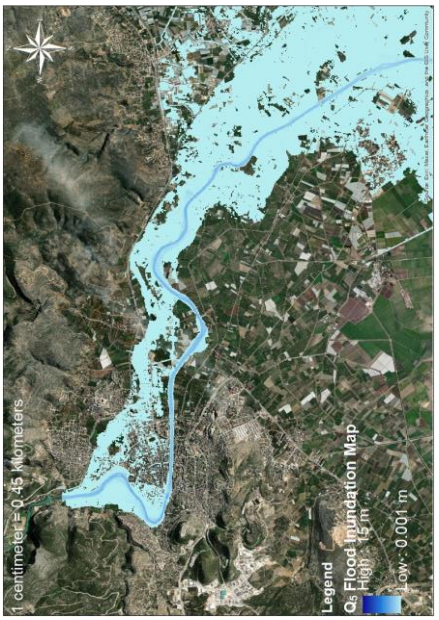

(b) 5-year flood

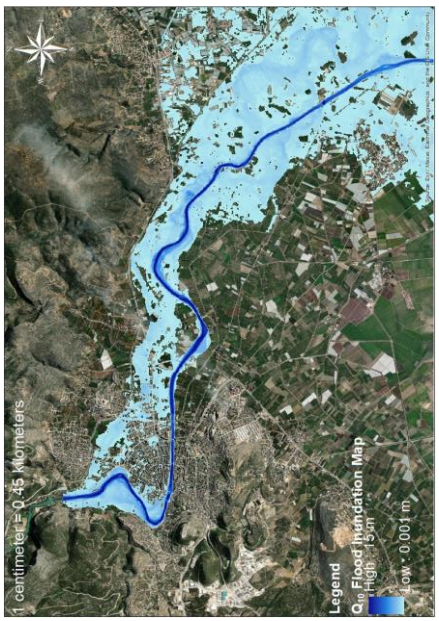

(c) 10-year flood

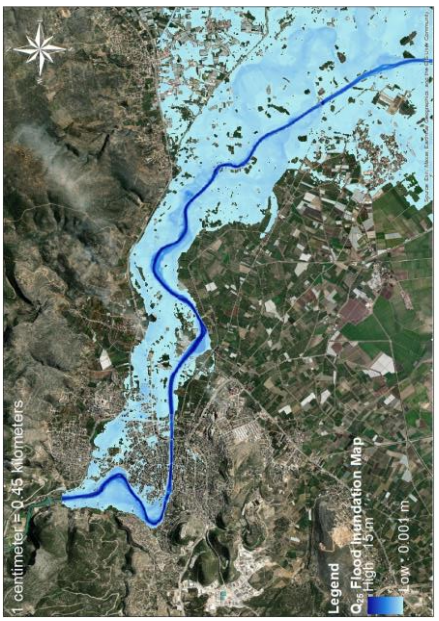

(d) 25-year flood

Figure 5.10. Flood inundation maps under stationary conditions (S0) (a) 2-year flood (b) 5-year flood (c) 10-year flood (d) 25-year flood (e) 50-year flood (f) 100-year flood (g) 500-year flood (Basemap source: ArcGIS World Imagery)

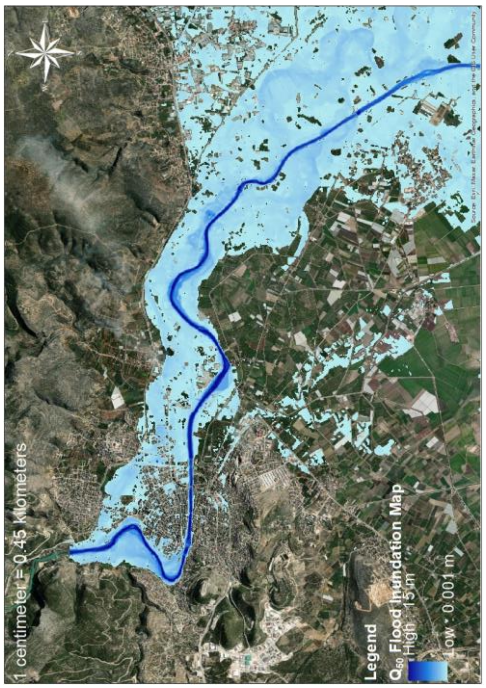

(e) 50-year flood

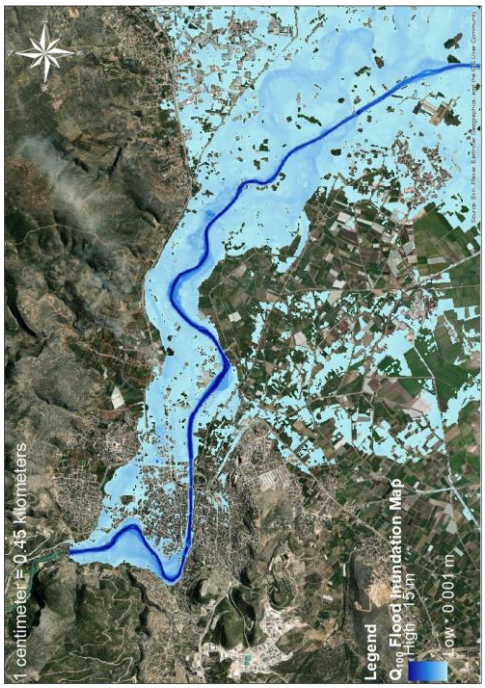

(f) 100-year flood

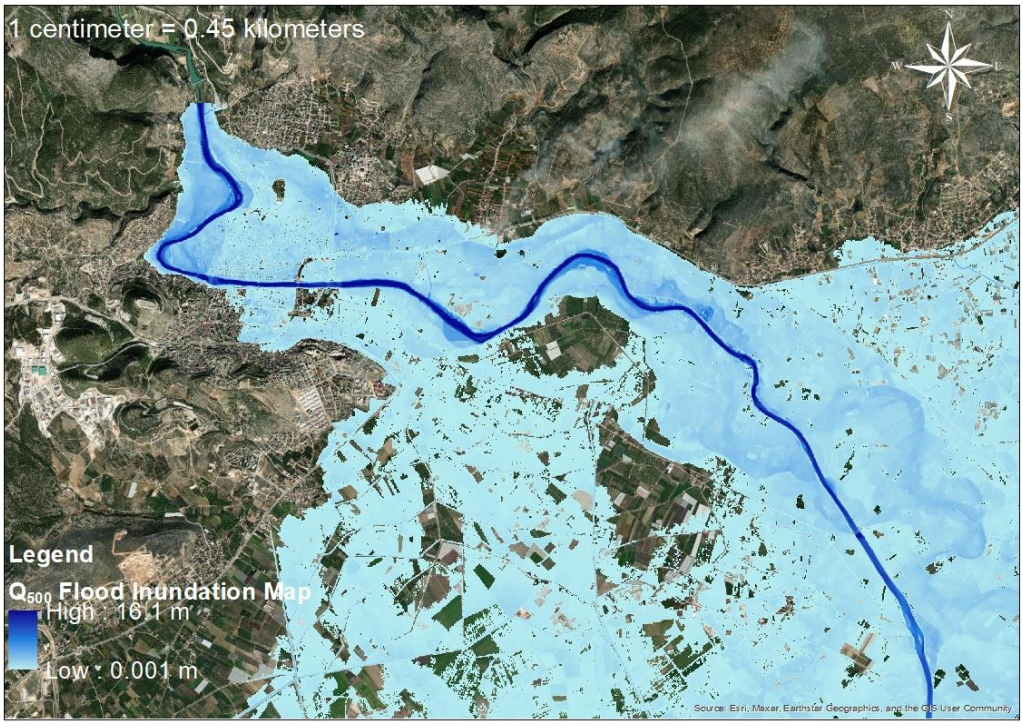

(g) 500-year flood

Figure 5.10. (cont'd)

5.4.3 Flood inundation maps of S1

The flood-inundated areas are considerably reduced compared to the S0 scenario due to the low peak discharges (see Table 5.18). The flood-inundated area by a 500-year flood event is about 6.5 times greater than the area flooded by a 2-year flood event (see Table 5.19). Flood inundation maps of S1 are given in Figure 5.11.

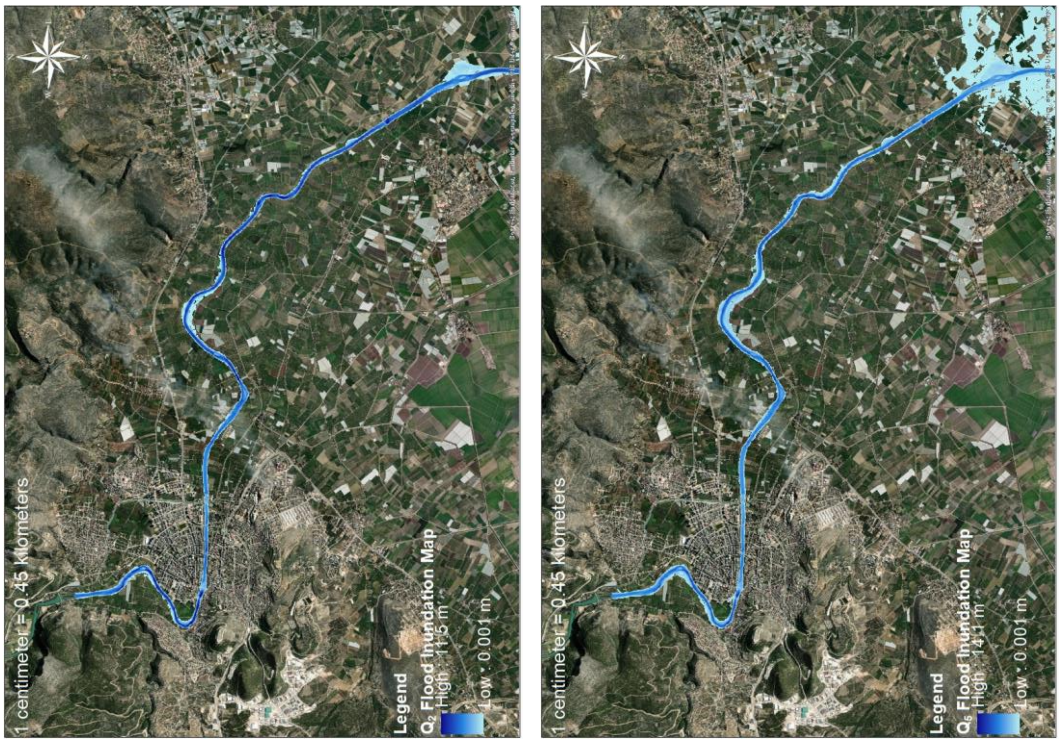

(a) 2-year flood (b) 5-year flood

Figure 5.11. Flood inundation maps under nonstationary conditions (S1) (a) 2-year flood (b) 5-year flood (c) 10-year flood (d) 25-year flood (e) 50-year flood (f) 100-year flood (g) 500-year flood (Basemap source: ArcGIS World Imagery)

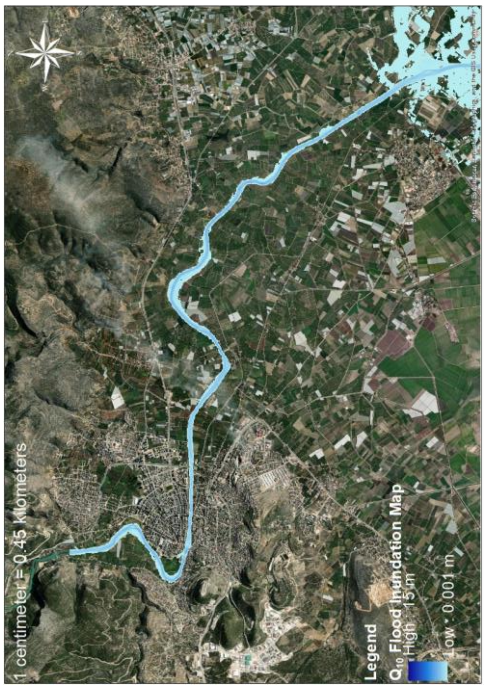

(c) 10-year flood

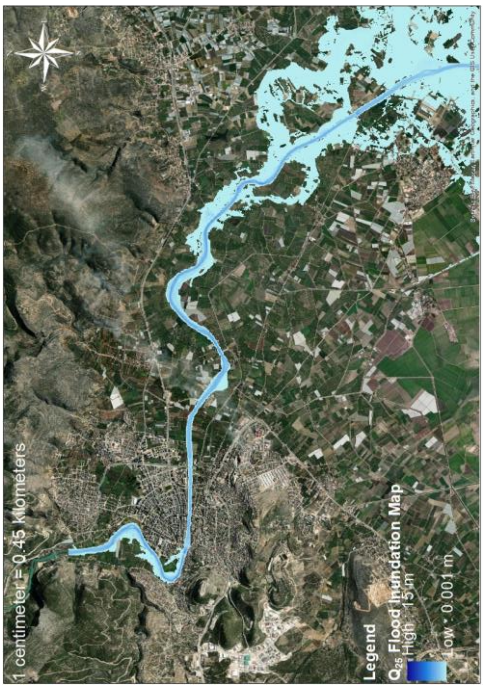

(d) 25-year flood

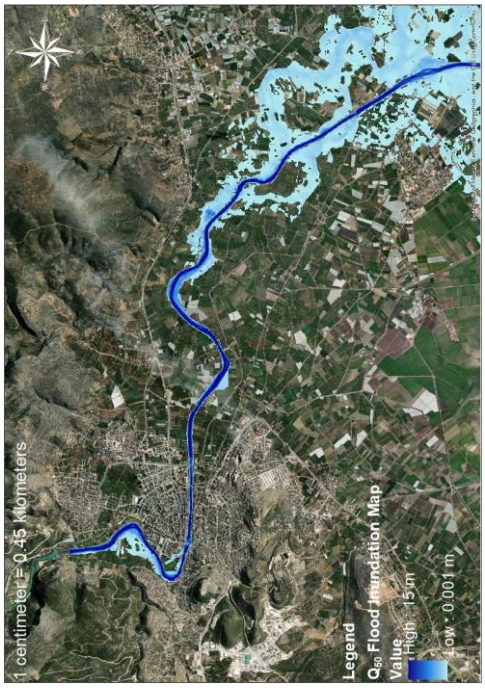

(e) 50-year flood

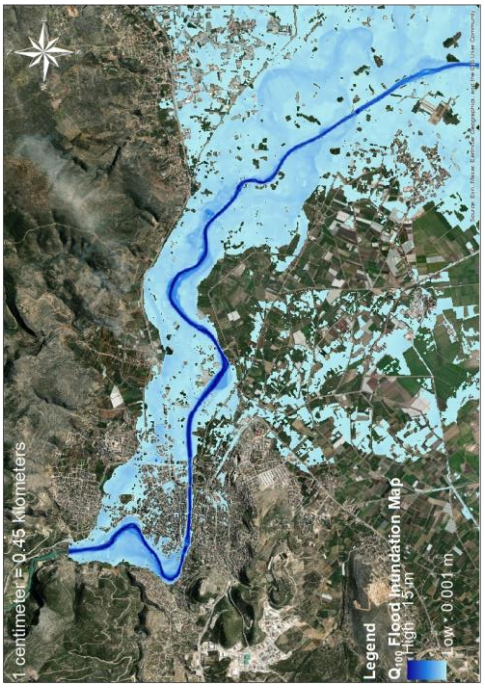

(f) 100-year flood

Figure 5.11. (cont'd)

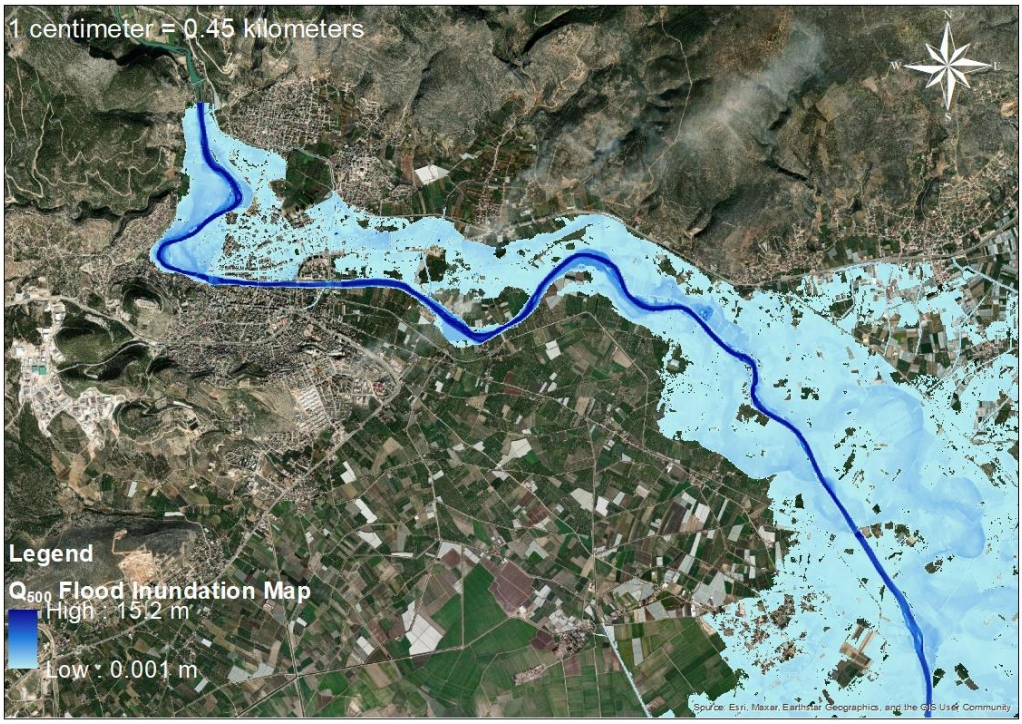

(g) 500-year flood

Figure 5.11. (cont'd)

5.4.4 Flood inundation maps of S2

In the case of 2-year, 5-year, 10-year, and 25-year flood events, flood-inundated areas are quite low compared to S0 (see Table 5.19). In the case of 50-year and 100-year flood events, the flooded areas are very similar compared to S0, while in the case of 500-year flood events, the flooded area is greater for S2 compared to S0 (see Table 5.19). This scenario is actually the worst-case scenario because the flood mitigation capacities of major hydraulic structures in the basin (i.e., dams) are ignored by assuming them to be at their full reservoir levels. Flood inundation maps of S2 are given in Figure 5.12.

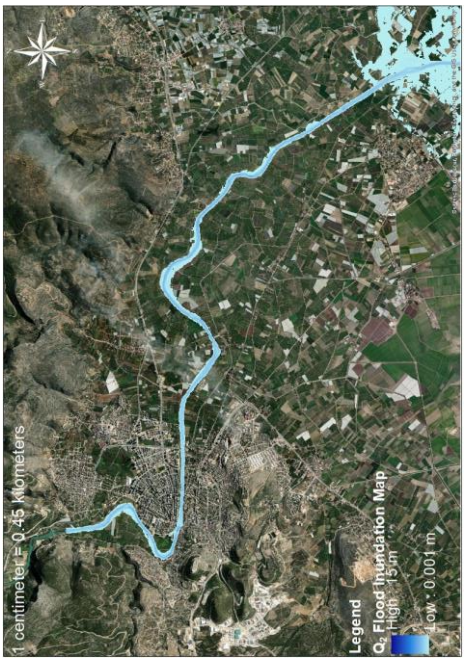

(a) 2-year flood

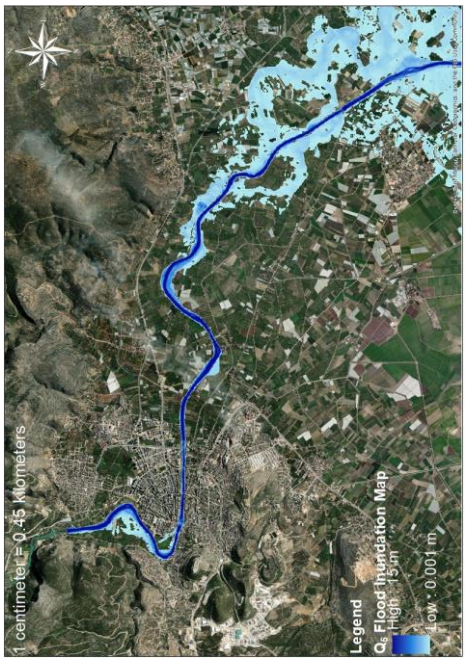

(b) 5-year flood

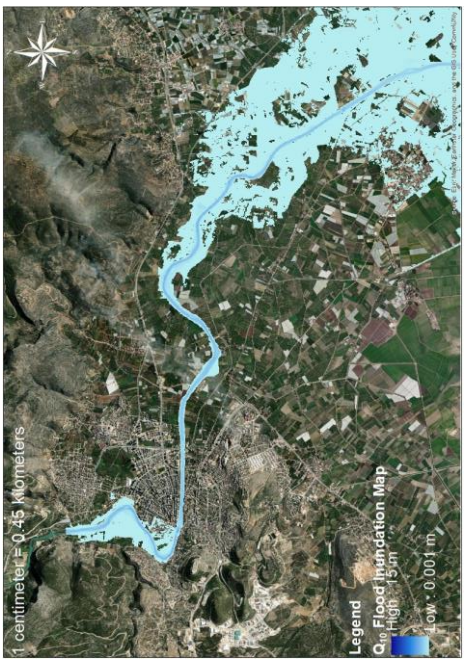

(c) 10-year flood

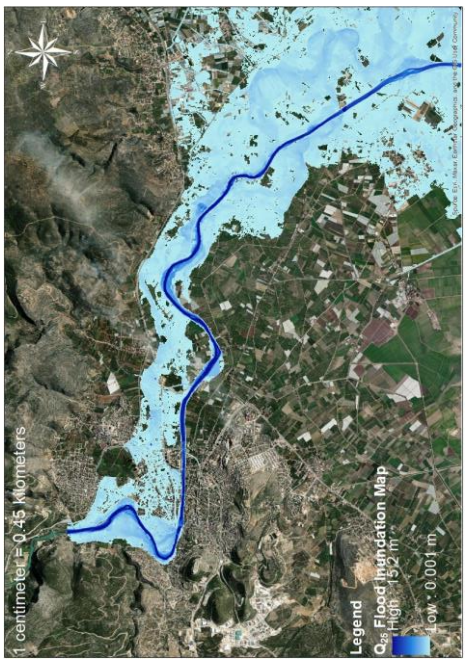

(d) 25-year flood

Figure 5.12. Flood inundation maps of S2 (a) 2-year flood (b) 5-year flood (c) 10-year flood (d) 25-year flood (e) 50-year flood (f) 100-year flood (g) 500-year flood (Basemap source: ArcGIS World Imagery)

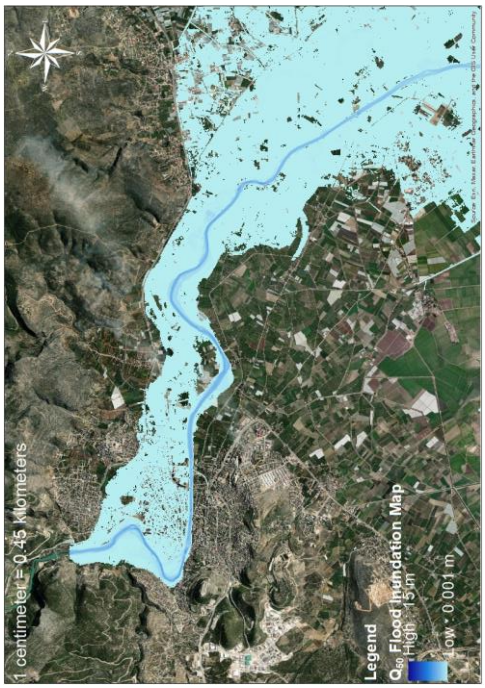

(e) 50-year flood

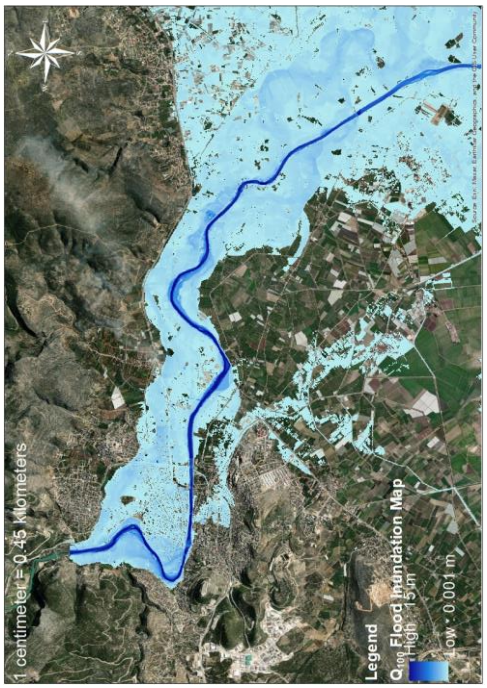

(f) 100-year flood

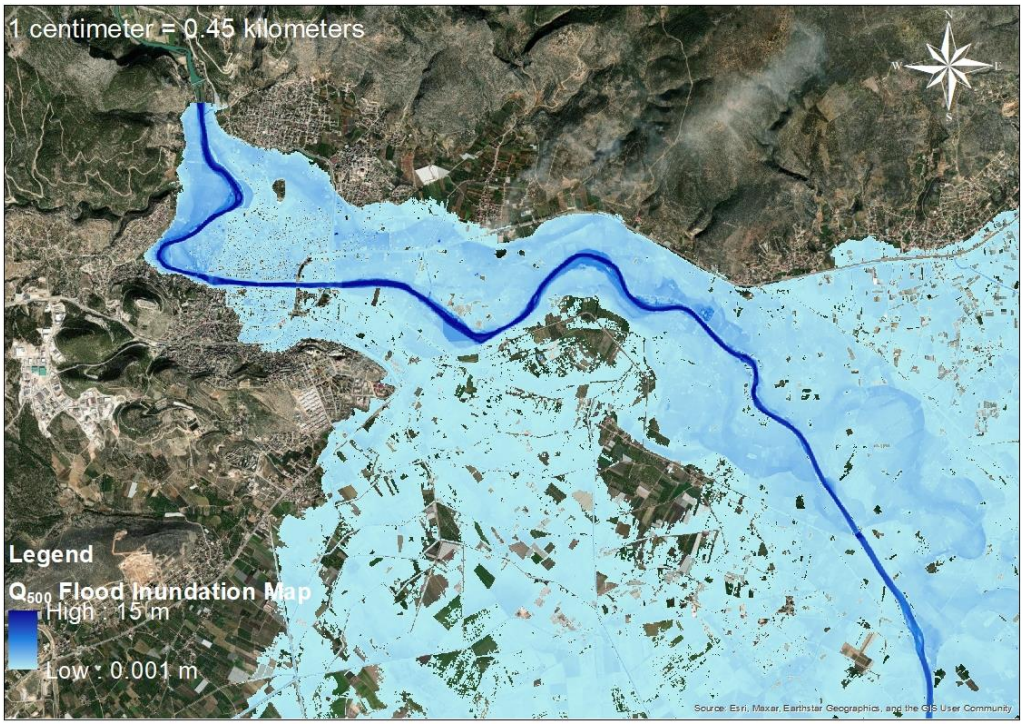

(g) 500-year flood

Figure 5.12. (cont'd)

5.4.5 Flood inundation maps of S3

This scenario assesses the AMFS, which is obtained from the hydrological model with M5 RCM under stationary conditions. S3 is the stationary version of S1. Calculated peak discharge values are approximately 1.2 times greater than the discharge values of S1 in the case of 2-year, 5-year, 10-year, 25-year, 50-year, and 100-year flood events. On the other hand, it is 1.5 times greater in the case of the 500-year flood event (see Table 5.18). Flood inundation maps of S3 are given in Figure 5.13.

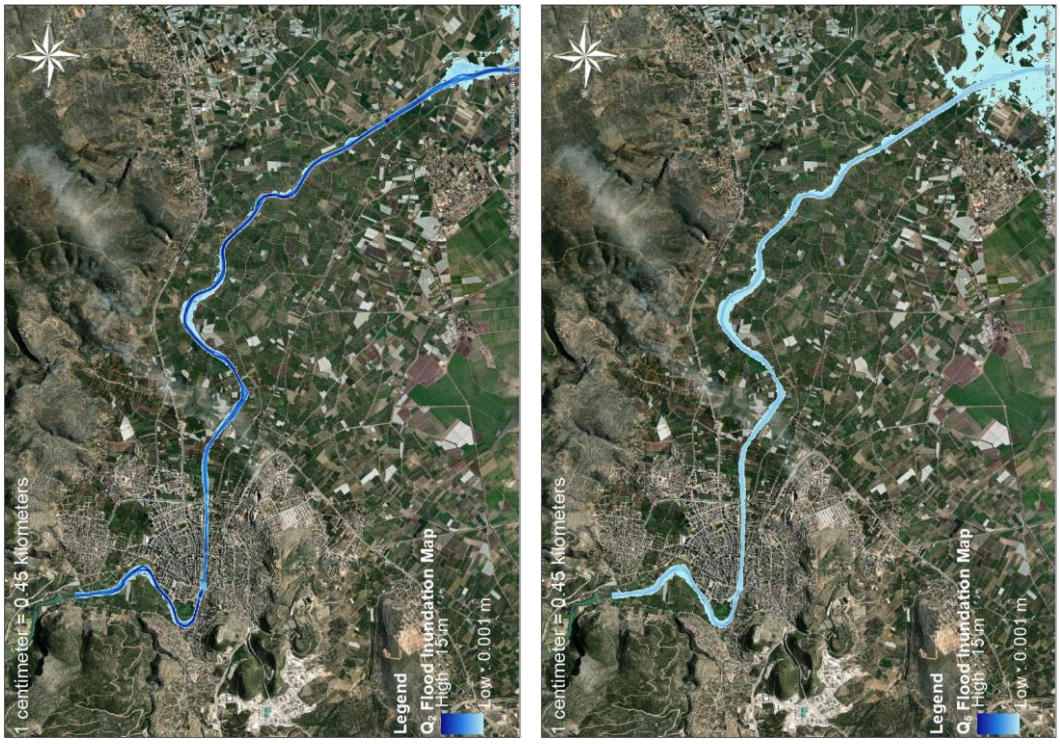

(a) 2-year flood (b) 5-year flood

Figure 5.13. Flood inundation maps of S3 (a) 2-year flood (b) 5-year flood (c) 10-year flood (d) 25-year flood (e) 50-year flood (f) 100-year flood (g) 500-year flood (Basemap source: ArcGIS World Imagery)

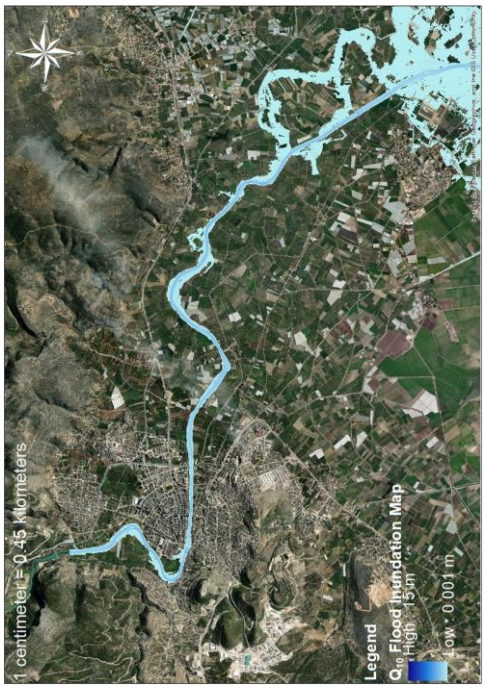

(c) 10-year flood

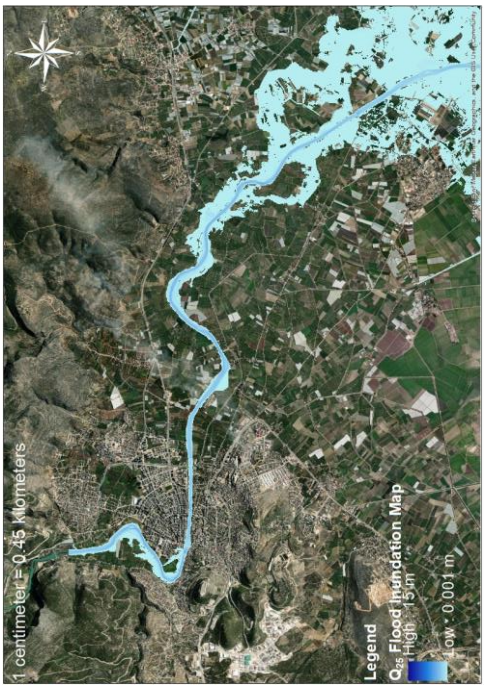

(d) 25-year flood

(e) 50-year flood

(f) 100-year flood

Figure 5.13. (cont'd)

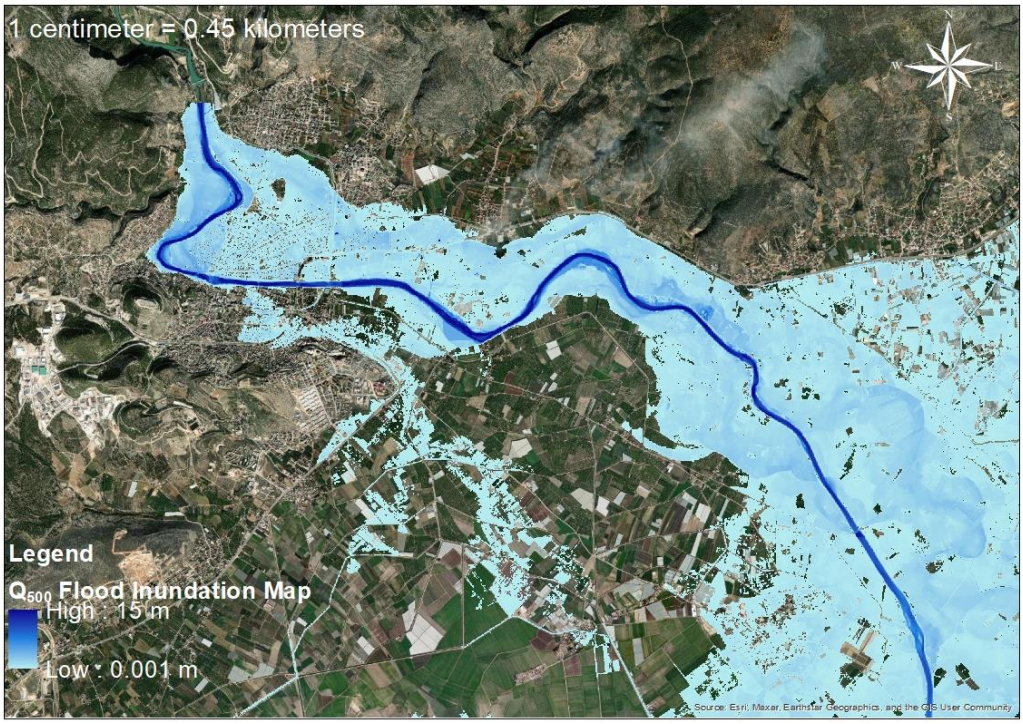

(g) 500-year flood

Figure 5.13. (cont'd)

5.4.6 Flood inundation maps of S4

S4 evaluates the impacts of both urbanization and CC. Urbanized areas are increased based on LULC change analysis. This analysis showed that urbanized areas are estimated to increase by 113% at the end of 2100. The urbanized area is increased by 113% by generating additional urbanized areas. These areas are generated near the newly urbanized areas, and they are represented with polygons in Figure 5.14.

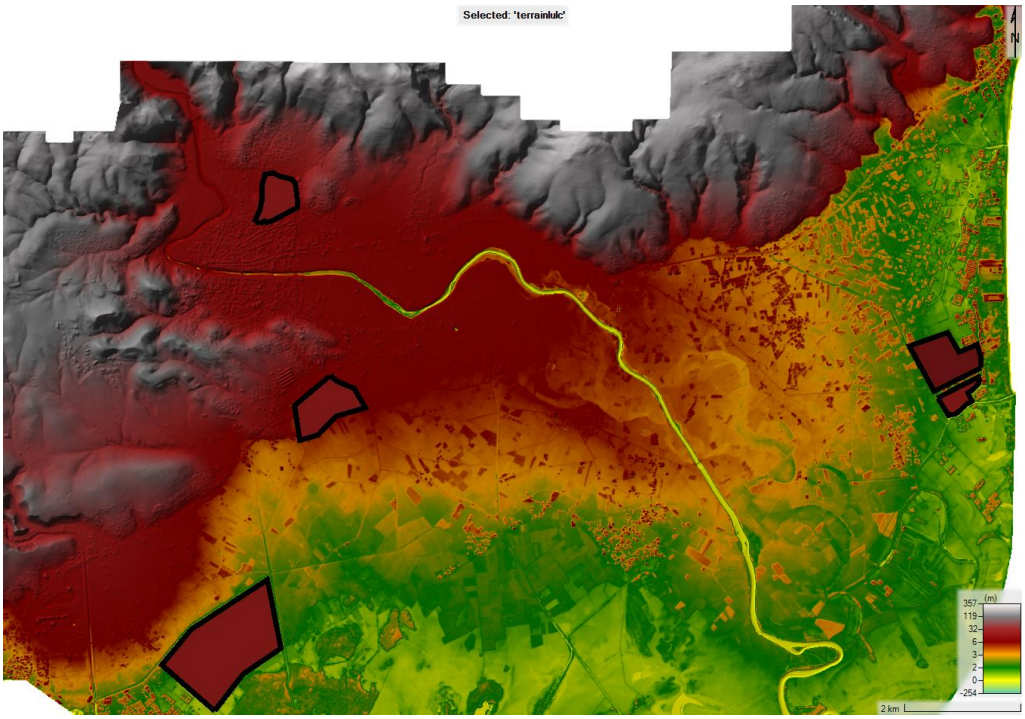

Figure 5.14. Added urbanized areas for S4 based on LULC projections

Flow hydrographs of S4 are the same as that of S1. The results showed that inundated areas increase by approximately 5 km^2 and 30% of the newly added urbanized areas are flooded (see Table 5.19). Flood inundation maps of S4 are given in Figure 5.15. It is crucial that urban-planning is carried out considering these flood inundation maps.

(a) 2-year flood

(b) 5-year flood

(c) 10-year flood

(d) 25-year flood

Figure 5.15. Flood inundation maps of S4 (a) 2-year flood (b) 5-year flood (c) 10-year flood (d) 25-year flood (e) 50-year flood (f) 100-year flood (g) 500-year flood (Basemap source: ArcGIS World Imagery)

(e) 50-year flood

(f) 100-year flood

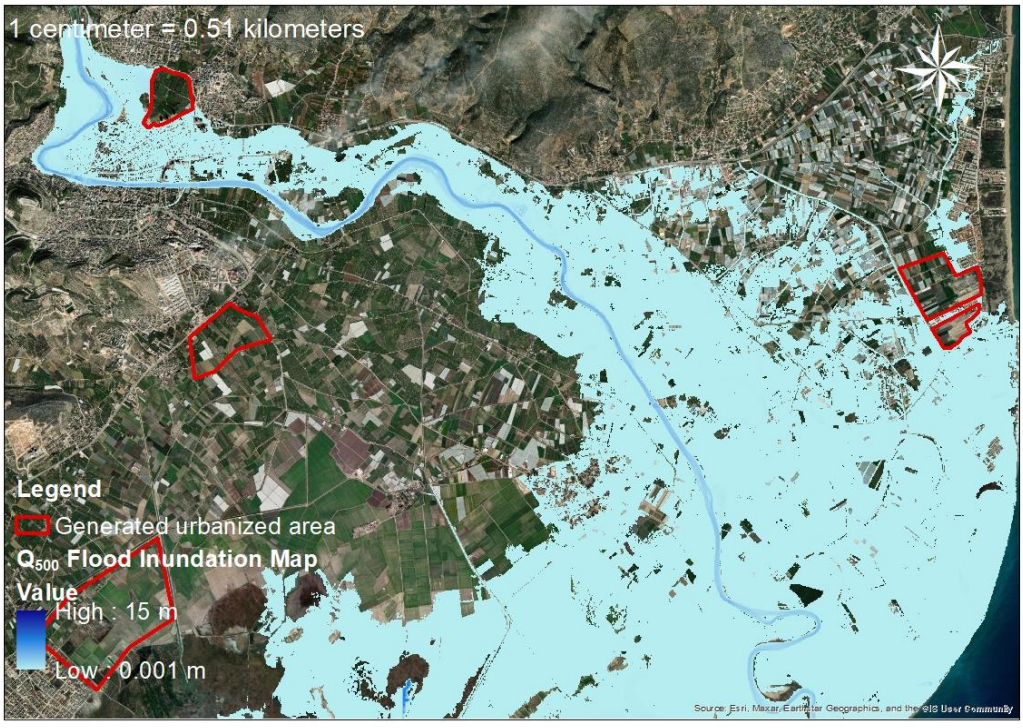

(g) 500-year flood

Figure 5.15. (cont'd)

5.5 Agent-based model

The results of ABM are given in this section. The box plots of average economic damages of 100 Realizations for each scenario are given in Figure 5.16. As shown in Figure 5.16, the average economic damage decreases as agents implement actions, and the government's actions are more effective than public actions. Public agents' actions resulted in a 35.4% and 19.7% decrease in the mean values for PubRand (public agent actions based on random values) and PubSur (public agent actions based on survey results) compared to the Base (no agents) scenario, respectively. The findings indicate that the assignment of random behavior to public agents may result in an overestimation of the reduction in economic damage. Consequently, the utilization of site-specific information is of paramount importance in order to achieve a realistic evaluation of flood consequences.

The added value of a survey that is used to collect information about public risk and coping perceptions instead of randomly assigning them is investigated by assuming the occurrence of the same flood event during each year of the 75-year simulation period. Figure 5.17 shows the change in total economic damage over time for both the PubRand and PubSur scenarios for the 500-year flood. The total economic damage initially decreases and stabilizes with time. Risk and coping perceptions of the individuals who experience floods increase at the initial stage of the simulation period. Thus, they take action, and total economic damage decreases with time. The economic damage value stabilizes for around nine years. It should be noted that these values are highly dependent on the threshold values for risk and coping perceptions. It can also be seen that the total economic damage for the PubRand scenario is less than the PubSur scenario, which supports the previous finding. It indicates that people's flood risk and flood coping perceptions are skewed towards lower-than-average values, which is a realistic outcome for Türkiye. Thus, especially for regions where flood awareness is limited (Türkkan & Hırca, 2021), surveys are essential for accurately modeling the impact of public action on economic damage reduction.

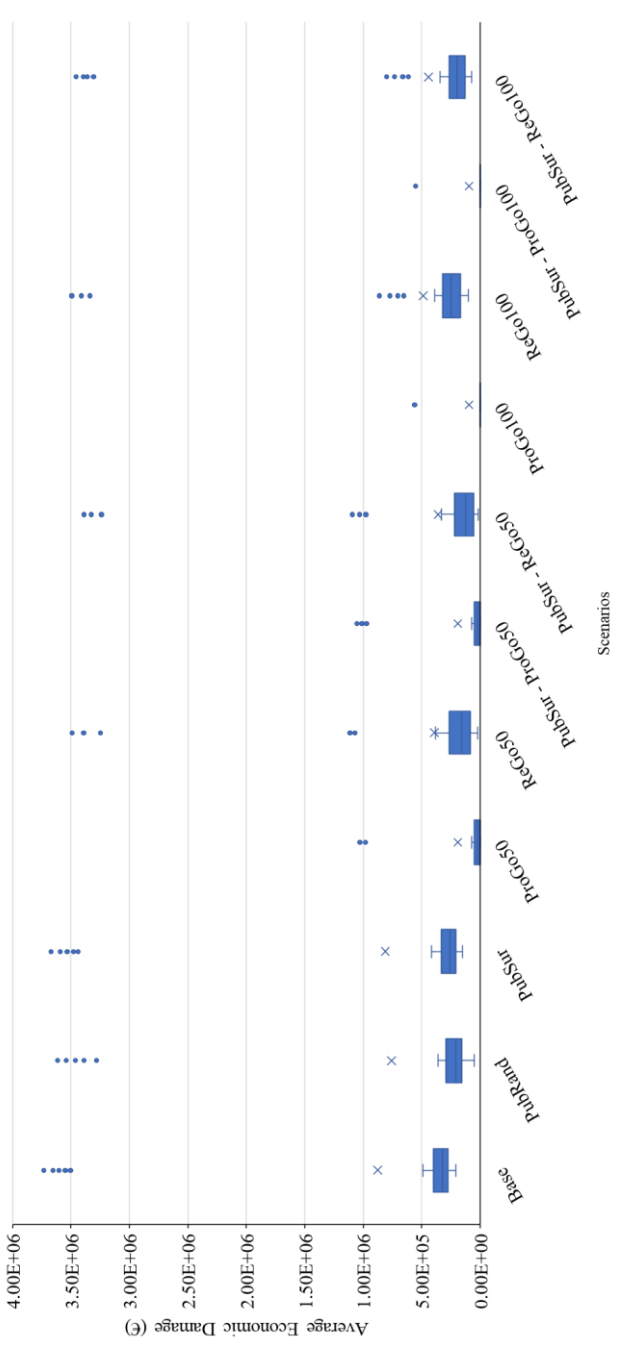

Figure 5.16. Box plots for average economic damage for each scenario

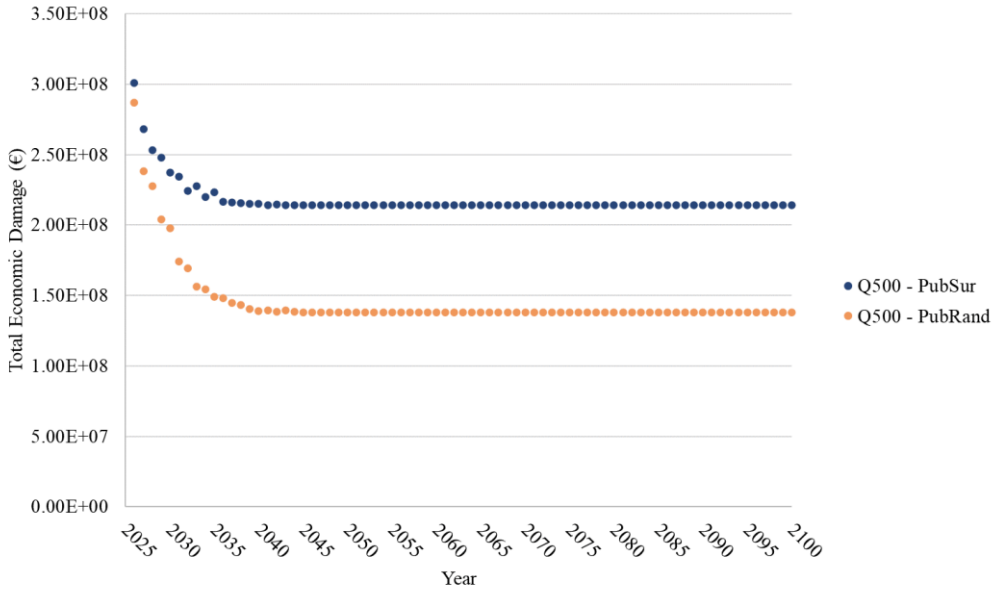

Figure 5.17. Change in total economic damage of PubSur and PubRand scenarios (Q_{500})

The box plots benefit–cost (B/C) ratios of 100 Realizations for scenarios with the government agent are given in Figure 5.18. It is observed that the B/C values of the scenarios with proactive government are greater than those with reactive government. It can also be seen that the B/C ratios of the scenarios with the government that take action against 50-year flood are greater than those of 100-year flood regardless of whether the government is proactive or reactive. Moreover, it can be said that taking action against a 50-year flood is more beneficial for the study area. The rationale behind this can be attributed to the high cost of implementing a 100-year flood action plan and the likelihood of 50-year floods to occur earlier in the simulation period but the low probability of occurrence of a 100-year flood event earlier in the simulation period of 75 years. Another interesting finding is that the B/C ratios of the scenarios with proactive government are always greater than 1.0, while they are less than 1.0 for 4% of Realizations of the scenarios with reactive government. Thus, the proactive behavior of the government is always feasible.

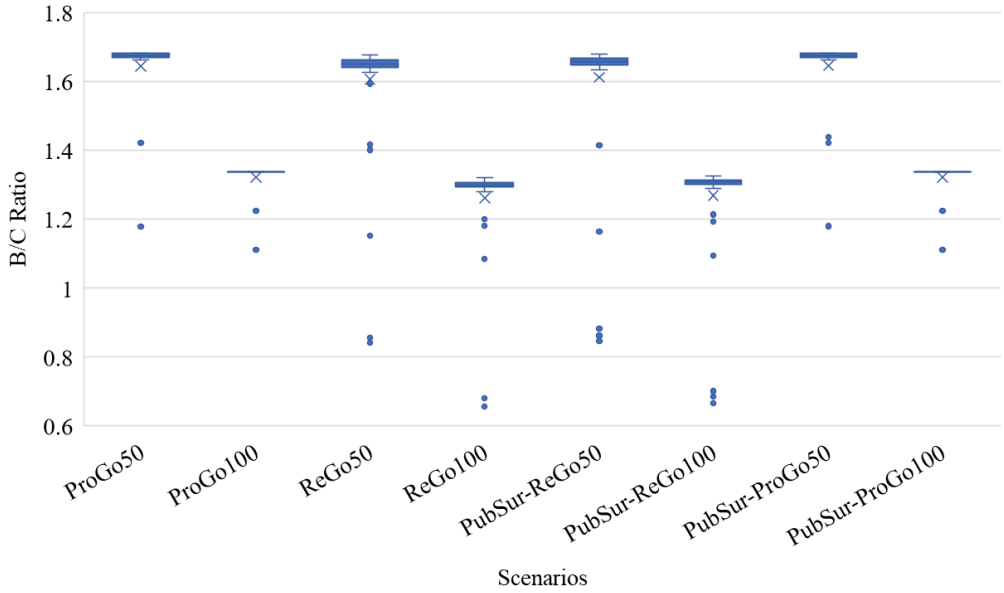

Figure 5.18. B/C ratios for Sc4-Sc11

It is observed that the timing of a severe flood (50-year, 100-year, or 500-year flood) affects total economic damage; thus, the following analysis is conducted to assess the significance of the timing of a severe flood. The Realizations are grouped into two: the first group includes the Realizations where a severe flood occurs within the initial 10 years of the simulation period (referred to as Early, denoted with E), while the second group has the rest of the Realizations (referred to as Late, denoted with L). The results of all scenarios except the base scenario are illustrated in Figure 5.19. It can be seen that the average damage of the scenarios with a reactive government in group E is less than the scenarios with a reactive government in group L. This is an expected result as an early occurrence of a severe flood prompts the reactive government to take action, resulting in decreased economic damage. On the other hand, scenarios with a proactive government that takes action against the 100-year flood exhibit very similar average economic damage values for both groups E and L. This is due to the fact that as the proactive government takes action at the very first stage, the timing of the flood event becomes unimportant.

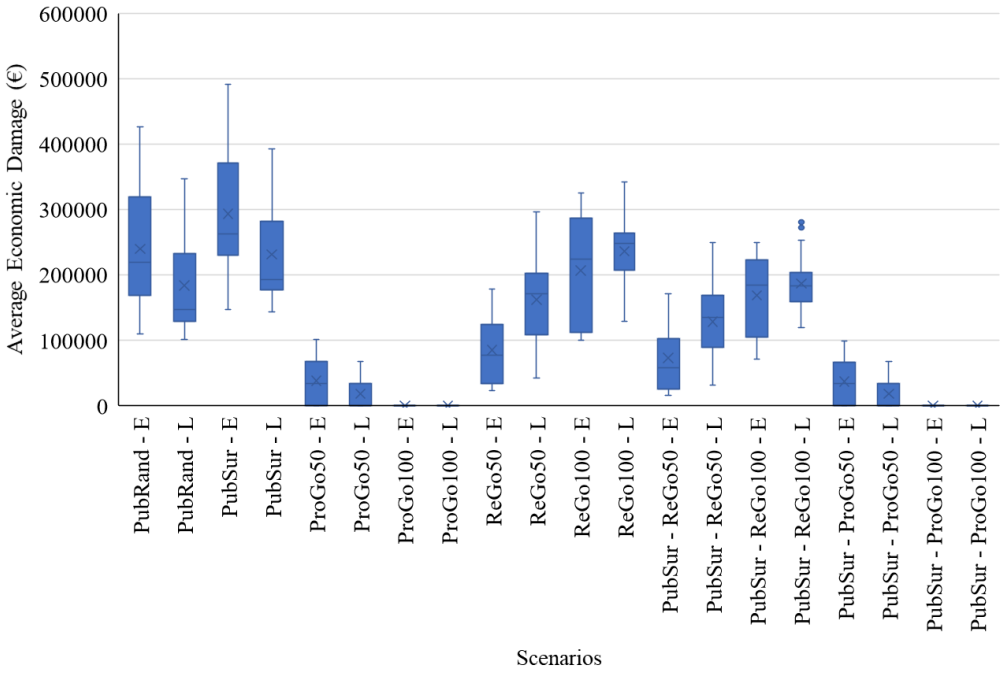

Figure 5.19. The effect of the timing of a serious flood event

The duration between flood events causes significant changes in economic damages. Figure 5.20 shows the economic damage change between two 500-year flood events for the PubSur scenario. To analyze the effect of the duration between two flood events 28 realizations are generated, and these realizations are designed as follows: i) there are only two 500-year flood events in the 75-year simulation duration, and ii) there are no flood events in the simulation duration. The change in the economic damage is calculated as the difference between the economic damage of the second flood event and the first flood event. Negative values show that economic damage decreases, while positive values show that economic damage increases. As seen from Figure 5.20, the rate of increase in economic damage is initially high. After around nine years, the rate of increase decreases. This shows that flood risk perception and coping perception values of the people tend to stabilize after around 9 years. In our study, around nine years, the change in the economic damage is becoming zero. This value is highly dependent on the selected threshold values for risk and coping perceptions. Figure 5.20 also implies that economic damage change values stabilize after 20 years. This shows the effect of timing on flood risk and flood coping

perception. People tend to forget the results of floods. Therefore, their flood risk perception and flood coping perception values decrease, and they do not take any action.

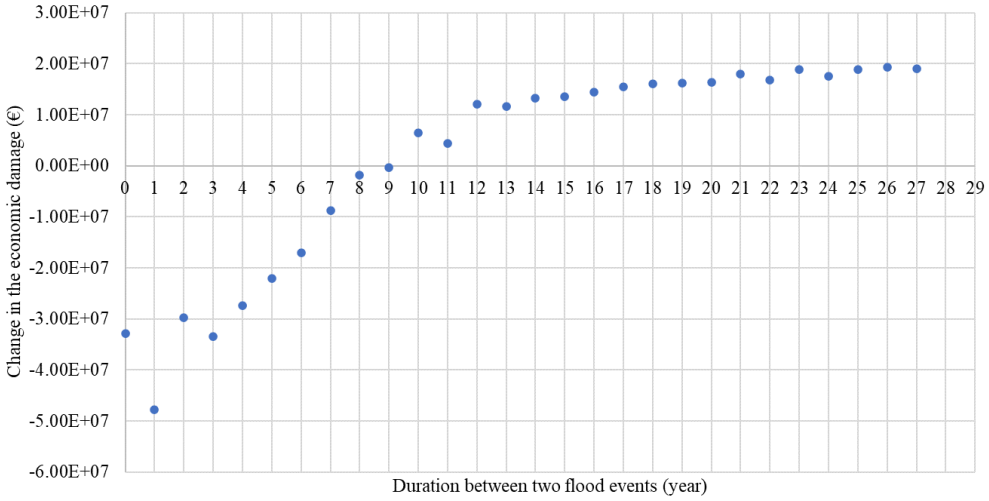

Figure 5.20. The effect of duration between two flood events on economic damage

Detailed analysis of the ABM is presented in our article titled " Integration of climate change impacts and agent-based model to flood risk evaluation in an urbanized area" which is given in Appendix B. This manuscript is under preparation for submission to a scientific journal.

5.6 Limitations of the study

The difficulties and limitations encountered during the study are summarized below:

- LULC analysis was conducted only between 2004 and 2021 due to the availability of satellite images and Google Earth images. The satellite image of 1985 is classified, but it could not be validated since a clear Google Earth image of that year is not available.
- During the development of the hydrological model, many difficulties and problems are encountered. The operation strategies of major reservoirs in the study basin are not available, so it was not possible to calibrate and validate

the model for the time period during which these structures were in operation. Thus, the hydrological model is calibrated and validated for the time period before the construction of the first major hydraulic structure. After the successful calibration and validation, the hydraulic structures are entered into the hydrologic model and their operation related parameters are calibrated. Then the model is tested with the hydraulic structures between 2016 and 2020.

- The hydrological model is run using daily data because the discharge values are available at the daily time step. However, rather than the peak discharge, 2D hydraulic model requires the hydrograph of a flood event as input. Thus, the flood hydrographs are generated using a Snyder Unit Hydrograph Model.
- The flood inundation maps are validated based on the information obtained from SHW and the study of Buldur et al. (2007) since flood inundation data is not available. The entering and leaving locations of the flood water and the flood-inundated neighborhoods are validated using the information obtained from SHW.
- The bridge dimensions obtained from SHW are not exact. Hence, minor problems occurred during the development of the hydraulic model. Necessary modifications are implemented to run the model.
- Manning's Roughness Coefficients are determined based on the CORINE Land Cover data (European Environment Agency, 2020) and the study of Papaioannou, et al. (2018).
- Economic damage values are calculated based on the study of Haer et al. (2020) because depth-damage curves are not available for Türkiye. Hence, the calculated economic damages bare some uncertainties.
- In ABM, the public agent behavior is designed based on risk perception and coping perception values. Functions and the coefficients used in these equations and threshold values are taken from the study of Tonn and Haer (2018). A sensitivity analysis is conducted for threshold values. However, a more detailed analysis necessary to develop site-specific threshold values.

CHAPTER 6

CONCLUSION

This study can be divided into six different parts: climate change analysis, land use/land cover change analysis, stationarity analysis, the hydrological model, the combined 1D/2D hydraulic model, and the agent-based model. The conclusions of each part are given under the related topics.

6.1 Climate change analysis

CC impacts are assessed by using temperature and precipitation projections of 17 RCMs from EURO-CORDEX (EURO-CORDEX, 2021). Precipitation and temperature data of these RCMs are downloaded and the hydrological model is run using the outputs of the RCMs for the calibration, validation and test periods. The calculated discharges and recorded discharges are analyzed based on R^2, $RMSE$, $PBIAS$, and NSE. EC-EARTH CCLM4-8-17, which is referred as M5 in this study, is selected as the best RCM with respect to discharges. In the study of Mesta et al. (2022), M5 is identified as one of the best-performing models in the spatial representation of climatology in the eastern part of the greater Mediterranean Basin which includes our study area. Thus, in this study temperature and precipitation projections of M5 are used in the hydrological model to include CC impacts into flood risk analysis.

6.2 Land use/land cover change analysis

LULC of the region is analyzed using historical satellite images and Google Earth. The analysis is conducted for 2004, 2013, 2017 and 2021. The results are analyzed for three periods: 2004 – 2013, 2013 – 2017, and 2017 – 2021. Agricultural land and

urbanized areas are the LULC classes that increased the most between 2004 and 2013 (24.86% and 12.29%, respectively). On the other hand, forestland decreased in this period (-16.23%). Urbanized areas continued to increase between 2013 and 2017 (8.56%), while there was no change in forestland in this period. Finally, between 2017 and 2021, urbanized areas increased 10.61%. Forestland, agricultural land and water bodies decreased in smaller amounts in this period (-0.21%, -0.31% and -0.71%, respectively). It can be seen that urbanized areas continuously increase in the region and this result is compatible with the other studies' findings that were conducted in the vicinity of Silifke (Alphan, 2003; Derse & Alphan, 2012; Zadbagher et al., 2018). Effect of increase in urbanized areas on flood risks in the study are are evaluated using 1D/2D hydraulic model in this study.

6.3 Nontationarity analysis

Findings of nonstationarity analysis provided within the scope of this thesis is presented in our article named "Nonstationary Frequency Analysis of Annual Maximum Flow Series: Climate Change versus Land Use / Land Cover Change" which is provided in Appendix A. A summary of its major findings is given here. AMFS are analyzed using seven covariates and six probability distributions for the study region. 841 NS models for each distribution are developed using all combinations of at most two covariates for location and scale parameters of the distribution. Finding the best combination is challenging; trying as many combinations as possible is a good idea, but it is time-consuming. Hence, the end-use of the study should be determined at the very first stage, and the performance of NS models should be evaluated accordingly.

Selecting the best distribution solely based on statistical measures may be misleading. The results of this study indicate that the GEV distribution performs the best among the other distributions with respect to AIC scores. Nevertheless, the best NS model's calculated 500-year peak discharge, Q_{500}, is 19 standard deviations outside the observed maximum annual discharge. Thus, selecting GEV distribution

to be used in flood risk analysis is not reasonable. For the basin, Gumbel distribution is selected as the best distribution, considering both the AIC scores and peak discharges. Q_{500} value of the best NS model with Gumbel distribution is approximately 1% greater than the maximum of AMFS. However, due to possible uncertainties in hydrological studies, peak discharges of good-performing NS models should be considered instead of only the best ones in flood management studies. RI and Temp are the covariates of the best NS model for Gumbel distribution. Another conclusion is that if the performance of the stationary model is not good, the performance of the NS models is not good either. For this reason, the performance of the stationary model might be used as an indicator to eliminate probability distributions.

The determination of the source of nonstationarity is of significant importance in the estimation of peak discharges. In the study area, NS models incorporating LULC-related covariates, namely RI and NDVI, demonstrate superior performance to those incorporating CC-related covariates. RI is the best-performing covariate across all probability distributions. Additionally, the use of NDVI as a LULC-related covariate, also demonstrates promising results. However, estimating LULC-related covariates for future scenarios may present certain challenges. While the estimation of NDVI is not straightforward, RI might be estimated adequately if basin management is well-planned for the future. Therefore, it is important to select covariates with consideration of their limitations.

6.4 Hydrological model

The development of the hydrological model for this study area is challenging due to the complexity of the basin and availability of limited data. The most problematic part of the hydrological model development is the existence of many hydraulic structures since the operational data of these structures cannot be obtained. For this reason, these hydraulic structures are modeled using a simplified approach: The hydrological model is developed considering the period before the construction of

the first major hydraulic structure. The calibration period is selected between 1965 and 1978, and the validation period is selected between 1981 and 1986. Then, to represent the rainfall-runoff behavior of the current basin, these structures are entered into the model, and they are represented with storage-discharge and elevation-storage, and elevation-area curves. The calibrated and validated model is tested between 2016 and 2020. The model results are satisfactory based on the statistical measures.

The hydrological model is run between 2025 and 2100 using the RCM outputs. AMFS is obtained between 2025 and 2100, and flood hydrographs for different return periods are generated for stationary and nonstationary conditions. The hydrographs are generated for five scenarios to investigate the effects of CC and LULC. For S2 (M5 RCM + NS model with time covariate + hydraulic structures are at full conditions), Q_{500} peak discharge is the maximum (2550.0 m^3/s), while for S1 (M5 RCM + NS model with time covariate), it is the lowest (1018.2 m^3/s). The results also showed a decrease in the peak discharges in the future. Q_{500} value (1589.9 m^3/s) for S3 (stationary model with M5 RCM) is less than the Q_{500} value (2256.2 m^3/s) for S0 (stationary model). Furthermore, when peak discharges of the same return periods are compared, peak discharges for S0 are greater than the others' peak discharges except the Q_{500} value for S2.

6.5 Combined 1D/2D hydraulic model

The combined 1D/2D hydraulic model is run for different return periods and five scenarios. The largest inundation occurs in the stationary scenario (S0) for 2, 5, 10, 25, 50 and 100-year floods. On the other hand, for 500-year flood, the inundated area of S2 (123.8 km^2) is the greatest which is the worst-case scenario that full reservoir conditions are considered. In contrast, the lowest inundation and calculated economic damage are observed in the nonstationary scenario (S1) due to the lowest peak discharges in this scenario. The inundated area of S1 for 2-year flood (12.2 km^2) is approximately five times lower than the inundated area of S0 (58.6 km^2).

On the other hand, this difference decreases for 500-year flood (79.6 km^2 and 117.1 km^2 for S1 and S0, respectively). However, the inundated area of the stationary scenario, S3 with a climate model (97.8 km^2) is greater than that of S1 and lower than that of S0 for 500-year flood. Moreover, in scenario S4, the urban area is increased according to the LULC change projections and this resulted in larger inundated area (84.5 km^2) than that of S1 for 500-year flood.

When economic damage values are compared for 500-year flood, it is greatest for S4 (1.46E+07 €). S2 (7.63E+06 €) and S0 (6.08E+06 €) comes after S4. In the case of the 100-year flood, the economic damage is the greatest for S0 (4.53E+06 €). The economic damage values are the same (7.34E+04 €) for S1 and S4 for the 2-year flood because the inundated areas are also the same (12.2 km^2). Calculated economic damage values are not fully realistic for Türkiye due to the use of not country-specific depth-damage curves (Huizinga et al., 2017) and unit costs (Haer et al., 2020). The curves generated for the European Continent (Huizinga et al., 2017) are used in this study. Hence, the economic damage estimations have some uncertainties. The results should be evaluated considering this fact. However, we believe that the relative evaluation of these scenarios is still useful.

6.6 Agent-based model

The necessity for FRM studies has increased significantly in light of the impacts of CC and urbanization increases. It is also essential to integrate the agents (i.e., stakeholders of the flood risks) into the FRM studies. Detailed results about ABM are presented in our article named “Integration of climate change impacts and agent-based model to flood risk evaluation in an urbanized area” given in Appendix B, and the major conclusions based on that article are summarized here.

The significance of the agents in FRM is demonstrated using 11 scenarios and 100 realizations in each of these scenarios in our study. Firstly, it is imperative that the public agent be included in FRM studies, and conducting a survey to evaluate the

public's behavior in the context of flood events is crucial. In this study, the average economic damage of the scenario in which the survey results are employed (2.59E+05 €) is found to be greater than that of the scenario with randomly generated values (2.09E+05 €). This illustrates the importance of the surveys. The absence of a survey in the study area precludes the realistic evaluation of the public's reactions to flood events. This is of particular importance in regions where flood awareness is limited. The economic damage is typically greater in scenarios with a reactive government than in those with a proactive government. For example, the average economic damage is 1.92E+05 € for the ProGo50 scenario (proactive government that takes action against a 50-year flood) while it is 3.93E+05 € for the ReGo50 scenario (reactive government that takes action against a 50-year flood). The lowest average economic damage value (9.58E+04 €) is observed in the PubSur-ProGo100 Scenario (Public agent actions based on survey results and proactive government that takes action against 100-year flood). This outcome demonstrates the necessity of integrating both public and government agents into the framework of FRM.

Another conclusion of this study is that the timing of a severe flood event is of significant importance. The economic damage value of the Realization that a serious flood event occurs earlier (e.g., 8.47E+04 € for ReGo50 scenario) is less than the Realization that a serious flood event occurs late (e.g., 1.62E+05 € for ReGo50 scenario). The timing of a serious flood event is particularly important for the reactive government. It can be seen that economic damage decreases 48% when a serious flood event occurs earlier for the scenarios with a reactive government.

B/C of the scenarios involving the government taking action against 50-year flood are greater than those involving the government taking action against 100-year flood. For the ProGo50 scenario, B/C varies between 1.18 and 1.68 with an average value of 1.65, while it changes between 1.11 and 1.34 with an average value of 1.32 for the ProGo100 scenario. The situation is similar in the scenarios with the reactive government as well. This is due to the high cost of the 100-year flood action. It can be inferred that B/C is always greater than 1.0 in the scenarios with the proactive government, while it is less than 1.0 for some Realizations in the scenarios with the

reactive government. This is a significant conclusion, as the consequences of flooding may be devastating destructive if the government is reactive and do not implement flood measure before experiencing major floods.

The final conclusion is that the public tends to forget the consequences of floods after approximately nine years. It should be noted that this value highly depends on the selected threshold values for risk and coping perceptions. Consequently, this also supports the significance of disseminating information about floods, as it is of paramount importance that the public is aware of the potential consequences of such events. It is imperative that the potential consequences of floods should not be underestimated. This is especially important for the regions where flood events occur frequently.

6.7 Future work

Some limitations were encountered during the study. Future work is suggested to overcome these limitations and improve findings of the study more realistic. Firstly, the number of respondents in the survey can be increased to get more realistic results. Furthermore, long-term data can be retained and collected from agents at different times. It is important to consider the advantages and disadvantages of this approach. Developed ABM can be also used in similar places. Secondly, specific studies for Türkiye can be conducted to get realistic economic damage results. Thirdly, the government agent action can be diversified, such as the construction of a dam upstream of the district center, river bed regulation, etc. and different actions can be also considered for the public agent. Finally, the coefficients and threshold values used in ABM can be calibrated based on a more detailed analysis.

REFERENCES

Abebe, Y., Ghorbani, A., Nikolic, I., Vojinovic, Z., & Sanchez, A. (2019). Flood risk management in Sint Maarten – A coupled agent-based and flood modelling method. *Journal of Environmental Management, 248*.

Adelekan, I., & Asiyanbi, A. (2016). Flood risk perception in flood-affected communities in Lagos, Nigeria. *Natural Hazards, 80*, 445-469.

Aik, D., Ismail, M., & Muharam, F. (2020). Land Use/Land Cover Changes and the Relationship with Land Surface Temperature Using Landsat and MODIS Imageries in Cameron Highlands, Malaysia. *Land, 9*. doi:http://dx.doi.org/10.3390/land9100372

Akaike, H. (1974). A New Look at the Statistical Model Identification. *IEEE Transactions On Automatic Control*, 716-723.

Akter, T., Quevauviller, P., Eisenreich, S., & Vaes, G. (2018). Impacts of climate and land use changes on flood risk management for the Schijn River, Belgium. *Environmental Science and Policy, 89*, 163-175.

Alam, A., Bhat, M., & Maheen, M. (2020). Using Landsat satellite data for assessing the land use and land cover change in Kashmir Valley. *GeoJournal, 85*, 1529-1543.

Alawamy, J., Balasundram, S., Hanif, A., & Sung, C. (2020). Detecting and Analyzing Land Use and Land Cover Changes in the Region of Al-Jabal Al-Akhdar, Libya Using Time-Series Landsat Data from 1985 to 2017. *Sustainability, 12*. doi:http://dx.doi.org/10.3390/su12114490

Alfieri, L., Feyen, L., Dottori, F., & Bianchi, A. (2015). Ensemble flood risk assessment in Europe under high end climate scenarios. *Global Environmental Change, 35*, 199-212.

Allam, M., Bakr, N., & Elbably, W. (2019). Multi-temporal assessment of land use/land cover change in arid region based on landsat satellite imagery:

Case study in Fayoum Region, Egypt. *Remote Sensing Applications: Society and Environment, 14*, 8-19.

Alphan, H. (2003). Land-use change and urbanization of Adana, Turkey. *Land Degradation & Development, 14*(6), 575-586.

Anzolin, G., Chaffe, P., Vrugt, J., & AghaKouchak, A. (2023). Using climate information as covariates to improve nonstationary flood frequency analysis in Brazil. *Hydrological Sciences Journal*, 645-654.

Arnell, N., & Gosling, S. (2016). The impacts of climate change on river flood risk at the global scale. *Climatic Change, 134*, 387-401.

Attems, M., Thaler, T., Genovese, E., & Fuchs, S. (2020). Implementation of property-level flood risk adaptation (PLFRA) measures: Choices and decisions. *WIREs Water, 7*(1).

Avand, M., Moradi, H., & Lasboyee, M. H. (2021). Using machine learning models, remote sensing, and GIS to investigate the effects of changing climates and land uses on flood probability. *Journal of Hydrology, 595*. doi:https://doi.org/10.1016/j.jhydrol.2020.125663

Aziz, R., Yucel, I., & Yozgatligil, C. (2020). Nonstationarity impacts on frequency analysis of yearly and seasonal extreme temperature in Turkey. *Atmospheric Research, 238*, 1-13.

Azizi, S., Ilderomi, A., & Noori, H. (2021). Investigating the effects of land use change on flood hydrograph using HEC-HMS hydrologic model (case study: Ekbatan Dam). *Natural Hazards, 109*, 145-160.

Bai, Y., Zhang, Z., & Zhao, W. (2019). Assessing the Impact of Climate Change on Flood Events Using HEC-HMS and CMIP5. *Water, Air, & Soil Pollution, 230*.

Balov, M. N. (2020). Influence of Climate Change on the Flood Disasters in Bursa, Turkey. *International Journal of Engineering Technologies IJET, 6*(4), 62-68.

Bangalore, M., Smith, A., & Veldkamp, T. (2019). Exposure to Floods, Climate Change, and Poverty in Vietnam. *Economics of Disasters and Climate Change, 3*, 79-99.

Bayazıt, Y., Koç, C., & Bakış, R. (2021). Urbanization impacts on flash urban floods in Bodrum Province, Turkey. *Hydrological Sciences Journal, 66*(1).

Bazrafshan, J., Cheraghalizadeh, M., & Shahgholian, K. (2022). Development of a Non-stationary Standardized Precipitation Evapotranspiration Index (NSPEI) for Drought Monitoring in a Changing Climate. *Water Resour Management*, 3523-3543.

Beckers, A., Dewals, B., Erpicum, S., Dujardin, S., Detrembleur, S., Teller, J., . . . Archambeau, P. (2013). Contribution of land use changes to future flood damage along the river Meuse in the Walloon region. *Natural Hazards and Earth System Sciences, 13*, 2301-2318.

Beden, N., & Keskin, A. (2021). Flood map production and evaluation of flood risks in situations of insufficient flow data. *Natural Hazards*, 2381-2408.

Begueria, S., Martinez, M., Serrano, S., Moreno, J., & Kenawy, A. (2010). Assessing trends in extreme precipitation events intensity and magnitude using non-stationary peaks-over-threshold analysis: a case study in northeast Spain from 1930 to 2006. *International Journal of Climatology, 31*(14), 2102-2114.

Betsholtz, A., & Nordlöf, B. (2017). *Potentials and limitations of 1D, 2D and coupled 1D-2D flood modelling in HEC-RAS A case study on Höje river (Master Thesis).* Lund: Lund University.

Bilici, Ö., & Everest, A. (2017). 29 ARALIK 2016 MERSİN SELİNİN METEOROLOJİK ANALİZİ VE İKLİM DEĞİŞİKLİĞİ BAĞLANTISI. *Doğu Coğrafya Dergisi*, 227-250.

Blöschl, G., Hall, J., Viglione, A., & al., e. (2019). Changing climate both increases and decreases European river floods. *Nature, 573*, 108-111.

Bormudoi, A., & Nagai, M. (2017). Perception of risk and coping capacity: A study in Jiadhal Basin, India. *International Journal of Disaster Risk Reduction, 21*, 376-383.

Bossa, A., Akpaca, J., Hounkpe, J., Yira, Y., & Badou, D. (2023). Non-Stationary Flood Discharge Frequency Analysis in West Africa. *GeoHazards, 4*(3), 316-327.

Botzen, W., Aerts, J., & van den Bergh, J. (2009). Dependence of flood risk perceptions on socioeconomic and objective risk factors. *Water Resources Research, 45*(10).

Brody, S. D., Highfield, W. E., & Blessing, R. (2015). An Analysis of the Effects of Land Use and Land Cover on Flood Lossesalong the Gulf of Mexico Coast from 1999 to 2009. *Journal of the American Water Resources Association, 51*(6), 1556-1567.

Bronstert, A. (2003). Floods and Climate Change: Interactions and Impacts. *Risk Analysis, 23*(3), 545-557.

Bubeck, P., Botzen, W., Kreibich, H., & Aerts, J. (2013). Detailed insights into the influence of flood-coping appraisals on mitigation behaviour. *Global Environmental Change, 23*(5), 1327-1338.

Bubeck, P., Botzen, W., Laudan, J., Aerts, J., & Thieken, A. (2018). Insights into Flood-Coping Appraisals of Protection Motivation Theory: Empirical Evidence from Germany and France. *Risk Analysis, 38*(6), 1239-1257.

Bubeck, P., Botzen, W., Suu, L., & Aerts, J. (2012). Do flood risk perceptions provide useful insights for flood risk management? Findings from central Vietnam. *Journal of Flood Risk Management, 5*(4), 295-302.

Bucak, T., Trolle, D., Tavşanoğlu, Ü., Çakıroğlu, A., Özen, A., Jeppesen, E., & Beklioğlu, M. (2018). Modeling the effects of climatic and land use changes on phytoplankton and water quality of the largest Turkish freshwater lake: Lake Beyşehir. *Science of Total Environment, 621*, 802-816.

Buchenrieder, G., Brandl, J., & Balgah, A. (2021). The Perception of Flood Risks: A Case Study of Babessi in Rural Cameroon. *International Journal of Disaster Risk Science, 12*, 1-21.

Buldur, A., Pınar, A., & Başaran, A. (2007). 05-07 MART 2004 TARİHLİ GÖKSU NEHRİTAŞKINI VE SİLİFKE'YE ETKİSİ. *Selçuk Üniversitesi Sosyal Bilimler Enstitüsü Dergisi*, 139-160.

Butchart, S. H., Walpole, M., Collen, B., van Strien, A., Scharlemann, J. P., Almond, R. E., & . . . Watson, R. (2010). Global Biodiversity: Indicators of Recent Declines. *Science, 328*(5982), 1164-1168.

Cabrera, J., & Lee, H. S. (2018). Impacts of Climate Change on Flood-Prone Areas in Davao Oriental, Philippines. *Water, 10*(7). doi:https://doi.org/10.3390/w10070893

Chang, H., & Franczyk, J. (2008). Climate Change, Land-Use Change, and Floods: Toward an Integrated Assessment. *Geography Compass*, 1549-1579.

Chen, M., Papadikis, K., & Jun, C. (2021). An investigation on the non-stationarity of flood frequency across the UK. *Journal of Hydrology, 597*.

Chen, Q., Chen, H., Zhang, J., Hou, Y., Shen, M., Chen, J., & Xu, C. (2020). Impacts of climate change and LULC change on runoff in the Jinsha River Basin. *Journal of Geographical Sciences, 30*, 85-102.

Chen, Y. –J., Lin, H. –J., Liou, J. –J., Cheng, C. –T., & Chen, Y. M. (2022). Assessment of Flood Risk Map under Climate Change RCP8.5 Scenarios in Taiwan. *Water, 14*(2), 207.

Cheng, L., AghaKouchak, A., Gilleland, E., & Katz, R. (2014). Non-stationary extreme value analysis in a changing climate. *Climatic Change, 127*, 353-369.

Coles, S. (2001). *An Introduction to Statistical Modeling of Extreme Values.* London: Springer.

Condon, L. E., Gangopadhyay, S., & Pruitt, T. (2015). Climate change and non-stationary flood risk for the upper Truckee River basin. *Hydrology and Earth System Sciences, 19*, 159-175.

Congalton, R. (1991). A review of assessing the accuracy of classifications of remotely sensed data. *Remote Sensing of Environment, 37*(1), 35-46.

Cortez, B., Pires, G., Diaz, A., Fonseca, H., & Oliveira, L. (2022). Nonstationary extreme precipitation in Brazil. *Hydrological Sciences Journal*, 1372-1383.

Costache, R., Pham, Q. B., Corodescu-Roşca, E., Cîmpianu, C., Hong, H., Thuy Linh, N. T., . . . Pham, B. T. (2020). Using GIS, remote sensing, and machine learning to highlight the correlation between the land-use/land-cover changes and flash-flood potential. *Remote Sensing, 12*(9), 1422.

Coughlan, M., Cronin, P., & Ryan, F. (2013). Survey research: Process and limitations. *International Journal of Therapy and Rehabilitation, 16*(1).

CRED & UNDRR. (2020). *Human cost of disasters: An overview of the last 20 years 200-2019.*

Cui, H., Jiang, S., Gao, B., Ren, L., Xiao, W., Wang, M., . . . Xu, C. (2023). On method of regional non-stationary flood frequency analysis under the influence of large reservoir group and climate change. *Journal of Hydrology*.

Dankers, R., & Feyen, L. (2008). Climate change impact on flood hazard in Europe: An assessment based on high-resolution climate simulations. *Journal of Geophysical Research, 113*. doi: https://doi.org/10.1029/2007JD009719

Dawson, R., Peppe, R., & Wang, M. (2011). An agent-based model for risk-based flood incident management. *Natural Hazards, 59*, 167-189.

Debele, S. E., Strupczewski, W. G., & Bogdanowicz, E. (2017). A comparison of three approaches to non-stationary flood frequency analysis. *Acta Geophysica, 65*, 863-883.

Deidda, R., Marrocu, M., Caroletti, G., Pusceddu, G., Langousis, G., Langousis, A., . . . Speranza, A. (2013). Regional climate models' performance in representing precipitation and temperature over selected Mediterranean areas. *Hydrology and Earth System Sciences, 17*, 5041-5059.

Deng, Z., Zhu, X., He, Q., & Tang, L. (2019). Land use/land cover classification using time series Landsat 8 images in a heavily urbanized area. *Advances in Space Research, 63*, 2144-2154.

Derse, M. A., & Alphan, H. (2012). Sürdürülebilir Arazi Kullanım Planlaması için Uzaktan Algılama Verilerine Dayalı Bölgesel Değişim Tespiti: Erdemli (Mersin) Örneği. *Ç.Ü. Fen ve Mühendislik Bilimleri Dergisi, 28*(5), 29-38.

Dezso, Z. B., Pongracz, R., & Barcza, Z. (2005). Analysis of land-use/land-cover change in the Carpathian Region based on remote sensing techniques. *Physics and Chemistry of the Earth, Parts A/B/C, 30*, 109-115.

Dino, I. G., & Akgül, C. M. (2019). Impact of climate change on the existing residential building stock in Turkey: An analysis on energy use, greenhouse gas emissions and occupant comfort. *Renewable Energy, 141*, 828-846.

DSİ Strateji Geliştirme Dairesi Başkanlığı. (2020). *2019 YILI FAALİYET RAPORU.* Retrieved from http://www.dsi.gov.tr/docs/stratejik-plan/dsi-2019-faaliyet-raporu.pdf?sfvrsn=2

Dubbelboer, J., Nikolic, I., Jenkins, K., & Hall, J. (2017). An Agent-Based Model of Flood Risk and Insurance. *Journal of Artificial Societies and Social Simulation, 20*(1).

Dudgeon, D., Arthington, A., Gessner, M., Kawabata, Z., Knowler, D., Leveque, C., . . . Sullivan, C. (2006). Freshwater biodiversity: importance, threats, status and conservation challenges. *Biological Reviews, 81*, 163-182.

Dutrieux, L. P., Verbesselt, J., Kooistra, L., & Herold, M. (2015). Monitoring forest cover loss using multiple data streams, a case study of a tropical dry forest in Bolivia. *ISPRS Journal of Photogrammetry and Remote Sensing*, 112-125.

Dutta, D., Wright, W., Nakayama, K., & Sugawara, Y. (2013). Design of Synthetic Impact Response Functions for Flood Vulnerability Assessment under Climate Change Conditions: Case Studies in Two Selected Coastal Zones in Australia and Japan. *Natural Hazards Review, 14*(1), 52-65.

Easterling, D., Meehl, G., Parmesan, C., Changnon, S., Karl, T., & Mearns, L. (2000). Climate Extremes: Observations, Modeling, and Impacts. *Science, 289*(5487), 2068-2074.

Eastoe, E. T. (2009). Modelling non-stationary extremes with application to surface level ozone. *Appl. Statist.*, 25-45.

El-Kawy, O., Rod, J., Ismail, H., & Suliman, A. (2011). Land use and land cover change detection in the western Nile delta of Egypt using remote sensing data. *Applied Geography, 31*, 483-494.

Erlat, E., Türkeş, M., & Aydin-Kandemir, F. (2021). Observed changes and trends in heatwave characteristics in Turkey since 1950. *Theoretical and Applied Climatology, 145*(1), 137-157.

EURO-CORDEX. (2021, December 21).

EURO-CORDEX. (2021, 12 21). *EURO-CORDEX Errata Page, Errata Table*. Retrieved from EURO-CORDEX: https://www.euro-cordex.net/078730/index.php.en

European Environment Agency. (2020). *CORINE Land Cover 2018 (vector), Europe, 6-yearly - version 2020_20u1, May 2020*. doi:https://doi.org/10.2909/71c95a07-e296-44fc-b22b-415f42acfdf0

Fan, F., Weng, Q., & Wang, Y. (2007). Land Use and Land Cover Change in Guangzhou, China, from 1998 to 2003, Based on Landsat TM/ETM+ Imagery. *Sensors, 7*, 1323-1342.

Faulkner, D., Warren, S., Spencer, P., & Sharkey, P. (2020). Can we still predict the future from the past? Implementing non-stationary flood frequency analysis in the UK. *Journal of Flood Risk Management, 13*(1).

Feng, B., Zhang, Y., & Bourke, R. (2021). Urbanization impacts on flood risks based on urban growth data and coupled flood models. *Natural Hazards, 106*, 613-627.

Feyen, L., Barredo, J. I., & Dankers, R. (2009). Implications of global warming and urban land use change on flooding in Europe. In *Water and Urban Development Paradigms* (pp. 217-225). London: CRC Press.

Feyen, L., Dankers, R., Bodis, K., Salamon, P., & Barredo, J. I. (2012). Fluvial flood risk in Europe in present and future climates. *Climatic Change, 112*, 47-62.

Flato, G., Marotzke, J., Abiodun, B., Braconnot, P., Chou, S., Collins, W., . . . Rummukainen, M. (2013). *Evaluation of Climate Models. In: Climate*

Change 2013: The Physical Science Basis." Contribution of Working Group I to the Fifth Assessment Report of the Intergovernmental Panel on Climate Change. Cambridge and New York: Cambridge University Press.

Fu, P., & Weng, Q. (2016). A time series analysis of urbanization induced land use and land cover change and its impact on land surface temperature with Landsat imagery. *Remote Sensing Environment, 175*, 205-214.

Fujihara, Y., Tanaka, K., Watanabe, T., Nagano, T., & Kojiri, T. (2008). Assessing the impacts of climate change on the water resources of the Seyhan River Basin in Turkey: Use of dynamically downscaled data for hydrologic simulations. *Journal of Hydrology, 353*, 33-48.

Game, P., Wang, M., Audra, P., & Gourbesville, P. (2023). Flood modelling for a real-time decision support system of the covered Lower Paillons River, Nice, France. *ournal of Hydroinformatics, 25*(5), 1884-1908.

Ganguli, P., & Coulibaly, P. (2017). Does nonstationarity in rainfall require nonstationary intensity–duration–frequency curves? *Hydrology and Earth System Sciences, 21*, 6461-6483.

Gao, L., Huang, J., Chen, X., Chen, Y., & Liu, M. (2017). Risk of Extreme Precipitation under Nonstationarity Conditions during the Second Flood Season in the Southeastern Coastal Region of China. *Journal of Hydrometeorology, 18*, 669-681.

Garijo, C., & Mediero, L. (2018). Influence of climate change on flood magnitude and seasonality in the Arga River catchment in Spain. *Acta Geophysica, 66*, 769-790.

Gilbert, N. (2008). *Agent-Based Models.* United States of America: Sage Publications.

Gilleland, E., & Katz, R. (2016). extRemes 2.0: An Extreme Value Analysis Package in R. *Journal of Statistical Software, 72*(8), 1-39.

Giorgi, F. (2006). Climate change hot-spots. *Geophysical Research Letters, 33*, 1-4.

Giorgi, F., & Gutowski Jr, W. J. (2015). Regional dynamical downscaling and the CORDEX initiative. *Annual review of environment and resources, 40*, 467-490.

Giorgi, F., & Lionello, P. (2008). Climate change projections for the Mediterranean region. *Global and Planetary Change, 63*, 90-104.

Göksel, Ç., & Balçık, F. B. (2019). Land Use and Land Cover Changes Using Spot 5 Pansharpen Images; A Case Study in Akdeniz District, Mersin-Turkey. *Turkish Journal of Engineering, 3*(1), 32-38.

Gu, X., Zhang, Q., Singh, V., Xiaoa, M., & Cheng, J. (2017). Nonstationarity-based evaluation of flood risk in the Pearl River basin: changingpatterns, causes and implications. *Hydrological Sciences Journal, 62*(2), 246-258.

Gül, G., Aşıkoğlu, Ö., Gül, A., Yaşoğlu, F., & Benzeden, E. (2013). Nonstationarity in Flood Time Series. *Journal of Hydrologic Engineering, 19*(7).

Gül, G., Rosbjerg, D., Gül, A., Ondracek, M., & Dikgola, K. (2010). Assessing climate change impacts on river flows and environmental flow requirements at catchment scale. *Ecohydrology*, 28-40.

Güler, M., Yomralıoğlu, T., & Reis, S. (2007). Using landsat data to determine land use/land cover changes in Samsun, Turkey. *Environmental Monitoring and Assessment, 127*, 155-167.

Guzha, A., Rufino, M., Okoth, S., Jacobs, S., & Nobrega, R. (2018). Impacts of land use and land cover change on surface runoff, discharge and low flows: Evidence from East Africa. *Journal of Hydrology: Regional Studies, 15*(2018), 49-67.

Haer, T., Botzen, W., de Moel, H., & Aerts, J. (2017). Integrating Household Risk Mitigation Behavior in FloodRisk Analysis: An Agent-Based Model Approach. *Risk Analysis, 37*(10), 1977-1992.

Haer, T., Husby, T. G., Botzen, W. J., & Aerts, J. C. (2020). The safe development paradox: An agent-based model for flood risk under climate change in the European Union. *Global Environmental Change, 60*.

Hallegatte, S., Ranger, N., Bhattacharya, S., Bachu, M., Priya, S., Dhore, K., . . . Herweijer, C. (2010). *Flood Risks, Climate Change Impacts and Adaptation Benefits in Mumbai: An Initial Assessment of Socio-Economic Consequences of Present and Climate Change Induced Flood Risks and of Possible Adaptation Options.* Paris: Organization for Economic Co-operation and Development Publishing.

Hammond, R. (2015). Considerations and best practices in agent-based modeling to inform policy. In *Assessing the use of agent-based models for tobacco regulation.* National Academies Press (US).

Hammond, R. (2015). Considerations and Best Practices in Agent-Based Modeling to Inform Policy. In *Assessing the Use of Agent-Based Models for Tobacco Regulation* (pp. 161-193). Washington DC: National Academies Press.

Harada, M., Maruya, Y., Kojima, T., Matsuoka, D., Nakagawa, Y., Kawahara, S., & Araki, F. (2020). Flood Frequency Analysis and Impact Assessment for Climate Change in the Nagara River Basin. *Journal of JSCE, 8*, 79-86.

Hassan, Z., Shabbir, R., Ahmad, S., Malik, A., Aziz, N., Butt, A., & Erum, S. (2016). Dynamics of land use and land cover change (LULCC) using geospatial techniques: a case study of Islamabad, Pakistan. *SpringerPlus, 5*(812).

Hassani-Mahmooei, B., & Parris, B. (2012). Climate change and internal migration patterns in Bangladesh: an agent-based model. *Environment and Development Economics, 17*(6), 763-780.

HEC-HMS. (2023, July 14). *Youtube*. Retrieved from HEC HMS Model Calibration Strategies: https://www.youtube.com/watch?v=t5uzhfK-kFA

Hesarkazzazi, S., Arabzadeh, R., Hajibabaei, M., Rauch, W., Kjeldsen, T., Prosdocimi, I., . . . Sitzenfrei, R. (2021). Stationary vs non-stationary modelling of flood frequency distribution across northwest England. *Hydrological Sciences Journal*, 729-744.

Hirabayashi, H., Mahendran, R., Koirala, S., Konoshima, L., Yamazaki, D., Watanabe, S., . . . Kanae, S. (2013). Global flood risk under climate change. *Nature Climate Change, 3*, 816-821.

Holley, J., McComas, K., Lambert, C., Snider, N., & Tucker, G. (2022). Responding to flood risk in Louisiana: the roles of place attachment, emotions, and location. *Natural Hazards, 113*, 615-640.

Hounkpe, J., Diekkrüger, B., Badou, D., & Afouda, A. (2015). Non-Stationary Flood Frequency Analysis in the Ouémé River Basin, Benin Republic. *Hydrology, 2*(4), 210-229.

Huang, C., Zhang, C., He, Y., Liu, Q., Li, H., Su, F., . . . Bridhikitti, A. (2020). Land Cover Mapping in Cloud-Prone Tropical Areas Using Sentinel-2 Data: Integrating Spectral Features with Ndvi Temporal Dynamics. *Remote Sensing, 12*(7).

Huizinga, J., De Moel, H., & Szewczyk, W. (2017). *Global flood depth-damage functions: Methodology and the database with guidelines.* Luxembourg: Publications Office of the European Union.

Hunter, D. (2002). *Risk Perception and Risk Tolerance in Aircraft Pilots.* Washington, DC: Office of Aerospace Medicine.

Hydrologic Engineering Center. (2023). *HEC-SSP Version 2.3.*

Igarashi, K., Koichiro, K., Tanaka, N., & Aranyabhaga, N. (2018). Prediction of the Impact of Climate Change and Land Use Change on Flood Discharge in

the Song Khwae District, Nan Province, Thailand. *Journal of Climate Change, 5*(1), 1-8.

İhlas Haber Ajansı. (2017, March 15). *Silifke'de Göksu ırmağının debisi yükseldi, bin 109 dekar alan zarar gördü.* Retrieved from İHA: https://www.iha.com.tr/mersin-haberleri/-1648015

IPCC. (2014). *Climate Change 2014 Synthesis Report.* Geneva.

IPCC. (2018). *An IPCC Special Report on the impacts of global warming of 1.5°C above pre-industrial levels and related global greenhouse gas emission pathways, in the context of strengthening the global response to the threat of climate change,... to eradicate poverty.*

IPCC. (2021). *Climate Change 2021: The Physical Science Basis. Contribution of Working Group I to the Sixth Assessment Report of the Intergovernmental Panel on Climate Change.* Cambridge University Press.

Isensee, L., Pinheiro, A., & Detzel, D. (2021). Dam Hydrological Risk and the Design Flood Under Non-stationary Conditions. *Water Resources Management*, 1499-1512.

Jaw, T., Li, J., Hsu, K. l., & Sorooshian, S. D. (2015). Evaluation for Moroccan dynamically downscaled precipitation from GCM CHAM5 and its regional hydrologic response. *Journal of Hydrology: Regional Studies*, 359-378.

Jenkins, K., Surminski, S., Hall, J., & Crick, F. (2017). Assessing surface water flood risk and management strategies under future climate change: Insights from an Agent-Based Model. *Science of the Total Environment, 595*, 159-168.

Jonkman, S., & Vrijling, J. (2008). Loss of life due to floods. *Journal of Flood Risk Management*, 43-56.

Kafy, A., Rahman, M., Faisal, A., Hasan, M., & Islam, M. (2020). Modelling future land use land cover changes and their impacts on land surface

temperatures in Rajshahi, Banghladesh. *Remote Sensing Applications: Society and Environment, 18*. doi:https://doi.org/10.1016/j.rsase.2020.100314

Kang, L., Jiang, S., Hu, X., & Li, C. (2019). Evaluation of Return Period and Risk in Bivariate Non-Stationary Flood Frequency Analysis. *Water, 11*(1).

Kara, F., & Yücel, İ. (2015). Climate change effects on extreme flows of water supply area in Istanbul: utility of regional climate models and downscaling method. *Environmental Monitoring and Assessment, 187*(580), 1-18.

Karagiannis, G., Chondrogiannis, S., Krausmann, E., & Turksezer, Z. (2017b). *Power Grid Recovery After NaturalHazard Impact.* European Commission.

Karagiannis, G., Turksezer, Z., Alfieri, L., Feyen, L., & Krausmann, E. (2017a). *Climate Change and Critical Infrastructure.* JRC.

Kentel, E., Yücel, İ., Mesta, B., Akgün, Ö., Özcan, C., Ercan, E., . . . Matur, İ. (2021). *TÜBİTAK Antalya Havzası'nda İklim Değişikliğinin Debi ve HES Enerji Üretimine Etkilerinin İncelenmesi Projesi (Pr No: 118Y365).* Ankara: TÜBİTAK.

Klijn, F., De Bruijn, K. M., Knoop, J., & Kwadijk, J. (2012). Assessment of the Netherlands' Flood Risk Management Policy Under Global Change. *AMBIO, 41*, 180-192.

Kostopoulou, E., & Jones, P. D. (2005). Assessment of climate extremes in the Eastern Mediterranean. *Meteorology and Atmospheric Physics, 89*(1), 69-85.

Kreibich, H., Bubeck, P., Van Vliet, M., & De Moel, H. (2015). A review of damage-reducing measures to manage fluvial flood risks in a changing climate. *Mitigation and Adaptation Strategies for Global Change* , 967-989.

Kuglitsch, F. G., Toreti, A., Xoplaki, E., Della-Marta, P. M., Zerefos, C. S., Türkeş, M., & Luterbacher, J. (2010). Heat wave changes in the eastern Mediterranean since 1960. *Geophysical Research Letters, 37*(4).

Landis, J., & Koch, G. (1977). The Measurement of Observer Agreement of Categorical Data. *Biometrics, 33*(1), 159-174.

Laudan, J. (2019). *Changing Susceptibility of Flood-prone Residents in Germany: Mental Coping and Mitigation Behaviour in the Context of Different Flood Types.* Potsdam: University of Potsdam.

Leclerc, M., & Ouarda, T. (2007). Non-stationary regional flood frequency analysis at ungauged sites. *Journal of Hydrology, 343*(3-4), 254-265.

Liu, D., Li, M., Li, Y., & Chen, H. (2022). Assessment of Public Flood Risk Perception and Influencing Factors: An Example of Jiaozuo City, China. *Sustainability, 14*(15).

Liu, D., Li, Y., Shen, X., Xie, Y., & Zhang, Y. (2018). Flood risk perception of rural households in western mountainous regions of Henan Province, China. *International Journal of Disaster Risk Reduction, 27*, 155-160.

Liu, W., Feng, Q., Engel, B., Yu, T., Zhang, X., & Qian, Y. (2023). A probabilistic assessment of urban flood risk and impacts of future climate change. *Journal of Hydrology, 618*.

Liu, Y., Chen, W., Li, L., Huang, J., Wang, X., Guo, Y., & Ji, G. (2023). Assessing the contribution of vegetation variation to streamflow variation in the Lancang River Basin, China. *Frontiers in Ecology and Evolution, 10*.

López, J., & Francés, F. (2013). Non-stationary flood frequency analysis in continental Spanish rivers, using climate and reservoir indices as external covariates. *Hydrology and Earth System Sciences, 17*(8), 3189-3203.

Lu, F., Song, X., Xiao, W., Zhu, K., & Xie, Z. (2019). Detecting the impact of climate and reservoirs on extreme floods using nonstationary frequency

models. *Stochastic Environmental Research and Risk Assessment, 34*, 169-182.

Luca, D., & Galasso, L. (2018). Stationary and Non-Stationary Frameworks for Extreme Rainfall Time Series in Southern Italy. *Water, 10*(10).

Madsen, H., Lawrence, D., Lang, M., Martinkova, M., & Kjeldsen, T. (2014). Review of trend analysis and climate change projections of extreme precipitation and floods in Europe. *Journal of Hydrology, 519*, 3634-3650.

Mahmood, R., Jia, S., & Zhu, W. (2019). Analysis of climate variability, trends, and prediction in the most active parts of the Lake Chad basin, Africa. *Scientific Reports*, 1-18.

Mahmoud, S. H., & Gan, T. Y. (2018). Urbanization and climate change implications in flood risk management: Developing an efficient decision support system for flood susceptibility mapping. *Science of the Total Environment, 636*, 152-167.

Manandhar, R., Odeh, I., & Ancev, T. (2009). Improving the Accuracy of Land Use and Land Cover Classification of Landsat Data Using Post-Classification Enhancement. *Remote Sensing, 1*, 330-344.

Mariotti, L., Coppola, E., Sylla, M., Giorgi, F., & Piani, C. (2011). Regional climate model simulation of projected 21st century climate change over an all-Africa domain: Comparison analysis of nested and driving model results. *Journal of Geophysical Research, 116*(d15111), 1-22.

Mehr, A. D., & Kahya, E. (2017). Climate Change Impacts on Catchment-Scale Extreme Rainfall Variability: Case Study of Rize Province, Turkey. *Journal of Hydrologic Engineering, 22*(3), 1-11.

Merz, B., Blöschl, G., Vorogushyn, S., Dottori, F., Aerts, J., Bates, P., . . . Macdonald, E. (2021). Causes, impacts and patterns of disastrous river floods. *Nature Reviews Earth & Environment*, 592-609.

Mesta, B., Akgun, O., & Kentel, E. (2024). Improving precipitation estimates for Turkey with multimodel ensemble: a comparison of nonlinear artificial neural network method with linear methods. *Neural Comput & Applic*.

Mesta, B., Sasaki, H., Nakaegawa, T., & Kentel, E. (2022). Changes in precipitation climatology for the Eastern Mediterranean using CORDEX RCMs, NHRCM and MRI-AGCM. *Atmospheric Research, 272*. doi:https://doi.org/10.1016/j.atmosres.2022.106140

Moriasi, D., Arnold, J., Van Liew, M., Bingner, R., Harmel, R., & Veith, T. (2007). Model evaluation guidelines for systematic quantification of accuracy in watershed simulations. *Trans. ASABE, 50*(3), 885-900. doi:http://dx.doi.org/10.13031/2013.23153

Moriasi, D., Gitau, M., Pai, N., & Daggupati, P. (2015). Hydrologic and Water Quality Models: Performance Measures and Evaluation Criteria. *American Society of Agricultural and Biological Engineers, 58*(6), 1763-1785. doi:10.13031/trans.58.10715

Mukherjee, F., & Singh, D. (2020). Assessing Land Use-Land Cover Change and Its Impact on Land Surface Temperature Using LANDSAT Data: A Comparison of Two Urban Areas in India. *Earth Systems and Environment, 4*, 385-407.

Muttitanon, W., & Tripathi, N. (2005). Land use/land cover changes in the coastal zone of Ban Don Bay, Thailand using Landsat 5 TM data. *International Journal of Remote Sensing, 26*(11), 2311-2323.

Netzel, L., Heldt, S., Engler, S., & Denecke, M. (2021). The importance of public risk perception for the effective management of pluvial floods in urban areas: A case study from Germany. *Journal of Flood Risk Management, 14*(2).

Nigussie, T., & Altunkaynak, A. (2019). Modeling the effect of urbanization on flood risk in Ayamama Watershed, Istanbul, Turkey, using the MIKE 21 FM model. *Natural Hazards, 99*, 1031-1047.

Ogras, S., & Onen, F. (2020). Flood Analysis with HEC-RAS: A Case Study of Tigris River. *Hindawi Advances in Civil Engineering*.

Oruc, S., Yücel, İ., & Yılmaz, A. (2022). Investigation of the Effect of Climate Change on Extreme Precipitation: Capital Ankara Case. *Teknik Dergi, 33*(2), 11749-11778.

Osei, M. A., Amekudzi, L. K., Omari-Sasu, A. Y., Yamba, E. I., Quansah, E., Aryee, J. N., & Preko, K. (n.d.). Estimation of the return periods of maxima rainfall and floods at the Pra River Catchment, Ghana, West Africa using the Gumbel extreme value theory. *Heliyon, 7*(5).

Otukei, J., & Blaschke, T. (2010). Land cover change assessment using decision trees, support vector machines and maximum likelihood classification algorithms. *International Journal of Applied Earth Observation and Geoinformation, 12S*, S27-S31.

Oubennaceur, K., Chokmani, K., Gauthier, Y., Ratte-Fortin, C., Homayouni, S., & Toussaint, J. –P. (2021). Flood Risk Assessment under Climate Change: The Petite Nation River Watershed. *Climate, 9*(125), 1-23.

Özdoğan, M. (2011). Modeling the impacts of climate change on wheat yields in Northwestern Turkey. *Agriculture, Ecosystems and Environment, 141*, 1-12.

Öztürk, T., Ceber, Z. P., Türkeş, M., & Kurnaz, M. L. (2015). Projections of climate change in the Mediterranean Basin by using downscaled global climate model outputs. *International Journal of Climatology, 35*, 4276-4292.

Papaioannou, G., Efstratiadis, A., Vasiliades, L., Loukas, A., Papalexiou, S. M., Koukouvinos, A., . . . Kossieris, P. (2018). An Operational Method for Flood Directive Implementation in Ungauged Urban Areas. *Hydrology, 5*, 24.

Patel, M. B. (2020). Flood frequency analysis using Gumbel distribution method at Garudeshwar Weir, Narmada Basin. *International Journal of Trend in Research and Development, 1*(7), 36-38.

Petchprayoon, P., Blanken, P. D., Ekkawatpanit, C., & Hussein, K. (2010). Hydrological impacts of land use/land cover change in alarge river basin in central–northern Thailand. *International Journal of Climatology, 30*, 1917-1930.

Pettorelli, N., Vik, J., Mysterud, A., Gaillard, J., Tucker, C., & Stenseth, N. (2005). Using the satellite-derived NDVI to assess ecological responses to environmental change. *Trends in ecology & evolution, 20*(9), 503-510.

Piani, C., Weedon, G. P., Best, M., Gomes, S. M., Viterbo, P., Hagemann, S., . . . Haerter, J. O. (2010). Statistical bias correction of global simulated daily precipitation and temperature for the application of hydrological models. *Journal of Hydrology, 395*(3-4), 199-215.

Poelmans, L., Van Rompaey, A., Ntegeka, V., & Willems, P. (2011). The relative impact of climate change and urban expansion on peak flows: a case study in central Belgium. *Hydrological Processes, 25*, 2846-2858.

Qu, C., Li, J., Yan, L., Yan, P., Cheng, F., & Lu, D. (2020). Non-Stationary Flood Frequency Analysis Using Cubic B-Spline-Based GAMLSS Model. *Water, 12*(7).

Radojevic, B. D., Breil, P., & Chocat, B. (2010). Assessing impact of global change on flood regimes. *International Journal of Climate Change Strategies and Management, 2*(2), 167-179.

Ranger, N., Hallegatte, S., Bhattacharya, S., Bachu, M., Priya, S., Dhore, K., . . . Morlot, J. (2011). An assessment of the potential impact of climate change on flood risk in Mumbai. *Climatic Change, 104*, 139-167.

Razmi, A., Golian, S., & Zahmatkesh, Z. (2017). Non-Stationary Frequency Analysis of Extreme Water Level: Application of Annual Maximum Series and Peak-over Threshold Approaches. *Water Resources Management, 31*, 2065-2083.

Read, L., & Vogel, R. (2015). Reliability, return periods, and risk under nonstationarity. *Water Resources Research, 51*(8), 6381-6398.

Richert, C., Erdlenbruch, K., & Figuieres, C. (2017). The determinants of households' flood mitigation decisions in France - on the possibility of feedback effects from past investments. *Ecological Economics, 131*, 342-352.

Ridha, T., Ross, A., & Mostafavi, A. (2022). Climate change impacts on infrastructure: Flood risk perceptions and evaluations of water systems in coastal urban areas. *International Journal of Disaster Risk Reduction, 73*.

Rigby, R., & Stasinopoulos, D. (2005). Generalized additive models for location, scale and shape, (with discussion). *Applied Statistics, 54*, 507-554.

Rincon, D., Velandia, J. F., Tsanis, I., & Khan, U. T. (2022). Stochastic Flood Risk Assessment under Climate Change Scenarios for Toronto, Canada Using CAPRA. *Water, 14*(227).

Rivera, J. A., & Arnould, G. (2020). Evaluation of the ability of CMIP6 models to simulate precipitation over Southwestern South America: Climatic features and long-term trends (1901–2014). *Atmospheric Research, 241*, 1-15.

Robi, M. A., Abebe, A., & Pingale, S. M. (2018). Flood hazard mapping under a climate change scenario in a Ribb catchment of Blue Nile River basin,

Ethiopia. *Applied Geomatics, 11*, 147-160. Retrieved from https://link.springer.com/article/10.1007/s12518-018-0249-8

Rogers, R. (1975). A Protection Motivation Theory of Fear Appeals and Attitude Change. *The Journal of Psychology, 91*(1), 93-114.

Salas, J., & Obeysekera, J. (2014). Revisiting the Concepts of Return Period and Riskfor Nonstationary Hydrologic Extreme Events. *Journal of Hydrologic Engineering, 19*(3), 554-568.

Sarhadi, A., & Soulis, E. (2017). Time-varying extreme rainfall intensity-duration-frequency curves in a changing climate. *Geophysical Research Letters, 44*(5), 2454-2463.

Sato, Y., Kojiri, T., Michihiro, Y., Suzuki, Y., & Nakakita, E. (2012). Estimates of Climate Change Impact on River Discharge in Japan Based on a Super-High- Resolution Climate Model. *Terrestrial, Atmospheric & Oceanic Sciences, 23*(5).

Şen, O., & Kahya, E. (2017). Determination of flood risk: A case study in the rainiest city of Turkey. *Environmental Modelling & Software, 93*, 296-309.

Sensoy, S. T., Akçakaya, A., Ekici, M., Demircan, M., Ulupinar, Y., ..., & Demirbaş, H. (2013). Trends in Turkey climate indices from 1960 to 2010. *6th Atmospheric science symposium, 24,* p. 26.

Serago, J., & Vogel, R. (2018). Parsimonious nonstationary flood frequency analysis. *Advances in Water Resources, 112*, 1-16.

Seyran, Z. (2009). *Aşağı Seyhan Ovasının Geçmişten Günümüze Arazi Kullanımındaki Değişiminin, Coğrafi Bilgi Sistemleri ve Uzaktan Algılama ile Belirlenmesi (Yayınlanmamış Yüksek Lisans Tezi).* Adana: Çukurova Üniversitesi, Fen Bilimleri Enstitüsü. Retrieved from http://libratez.cu.edu.tr/tezler/7642.pdf

Sharma, D., Das Gupta, A., & Babel, M. S. (2007). Spatial disaggregation of bias-corrected GCM precipitation for improved hydrologic simulation: Ping River Basin, Thailand. *Hydrology and Earth System Sciences, 11*(4), 1373-1390.

Singh, N., & Chinnasamy, P. (2021). Non-stationary flood frequency analysis and attribution of streamflow series: a case study of Periyar River, India. *Hydrological Sciences Journal*, 1866-1881.

Snyder, F. (1938). Synthetic unit graphs. *Trans. Am. Geophys. Union*, 447-454.

Solomon, O., & Prince, O. (2013). Flood frequency analysis of Osse river using Gumbel's distribution. *Civil and environmental research, 3*(10), 55-59.

Son, C., Lee, T., & Kwon, H. (2017). Integrating nonstationary behaviors of typhoon and non-typhoon extreme rainfall events in East Asia. *Scientific Reports*.

Song, X., Lu, F., Wang, H., Xiao, W., & Zhu, K. (2018). Penalized maximum likelihood estimators for the nonstationary Pearson type 3 distribution. *Journal of hydrology*, 579-589.

Sönmez, M. (2012). Adana Şehrinin Alansal Gelişimi ve Yakın Çevresinin Arazi Kullanımında Meydana Gelen Değişimler. *Türk Coğrafya Dergisi, 57*, 55-69.

Spinoni, J., Barbosa, P., Bucchignani, E., Cassano, J., Cavazos, T., Christensen, J. H., . . . Dosio, A. (2020). Future Global Meteorological Drought Hot Spots: A Study based on CORDEX Data. *Journal of Climate, 33*, 3635-3661.

Sraj, M., Viglione, A., Parajka, J., & Blöschl, G. (2016). The influence of non-stationarity in extreme hydrological events on flood frequency estimation. *Journal of Hydrology and Hydromechanics, 64*(4).

Šraj, M., Viglione, A., Parajka, J., & Blöschl, G. (2016). The influence of non-stationarity in extreme hydrological events on flood frequency estimation. *Journal of Hydrology and Hydromechanics, 64*(4), 426-437.

Story, M., & Congalton, R. (1986). Accuracy Assessment: A User's Perspective. *Photogrammetric Engineering and Remote Sensing, 52*, 397-399.

Sun, P., Liu, S., Jiang, H., Lü, Y., Liu, J., Lin, Y., & Liu, X. (2008). Hydrologic Effects of NDVI Time Series in a Context of Climatic Variability in an Upstream Catchment of the Minjiang River. *JAWRA Journal of the American Water Resources Association, 44*(5), 1132-1143.

Sun, P., Wen, Q., Zhang, Q., Singh, V., Sun, Y., & Li, J. (2018). Nonstationarity-based evaluation of flood frequency and flood risk in the Huai River basin, China. *Journal of Hydrology, 567*, 393-404.

Swain, D., Wing, O., Bates, P., Done, J., Johnson, K., & Cameron, D. (2020). Increased Flood Exposure Due to Climate Change and Population Growth in the United States. *Earth's Future, 8*(11).

Szwagrzyk, M., Kaim, D., Price, B., Wypych, A., Grabska, E., & Kozak, J. (2018). Impact of forecasted land use changes on flood risk in the Polish Carpathians. *Natural Hazards, 94*, 227-240.

Tabari, H. (2020). Climate change impact on flood and extreme precipitation increases with water availability. *Scientific Reports, 10*.

Tan, K., Lim, H., MatJafri, M., & Abdullah, K. (2010). Landsat data to evaluate urban expansion and determine land use/land cover changes in Penang Island, Malaysia. *Environmental Earth Sciences, 60*, 1509-1521.

Tanaka, T., Kiyohara, K., & Tachikawa, Y. (2020). Comparison of fluvial and pluvial flood risk curves in urban cities derived from a large ensemble climate simulation dataset: A case study in Nagoya, Japan. *Journal of Hydrology, 584*.

Tayanç, M., İm, U., Doğruel, M., & Karaca, M. (2009). Climate change in Turkey for the last half century. *Climatic Change, 94*(3), 483-502.

Tian, Y., Bai, X., Wang, S., Qin, L., & Li, Y. (2017). Spatial-temporal changes of vegetation cover in Guizhou Province, Southern China. *Chinese Geographical Science*, 25-38.

Tonn, G., & Guikema, S. (2018). An Agent-Based Model of Evolving Community Flood Risk. *Risk Analysis, 38*(6), 1258-1278.

Tonn, G., Guikema, S., & Zaitchik, B. (2020). Simulating Behavioral Influences on Community Flood Risk under Future Climate Scenarios. *Risk Analysis, 40*(4), 884-898.

Toros, H. (2012). Spatio-temporal variation of daily extreme temperatures over Turkey. *International Journal of Climatology, 32*(7), 1047-1055.

Tübitak MAM Çevre Enstitüsü. (2013). *Havza Koruma Eylem Planlarının Hazırlanması-Doğu Akdeniz Havzası.* Ankara. Retrieved from https://www.tarimorman.gov.tr/SYGM/Belgeler/havza%20koruma%20eylem%20planlar%C4%B1/Dogu_Akdeniz_web.pdf

Turkish Statistical Institute. (2024). *Adrese Dayalı Nüfus Kayıt Sistemi Sonuçları*. Retrieved from Merkezi Dağıtım Sistemi.

Türkiye İstatistik Kurumu. (2018). *Nüfus Projeksiyonları, 2018-2080*. Retrieved from Türkiye İstatistik Kurumu: http://www.tuik.gov.tr/PreHaberBultenleri.do?id=30567

Türkiye İstatistik Kurumu. (2024). *İstatistik Veri Portalı*. Retrieved from TÜİK: https://data.tuik.gov.tr/Kategori/GetKategori?p=Nufus-ve-Demografi-109

Türkkan, G., & Hırca, T. (2021). The investigation of food risk perception as a quantitative analysis from socio-demographic perspective. *Natural Hazards*, 715-733.

U.S. Army Corps of Engineers. (2000). *HEC-HMS Technical Reference Manual.* Davis, CA.

U.S. Army Corps of Engineers. (2013). *HEC-HMS Hydrologic Modeling System, User's Manual, Version 4.0.* ccc.

U.S. Army Corps of Engineers. (2024). *HEC-HMS Hydrologic Modeling System, User's Manual, Version 4.9.* Davis, CA.

Unal, Y. S., Tan, E., & Mentes, S. S. (2013). Summer heat waves over western Turkey between 1965 and 2006. *Theoretical and Applied Climatology, 112*(1), 339-350.

Villarini, G., Serinaldi, F., Smith, J., & Krajewski, W. (2009). On the stationarity of annual flood peaks in the continental United States during the 20th century. *Water Resources Research, 45*(8).

Walther, G., Post, E., Convey, P., Menzel, A., Parmesan, C., Beebee, T., . . . Bairlein, F. (2002). Ecological responses to recent climate change. *Nature, 416*(6879), 389-395.

WCRP CORDEX. (n.d.). *What is regional downscaling?* Retrieved from CORDEX: https://cordex.org/about/what-is-regional-downscaling/

Wi, S., Valdes, J., Steinschneider, S., & Kim, T. (2016). Non-stationary frequency analysis of extreme precipitation in South Korea using peaks-over-threshold and annual maxima. *Stochastic Environmental Research and Risk Assessment*, 583-606.

Wilby, R. L., Beven, K. J., & Reynard, N. S. (2008). Climate change and fluvial flood risk in the UK: more of the same? *Hydrological Processes, 22,* 2511-2523.

Wilensky, U. (1999). NetLogo. Evanston, IL, USA. Retrieved from http://ccl.northwestern.edu/netlogo/

Wing, O., Lehman, W., Bates, P., Sampson, C., Quinn, N., Smith, A., . . . Kousky, C. (2022). Inequitable patterns of US flood risk in the Anthropocene. *Nature Climate Change*, 156-162.

Xu, X., Wang, Y. C., Kalcic, M., Muenich, R. L., Yang, Y. C., & Scavia, D. (2019). Evaluating the impact of climate change on fluvial flood risk in a mixed-use watershed. *Environmental Modeling & Software, 122*.

Yalcin, E. (2019). Two-dimensional hydrodynamic modelling for urban flood risk assessment using unmanned aerial vehicle imagery: A case study of Kirsehir, Turkey. *Journal of Flood Risk Management, 12*(S1).

Yan, L., Li, L., Yan, P., He, H., Li, J., & Lu, D. (2019). Nonstationary Flood Hazard Analysis in Response to Climate Change and Population Growth. *Water, 11*(9).

Yang, T., & Liu, W. (2020). A General Overview of the Risk-Reduction Strategies for Floods and Droughts. *Sustainability, 12*(7).

Yeğin, M. (2015). *Master's Thesis: Flood risk mapping using economic, environmental and social dimensions.* Ankara: Middle East Technical University.

Yilmaz, A. G. (2015). The effects of climate change on historical and future extreme rainfall in Antalya, Turkey. *Hydrological Sciences Journal - Journal des Sciences Hydrologiques, 60*(12), 2148-2162.

Yilmaz, A., Imteaz, M., Shanableh, A., Al-Ruzouq, R., Atabay, S., & Haddad, K. (2023). A Non-Stationarity Analysis of Annual Maximum Floods: A Case Study of Campaspe River Basin, Australia. *Water, 15*(20).

Yin, J., Yin, Z., Zhong, H., Xu, S., Hu, X., Wang, J., & Wu, J. (2011). Monitoring urban expansion and land use/land cover changes of Shanghai metropolitan area during the transitional economy (1979-2009) in China. *Environmental Monitoring and Assessment, 177*, 609-621.

Yucel, I., Güventürk, A., & Sen, O. L. (2015). Climate change impacts on snowmelt runoff for mountainous transboundary basins in eastern Turkey. *International Journal of Climatology, 35*(2), 215-228.

Yüksel Proje. (2017). *Doğu Akdeniz Havzası Master Plan Raporu.* Ankara.

Zaalberg, R., Midden, C., Meijnders, A., & McCalley, T. (2009). Prevention, Adaptation, and Threat Denial: Flooding Experiences in the Netherlands. *Risk Analysis, 29*(12), 1759-1778.

Zadbagher, E., Becek, K., & Berberoglu, S. (2018). Modeling land use/land cover change using remote sensing and geographic information systems: case study of the Seyhan Basin, Turkey. *Environmental Monitoring and Assessment, 190*, 494.

Zaidi, S., Akbari, A., Samah, A., Kong, N., & Gisen, J. (2017). Landsat-5 Time Series Analysis for Land Use/Land Cover Change Detection Using NDVI and Semi-Supervised Classification Techniques. *Polish Journal of Environmental Studies, 26*(6), 2833-2840.

Zhai, G., Sato, T., Fukuzono, T., Ikeda, S., & Yoshida, K. (2006). WILLINGNESS TO PAY FOR FLOOD RISK REDUCTION AND ITS DETERMINANTS IN JAPAN. *Journal of the American Water Resources Association*, *42*(4), 927-940.

Zhou, Q., Leng, G., Su, J., & Ren, Y. (2019). Comparison of urbanization and climate change impacts on urban flood volumes: Importance of urban planning and drainage adaptation. *Science of The Total Environment*, 24-33.

Zhuo, L., & Han, D. (2020). Agent-based modelling and flood risk management: A compendious literature review. *Journal of Hydrology, 591*.

APPENDICES

A. Paper 1: Nonstationary Frequency Analysis of Annual Maximum Flow Series: Climate Change versus Land Use / Land Cover Change

M. Yegin[1], G. Karakaya[2], E. Kentel[1]

[1] Department of Civil Engineering, Middle East Technical University, Ankara 06800, Türkiye

[2] Department of Business Administration, Middle East Technical University, Ankara 06800, Türkiye

Murat Yegin	Gulsah Karakaya	Elcin Kentel
myegin@metu.edu.tr	kgulsah@metu.edu.tr	ekentel@metu.edu.tr

ACKNOWLEDGMENTS

This study was supported by Scientific and Technological Research Council of Turkey (TUBITAK) under the Grant Number 220N054. The authors thank to TUBITAK for their supports. We want to thank Anil Can Yildirim for his help in processing satellite images for NDVI calculations.

ABSTRACT

Accurately calculating flood peak discharges is vital in flood risk management. Flood management under stationary conditions may fail due to the ignorance of climate change (CC) and land use/land cover change (LULC), which necessitates nonstationarity flood frequency analysis. This study addresses the challenges of selecting appropriate probability distributions and covariates for nonstationary (NS) frequency analysis of annual maximum flow series (AMFS). In this study, six different probability distributions, normal, log-normal, logistic, gamma, Gumbel, and Generalized Extreme Value (GEV) distributions, and seven different covariates, time, reservoir index, annual maximum precipitation, annual average temperature,

annual total precipitation, population, and Normalized Difference Vegetation Index (NDVI), are analyzed for Silifke, Türkiye. Based on Akaike Information Criterion (AIC) scores, the GEV distribution performed better than others. However, calculated 500-year return period flood (Q_{500}) values with the best NS model of the GEV distribution were an outlier (i.e., almost 19 standard deviations outside the average observed AMFS). Thus, AIC scores alone may be misleading. When AIC scores and calculated Q_{500} values are evaluated together, Gumbel is identified as the best distribution for modeling AMFS in the study area. Moreover, LULC-related covariates are determined to govern the nonstationarity rather than CC-related covariates in the study area. The reservoir index is determined as the most representative covariate for AMFS, while NDVI, which is used as a covariate in nonstationarity frequency studies for the first time, also appeared in many of the good-performing NS models.

Keywords Nonstationarity, Covariates of land use/land cover and climate change, Normalized Difference Vegetation Index, Reservoir Index, Annual Maximum Flow Series

1. INTRODUCTION

In designing hydraulic structures, it is typical to assume that extreme events are stationary (Salas & Obeysekera, 2014; Read and Vogel, 2015); however, nonstationarity exists in nature. Factors such as human interventions in the river basin, land use and land cover (LULC) changes, and climate change (CC) contribute to nonstationarity (Salas & Obeysekera, 2014; Chen et al., 2020). Therefore, nonstationary (NS) frequency analysis is becoming more common in hydro-climatology studies.

NS models are commonly generated using time as the only covariate (Wi et al., 2016; Sarhadi & Soulis, 2017; Son et al., 2017; Cortez et al., 2022). However, recent studies consider additional covariates like average temperature and annual maximum precipitation to investigate the impacts of nonstationarity on extreme hydrological events such as floods and droughts (Leclerc & Ouarda, 2007; Gül et al., 2013;

Condon et al., 2015; Hounkpe et al., 2015; Sraj et al., 2016; Debele et al., 2017; Serago & Vogel, 2018; Sun et al., 2018; Kang et al., 2019; Faulkner et al., 2020; Qu et al., 2020; Hesarkazzazi et al., 2021; Isensee et al., 2021; Bazrafshan et al., 2022; Cui et al., 2023). For example, Yan et al. (2019) used two physical covariates, rainfall and population, besides time in their nonstationarity analysis to evaluate the effects of CC and population growth on flood hazard at two locations in China. They found that physical covariates outperformed time as explanatory variables in their study areas. NS models with physical covariates produced more reasonable flood hazard estimates than those with only time covariate. Chen et al. (2021) modeled the peak flow series of 158 stream gages across the UK. They used nine different covariates, namely time, annual rainfall amount, annual maximum daily rainfall, global average temperature, regional temperature, the North Atlantic Oscillation, the Arctic Oscillation, the East Atlantic Pattern, and the Scandinavia Pattern with log-normal, gamma, inverse-Gaussian, reverse Gumbel, and Weibull distributions to model peak flows. Their results showed that NS models with physical covariates were superior for most stations, and particularly rainfall-related covariates represented flood nonstationarity better than other covariates.

In NS frequency analysis of extreme flows, General Extreme Value (GEV) distribution is widely used (Leclerc & Ouarda, 2007; Gül et al., 2013; Condon et al., 2015; Hounkpe et al., 2015; Sraj et al., 2016; Gao et al., 2016; Faulkner et al., 2020; Singh & Chinnasamy, 2021; Anzolin et al., 2023; Bossa et al., 2023; Yilmaz et al., 2023). Normal, log-normal, Gumbel, gamma and logistic distributions are also used by many researchers (Beguería et al., 2011; Cheng et al., 2014; Condon et al., 2015; Debele et al., 2017; Ganguli & Coulibaly, 2017; Hesarkazzazi et al., 2017; Cortez et al., 2022) in the frequency analysis of the hydrometeorological parameters like annual maximum rainfall and annual maximum discharge.

Nonstationarity analysis of the annual maximum flow series (AMFS) is crucial in understanding the probable effects of extreme events such as floods (Villarini et al., 2009). In developing NS models, selection of suitable distribution models together with suitable covariates is very important and has become a research interest in the

last two decades. Therefore, this study aims to develop well-performing NS models using different covariates and distribution models for AMFS. Silifke, which experienced severe floods, was selected as the study area. Silifke, located in the Mediterranean region of Turkey, is predicted to be one of the most vulnerable regions to CC (Giorgi and Lionello, 2008). Besides CC, the region is also experiencing significant LULC change, which is also expected to contribute to nonstationarity on AMFS.

This study introduces a new covariate, the Normalized Difference Vegetation Index (NDVI), to the NS frequency analysis to represent the impact of LULC change on AMFS. NDVI quantifies vegetation greenness and provides information about vegetation density. It is mainly used to monitor vegetation and plant responses to environmental change and assess trophic interactions in the literature (Pettorelli et al., 2005; Dutrieux et al., 2015; Tian et al., 2017; Huang et al., 2020). In our study, we used NDVI as a covariate. The primary motivation for incorporating NDVI into this study is its potential influence on streamflow, supported by findings from Sun et al. (2008) and Liu et al. (2023) that state a negative correlation between NDVI and streamflow.

This study conducts NS frequency analysis of AMFS by employing commonly used probability distributions and covariates in the literature. Akaike Information Criterion (AIC) score (Akaike, 1974) is used to identify the best NS models. The covariates are categorized as CC-related and LULC-related, and their performances are examined. Moreover, to the best of our knowledge, this is the first study that uses NDVI as a potential covariate besides the commonly used ones in the NS analysis of AMFS.

2. MATERIALS & METHODS

2.1.Study Area and Data Sources

Stream gage E17A014 is located on Göksu River, just upstream of Silifke. Its catchment area is approximately 10300 km^2 (Fig. 1) and hosts several large dams that have significant effect on the streamflow. Among these dams, Gezende Dam,

the first major dam in the basin, started to operate in 1994, while Ermenek Dam, the last major dam in the basin, started its operation in 2009.

Daily flow data of E17A014 spanning from 1984 to 2020 has been taken from the State Hydraulic Works, and then AMFS is derived from the dataset. This period's average annual maximum flow is 556 m^3/s, while the minimum and maximum values are 151 m^3/s and 1833 m^3/s, respectively. Annual maximum precipitation, annual total precipitation, and annual average temperature data are obtained from the Turkish State Meteorological Service, while population data is taken from the Turkish Statistical Institute (Turkish Statistical Institute, 2024). The average annual maximum precipitation is 47.7 mm and ranges between 29.8 mm and 67.5 mm for 1984-2020. On the other hand, the average temperature in the region is around 7.3°C for the same period. Finally, NDVI is calculated using satellite images from the US Geological Survey (i.e., Landsat-5 image courtesy of the U.S. Geological Survey and Landsat-8 image courtesy of the U.S. Geological Survey).

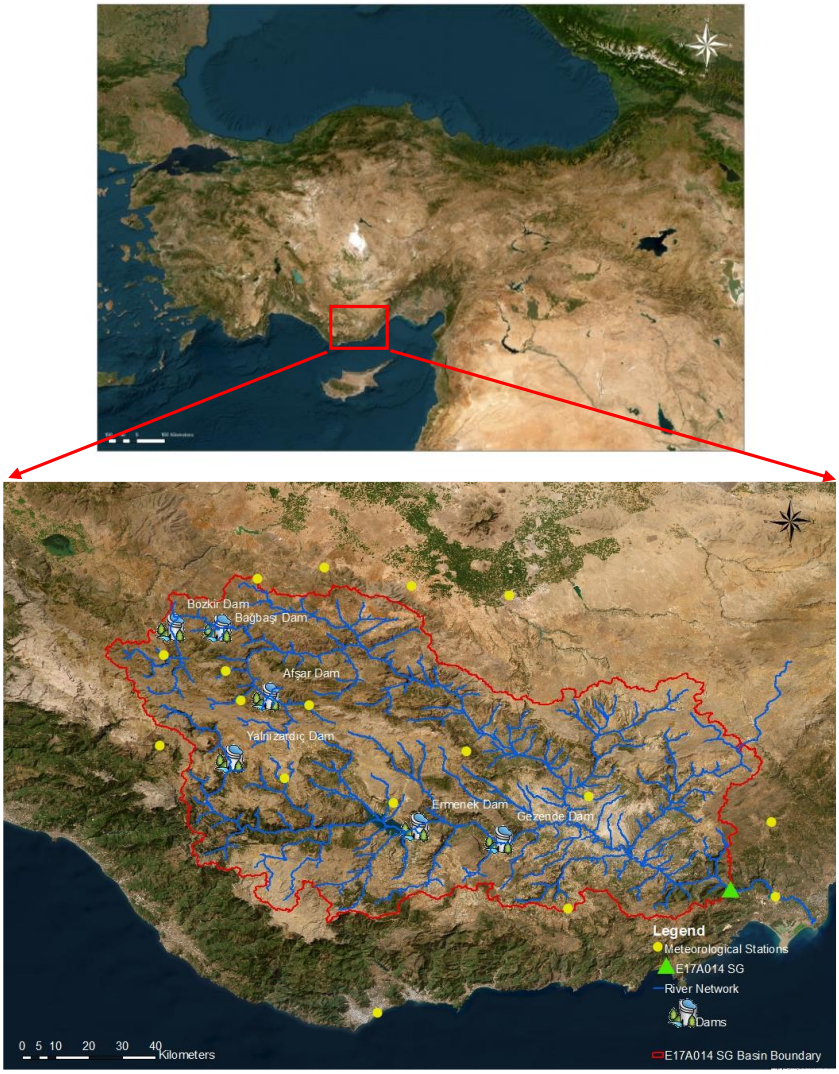

Fig. 1 The study area (Source: Esri, Maxar, Earthstar Geographics, and the GIS User Community)

2.2.Candidate Explanatory Covariates

To examine the effects of CC and LULC on AMFS, representative covariates from each category are identified based on the literature review. That is, annual maximum precipitation (MP), annual total precipitation (TP), and annual average temperature (Temp) to analyze CC effects (Condon et al., 2015; Yan et al., 2019; Chen et al., 2021), whereas reservoir index (RI) and population (Pop) for LULC changes

(Villarini et al., 2009; Lopez & Frances, 2013; Yan et al., 2019) are selected. As being another commonly used covariate indicator of both CC and LULC, time is also employed in our analysis.

In addition to these six covariates, NDVI is also included as one of the LULC-related covariates. This is due to the increase in urbanization around the study area, as supported by Alphan (2003), Derse & Alphan (2012), and Göksel & Balçık (2019). Hence, a total of seven covariates are evaluated in this study.

There are 17 meteorological stations (MSs) in and around E17A014 Basin (Fig. 1). Available data from these MSs are used in Thiessen Polygons Method to obtain areal average temperature and precipitation values for the basin.

As shown in Fig. 1, there are several large dams in the basin that affect the AMFS at its outlet. Therefore, RI is used as the covariate to characterize the impact of these reservoirs on the AMFS. RI was first proposed by Lopez and Frances (2013) as an indicator of reservoir impacts on streamflow and is formulated as follows:

$$RI = \sum_{i=1}^{N} \left(\frac{A_i}{A_T}\right) \times \left(\frac{C_i}{C_T}\right) \quad (1)$$

where N is the number of reservoirs located upstream of the stream gage, A_i is the catchment area (km^2) of the reservoir i, A_T is the catchment area (km^2), C_i is the capacity of the reservoir i (hm^3), and C_T is the average annual discharge (hm^3) at the stream gage.

The basin spans across various districts of different cities. The population of the study area is estimated using censuses of these cities. The population increased until 2000, decreased until 2007, and has been increasing in this region recently. Thus, the population is assessed as an indicator of LULC.

In this study, NDVI is estimated using Landsat-5 and Landsat-8 images provided by the U.S. Geological Survey, and the analysis is conducted using the ArcGIS program. Landsat-5 and Landsat-8 images consist of seven and eleven spectral bands, respectively. Each cell of these images has its band values that are used to calculate

an average NDVI value for the basin. NDVI values for Landsat-5 and Landsat-8 are calculated as follows:

$$NDVI = \frac{Band\ 4 - Band\ 3}{Band\ 4 + Band\ 3} \qquad Landsat - 5 \tag{2}$$

$$NDVI = \frac{Band\ 5 - Band\ 4}{Band\ 4 + Band\ 3} \qquad Landsat - 8 \tag{3}$$

2.3.Changes in the Candidate Covariates and AMFS over Time

Temporal variations in each covariate, together with AMFS, are shown in Fig. 2. As can be seen from Fig. 2 (a), there is a notable jump in RI in 2009 when Ermenek Dam, the largest reservoir volume in the basin, became operational (see Fig. 2 (a)). It can be observed that AMFS has lower annual maximum flows after 2004 compared to the 1984-2004 period. Higher NDVI values are observed after 2004, indicating a correlation between lower maximum flows and higher NDVI values. On the other hand, MP and TP exhibit oscillations similar to those of AMFS. With some shifts, the oscillations seem to be compatible. Temp also oscillates but there is not any observable relation with that of AMFS oscillations. Similarly, Pop does not show any obvious correlation with AMFS. Hence, it is not straightforward to determine the best covariate or covariate combinations from these plots. Developing NS models by testing all combinations of these seven covariates for both location and scale parameters is impractical. Thus, a trial-and-error process is employed to find the best NS model. Initially, NS models are developed based on the combinations that are commonly used in the literature. After that, the number of covariates is restricted to two for each distribution parameter (i.e., location and scale), and all possible combinations are explored. The details of model development will be provided in the next section.

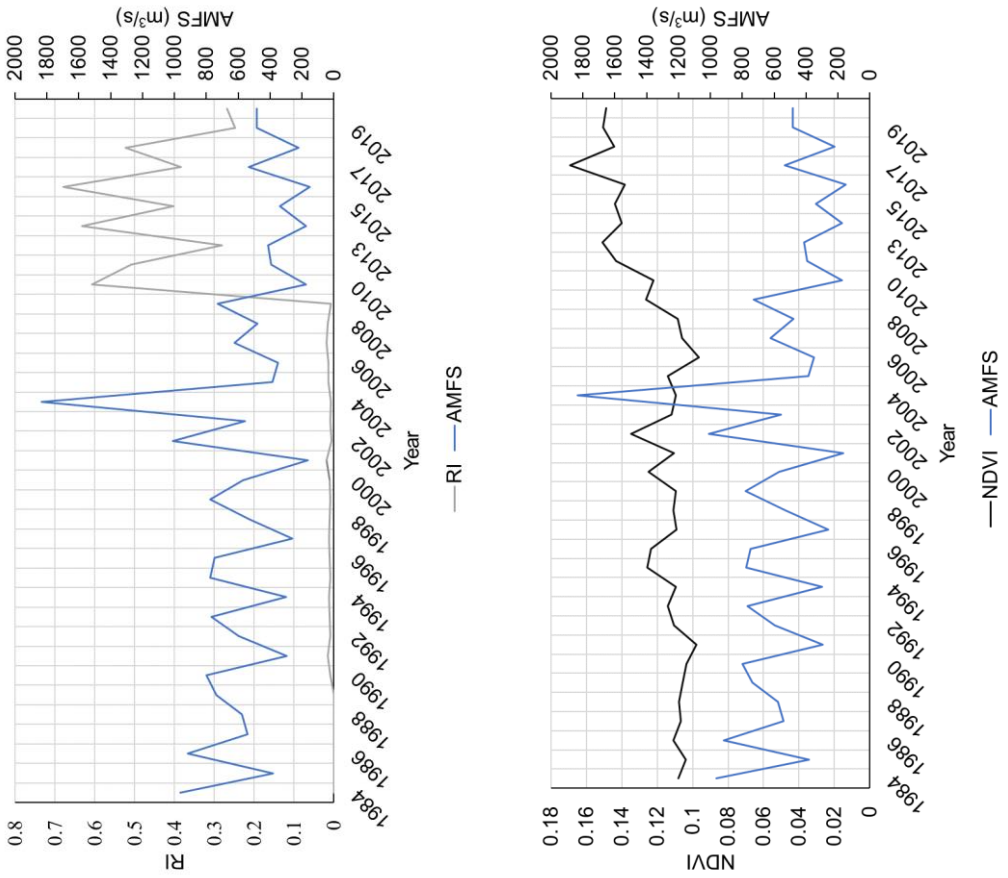

(a) RI vs AMFS (b) NDVI vs AMFS

Fig. 2 Temporal variation of the covariates and AMFS

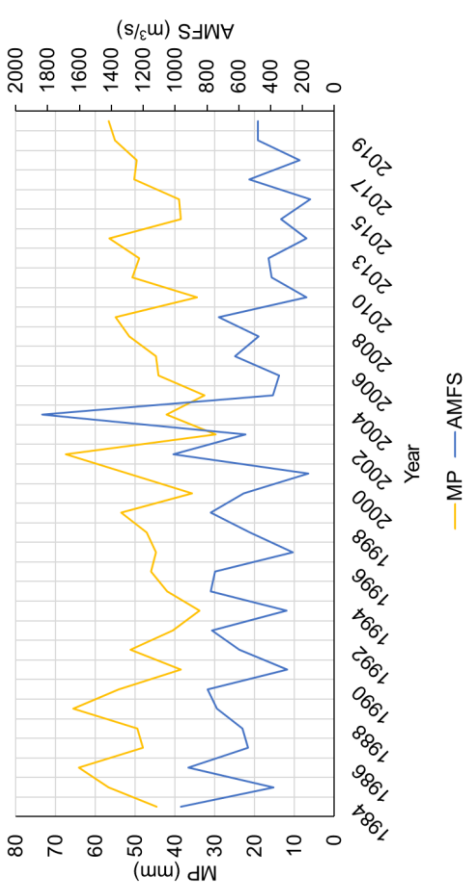

(c) MP vs AMFS

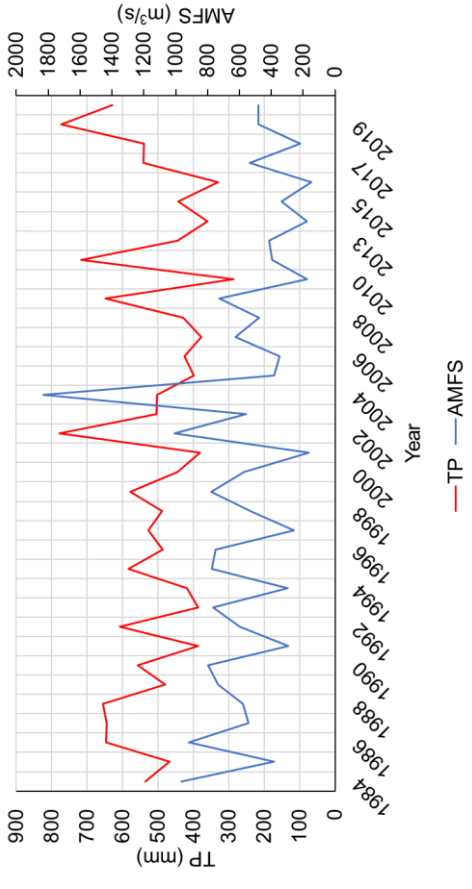

(d) TP vs AMFS

Fig. 2 (cont'd)

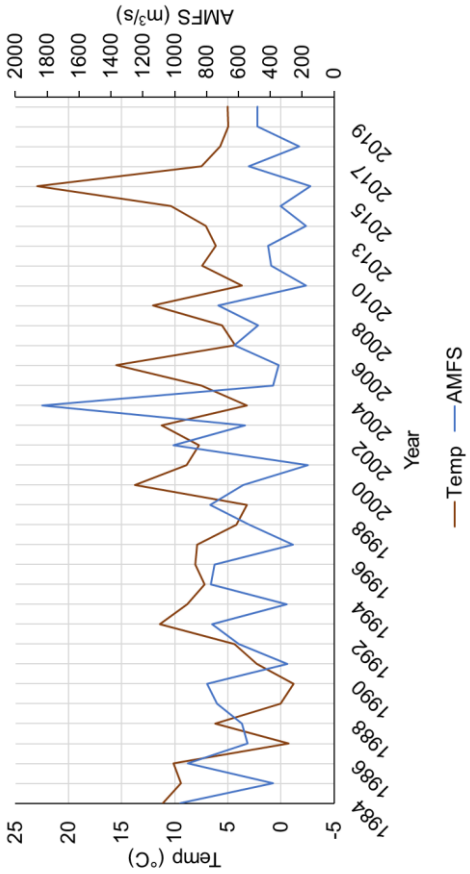

(e) Temp vs AMFS

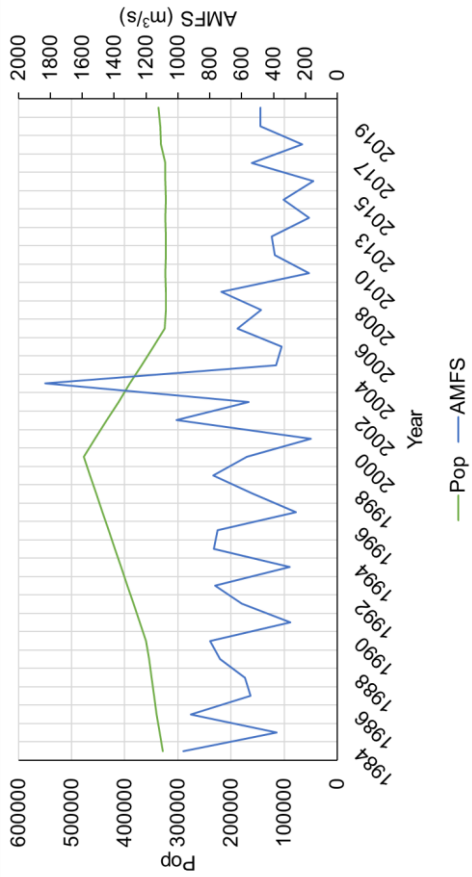

(f) Pop vs AMFS

Fig. 2 (cont'd)

2.4.Methodology

In developing NS models for AMFS of E17A014, the commonly used distributions families, normal, Pearson type III, GEV and logistic families are considered, and six probability distributions from these families, namely normal, log-normal, gamma, GEV, Gumbel, and logistic are employed. The probability density functions of these distributions are given in Table 1. Two different R Packages are used in the development of the NS models: the extRemes package (Gilleland, 2022) and the Generalized Additive Model for Location Scale and Shape (GAMLSS) package (Rigby & Stasinopoulos, 2005).

Table 1 Distribution functions

Name	Probability Density Function	
Normal (No)	$f(x) = \frac{e^{-(x-\mu)^2/(2\sigma^2)}}{\sigma\sqrt{2\pi}}$	
Log-normal (LogNo)	$f(x) = \frac{e^{-((\ln((x-\mu)/\sigma))^2/(2\xi^2)}}{(x-\mu)\xi\sqrt{2\pi}}$	$x > \mu$ $\sigma, \xi > 0$
Gamma (Ga)	$f(x) = \frac{\left(\frac{x-\mu}{\sigma}\right)^{\xi-1} e^{\left(-\frac{x-\mu}{\sigma}\right)}}{\sigma\Gamma(\xi)}$	$x \geq \mu$ $\xi, \sigma > 0$
GEV	$f(x) = \frac{1}{\sigma}\left[1 - \frac{\xi}{\sigma}(x - \mu)\right]^{\left(\frac{1-\xi}{\xi}\right)} e^{\left\{-\left[1-\frac{\xi}{\sigma}(x-\mu)\right]^{\frac{1}{\xi}}\right\}}$	$\mu + \frac{\sigma}{\xi} < x < \infty$
Gumbel (Gu)	$f(x) = \frac{1}{\sigma} e^{\frac{x-\mu}{\sigma}} e^{-e^{\frac{x-\mu}{\sigma}}}$	
Logistic (Lo)	$f(x) = \frac{1}{\sigma} \frac{e^{-(x-\mu)/\sigma}}{[1 + e^{-(x-\mu)/\sigma}]^2}$	

μ: Location parameter, σ: Scale parameter, ξ: Shape parameter, Γ: Gamma function

For each distribution, first, a set of NS models is developed, considering the previously developed models in the literature and adding NDVI to some of them. This set has 93 NS models and is referred to as the Initial Set, "IS".

The performances of NS models are evaluated based on their AIC scores (Akaike, 1974):

$$AIC = (-2)\log_e L + 2K \quad (4)$$

where K is the number of parameters in the model, L is the maximum likelihood of the model, and smaller AIC values indicate better models.

Besides the NS models in IS, new models that use combinations of better-performing covariates are intended to be developed to represent a diverse range of models. However, this process is not straightforward as knowing which combinations of the covariates will result in good NS models before their development is impossible. Therefore, the number of covariates is restricted to at most two for each location and scale parameter, and all possible combinations are explored. For each distribution, a set of 840 NS models are developed, and this set is referred to as "All2":

$$Total\ number\ of\ NS\ models = \sum_{k=0}^{2} \binom{n}{k} \times \sum_{r=0}^{2} \binom{n}{r} - 1 \quad (5)$$

where n is the total number of covariates, which is seven, k is the number of covariates used to represent the location parameter, and r is the number of covariates used to represent the scale parameter. We subtract one to ensure that only models with at least one covariate are considered.

In the results section, the models' performances in All2 and IS are compared to assess the advantages of developing all possible NS models with at most two covariates in each parameter against the traditional approach of developing a limited number of NS models with predetermined covariate combinations. Stationary (S) models are also developed to compare their performances against those of NS models.

Moreover, 5-year flow (Q_5) and 500-year return period flood (Q_{500}) values are calculated to check whether the models with good performances have reasonable peak discharge values. In the calculations, the approach of Eastoe & Tawn (2009) is followed. That is, first, a specific discharge value is selected, and the exceedance probability of this value is calculated for each year. Afterwards, the average of these exceedance probabilities is found. If this average value matches the desired value, the selected discharge value is considered accurate. Otherwise, a new discharge value is selected, and the process is repeated until the desired exceedance probability is achieved. This return level is referred as marginal return level in the study of Eastoe & Tawn (2009).

3. RESULTS

AIC scores of the S model, the best of IS, and the best of All2 for each distribution, together with the improvements in AIC scores, are represented in Fig. 3. It can be seen that the performances of the best NS models, both for IS and All2, are better than the S models across all distributions. It can be observed that the improvement from the S model to the best of IS ranges between 13 and 24, whereas it ranges between 18 and 27 for the best of All2. On the other hand, the improvement from the best of IS to the best of All2 is between 1.7 and 7.4.

When the distributions of good-performing models are analyzed, it is seen that better NS models are developed with GEV, Gumbel, and log-normal distributions. Moreover, the improvements in the AIC scores from the best of IS to the best of All2 are less than 5 for these three distributions. Thus, it can be concluded that developing a limited number of NS models (like those in IS) with good-performing distributions will result in good-performing NS models. In other words, the added benefit of developing all NS models with all possible combinations of two covariates may not be necessary if good-performing distributions are used.

It can also be seen from Fig. 3 that AIC scores of S models with GEV, Gumbel, log-normal, and gamma distributions are close to each other and better than those with logistic and normal distributions. For logistic and normal distributions, besides S models, NS models also have the highest AIC scores. Thus, performances of S models can be used as an indicator of the performances of the corresponding NS models of the same distributions and be used in selecting potential distributions to be used in the NS frequency analysis. It is concluded that normal and logistic distributions do not perform as good as GEV, Gumbel, log-normal and gamma distributions to model AMFS for the study area.

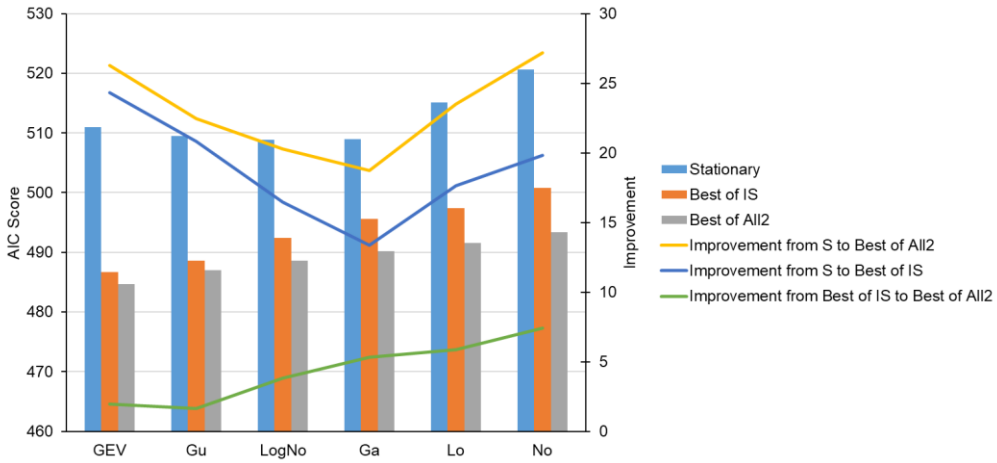

Fig. 3 AIC scores of the best models and improvement between different sets

Fig. 4 shows the box plots for AIC scores of the models in All2, in IS, and the best 20 NS models for each distribution. As can be seen from the box plots of the best 20 NS models in Fig. 4, GEV and Gumbel distributions yield the lowest AIC scores. Gumbel distribution also has a narrow range for the best 20 NS models. Normal and logistic distributions have large number of relatively bad performing NS models both in IS and All2. Moreover, the normal distribution presents numerous outliers, with the worst AIC scores. These findings support our initial conclusion of normal and logistic distributions not being suitable for the study area. Another interesting observation from Fig. 4 is that although the narrowest variation in AIC scores of best 20 NS models is for the GEV distribution, the variations in IS and All2 of the GEV distribution are considerably wide. Therefore, if a limited number of NS models with the GEV distribution are developed, that set may not include good-performing models.

The top-performing 20 NS models in All2 for each probability distribution are identified. Among these models employing the same covariates in the same parameters are compared and those with higher AIC scores are selected. This process yields a set comprising 55 NS models, indicating that a substantial proportion of covariate combinations perform relatively well regardless of the distribution. However, it should be noted that for gamma, logistic, and normal distributions, most of these 20 best-performing models are not located in IS but in All2.

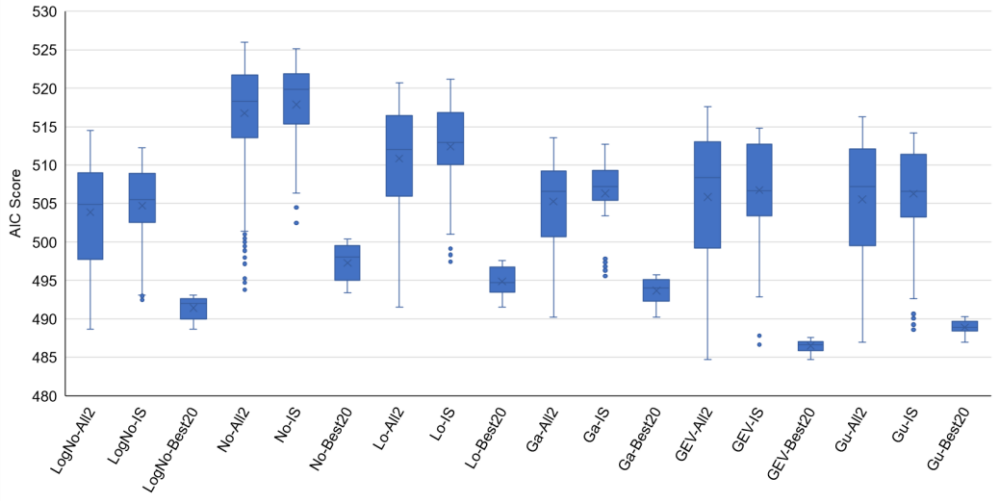

Fig. 4 Box plots for AIC scores of the models in All2, IS, and the best 20 NS models

Table 2 presents the Q_{500} values of the best NS models and the minimum and maximum Q_{500} values of the NS models in All2. The variance is highest for GEV distribution, where Q_{500} values vary between 1844.2 m^3/s and 19395.4 m^3/s. The log-normal distribution also demonstrates high variance. On the other hand, the variance of Gumbel distribution is the lowest, with the logistic distribution exhibiting similar characteristics. Since Q_{500} values are frequently used in flood risk analysis and it may not be possible to identify the best nonstationary model every time, distributions that give reasonable Q_{500} values for all nonstationary models should be used. Of course, the nonstationary models with good performances and realistic Q_{500} values should be preferred.

Table 2 Calculated Q_{500} values for the models in All2

	Q_{500} of the best NS model (m^3/s)	Minimum Q_{500} (m^3/s)	Maximum Q_{500} (m^3/s)
LogNo	1651.8	1572.9	5384.7
No	1872.5	1291.7	2762.6
Lo	1734.9	1284.0	2102.7
Ga	1705.2	1361.1	3215.5
GEV	7774.2	1844.2	19395.4
Gu	1853.1	1423.5	2510.4

Fig. 5 demonstrates the calculated Q_{500} values for all 55 NS as well as S models. Q_{500} values of most NS models are significantly higher than those of the S model for both GEV and log-normal distributions, justifying the necessity of developing NS models, especially for flood risk analysis. It can be observed from Fig. 5 that Q_{500} values for GEV and log-normal distributions oscillate a lot. The recorded maximum discharge value of E17A014 SG is 1833 m^3/s between 1961 and 2024, while the Q_{500} value of the best NS model of GEV distribution is notably higher at 7774 m^3/s. This value is an outlier among the observed AMFS, which is approximately 19 standard deviations away from the maximum observed AMFS. Therefore, although the best NS model belongs to the GEV distribution (see Fig. 3), it is impractical to use this model to generate extreme streamflow values. A similar problem is also identified by Song et al. (2018). They stated that the Maximum Likelihood Estimation method may lead to unreasonable results in the parameter estimation of NS models for the GEV distribution. On the other hand, log-normal and gamma distributions have good performances, too. The calculated peak discharge values for the 500-year return period flood of the best NS models with log-normal and gamma distributions are also acceptable. Lastly, the AIC scores of the NS models with Gumbel distribution are lower than those with log-normal and gamma distributions (see Fig. 3). Hence, Gumbel distribution emerges as the most suitable probability distribution for modeling AMFS, which many researchers use in the literature (Solomon & Prince, 2013; Osei et al., 2021; Patel, 2020; Game et al., 2023). For Gumbel distribution, the improvement in AIC from the best of IS to the best of All2 is around 1.5 (see Fig. 3), indicating that the added benefit of developing 840 NS models is insignificant. When AIC scores (see Fig. 3) and Q_{500} values (Fig. 5) are evaluated together, these results suggest that developing good NS models with commonly used covariates in the literature is likely when a suitable distribution is selected. In other words, developing NS models with all combinations may not be necessary to identify good NS models. However, it should be noted that uncertainty is inherent in the nature of hydrological events. Thus, it is worth checking the Q_{500} values of other NS models with lower AIC scores. For example, consider the case of Gumbel distribution, where

the NS model yielding the maximum Q_{500} value has an AIC score of 489.8, which is just 0.6% greater than that of the best NS model with Gumbel distribution. On the other hand, the difference between the Q_{500} values of these two models is 657.3 m^3/s, which is an important difference for flood management studies. Thus, investigating the Q_{500} values of the NS models with reasonable AIC scores is crucial.

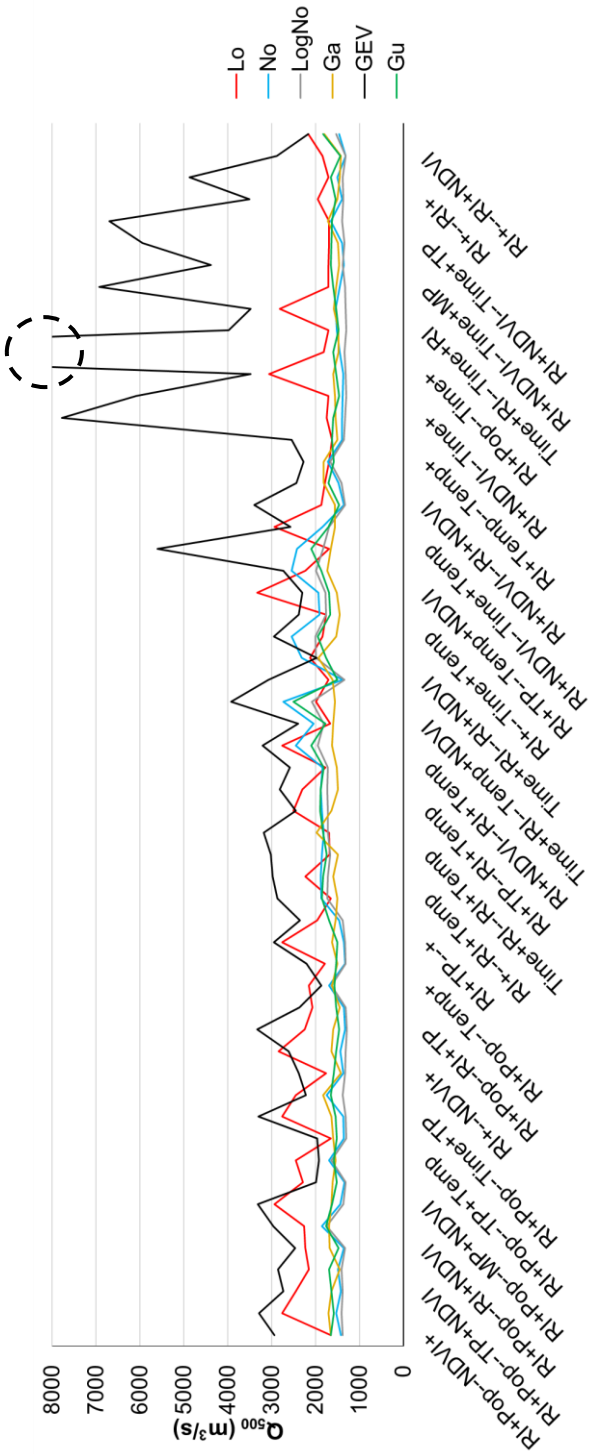

Fig. 5 Calculated Q_{500} values for the best 55 NS models and S models. The circle marks the NS model of the GEV distribution that has Q_{500} of 17590.3 m^3/s (see Table 2). "- -" separates the location and scale parameters

To identify the covariates with the potential to yield good NS models, top-performing 20 NS models of each probability distribution are selected, and the frequency of occurrence of each covariate within these models is shown in Fig. 6. As can be observed from Fig. 6 that RI is consistently the most frequently selected covariate for the location parameter across all probability distributions. For gamma and log-normal distributions, population emerges as another significant covariate for the location parameter. On the other hand, it is not possible to identify a favored covariate for the scale parameter. Moreover, for Gumbel distribution, RI, average temperature, and NDVI are the most frequently selected covariates for the scale parameter.

It should be stated that LULC-related covariates are selected more frequently than CC-related covariates for all distributions in the best 20 NS models. This suggests that the effect of LULC on AMFS is more pronounced than that of CC in the study area. Therefore, critical processes that may affect streamflow in the study regions should be thoroughly investigated first, and NS models using indicators of these processes as covariates have to be evaluated. For example, for Gumbel distribution, as being the suggested distribution, the AIC value of the best NS model that uses CC-related covariates is 496.7, while it is 487.1 with LULC-related covariates (see Table 3).

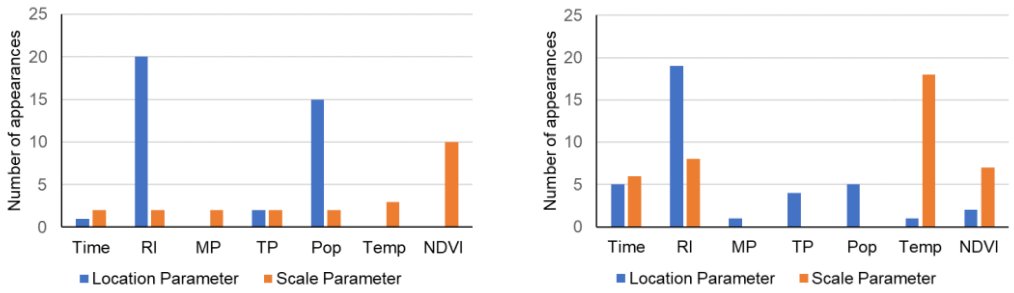

(a) LogNo (b) No

Fig. 6 Number of appearances of each covariate in the best 20 NS models

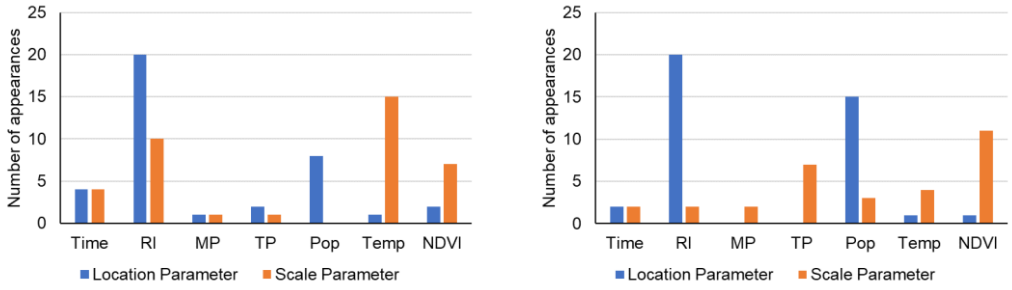

(c) Lo

(d) Ga

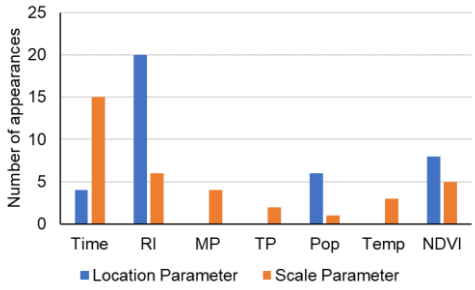

(e) GEV

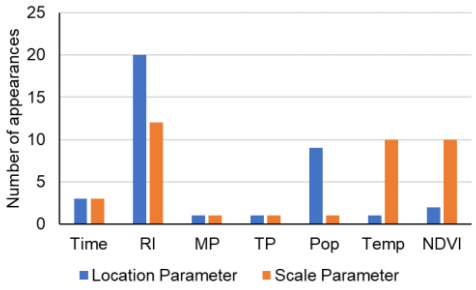

(f) Gu

Fig. 6 (cont'd)

Table 3 shows the AIC scores of the best NS model for each distribution and the combinations of the covariates. These combinations include models employing only CC-related covariates (time, MP, TP, and temp), only LULC-related covariates (time, RI, Pop, and NDVI), and models using both types of covariates. As evident from the AIC scores in Table 3, using only LULC-related covariates for all distributions resulted in better NS models than models using only CC-related covariates. For normal and logistic distributions, using LULC-related covariates improved AIC scores slightly in comparison with CC-related covariates (i.e., 2.3 and 3.6 for normal and logistic distributions, respectively). This suggests that LULC-related covariates are more effective than CC-related covariates on AMFS for this basin. In addition to this, using both types of covariates did not result in better models while compared to the models with only LULC-related covariates. The AIC scores of the best NS models did not change for log-normal, gamma and GEV while it is increased by 0.1 for Gumbel distribution.

Fig. 7 shows the box plots for the models in All2 with only CC-related covariates, LULC-related covariates, and both types of covariates. It can be seen that No-CC, No-Both, and Lo-CC have many outliers. LogNo-LULC, LogNo-Both, GEV-LULC, GEV-Both, Gu-LULC, and Gu-Both have smaller AIC scores. The models with CC-related covariates generally have higher AIC scores than others, which supports the importance of including LULC-related covariates in NS models.

Table 3 The impacts of CC and LULC-related covariates on the AIC Scores

	AIC Score of the best model	Covariates used in the best NS model						
		Time	MP	TP	Temp	RI	Pop	NDVI
NS models with only CC covariates								
LogNo-CC	495.1	L		L				
No-CC	500.8	L+S		L	S			
Lo-CC	498.2	L+S		L	S			
Ga-CC	498.6	L	S	L				
GEV-CC	496.8	L		L				
Gu-CC	496.7	L		L				
NS models with only LULC covariates								
LogNo-LULC	488.6					L	L	S
No-LULC	498.5	L				L+S		S
Lo-LULC	494.6	L				L+S		S
Ga-LULC	490.2	S				L	L	S
GEV-LULC	484.7	S				L		L
Gu-LULC	487.1	L				L+S		S
NS models with both CC & LULC covariates								
LogNo	488.6					L	L	S
No	493.4				S	L+S		
Lo	491.5				S	L+S		
Ga	490.2	S				L	L	S
GEV	484.7	S				L		L
Gu	487.0				S	L+S		

L: Location Parameter, S: Scale Parameter

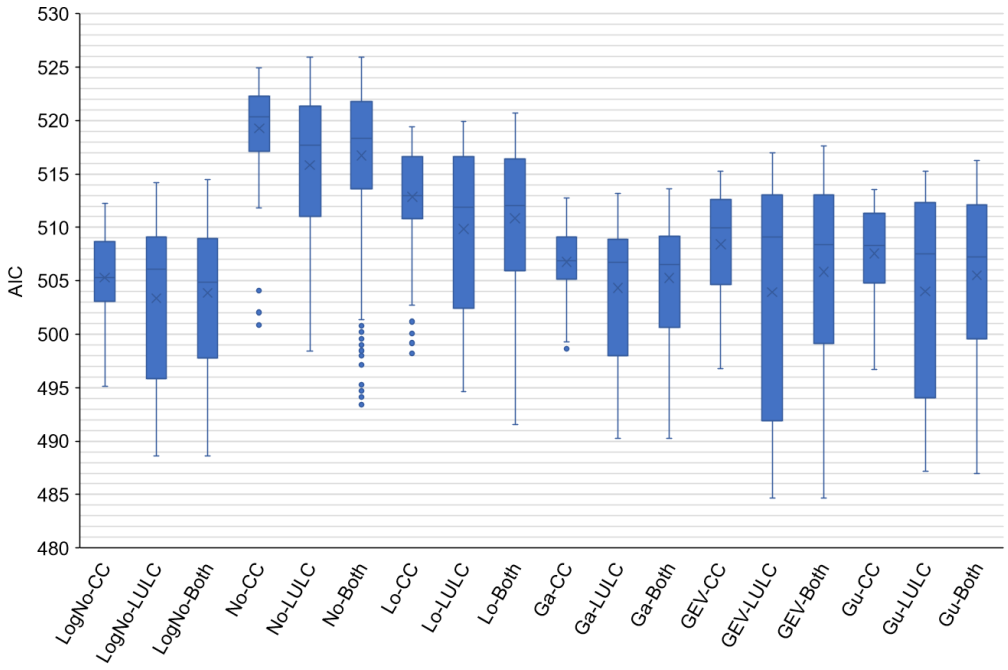

Fig. 7 Box plots for the models with only CC-related, only LULC-related, and both types of covariates

Streamflow values (both extremes, Q_{500} and Q_5) generated using NS models are calculated for all distributions and shown in Fig. 8. As mentioned above, despite GEV distribution exhibiting the lowest AIC scores, calculated Q_{500} values are outliers for many models (i.e., Q_{500} of the best GEV model is 7774.2 m^3/s and it is approximately 19 standard deviations away from the observed maximum AMFS.) Q_{500} values of best NS models for other distributions are more or less the same (see Table 2). Q_{500} value of the best NS model with Gumbel distribution is 1853.1 m^3/s, and this value is approximately 1% greater than the maximum observed discharge value. As shown in Fig. 8 (b), Q_5 values of NS models with GEV distribution oscillate significantly and many outliers exist. The straight line in Fig. 8 (b) represents the average of the AMFS over a 63-year observation period (i.e., 1984-2020), and most of the outliers of GEV distribution in All2 are not observed in this period. It can also be seen that there are no outliers for the best 20 NS models for Q_{500} and Q_5 values in any distribution.

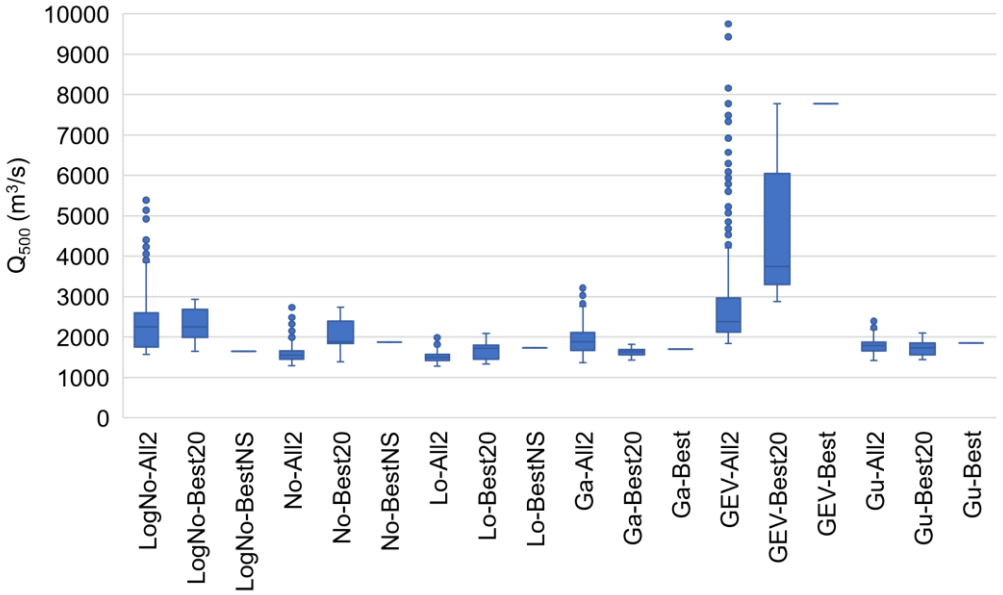

(a)

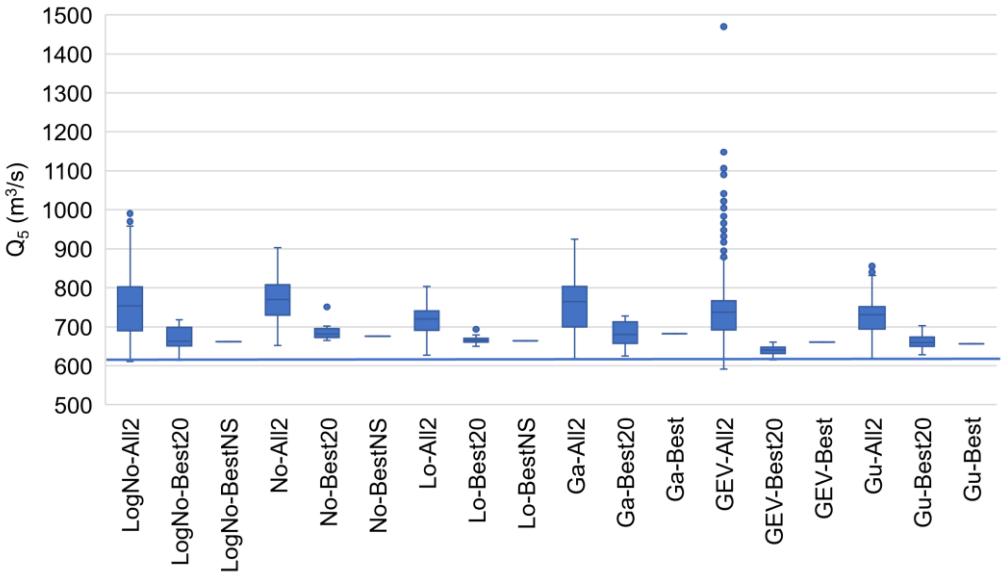

(b)

Fig. 8 (a) Q_{500} (m^3/s) values for the NS models (b) Q_5 (m^3/s) values for the NS models. The solid horizontal line is the average of observed discharges.

4. CONCLUSION

Traditional flood management relies on stationarity assumption, however, analyzing AMFS under nonstationary conditions is essential. In flood studies, selection of the

appropriate probability distribution and covariates is important for developing representative nonstationary models.

In this study, six different probability distributions and seven different covariates are analyzed to characterize a suitable NS model for the study area. 93 NS models (IS) are generated as an initial step, and after that, 840 NS models (All2) are generated using two covariates at most for each statistical parameter. The best NS models in these two sets differ with respect to their AIC scores. The performance differences between these two NS models are high for normal and logistic distributions and low for GEV and Gumbel distributions. It should be noted that finding the best NS model with the best combination of covariates is a challenging task; trying as many combinations as possible is a good idea, but it might be time-consuming. However, choosing a good-performing probability distribution can reduce the need for extensive covariate selection.

Selecting the best distribution based on some statistical measures might be deceptive. In this study, GEV distribution performs best among the others according to AIC scores. However, the best NS model's calculated peak discharge, Q_{500}, value is far from the observed maximum annual discharges. Thus, the appropriate distribution should be selected considering the end-use of the study. For the basin, Gumbel distribution is selected as the best distribution, considering both the AIC scores and peak discharges. Q_{500} value of the best NS model with Gumbel distribution is approximately 1% greater than the maximum of AMFS. Furthermore, there is no significant difference between the best NS models of set IS and All2. Hence, good-performing NS models can be developed without so much effort with Gumbel distribution. However, due to the uncertainty in hydrological processes, the peak discharges of the NS models that perform well should also be considered in flood management studies. RI and Temp are used in the best NS model for Gumbel distribution. Another conclusion is that if the performance of the S model is not good, the performance of the NS models is not good either. For this reason, the performance of the S model might be used as an indicator to eliminate probability distributions.

Determining the source of the nonstationarity is important in estimating peak discharges. In our study area, NS models with LULC-related covariates perform better than those with CC-related covariates. RI is the best-performing covariate for all probability distributions. In addition, NDVI, which is used as an LULC-related covariate for the first time, performs well. However, estimating the LULC-related covariates for the future may not be straightforward. While the estimation of NDVI is not easy, RI might be estimated well enough if the basin management is well-planned for the future. Hence, the covariates should also be selected considering their limitations.

REFERENCES

Abebe, Y., Ghorbani, A., Nikolic, I., Vojinovic, Z., & Sanchez, A. (2019). Flood risk management in Sint Maarten – A coupled agent-based and flood modelling method. *Journal of Environmental Management, 248*.

Adelekan, I., & Asiyanbi, A. (2016). Flood risk perception in flood-affected communities in Lagos, Nigeria. *Natural Hazards, 80,* 445-469.

Aik, D., Ismail, M., & Muharam, F. (2020). Land Use/Land Cover Changes and the Relationship with Land Surface Temperature Using Landsat and MODIS Imageries in Cameron Highlands, Malaysia. *Land, 9*. doi:http://dx.doi.org/10.3390/land9100372

Akaike, H. (1974). A New Look at the Statistical Model Identification. *IEEE Transactions On Automatic Control*, 716-723.

Akter, T., Quevauviller, P., Eisenreich, S., & Vaes, G. (2018). Impacts of climate and land use changes on flood risk management for the Schijn River, Belgium. *Environmental Science and Policy, 89*, 163-175.

Alam, A., Bhat, M., & Maheen, M. (2020). Using Landsat satellite data for assessing the land use and land cover change in Kashmir Valley. *GeoJournal, 85,* 1529-1543.

Alawamy, J., Balasundram, S., Hanif, A., & Sung, C. (2020). Detecting and Analyzing Land Use and Land Cover Changes in the Region of Al-Jabal Al-Akhdar, Libya Using Time-Series Landsat Data from 1985 to 2017. *Sustainability, 12*. doi:http://dx.doi.org/10.3390/su12114490

Alfieri, L., Feyen, L., Dottori, F., & Bianchi, A. (2015). Ensemble flood risk assessment in Europe under high end climate scenarios. *Global Environmental Change, 35*, 199-212.

Allam, M., Bakr, N., & Elbably, W. (2019). Multi-temporal assessment of land use/land cover change in arid region based on landsat satellite imagery: Case study in Fayoum Region, Egypt. *Remote Sensing Applications: Society and Environment, 14*, 8-19.

Alphan, H. (2003). Land-use change and urbanization of Adana, Turkey. *Land Degradation & Development, 14*(6), 575-586.

Anzolin, G., Chaffe, P., Vrugt, J., & AghaKouchak, A. (2023). Using climate information as covariates to improve nonstationary flood frequency analysis in Brazil. *Hydrological Sciences Journal*, 645-654.

Arnell, N., & Gosling, S. (2016). The impacts of climate change on river flood risk at the global scale. *Climatic Change, 134*, 387-401.

Attems, M., Thaler, T., Genovese, E., & Fuchs, S. (2020). Implementation of property-level flood risk adaptation (PLFRA) measures: Choices and decisions. *WIREs Water, 7*(1).

Avand, M., Moradi, H., & Lasboyee, M. H. (2021). Using machine learning models, remote sensing, and GIS to investigate the effects of changing climates and land uses on flood probability. *Journal of Hydrology, 595*. doi:https://doi.org/10.1016/j.jhydrol.2020.125663

Aziz, R., Yucel, I., & Yozgatligil, C. (2020). Nonstationarity impacts on frequency analysis of yearly and seasonal extreme temperature in Turkey. *Atmospheric Research, 238*, 1-13.

Azizi, S., Ilderomi, A., & Noori, H. (2021). Investigating the effects of land use change on flood hydrograph using HEC-HMS hydrologic model (case study: Ekbatan Dam). *Natural Hazards, 109*, 145-160.

Bai, Y., Zhang, Z., & Zhao, W. (2019). Assessing the Impact of Climate Change on Flood Events Using HEC-HMS and CMIP5. *Water, Air, & Soil Pollution, 230*.

Balov, M. N. (2020). Influence of Climate Change on the Flood Disasters in Bursa, Turkey. *International Journal of Engineering Technologies IJET, 6*(4), 62-68.

Bangalore, M., Smith, A., & Veldkamp, T. (2019). Exposure to Floods, Climate Change, and Poverty in Vietnam. *Economics of Disasters and Climate Change, 3*, 79-99.

Bayazıt, Y., Koç, C., & Bakış, R. (2021). Urbanization impacts on flash urban floods in Bodrum Province, Turkey. *Hydrological Sciences Journal, 66*(1).

Bazrafshan, J., Cheraghalizadeh, M., & Shahgholian, K. (2022). Development of a Non-stationary Standardized Precipitation Evapotranspiration Index (NSPEI) for Drought Monitoring in a Changing Climate. *Water Resour Management*, 3523-3543.

Beckers, A., Dewals, B., Erpicum, S., Dujardin, S., Detrembleur, S., Teller, J., . . . Archambeau, P. (2013). Contribution of land use changes to future flood damage along the river Meuse in the Walloon region. *Natural Hazards and Earth System Sciences, 13*, 2301-2318.

Beden, N., & Keskin, A. (2021). Flood map production and evaluation of flood risks in situations of insufficient flow data. *Natural Hazards*, 2381-2408.

Begueria, S., Martinez, M., Serrano, S., Moreno, J., & Kenawy, A. (2010). Assessing trends in extreme precipitation events intensity and magnitude using non-stationary peaks-over-threshold analysis: a case study in northeast Spain from 1930 to 2006. *International Journal of Climatology, 31*(14), 2102-2114.

Betsholtz, A., & Nordlöf, B. (2017). *Potentials and limitations of 1D, 2D and coupled 1D-2D flood modelling in HEC-RAS A case study on Höje river (Master Thesis).* Lund: Lund University.

Bilici, Ö., & Everest, A. (2017). 29 ARALIK 2016 MERSİN SELİNİN METEOROLOJİK ANALİZİ VE İKLİM DEĞİŞİKLİĞİ BAĞLANTISI. *Doğu Coğrafya Dergisi*, 227-250.

Blöschl, G., Hall, J., Viglione, A., & al., e. (2019). Changing climate both increases and decreases European river floods. *Nature, 573*, 108-111.

Bormudoi, A., & Nagai, M. (2017). Perception of risk and coping capacity: A study in Jiadhal Basin, India. *International Journal of Disaster Risk Reduction, 21*, 376-383.

Bossa, A., Akpaca, J., Hounkpe, J., Yira, Y., & Badou, D. (2023). Non-Stationary Flood Discharge Frequency Analysis in West Africa. *GeoHazards, 4*(3), 316-327.

Botzen, W., Aerts, J., & van den Bergh, J. (2009). Dependence of flood risk perceptions on socioeconomic and objective risk factors. *Water Resources Research, 45*(10).

Brody, S. D., Highfield, W. E., & Blessing, R. (2015). An Analysis of the Effects of Land Use and Land Cover on Flood Lossesalong the Gulf of Mexico Coast from 1999 to 2009. *Journal of the American Water Resources Association, 51*(6), 1556-1567.

Bronstert, A. (2003). Floods and Climate Change: Interactions and Impacts. *Risk Analysis, 23*(3), 545-557.

Bubeck, P., Botzen, W., Kreibich, H., & Aerts, J. (2013). Detailed insights into the influence of flood-coping appraisals on mitigation behaviour. *Global Environmental Change, 23*(5), 1327-1338.

Bubeck, P., Botzen, W., Laudan, J., Aerts, J., & Thieken, A. (2018). Insights into Flood-Coping Appraisals of Protection Motivation Theory: Empirical Evidence from Germany and France. *Risk Analysis, 38*(6), 1239-1257.

Bubeck, P., Botzen, W., Suu, L., & Aerts, J. (2012). Do flood risk perceptions provide useful insights for flood risk management? Findings from central Vietnam. *Journal of Flood Risk Management, 5*(4), 295-302.

Bucak, T., Trolle, D., Tavşanoğlu, Ü., Çakıroğlu, A., Özen, A., Jeppesen, E., & Beklioğlu, M. (2018). Modeling the effects of climatic and land use changes on phytoplankton and water quality of the largest Turkish freshwater lake: Lake Beyşehir. *Science of Total Environment, 621,* 802-816.

Buchenrieder, G., Brandl, J., & Balgah, A. (2021). The Perception of Flood Risks: A Case Study of Babessi in Rural Cameroon. *International Journal of Disaster Risk Science, 12*, 1-21.

Buldur, A., Pınar, A., & Başaran, A. (2007). 05-07 MART 2004 TARİHLİ GÖKSU NEHRİTAŞKINI VE SİLİFKE'YE ETKİSİ. *Selçuk Üniversitesi Sosyal Bilimler Enstitüsü Dergisi*, 139-160.

Butchart, S. H., Walpole, M., Collen, B., van Strien, A., Scharlemann, J. P., Almond, R. E., & . . . Watson, R. (2010). Global Biodiversity: Indicators of Recent Declines. *Science, 328*(5982), 1164-1168.

Cabrera, J., & Lee, H. S. (2018). Impacts of Climate Change on Flood-Prone Areas in Davao Oriental, Philippines. *Water, 10*(7). doi:https://doi.org/10.3390/w10070893

Chang, H., & Franczyk, J. (2008). Climate Change, Land-Use Change, and Floods: Toward an Integrated Assessment. *Geography Compass*, 1549-1579.

Chen, M., Papadikis, K., & Jun, C. (2021). An investigation on the non-stationarity of flood frequency across the UK. *Journal of Hydrology, 597*.

Chen, Q., Chen, H., Zhang, J., Hou, Y., Shen, M., Chen, J., & Xu, C. (2020). Impacts of climate change and LULC change on runoff in the Jinsha River Basin. *Journal of Geographical Sciences, 30*, 85-102.

Chen, Y. –J., Lin, H. –J., Liou, J. –J., Cheng, C. –T., & Chen, Y. M. (2022). Assessment of Flood Risk Map under Climate Change RCP8.5 Scenarios in Taiwan. *Water, 14*(2), 207.

Cheng, L., AghaKouchak, A., Gilleland, E., & Katz, R. (2014). Non-stationary extreme value analysis in a changing climate. *Climatic Change, 127*, 353-369.

Coles, S. (2001). *An Introduction to Statistical Modeling of Extreme Values.* London: Springer.

Condon, L. E., Gangopadhyay, S., & Pruitt, T. (2015). Climate change and non-stationary flood risk for the upper Truckee River basin. *Hydrology and Earth System Sciences, 19*, 159-175.

Congalton, R. (1991). A review of assessing the accuracy of classifications of remotely sensed data. *Remote Sensing of Environment, 37*(1), 35-46.

Cortez, B., Pires, G., Diaz, A., Fonseca, H., & Oliveira, L. (2022). Nonstationary extreme precipitation in Brazil. *Hydrological Sciences Journal*, 1372-1383.

Costache, R., Pham, Q. B., Corodescu-Roşca, E., Cîmpianu, C., Hong, H., Thuy Linh, N. T., . . . Pham, B. T. (2020). Using GIS, remote sensing, and machine learning to highlight the correlation between the land-use/land-cover changes and flash-flood potential. *Remote Sensing, 12*(9), 1422.

Coughlan, M., Cronin, P., & Ryan, F. (2013). Survey research: Process and limitations. *International Journal of Therapy and Rehabilitation, 16*(1).

CRED & UNDRR. (2020). *Human cost of disasters: An overview of the last 20 years 200-2019.*

Cui, H., Jiang, S., Gao, B., Ren, L., Xiao, W., Wang, M., . . . Xu, C. (2023). On method of regional non-stationary flood frequency analysis under the influence of large reservoir group and climate change. *Journal of Hydrology*.

Dankers, R., & Feyen, L. (2008). Climate change impact on flood hazard in Europe: An assessment based on high-resolution climate simulations. *Journal of Geophysical Research, 113*. doi: https://doi.org/10.1029/2007JD009719

Dawson, R., Peppe, R., & Wang, M. (2011). An agent-based model for risk-based flood incident management. *Natural Hazards, 59*, 167-189.

Debele, S. E., Strupczewski, W. G., & Bogdanowicz, E. (2017). A comparison of three approaches to non-stationary flood frequency analysis. *Acta Geophysica, 65*, 863-883.

Deidda, R., Marrocu, M., Caroletti, G., Pusceddu, G., Langousis, G., Langousis, A., . . . Speranza, A. (2013). Regional climate models' performance in representing precipitation and temperature over selected Mediterranean areas. *Hydrology and Earth System Sciences, 17*, 5041-5059.

Deng, Z., Zhu, X., He, Q., & Tang, L. (2019). Land use/land cover classification using time series Landsat 8 images in a heavily urbanized area. *Advances in Space Research, 63*, 2144-2154.

Derse, M. A., & Alphan, H. (2012). Sürdürülebilir Arazi Kullanım Planlaması için Uzaktan Algılama Verilerine Dayalı Bölgesel Değişim Tespiti: Erdemli (Mersin) Örneği. *Ç.Ü. Fen ve Mühendislik Bilimleri Dergisi, 28*(5), 29-38.

Dezso, Z. B., Pongracz, R., & Barcza, Z. (2005). Analysis of land-use/land-cover change in the Carpathian Region based on remote sensing techniques. *Physics and Chemistry of the Earth, Parts A/B/C, 30*, 109-115.

Dino, I. G., & Akgül, C. M. (2019). Impact of climate change on the existing residential building stock in Turkey: An analysis on energy use, greenhouse gas emissions and occupant comfort. *Renewable Energy, 141*, 828-846.

DSİ Strateji Geliştirme Dairesi Başkanlığı. (2020). *2019 YILI FAALİYET RAPORU.* Retrieved from http://www.dsi.gov.tr/docs/stratejik-plan/dsi-2019-faaliyet-raporu.pdf?sfvrsn=2

Dubbelboer, J., Nikolic, I., Jenkins, K., & Hall, J. (2017). An Agent-Based Model of Flood Risk and Insurance. *Journal of Artificial Societies and Social Simulation, 20*(1).

Dudgeon, D., Arthington, A., Gessner, M., Kawabata, Z., Knowler, D., Leveque, C., . . . Sullivan, C. (2006). Freshwater biodiversity: importance, threats, status and conservation challenges. *Biological Reviews, 81*, 163-182.

Dutrieux, L. P., Verbesselt, J., Kooistra, L., & Herold, M. (2015). Monitoring forest cover loss using multiple data streams, a case study of a tropical dry forest in Bolivia. *ISPRS Journal of Photogrammetry and Remote Sensing*, 112-125.

Dutta, D., Wright, W., Nakayama, K., & Sugawara, Y. (2013). Design of Synthetic Impact Response Functions for Flood Vulnerability Assessment under

Climate Change Conditions: Case Studies in Two Selected Coastal Zones in Australia and Japan. *Natural Hazards Review, 14*(1), 52-65.

Easterling, D., Meehl, G., Parmesan, C., Changnon, S., Karl, T., & Mearns, L. (2000). Climate Extremes: Observations, Modeling, and Impacts. *Science, 289*(5487), 2068-2074.

Eastoe, E. T. (2009). Modelling non-stationary extremes with application to surface level ozone. *Appl. Statist.*, 25-45.

El-Kawy, O., Rod, J., Ismail, H., & Suliman, A. (2011). Land use and land cover change detection in the western Nile delta of Egypt using remote sensing data. *Applied Geography, 31*, 483-494.

Erlat, E., Türkeş, M., & Aydin-Kandemir, F. (2021). Observed changes and trends in heatwave characteristics in Turkey since 1950. *Theoretical and Applied Climatology, 145*(1), 137-157.

EURO-CORDEX. (2021, December 21).

EURO-CORDEX. (2021, 12 21). *EURO-CORDEX Errata Page, Errata Table*. Retrieved from EURO-CORDEX: https://www.euro-cordex.net/078730/index.php.en

European Environment Agency. (2020). *CORINE Land Cover 2018 (vector), Europe, 6-yearly - version 2020_20u1, May 2020*. doi:https://doi.org/10.2909/71c95a07-e296-44fc-b22b-415f42acfdf0

Fan, F., Weng, Q., & Wang, Y. (2007). Land Use and Land Cover Change in Guangzhou, China, from 1998 to 2003, Based on Landsat TM/ETM+ Imagery. *Sensors, 7*, 1323-1342.

Faulkner, D., Warren, S., Spencer, P., & Sharkey, P. (2020). Can we still predict the future from the past? Implementing non-stationary flood frequency analysis in the UK. *Journal of Flood Risk Management, 13*(1).

Feng, B., Zhang, Y., & Bourke, R. (2021). Urbanization impacts on flood risks based on urban growth data and coupled flood models. *Natural Hazards, 106*, 613-627.

Feyen, L., Barredo, J. I., & Dankers, R. (2009). Implications of global warming and urban land use change on flooding in Europe. In *Water and Urban Development Paradigms* (pp. 217-225). London: CRC Press.

Feyen, L., Dankers, R., Bodis, K., Salamon, P., & Barredo, J. I. (2012). Fluvial flood risk in Europe in present and future climates. *Climatic Change, 112*, 47-62.

Flato, G., Marotzke, J., Abiodun, B., Braconnot, P., Chou, S., Collins, W., . . . Rummukainen, M. (2013). *Evaluation of Climate Models. In: Climate Change 2013: The Physical Science Basis." Contribution of Working Group I to the Fifth Assessment Report of the Intergovernmental Panel on Climate Change.* Cambridge and New York: Cambridge University Press.

Fu, P., & Weng, Q. (2016). A time series analysis of urbanization induced land use and land cover change and its impact on land surface temperature with Landsat imagery. *Remote Sensing Environment, 175*, 205-214.

Fujihara, Y., Tanaka, K., Watanabe, T., Nagano, T., & Kojiri, T. (2008). Assessing the impacts of climate change on the water resources of the Seyhan River Basin in Turkey: Use of dynamically downscaled data for hydrologic simulations. *Journal of Hydrology, 353*, 33-48.

Game, P., Wang, M., Audra, P., & Gourbesville, P. (2023). Flood modelling for a real-time decision support system of the covered Lower Paillons River, Nice, France. *ournal of Hydroinformatics, 25*(5), 1884-1908.

Ganguli, P., & Coulibaly, P. (2017). Does nonstationarity in rainfall require nonstationary intensity–duration–frequency curves? *Hydrology and Earth System Sciences, 21*, 6461-6483.

Gao, L., Huang, J., Chen, X., Chen, Y., & Liu, M. (2017). Risk of Extreme Precipitation under Nonstationarity Conditions during the Second Flood Season in the Southeastern Coastal Region of China. *Journal of Hydrometeorology, 18*, 669-681.

Garijo, C., & Mediero, L. (2018). Influence of climate change on flood magnitude and seasonality in the Arga River catchment in Spain. *Acta Geophysica, 66*, 769-790.

Gilbert, N. (2008). *Agent-Based Models.* United States of America: Sage Publications.

Gilleland, E., & Katz, R. (2016). extRemes 2.0: An Extreme Value Analysis Package in R. *Journal of Statistical Software, 72*(8), 1-39.

Giorgi, F. (2006). Climate change hot-spots. *Geophysical Research Letters, 33*, 1-4.

Giorgi, F., & Gutowski Jr, W. J. (2015). Regional dynamical downscaling and the CORDEX initiative. *Annual review of environment and resources, 40*, 467-490.

Giorgi, F., & Lionello, P. (2008). Climate change projections for the Mediterranean region. *Global and Planetary Change, 63*, 90-104.

Göksel, Ç., & Balçık, F. B. (2019). Land Use and Land Cover Changes Using Spot 5 Pansharpen Images; A Case Study in Akdeniz District, Mersin-Turkey. *Turkish Journal of Engineering, 3*(1), 32-38.

Gu, X., Zhang, Q., Singh, V., Xiaoa, M., & Cheng, J. (2017). Nonstationarity-based evaluation of flood risk in the Pearl River basin: changingpatterns, causes and implications. *Hydrological Sciences Journal, 62*(2), 246-258.

Gül, G., Aşıkoğlu, Ö., Gül, A., Yaşoğlu, F., & Benzeden, E. (2013). Nonstationarity in Flood Time Series. *Journal of Hydrologic Engineering, 19*(7).

Gül, G., Rosbjerg, D., Gül, A., Ondracek, M., & Dikgola, K. (2010). Assessing climate change impacts on river flows and environmental flow requirements at catchment scale. *Ecohydrology*, 28-40.

Güler, M., Yomralıoğlu, T., & Reis, S. (2007). Using landsat data to determine land use/land cover changes in Samsun, Turkey. *Environmental Monitoring and Assessment, 127*, 155-167.

Guzha, A., Rufino, M., Okoth, S., Jacobs, S., & Nobrega, R. (2018). Impacts of land use and land cover change on surface runoff, discharge and low flows: Evidence from East Africa. *Journal of Hydrology: Regional Studies, 15*(2018), 49-67.

Haer, T., Botzen, W., de Moel, H., & Aerts, J. (2017). Integrating Household Risk Mitigation Behavior in FloodRisk Analysis: An Agent-Based Model Approach. *Risk Analysis, 37*(10), 1977-1992.

Haer, T., Husby, T. G., Botzen, W. J., & Aerts, J. C. (2020). The safe development paradox: An agent-based model for flood risk under climate change in the European Union. *Global Environmental Change, 60*.

Hallegatte, S., Ranger, N., Bhattacharya, S., Bachu, M., Priya, S., Dhore, K., . . . Herweijer, C. (2010). *Flood Risks, Climate Change Impacts and Adaptation Benefits in Mumbai: An Initial Assessment of Socio-Economic Consequences of Present and Climate Change Induced Flood Risks and of Possible Adaptation Options.* Paris: Organization for Economic Co-operation and Development Publishing.

Hammond, R. (2015). Considerations and best practices in agent-based modeling to inform policy. In *Assessing the use of agent-based models for tobacco regulation.* National Academies Press (US).

Hammond, R. (2015). Considerations and Best Practices in Agent-Based Modeling to Inform Policy. In *Assessing the Use of Agent-Based Models for Tobacco Regulation* (pp. 161-193). Washington DC: National Academies Press.

Harada, M., Maruya, Y., Kojima, T., Matsuoka, D., Nakagawa, Y., Kawahara, S., & Araki, F. (2020). Flood Frequency Analysis and Impact Assessment for Climate Change in the Nagara River Basin. *Journal of JSCE, 8*, 79-86.

Hassan, Z., Shabbir, R., Ahmad, S., Malik, A., Aziz, N., Butt, A., & Erum, S. (2016). Dynamics of land use and land cover change (LULCC) using geospatial techniques: a case study of Islamabad, Pakistan. *SpringerPlus, 5*(812).

Hassani-Mahmooei, B., & Parris, B. (2012). Climate change and internal migration patterns in Bangladesh: an agent-based model. *Environment and Development Economics, 17*(6), 763-780.

HEC-HMS. (2023, July 14). *Youtube*. Retrieved from HEC HMS Model Calibration Strategies: https://www.youtube.com/watch?v=t5uzhfK-kFA

Hesarkazzazi, S., Arabzadeh, R., Hajibabaei, M., Rauch, W., Kjeldsen, T., Prosdocimi, I., . . . Sitzenfrei, R. (2021). Stationary vs non-stationary modelling of flood frequency distribution across northwest England. *Hydrological Sciences Journal*, 729-744.

Hirabayashi, H., Mahendran, R., Koirala, S., Konoshima, L., Yamazaki, D., Watanabe, S., . . . Kanae, S. (2013). Global flood risk under climate change. *Nature Climate Change, 3*, 816-821.

Holley, J., McComas, K., Lambert, C., Snider, N., & Tucker, G. (2022). Responding to flood risk in Louisiana: the roles of place attachment, emotions, and location. *Natural Hazards, 113*, 615-640.

Hounkpe, J., Diekkrüger, B., Badou, D., & Afouda, A. (2015). Non-Stationary Flood Frequency Analysis in the Ouémé River Basin, Benin Republic. *Hydrology, 2*(4), 210-229.

Huang, C., Zhang, C., He, Y., Liu, Q., Li, H., Su, F., . . . Bridhikitti, A. (2020). Land Cover Mapping in Cloud-Prone Tropical Areas Using Sentinel-2

Data: Integrating Spectral Features with Ndvi Temporal Dynamics. *Remote Sensing, 12*(7).

Huizinga, J., De Moel, H., & Szewczyk, W. (2017). *Global flood depth-damage functions: Methodology and the database with guidelines.* Luxembourg: Publications Office of the European Union.

Hunter, D. (2002). *Risk Perception and Risk Tolerance in Aircraft Pilots.* Washington, DC: Office of Aerospace Medicine.

Hydrologic Engineering Center. (2023). *HEC-SSP Version 2.3.*

Igarashi, K., Koichiro, K., Tanaka, N., & Aranyabhaga, N. (2018). Prediction of the Impact of Climate Change and Land Use Change on Flood Discharge in the Song Khwae District, Nan Province, Thailand. *Journal of Climate Change, 5*(1), 1-8.

İhlas Haber Ajansı. (2017, March 15). *Silifke'de Göksu ırmağının debisi yükseldi, bin 109 dekar alan zarar gördü.* Retrieved from İHA: https://www.iha.com.tr/mersin-haberleri/-1648015

IPCC. (2014). *Climate Change 2014 Synthesis Report.* Geneva.

IPCC. (2018). *An IPCC Special Report on the impacts of global warming of 1.5°C above pre-industrial levels and related global greenhouse gas emission pathways, in the context of strengthening the global response to the threat of climate change,... to eradicate poverty.*

IPCC. (2021). *Climate Change 2021: The Physical Science Basis. Contribution of Working Group I to the Sixth Assessment Report of the Intergovernmental Panel on Climate Change.* Cambridge University Press.

Isensee, L., Pinheiro, A., & Detzel, D. (2021). Dam Hydrological Risk and the Design Flood Under Non-stationary Conditions. *Water Resources Management*, 1499-1512.

Jaw, T., Li, J., Hsu, K. l., & Sorooshian, S. D. (2015). Evaluation for Moroccan dynamically downscaled precipitation from GCM CHAM5 and its regional hydrologic response. *Journal of Hydrology: Regional Studies*, 359-378.

Jenkins, K., Surminski, S., Hall, J., & Crick, F. (2017). Assessing surface water flood risk and management strategies under future climate change: Insights from an Agent-Based Model. *Science of the Total Environment, 595*, 159-168.

Jonkman, S., & Vrijling, J. (2008). Loss of life due to floods. *Journal of Flood Risk Management*, 43-56.

Kafy, A., Rahman, M., Faisal, A., Hasan, M., & Islam, M. (2020). Modelling future land use land cover changes and their impacts on land surface temperatures in Rajshahi, Banghladesh. *Remote Sensing Applications: Society and Environment, 18*. doi:https://doi.org/10.1016/j.rsase.2020.100314

Kang, L., Jiang, S., Hu, X., & Li, C. (2019). Evaluation of Return Period and Risk in Bivariate Non-Stationary Flood Frequency Analysis. *Water, 11*(1).

Kara, F., & Yücel, İ. (2015). Climate change effects on extreme flows of water supply area in Istanbul: utility of regional climate models and downscaling method. *Environmental Monitoring and Assessment, 187*(580), 1-18.

Karagiannis, G., Chondrogiannis, S., Krausmann, E., & Turksezer, Z. (2017b). *Power Grid Recovery After NaturalHazard Impact.* European Commission.

Karagiannis, G., Turksezer, Z., Alfieri, L., Feyen, L., & Krausmann, E. (2017a). *Climate Change and Critical Infrastructure.* JRC.

Kentel, E., Yücel, İ., Mesta, B., Akgün, Ö., Özcan, C., Ercan, E., . . . Matur, İ. (2021). *TÜBİTAK Antalya Havzası'nda İklim Değişikliğinin Debi ve HES Enerji Üretimine Etkilerinin İncelenmesi Projesi (Pr No: 118Y365).* Ankara: TÜBİTAK.

Klijn, F., De Bruijn, K. M., Knoop, J., & Kwadijk, J. (2012). Assessment of the Netherlands' Flood Risk Management Policy Under Global Change. *AMBIO, 41*, 180-192.

Kostopoulou, E., & Jones, P. D. (2005). Assessment of climate extremes in the Eastern Mediterranean. *Meteorology and Atmospheric Physics, 89*(1), 69-85.

Kreibich, H., Bubeck, P., Van Vliet, M., & De Moel, H. (2015). A review of damage-reducing measures to manage fluvial flood risks in a changing climate. *Mitigation and Adaptation Strategies for Global Change* , 967-989.

Kuglitsch, F. G., Toreti, A., Xoplaki, E., Della-Marta, P. M., Zerefos, C. S., Türkeş, M., & Luterbacher, J. (2010). Heat wave changes in the eastern Mediterranean since 1960. *Geophysical Research Letters, 37*(4).

Landis, J., & Koch, G. (1977). The Measurement of Observer Agreement of Categorical Data. *Biometrics, 33*(1), 159-174.

Laudan, J. (2019). *Changing Susceptibility of Flood-prone Residents in Germany: Mental Coping and Mitigation Behaviour in the Context of Different Flood Types.* Potsdam: University of Potsdam.

Leclerc, M., & Ouarda, T. (2007). Non-stationary regional flood frequency analysis at ungauged sites. *Journal of Hydrology, 343*(3-4), 254-265.

Liu, D., Li, M., Li, Y., & Chen, H. (2022). Assessment of Public Flood Risk Perception and Influencing Factors: An Example of Jiaozuo City, China. *Sustainability, 14*(15).

Liu, D., Li, Y., Shen, X., Xie, Y., & Zhang, Y. (2018). Flood risk perception of rural households in western mountainous regions of Henan Province, China. *International Journal of Disaster Risk Reduction, 27*, 155-160.

Liu, W., Feng, Q., Engel, B., Yu, T., Zhang, X., & Qian, Y. (2023). A probabilistic assessment of urban flood risk and impacts of future climate change. *Journal of Hydrology, 618*.

Liu, Y., Chen, W., Li, L., Huang, J., Wang, X., Guo, Y., & Ji, G. (2023). Assessing the contribution of vegetation variation to streamflow variation in the Lancang River Basin, China. *Frontiers in Ecology and Evolution, 10*.

López, J., & Francés, F. (2013). Non-stationary flood frequency analysis in continental Spanish rivers, using climate and reservoir indices as external covariates. *Hydrology and Earth System Sciences, 17*(8), 3189-3203.

Lu, F., Song, X., Xiao, W., Zhu, K., & Xie, Z. (2019). Detecting the impact of climate and reservoirs on extreme floods using nonstationary frequency models. *Stochastic Environmental Research and Risk Assessment, 34*, 169-182.

Luca, D., & Galasso, L. (2018). Stationary and Non-Stationary Frameworks for Extreme Rainfall Time Series in Southern Italy. *Water, 10*(10).

Madsen, H., Lawrence, D., Lang, M., Martinkova, M., & Kjeldsen, T. (2014). Review of trend analysis and climate change projections of extreme precipitation and floods in Europe. *Journal of Hydrology, 519*, 3634-3650.

Mahmood, R., Jia, S., & Zhu, W. (2019). Analysis of climate variability, trends, and prediction in the most active parts of the Lake Chad basin, Africa. *Scientific Reports*, 1-18.

Mahmoud, S. H., & Gan, T. Y. (2018). Urbanization and climate change implications in flood risk management: Developing an efficient decision support system for flood susceptibility mapping. *Science of the Total Environment, 636*, 152-167.

Manandhar, R., Odeh, I., & Ancev, T. (2009). Improving the Accuracy of Land Use and Land Cover Classification of Landsat Data Using Post-Classification Enhancement. *Remote Sensing, 1,* 330-344.

Mariotti, L., Coppola, E., Sylla, M., Giorgi, F., & Piani, C. (2011). Regional climate model simulation of projected 21st century climate change over an all-Africa domain: Comparison analysis of nested and driving model results. *Journal of Geophysical Research, 116*(d15111), 1-22.

Mehr, A. D., & Kahya, E. (2017). Climate Change Impacts on Catchment-Scale Extreme Rainfall Variability: Case Study of Rize Province, Turkey. *Journal of Hydrologic Engineering, 22*(3), 1-11.

Merz, B., Blöschl, G., Vorogushyn, S., Dottori, F., Aerts, J., Bates, P., . . . Macdonald, E. (2021). Causes, impacts and patterns of disastrous river floods. *Nature Reviews Earth & Environment,* 592-609.

Mesta, B., Akgun, O., & Kentel, E. (2024). Improving precipitation estimates for Turkey with multimodel ensemble: a comparison of nonlinear artificial neural network method with linear methods. *Neural Comput & Applic*.

Mesta, B., Sasaki, H., Nakaegawa, T., & Kentel, E. (2022). Changes in precipitation climatology for the Eastern Mediterranean using CORDEX RCMs, NHRCM and MRI-AGCM. *Atmospheric Research, 272*. doi:https://doi.org/10.1016/j.atmosres.2022.106140

Moriasi, D., Arnold, J., Van Liew, M., Bingner, R., Harmel, R., & Veith, T. (2007). Model evaluation guidelines for systematic quantification of accuracy in watershed simulations. *Trans. ASABE, 50*(3), 885-900. doi:http://dx.doi.org/10.13031/2013.23153

Moriasi, D., Gitau, M., Pai, N., & Daggupati, P. (2015). Hydrologic and Water Quality Models: Performance Measures and Evaluation Criteria. *American Society of Agricultural and Biological Engineers, 58*(6), 1763-1785. doi:10.13031/trans.58.10715

Mukherjee, F., & Singh, D. (2020). Assessing Land Use-Land Cover Change and Its Impact on Land Surface Temperature Using LANDSAT Data: A Comparison of Two Urban Areas in India. *Earth Systems and Environment, 4*, 385-407.

Muttitanon, W., & Tripathi, N. (2005). Land use/land cover changes in the coastal zone of Ban Don Bay, Thailand using Landsat 5 TM data. *International Journal of Remote Sensing, 26*(11), 2311-2323.

Netzel, L., Heldt, S., Engler, S., & Denecke, M. (2021). The importance of public risk perception for the effective management of pluvial floods in urban areas: A case study from Germany. *Journal of Flood Risk Management, 14*(2).

Nigussie, T., & Altunkaynak, A. (2019). Modeling the effect of urbanization on flood risk in Ayamama Watershed, Istanbul, Turkey, using the MIKE 21 FM model. *Natural Hazards, 99*, 1031-1047.

Ogras, S., & Onen, F. (2020). Flood Analysis with HEC-RAS: A Case Study of Tigris River. *Hindawi Advances in Civil Engineering*.

Oruc, S., Yücel, İ., & Yılmaz, A. (2022). Investigation of the Effect of Climate Change on Extreme Precipitation: Capital Ankara Case. *Teknik Dergi, 33*(2), 11749-11778.

Osei, M. A., Amekudzi, L. K., Omari-Sasu, A. Y., Yamba, E. I., Quansah, E., Aryee, J. N., & Preko, K. (n.d.). Estimation of the return periods of maxima rainfall and floods at the Pra River Catchment, Ghana, West Africa using the Gumbel extreme value theory. *Heliyon, 7*(5).

Otukei, J., & Blaschke, T. (2010). Land cover change assessment using decision trees, support vector machines and maximum likelihood classification algorithms. *International Journal of Applied Earth Observation and Geoinformation, 12S*, S27-S31.

Oubennaceur, K., Chokmani, K., Gauthier, Y., Ratte-Fortin, C., Homayouni, S., & Toussaint, J. –P. (2021). Flood Risk Assessment under Climate Change: The Petite Nation River Watershed. *Climate, 9*(125), 1-23.

Özdoğan, M. (2011). Modeling the impacts of climate change on wheat yields in Northwestern Turkey. *Agriculture, Ecosystems and Environment, 141*, 1-12.

Öztürk, T., Ceber, Z. P., Türkeş, M., & Kurnaz, M. L. (2015). Projections of climate change in the Mediterranean Basin by using downscaled global climate model outputs. *International Journal of Climatology, 35*, 4276-4292.

Papaioannou, G., Efstratiadis, A., Vasiliades, L., Loukas, A., Papalexiou, S. M., Koukouvinos, A., . . . Kossieris, P. (2018). An Operational Method for Flood Directive Implementation in Ungauged Urban Areas. *Hydrology, 5*, 24.

Patel, M. B. (2020). Flood frequency analysis using Gumbel distribution method at Garudeshwar Weir, Narmada Basin. *International Journal of Trend in Research and Development, 1*(7), 36-38.

Petchprayoon, P., Blanken, P. D., Ekkawatpanit, C., & Hussein, K. (2010). Hydrological impacts of land use/land cover change in alarge river basin in central–northern Thailand. *International Journal of Climatology, 30*, 1917-1930.

Pettorelli, N., Vik, J., Mysterud, A., Gaillard, J., Tucker, C., & Stenseth, N. (2005). Using the satellite-derived NDVI to assess ecological responses to environmental change. *Trends in ecology & evolution, 20*(9), 503-510.

Piani, C., Weedon, G. P., Best, M., Gomes, S. M., Viterbo, P., Hagemann, S., . . . Haerter, J. O. (2010). Statistical bias correction of global simulated daily precipitation and temperature for the application of hydrological models. *Journal of Hydrology, 395*(3-4), 199-215.

Poelmans, L., Van Rompaey, A., Ntegeka, V., & Willems, P. (2011). The relative impact of climate change and urban expansion on peak flows: a case study in central Belgium. *Hydrological Processes, 25*, 2846-2858.

Qu, C., Li, J., Yan, L., Yan, P., Cheng, F., & Lu, D. (2020). Non-Stationary Flood Frequency Analysis Using Cubic B-Spline-Based GAMLSS Model. *Water, 12*(7).

Radojevic, B. D., Breil, P., & Chocat, B. (2010). Assessing impact of global change on flood regimes. *International Journal of Climate Change Strategies and Management, 2*(2), 167-179.

Ranger, N., Hallegatte, S., Bhattacharya, S., Bachu, M., Priya, S., Dhore, K., . . . Morlot, J. (2011). An assessment of the potential impact of climate change on flood risk in Mumbai. *Climatic Change, 104*, 139-167.

Razmi, A., Golian, S., & Zahmatkesh, Z. (2017). Non-Stationary Frequency Analysis of Extreme Water Level: Application of Annual Maximum Series and Peak-over Threshold Approaches. *Water Resources Management, 31*, 2065-2083.

Read, L., & Vogel, R. (2015). Reliability, return periods, and risk under nonstationarity. *Water Resources Research, 51*(8), 6381-6398.

Richert, C., Erdlenbruch, K., & Figuieres, C. (2017). The determinants of households' flood mitigation decisions in France - on the possibility of feedback effects from past investments. *Ecological Economics, 131*, 342-352.

Ridha, T., Ross, A., & Mostafavi, A. (2022). Climate change impacts on infrastructure: Flood risk perceptions and evaluations of water systems in coastal urban areas. *International Journal of Disaster Risk Reduction, 73*.

Rigby, R., & Stasinopoulos, D. (2005). Generalized additive models for location, scale and shape, (with discussion). *Applied Statistics, 54*, 507-554.

Rincon, D., Velandia, J. F., Tsanis, I., & Khan, U. T. (2022). Stochastic Flood Risk Assessment under Climate Change Scenarios for Toronto, Canada Using CAPRA. *Water, 14*(227).

Rivera, J. A., & Arnould, G. (2020). Evaluation of the ability of CMIP6 models to simulate precipitation over Southwestern South America: Climatic features and long-term trends (1901–2014). *Atmospheric Research, 241*, 1-15.

Robi, M. A., Abebe, A., & Pingale, S. M. (2018). Flood hazard mapping under a climate change scenario in a Ribb catchment of Blue Nile River basin, Ethiopia. *Applied Geomatics, 11*, 147-160. Retrieved from https://link.springer.com/article/10.1007/s12518-018-0249-8

Rogers, R. (1975). A Protection Motivation Theory of Fear Appeals and Attitude Change. *The Journal of Psychology, 91*(1), 93-114.

Salas, J., & Obeysekera, J. (2014). Revisiting the Concepts of Return Period and Riskfor Nonstationary Hydrologic Extreme Events. *Journal of Hydrologic Engineering, 19*(3), 554-568.

Sarhadi, A., & Soulis, E. (2017). Time-varying extreme rainfall intensity-duration-frequency curves in a changing climate. *Geophysical Research Letters, 44*(5), 2454-2463.

Sato, Y., Kojiri, T., Michihiro, Y., Suzuki, Y., & Nakakita, E. (2012). Estimates of Climate Change Impact on River Discharge in Japan Based on a Super-High- Resolution Climate Model. *Terrestrial, Atmospheric & Oceanic Sciences, 23*(5).

Şen, O., & Kahya, E. (2017). Determination of flood risk: A case study in the rainiest city of Turkey. *Environmental Modelling & Software, 93*, 296-309.

Sensoy, S. T., Akçakaya, A., Ekici, M., Demircan, M., Ulupinar, Y., ..., & Demirbaş, H. (2013). Trends in Turkey climate indices from 1960 to 2010. *6th Atmospheric science symposium, 24*, p. 26.

Serago, J., & Vogel, R. (2018). Parsimonious nonstationary flood frequency analysis. *Advances in Water Resources, 112*, 1-16.

Seyran, Z. (2009). *Aşağı Seyhan Ovasının Geçmişten Günümüze Arazi Kullanımındaki Değişiminin, Coğrafi Bilgi Sistemleri ve Uzaktan Algılama ile Belirlenmesi (Yayınlanmamış Yüksek Lisans Tezi).* Adana: Çukurova Üniversitesi, Fen Bilimleri Enstitüsü. Retrieved from http://libratez.cu.edu.tr/tezler/7642.pdf

Sharma, D., Das Gupta, A., & Babel, M. S. (2007). Spatial disaggregation of bias-corrected GCM precipitation for improved hydrologic simulation: Ping River Basin, Thailand. *Hydrology and Earth System Sciences, 11*(4), 1373-1390.

Singh, N., & Chinnasamy, P. (2021). Non-stationary flood frequency analysis and attribution of streamflow series: a case study of Periyar River, India. *Hydrological Sciences Journal*, 1866-1881.

Snyder, F. (1938). Synthetic unit graphs. *Trans. Am. Geophys. Union*, 447-454.

Solomon, O., & Prince, O. (2013). Flood frequency analysis of Osse river using Gumbel's distribution. *Civil and environmental research*, *3*(10), 55-59.

Son, C., Lee, T., & Kwon, H. (2017). Integrating nonstationary behaviors of typhoon and non-typhoon extreme rainfall events in East Asia. *Scientific Reports*.

Song, X., Lu, F., Wang, H., Xiao, W., & Zhu, K. (2018). Penalized maximum likelihood estimators for the nonstationary Pearson type 3 distribution. *Journal of hydrology*, 579-589.

Sönmez, M. (2012). Adana Şehrinin Alansal Gelişimi ve Yakın Çevresinin Arazi Kullanımında Meydana Gelen Değişimler. *Türk Coğrafya Dergisi, 57*, 55-69.

Spinoni, J., Barbosa, P., Bucchignani, E., Cassano, J., Cavazos, T., Christensen, J. H., . . . Dosio, A. (2020). Future Global Meteorological Drought Hot Spots: A Study based on CORDEX Data. *Journal of Climate, 33*, 3635-3661.

Sraj, M., Viglione, A., Parajka, J., & Blöschl, G. (2016). The influence of non-stationarity in extreme hydrological events on flood frequency estimation. *Journal of Hydrology and Hydromechanics, 64*(4).

Šraj, M., Viglione, A., Parajka, J., & Blöschl, G. (2016). The influence of non-stationarity in extreme hydrological events on flood frequency estimation. *Journal of Hydrology and Hydromechanics, 64*(4), 426-437.

Story, M., & Congalton, R. (1986). Accuracy Assessment: A User's Perspective. *Photogrammetric Engineering and Remote Sensing, 52*, 397-399.

Sun, P., Liu, S., Jiang, H., Lü, Y., Liu, J., Lin, Y., & Liu, X. (2008). Hydrologic Effects of NDVI Time Series in a Context of Climatic Variability in an Upstream Catchment of the Minjiang River. *JAWRA Journal of the American Water Resources Association, 44*(5), 1132-1143.

Sun, P., Wen, Q., Zhang, Q., Singh, V., Sun, Y., & Li, J. (2018). Nonstationarity-based evaluation of flood frequency and flood risk in the Huai River basin, China. *Journal of Hydrology, 567*, 393-404.

Swain, D., Wing, O., Bates, P., Done, J., Johnson, K., & Cameron, D. (2020). Increased Flood Exposure Due to Climate Change and Population Growth in the United States. *Earth's Future, 8*(11).

Szwagrzyk, M., Kaim, D., Price, B., Wypych, A., Grabska, E., & Kozak, J. (2018). Impact of forecasted land use changes on flood risk in the Polish Carpathians. *Natural Hazards, 94*, 227-240.

Tabari, H. (2020). Climate change impact on flood and extreme precipitation increases with water availability. *Scientific Reports, 10*.

Tan, K., Lim, H., MatJafri, M., & Abdullah, K. (2010). Landsat data to evaluate urban expansion and determine land use/land cover changes in Penang Island, Malaysia. *Environmental Earth Sciences, 60,* 1509-1521.

Tanaka, T., Kiyohara, K., & Tachikawa, Y. (2020). Comparison of fluvial and pluvial flood risk curves in urban cities derived from a large ensemble climate simulation dataset: A case study in Nagoya, Japan. *Journal of Hydrology, 584*.

Tayanç, M., İm, U., Doğruel, M., & Karaca, M. (2009). Climate change in Turkey for the last half century. *Climatic Change, 94*(3), 483-502.

Tian, Y., Bai, X., Wang, S., Qin, L., & Li, Y. (2017). Spatial-temporal changes of vegetation cover in Guizhou Province, Southern China. *Chinese Geographical Science,* 25-38.

Tonn, G., & Guikema, S. (2018). An Agent-Based Model of Evolving Community Flood Risk. *Risk Analysis, 38*(6), 1258-1278.

Tonn, G., Guikema, S., & Zaitchik, B. (2020). Simulating Behavioral Influences on Community Flood Risk under Future Climate Scenarios. *Risk Analysis, 40*(4), 884-898.

Toros, H. (2012). Spatio-temporal variation of daily extreme temperatures over Turkey. *International Journal of Climatology, 32*(7), 1047-1055.

Tübitak MAM Çevre Enstitüsü. (2013). *Havza Koruma Eylem Planlarının Hazırlanması-Doğu Akdeniz Havzası.* Ankara. Retrieved from https://www.tarimorman.gov.tr/SYGM/Belgeler/havza%20koruma%20eylem%20planlar%C4%B1/Dogu_Akdeniz_web.pdf

Turkish Statistical Institute. (2024). *Adrese Dayalı Nüfus Kayıt Sistemi Sonuçları*. Retrieved from Merkezi Dağıtım Sistemi.

Türkiye İstatistik Kurumu. (2018). *Nüfus Projeksiyonları, 2018-2080*. Retrieved from Türkiye İstatistik Kurumu: http://www.tuik.gov.tr/PreHaberBultenleri.do?id=30567

Türkiye İstatistik Kurumu. (2024). *İstatistik Veri Portalı*. Retrieved from TÜİK: https://data.tuik.gov.tr/Kategori/GetKategori?p=Nufus-ve-Demografi-109

Türkkan, G., & Hırca, T. (2021). The investigation of food risk perception as a quantitative analysis from socio-demographic perspective. *Natural Hazards*, 715-733.

U.S. Army Corps of Engineers. (2000). *HEC-HMS Technical Reference Manual.* Davis, CA.

U.S. Army Corps of Engineers. (2013). *HEC-HMS Hydrologic Modeling System, User's Manual, Version 4.0.* ccc.

U.S. Army Corps of Engineers. (2024). *HEC-HMS Hydrologic Modeling System, User's Manual, Version 4.9.* Davis, CA.

Unal, Y. S., Tan, E., & Mentes, S. S. (2013). Summer heat waves over western Turkey between 1965 and 2006. *Theoretical and Applied Climatology, 112*(1), 339-350.

Villarini, G., Serinaldi, F., Smith, J., & Krajewski, W. (2009). On the stationarity of annual flood peaks in the continental United States during the 20th century. *Water Resources Research, 45*(8).

Walther, G., Post, E., Convey, P., Menzel, A., Parmesan, C., Beebee, T., . . . Bairlein, F. (2002). Ecological responses to recent climate change. *Nature, 416*(6879), 389-395.

WCRP CORDEX. (n.d.). *What is regional downscaling?* Retrieved from CORDEX: https://cordex.org/about/what-is-regional-downscaling/

Wi, S., Valdes, J., Steinschneider, S., & Kim, T. (2016). Non-stationary frequency analysis of extreme precipitation in South Korea using peaks-over-threshold and annual maxima. *Stochastic Environmental Research and Risk Assessment*, 583-606.

Wilby, R. L., Beven, K. J., & Reynard, N. S. (2008). Climate change and fluvial flood risk in the UK: more of the same? *Hydrological Processes, 22*, 2511-2523.

Wilensky, U. (1999). NetLogo. Evanston, IL, USA. Retrieved from http://ccl.northwestern.edu/netlogo/

Wing, O., Lehman, W., Bates, P., Sampson, C., Quinn, N., Smith, A., . . . Kousky, C. (2022). Inequitable patterns of US flood risk in the Anthropocene. *Nature Climate Change*, 156-162.

Xu, X., Wang, Y. C., Kalcic, M., Muenich, R. L., Yang, Y. C., & Scavia, D. (2019). Evaluating the impact of climate change on fluvial flood risk in a mixed-use watershed. *Environmental Modeling & Software, 122*.

Yalcin, E. (2019). Two-dimensional hydrodynamic modelling for urban flood risk assessment using unmanned aerial vehicle imagery: A case study of Kirsehir, Turkey. *Journal of Flood Risk Management*, *12*(S1).

Yan, L., Li, L., Yan, P., He, H., Li, J., & Lu, D. (2019). Nonstationary Flood Hazard Analysis in Response to Climate Change and Population Growth. *Water, 11*(9).

Yang, T., & Liu, W. (2020). A General Overview of the Risk-Reduction Strategies for Floods and Droughts. *Sustainability, 12*(7).

Yeğin, M. (2015). *Master's Thesis: Flood risk mapping using economic, environmental and social dimensions.* Ankara: Middle East Technical University.

Yilmaz, A. G. (2015). The effects of climate change on historical and future extreme rainfall in Antalya, Turkey. *Hydrological Sciences Journal - Journal des Sciences Hydrologiques, 60*(12), 2148-2162.

Yilmaz, A., Imteaz, M., Shanableh, A., Al-Ruzouq, R., Atabay, S., & Haddad, K. (2023). A Non-Stationarity Analysis of Annual Maximum Floods: A Case Study of Campaspe River Basin, Australia. *Water, 15*(20).

Yin, J., Yin, Z., Zhong, H., Xu, S., Hu, X., Wang, J., & Wu, J. (2011). Monitoring urban expansion and land use/land cover changes of Shanghai metropolitan area during the transitional economy (1979-2009) in China. *Environmental Monitoring and Assessment, 177,* 609-621.

Yucel, I., Güventürk, A., & Sen, O. L. (2015). Climate change impacts on snowmelt runoff for mountainous transboundary basins in eastern Turkey. *International Journal of Climatology, 35*(2), 215-228.

Yüksel Proje. (2017). *Doğu Akdeniz Havzası Master Plan Raporu.* Ankara.

Zaalberg, R., Midden, C., Meijnders, A., & McCalley, T. (2009). Prevention, Adaptation, and Threat Denial: Flooding Experiences in the Netherlands. *Risk Analysis*, *29*(12), 1759-1778.

Zadbagher, E., Becek, K., & Berberoglu, S. (2018). Modeling land use/land cover change using remote sensing and geographic information systems: case study of the Seyhan Basin, Turkey. *Environmental Monitoring and Assessment, 190,* 494.

Zaidi, S., Akbari, A., Samah, A., Kong, N., & Gisen, J. (2017). Landsat-5 Time Series Analysis for Land Use/Land Cover Change Detection Using NDVI and Semi-Supervised Classification Techniques. *Polish Journal of Environmental Studies, 26*(6), 2833-2840.

Zhai, G., Sato, T., Fukuzono, T., Ikeda, S., & Yoshida, K. (2006). WILLINGNESS TO PAY FOR FLOOD RISK REDUCTION AND ITS DETERMINANTS

IN JAPAN. *Journal of the American Water Resources Association, 42*(4), 927-940.

Zhou, Q., Leng, G., Su, J., & Ren, Y. (2019). Comparison of urbanization and climate change impacts on urban flood volumes: Importance of urban planning and drainage adaptation. *Science of The Total Environment*, 24-33.

Zhuo, L., & Han, D. (2020). Agent-based modelling and flood risk management: A compendious literature review. *Journal of Hydrology, 591*.

STATEMENTS & DECLARATIONS

Ethical Approval

Not applicable

Consent to Participate

Not applicable

Consent to Publish

Not applicable

Author Contributions

Murat Yegin, Gulsah Karakaya and Elcin Kentel contributed to the design of the work. Material preparation, data collection and analysis were carried out by Murat Yegin. Interpretation of data and results were carried out by Murat Yegin, Gulsah Karakaya and Elcin Kentel. The first draft of the manuscript was written by Murat Yegin and Murat Yegin, Gulsah Karakaya and Elcin Kentel revised it critically. Murat Yegin, Gulsah Karakaya and Elcin Kentel read and approved the final manuscript.

Funding

This study was supported by Scientific and Technological Research Council of Turkey (TUBITAK) under the Grant Number 220N054.

Competing Interests

The authors declare that they have no conflict of interest.

Availability of data and materials

The datasets generated during and/or analyzed during the current study are available from the corresponding author on reasonable request.

B. Paper 2: Integration of climate change impacts and agent-based model to flood risk evaluation in an urbanized area

M. Yegin[1], S. Nabinejad[2], G. Karakaya[3], H. Schuttrumpf[2], E. Kentel[1]

[1] Department of Civil Engineering, Middle East Technical University, Ankara 06800, Türkiye

[2] Institute of Hydraulic Engineering and Water Resources Management, RWTH Aachen University, Aachen 52074, Germany

[3] Department of Business Administration, Middle East Technical University, Ankara 06800, Türkiye

ABSTRACT

Floods are among the most devastating natural hazards. Flood hazards cannot be prevented, but the consequences of floods can be reduced by taking necessary actions. Nevertheless, public actions are also very important in reducing flood consequences; in traditional flood risk management studies, government actions are included. In recent years, public actions have started to be included in the studies by using agent-based models (ABM). This study analyzes the impact of both climate change and agent impacts on flood risk in an urbanized area. 17 different regional climate models (RCM) were downloaded and analyzed for climate change analysis. The best RCM was selected based on some statistical measures, and the outputs of the best RCM were used in the hydrological model. The hydrological model was run between 2025 and 2100. The combined 1D/2D hydraulic model was run for each year using different flood hydrographs (i.e., 2-year, 5-year,…,500-year). In ABM, two different agents were included: i) public agent and ii) government agent. Decision analysis of the public agent is designed based on the individuals' flood risk perception and flood coping perception values. A survey was conducted in the study area to evaluate these parameters. In most of the studies, these parameters are randomly assigned. On the other hand, two different behavior types are used for the

government agent: i) Proactive behavior and ii) Reactive behavior. In this study, 11 different scenarios and 100 Realizations were generated to analyze CC and ABM on flood risks. The study's main findings are: i) Climate change is an important parameter and should be integrated into the hydrologic and hydraulic models for future simulations. ii) In our study area, the economic damage of the scenario with the survey results is greater than that with the random values. Thus, conducting the survey is crucial for the study area; iii) Government actions and behavior types of the government are important. In our study area, the benefit-cost ratio (B/C) of the scenarios with the government which takes action against a 50-year flood event is greater than the scenarios with the government which takes action against a 100-year flood event. Another important finding is that the B/C of some Realizations is lower than 1.0 for the scenarios with reactive government, while it is always greater than 1.0 if the government is proactive; iv) Timing of the severe flood event is effective on the average economic damage. The Realizations that a serious flood event occurred earlier (in the first 10 years of the simulation) have less average economic damage than the others due to the earlier actions. Thus, it is important to take action earlier, considering the possible future flood consequences; v) The public agent tends to forget the consequences of the floods around 9 years. Hence, it is important to educate the public and raise awareness about the floods in the study area.

1. INTRODUCTION

Floods are one of the most destructive natural hazards in the world (CRED and UNDRR, 2020). Although they cannot be prevented entirely, their consequences may be reduced significantly by taking the necessary mitigation and adaptation measures (Jonkman & Vrijling, 2008; Kreibich et al., 2015; Yang & Liu, 2020; Merz et al., 2021). These measures, which will be referred to as actions from here on for the sake of simplicity, can be taken by the public, the government, or both.

Traditional flood risk management (FRM) studies typically employ hydrological models to develop hydrographs of flood events with different return periods and hydraulic models to generate corresponding flood inundation maps. Afterwards, with

the help of these inundation maps and depth-damage curves, the economic, social, and environmental risks are calculated. However, thisapproach has two main shortcomings: i) it ignores the effects of climate change, and ii) it fails to account for potential impacts of actions.

Climate change (CC) is regarded as one of the most important drivers behind the changing frequency and intensity of floods worldwide (Bronstert, 2003; Hirabayashi et al., 2013; Swain et al., 2020). Thus, many researchers intended to integrate climate change impacts on traditional FRM (Ranger et al., 2011; Hirabayashi et al., 2013; Arnell & Gosling, 2016; Zhou et al., 2019; Tabari, 2020). Future flood risks are tried to be evaluated using the outputs of regional and global climate models in this study.

In traditional FRM studies, typically, the behaviors of the agents/stakeholders (i.e., the public, the government, or both) are overlooked. Although the involvement of stakeholders' behavior is crucial (Haer et al., 2020), there are a few studies in which the behaviors of the stakeholders are considered in FRM (Dubbelboer et al., 2016; Haer et al., 2017; Tonn & Guikema, 2018; Haer et al., 2020). These studies employed Agent-Based Model (ABM), which has been proposed to include stakeholders' behavior in the analysis. ABM is an analytical method for the social sciences that enables a researcher to create, analyze, and experiment with models composed of agents that interact within an environment (Gilbert, 2008). Actions taken by the stakeholders are integrated into flood risk analysis in a number of limited studies, such as Dawson et al. (2011), Haer et al. (2017), Tonn and Guikema (2018), and Haer et al. (2020). However, in most studies, random behaviors are assigned to the people living in flood-prone areas, or the analysis is carried out based on some hypothetical scenarios. This is because even though the incorporation of site-specific data to represent the behaviors of agents is expected to improve the accuracy of the analysis, it can be rather costly (Coughlan et al., 2013) and time-consuming, so its added value should be assessed. One of the main contributions of this study is to analyze the effects of the surveys on ABM.

Silifke, which has encountered numerous flood events over the past decade is chosen as the study area. Göksu River, which is one of the longest rivers in Turkey, runs through Silifke and discharges to the Mediterranean Sea. Silifke is quite suitable for analyzing the impact of both climate change and the actions of the stakeholders on floods due to historical floods in Silifke and the results of climate change studies conducted in the region (Aziz et al., 2020; Kentel et al., 2021).

The main objective of this study is to integrate both the effects of climate change and the actions of stakeholders into FRM analysis to develop more effective and resilient FRM strategies tailored to the specific needs and conditions of the study area. A hydrological model is developed for the study area to generate flood hydrographs of various return periods using precipitation and temperature predictions of the best-performing climate model for the period spanning from 2025 to 2100. A combined 1D/2D hydraulic model is developed to generate corresponding flood inundation maps. Finally, an ABM is generated to integrate the actions of agents (i.e., the public and the government) regarding flood risks. A survey is conducted to realistically represent the spatial distribution of behavior of the public agent (represented by the individuals living in the study area), while the government agent is designed based on two different management strategies, namely proactive and reactive.

This study is one of the first studies that integrates a hydrological model, a combined 1D/2D hydraulic model, and an ABM to evaluate CC impacts and behavior of the agents in micro-scale flood risk assessment. It is also crucial for Turkey because it is the first flood risk study that integrates both CC impacts and ABM. The study results highlight the significance of the timing of a major flood event on economic damage, the importance of the management strategies of the government and the realistic identification of economic damage calculated using site-specific information collected through surveys.

2. BACKGROUND

2.1.Flood risk and climate change

Intergovernmental Panel on Climate Change (IPCC) – Working groups I, II, and III (IPCC, 2014) define "Climate Change (CC)" as changes in the climate system that may be due to natural internal processes or external forcings such as persistent anthropogenic changes in the atmospheric composition or land use. Due to CC, precipitation and temperature trends are significantly altered compared to the current conditions or the pre-industrial era, and the natural systems are strongly affected (Easterling et al., 2000; Giorgi & Lionello, 2008; Mariotti et al., 2011; IPCC, 2014, 2018; Mahmood et al., 2019). Changes in the frequencies and intensities of extreme weather conditions, such as floods and droughts, are the most commonly encountered consequences of CC.

Recently, studies on the impact of CC on different types of floods (fluvial, pluvial, or coastal floods) have appeared in the literature. Hirabayashi et al. (2013) worked on global flood risk under CC using the outputs of 11 climate models. They calculated the peak discharge of the 100-year return period for the 20th century, estimated the return period of this discharge in the 21st century, and compared them. They found a significant increase in flood frequency in Southeast Asia, Peninsular India, eastern Africa, and the northern half of the Andes. In a more recent study by Arnell and Gosling (2016), the impacts of CC on river floods at the global scale are studied using the results of 21 climate models. Changes in the magnitude, return period of the flood peaks, flood-prone population, and flood-prone cropland for the 100-year flood event in 2050 were selected as indicators, and flood hazard was calculated based on these indicators. The study results showed the variations of flood risk under different climate models; moreover, the primary reason for this variation was identified as the precipitation projections of the climate models. Blöschl et al.(2019) studied the effect of climate change on European river floods by analyzing the observed flood discharges in the past five decades in Europe. They found that regional flood discharge trends range between an increase of about 11 % and a

decrease of about 23 % per decade. Oubennaceur et al. (2021) investigated the flood risk under CC for 2050 and 2080 in Quebec. They used one climate model and two different RCPs. They concluded that flood peaks and flood damages show a minor decrease in the future. Many studies conclude that CC affects flood risks (Hallegatte et al., 2010; Bai et al., 2019; Bangalore et al., 2019; Xu et al., 2019; Tanaka et al., 2020; Wing et al., 2022; Liu et al., 2023).

In Turkey, although there are many studies on floods (Yegin, 2015; Nigussie & Altunkaynak, 2019; Yalcin, 2019; Ogras & Onen, 2020; Bayazıt et al., 2021; Beden & Keskin, 2021), research on CC impacts on floods are very limited. One of the earliest studies was carried out by Gül et al. (2010) and flood frequency estimation methods under different climatologic and geographic conditions were carried out. In a study conducted by Şen and Kahya (2017), combined hydrological and hydraulic models were used to estimate surface and peak flows. They calculated these flows using historical observations and CC scenarios, concluding that the peak discharges would decrease due to CC in Rize. Bilici and Everest (2017) studied the relationship between the December 29, 2016 Mersin Flood and CC. They also studied the other causes of major floods in Mersin; however, numerical modeling was not conducted.

2.2.Agent-Based Model

ABM is an approach to modeling complex social dynamics. Agents in the model are represented as autonomous individuals, and different rules are assigned to the agents to simulate their behaviors. ABM is used in many areas, such as biology, social sciences, economics and finance, land use, and anthropology (Hammond, 2015).

In traditional flood risk analysis, possible actions that the government or the people can take are ignored. The government may adopt flood mitigation strategies proactively, regardless of flood experience, or reactively after experiencing floods. On the other hand, people's risk and coping perceptions are the two main factors that reflect people's tendency to take actions to decrease flood consequences (Zhai et al., 2006; Bubeck et al., 2012; Attems et al., 2020), may evolve with time and vary with spatial factors such as proximity to the river. Integrating these potential actions and

perceptions into FRM studies is a major challenge. Until recently, this need was not recognized since numerical modeling approaches are lacking in including people's and the government's behavior; however, ABM addresses this gap by incorporating the behaviors of agents in FRM.

Integration of ABM into FRM has limited applications. Dawson et al. (2010) estimated the vulnerability of people to flood under different storm surge conditions, defense scenarios, evacuation strategies, and flood warning times by coupling ABM with a hydrodynamic model in the coastal town of Towyn in the United Kingdom. They assessed agents' behavior based on age, sex, employment, and household size and randomly assigned locations to the agents. In a more recent study, Haer et al. (2017) integrated household risk mitigation behavior into FRM in Heijplaat, Rotterdam. They analyzed households' behavior under three different economic decision models: i) expected utility theory, ii) prospect theory, and iii) a prospect theory model They showed that future flood risk may be underestimated if human behavior is neglected in FRM. Tonn and Guikema (2018) developed an ABM that analyzes the impacts of community policies and individual decisions on community flood risk. Individuals' decisions were determined based on risk and coping perceptions, which were calculated based on parameters including the number of flood experiences, the number of near-miss flood experiences, and individual mitigation efforts. They concluded that community mitigation decreases future flood damage. One of the rare studies in which CC and ABM are used together is carried out by Haer et al. (2020). Using a scenario-based approach, they developed an ABM, where the government and the households were the main agents, to study flood risk under CC in the European Union. They found that the effects of extreme flood events (such as a 1000-year flood event) are more significant (economical damage is higher) for the proactive government than the reactive government, which provides high protection levels in large metropolitan areas. Zhuo and Han (2020) conducted a detailed literature review of ABM and FRM. They identified three topics: real-time flood emergency management, long-term flood adaptation planning, and flood hydrological planning, where ABM has been used, and addressed different research

challenges. They emphasized the potential contribution of ABM to future FRM studies.

2.2.1. Risk and Coping Perceptions

The risk-reducing behavior of individuals against natural hazards is interpreted using the Protection Motivation Theory (PMT) introduced by Rogers (1975) and has become very popular nowadays. Risk perception and coping perception are the two main cognitive processes of PMT.

Risk and coping perceptions are the two main factors that reflect people's tendency to take action to decrease flood consequences (Zhai et al., 2006; Bubeck et al., 2012; Attems et al., 2019). Risk and coping perceptions of people vary with time (i.e., flood experience) and space (i.e., proximity to the river). Thus, the actions of people should be quantified considering temporal and spatial dimensions in ABM.

Risk perception is a time-dependent parameter used to identify and evaluate risk associated with hazardous events (Hunter, 2022). People's risk perception regarding floods is investigated in a few studies. Botzen et al. (2009) evaluated how geographical and socioeconomic characteristics, flood experience, flood threat knowledge, and risk attitude influence flood risk perception in the Netherlands. They found that flood risk perception is generally low. They also stated that flood risk awareness may be improved by educating people about the causes of floods. In a recent study, Netzel et al. (2020) analyzed the importance of public risk perception for efficiently managing pluvial floods at two case study sites in Western Germany through a questionnaire-based telephone survey. Their findings revealed that personal and global risk perceptions should be distinguished. They observed that global risk perception was high while personal risk perception was relatively low among the participants. Furthermore, they analyzed the impacts of some parameters on risk perception and found that personal risk perception, education, housing conditions, and knowledge influence people's behavior in terms of mitigation. Liu et al. (2022) studied flood risk perception and effecting factors in Jiaozuo City, China. They assessed demographic factors, residential conditions, and other factors (e.g.

flood experience, adaptation measures), and found that people with lower levels of education and income, fewer flood experiences, as well those being married, living in rural areas, or near rivers/reservoirs had a higher flood risk perception than others.

Coping perception, which refers to the way people perceive their ability to handle and manage challenging circumstances, is an essential parameter in terms of protective behavior. Bubeck et al. (2012, 2018) stated that coping perception predicts protective behavior better than risk perception. Zaalberg et al. (2009) studied the flooding experiences in the Netherlands and investigated whether previous exposure to flooding significantly influenced residents' motivation to manage future flood events adequately. They found that people with flood experience exhibited strong emotional responses, increased concerns about future flooding, and increased perception of vulnerability to future floods. Laudan (2019) examined the damage-driving factors of flash floods and river floods in Germany. Furthermore, he assessed the psychological impacts on the coping ability of flood-affected households. He found that damage-driving factors are different for flash floods and river floods, and flood types weakly influence the coping perception of people.

Risk and coping perceptions are important indicators of people's decisions on whether to take action or not. Thus, these two factors are included in the FRM framework through ABM in this study.

3. DATA & METHODS

3.1.Study Area and Data

Göksu River, which is approximately 271 km, is one of the longest rivers in Turkey. It runs through Silifke and discharges to the Mediterranean Sea. Silifke, a district of Mersin located at the downstream part of Göksu River, is selected as the study area because of the number of flood events in recent years. In the 2004 flood, 4,887.3 da agricultural area and many residential areas were flooded. Economic damage was determined as approximately $ 6 million (Buldur et al., 2007). In the 2017 flood, 1,109 da agricultural areas were flooded, and economic damage was calculated as

approximately $ 370,000 (İhlas Haber Ajansı, 2017). The population of Silifke in 2023 is around 137,047 (Turkish Statistical Institute, 2024). Lidar point cloud data of the study area with 1 m resolution was obtained from the Ministry of Environment, Urbanization, and Climate Change. It covers approximately 500 $km^{2,}$ and its resolution is 1 m. The spatial data regarding the locations of buildings is also taken from the same institution. There are approximately 29,000 buildings in the study area. On the other hand, the bathymetry of Göksu River is obtained from the State Hydraulic Works (SHW), and the resolution of bathymetry data is 1 m as well. The bathymetry data covers the river section between the point where Göksu River discharges to sea and 8 km upstream of Silifke District Center. A digital elevation model is generated using lidar point cloud data and the bathymetry of the Göksu River. The photographs from the study area are given in Figure 1.

Figure 1. Photographs from the study area

There are 17 meteorological stations (MSs) in and around E17A014 Basin (see Figure 2). The observed minimum temperature in the basin is -28°C while the maximum is 46.7 °C. On the other hand, the maximum precipitation amount is observed as 168.6 mm. The recorded maximum discharge is 1996.0 m^3/s at E17A014 stream gage and this value is recorded during the flood event in 2004. This value is actually greater than 1996 m^3/s, but the stream gage could not record the real value because it was damaged during the flood event. The average discharge value is 100.6 m^3/s for this stream gage, which is located just upstream of the center of Silifke. The study area is shown in Figure.

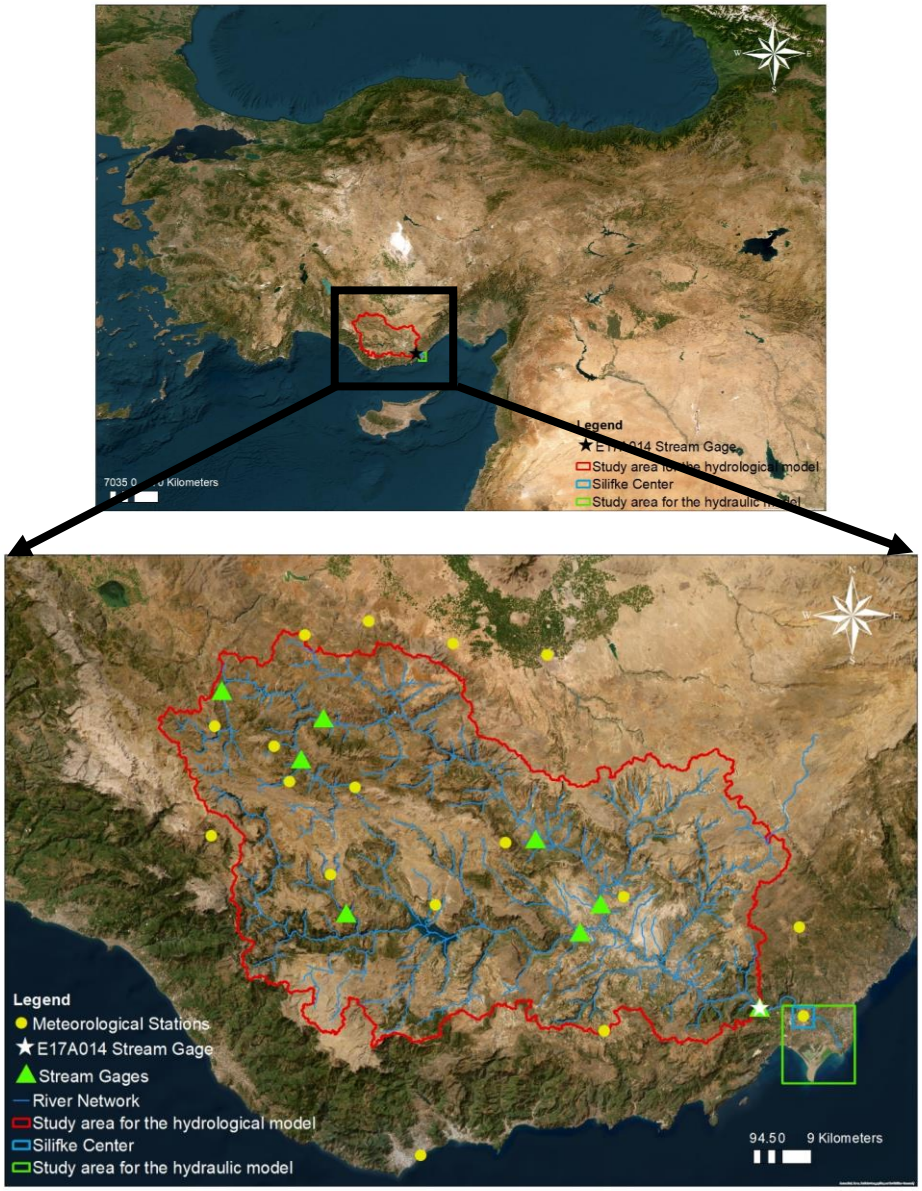

Figure 2. Location of the study area (Source: Esri, Maxar, Earthstar Geographics, and the GIS User Community)

3.2.Methods

The flowchart of the methodology is given in Figure 3. Three different models are developed within the context of this study. Firstly, a hydrological model to simulate the rainfall-runoff behavior of the catchment is developed to determine inundated areas. After calibration and validation of the model, a combined 1D/2D hydraulic

model is developed. Finally, using the combined 1D/2D hydrodynamic model outputs, an ABM covering the period from 2025 to 2100 is framed to incorporate the behaviors of the agents and evaluate their impacts on flood risks. Detailed information about each model is provided in the following sections.

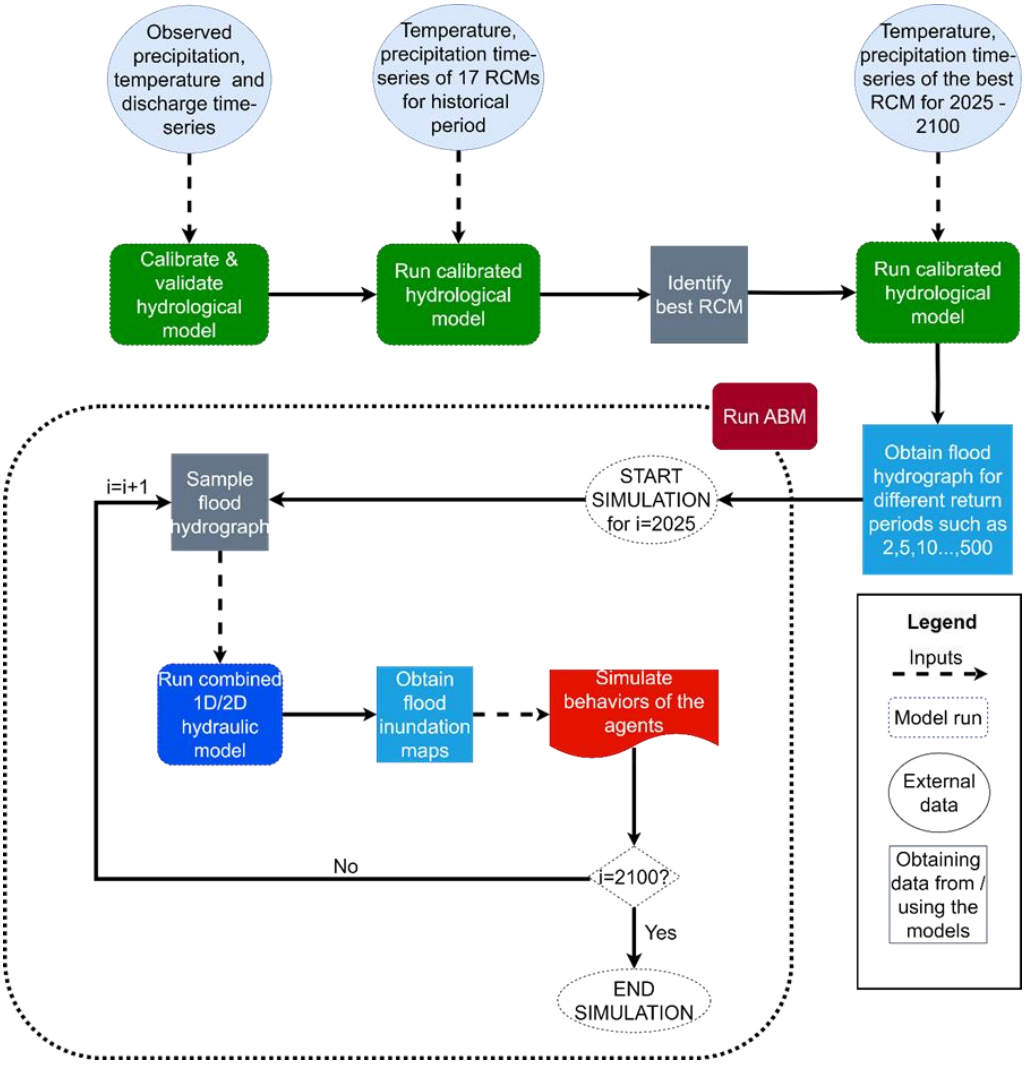

Figure 3. The flowchart of the methodology

The hydrological model of the study area is developed using the Hydrologic Engineering Center's Hydrologic Modeling System (HEC-HMS) of the US Army Corps of Engineers. The hydrologic model is calibrated using daily streamflow observation of E17A014 Stream Gage (SG), whose drainage area is approximately 10.300 km^2. E17A014 is located 8 km upstream of Silifke (see Figure).

Daily streamflow measurements of E17A014 SG are available between 1960 and 2023. However, many hydraulic structures are located along Göksu River within the basin boundary, and daily operational data of these hydraulic structures are unavailable. Without this information, developing a realistic hydrologic model is not possible. Thus, the hydrologic model is developed, calibrated, and validated for the period before the construction of the major hydraulic structures. The hydraulic structures (i.e., elevation-storage-discharge curves) are integrated into the calibrated model accordingly.

Gezende Dam is the first major hydraulic structure constructed in the basin in 1994. In addition to streamflow data, daily temperature and daily rainfall data are required as inputs for the hydrological model. There are 17 meteorological stations (MSs) in and around E17A014 Basin (see Figure 2). Available data from these MSs are used in Thiessen Polygons Method to obtain areal average temperature and precipitation values for the basin. Discharge, temperature, and rainfall data for the model area are available between 1965-1978 and 1981-1986. Thus, the calibration and validation periods are selected as 1965-1978 and 1981-1986, respectively. The performance of the hydrological model is tested for the 2016 – 2020 period after the dams are embedded into the model.

The hydrological model is run with the temperature and precipitation time series obtained from the best climate model for the 2025-2100 period, and annual maximum discharges are obtained. Generalized logistic distribution is fitted to the annual maximum discharge series using the HEC-SSP software and peak discharges for different return periods (i.e., 2-, 5-, 10-, 25-, 50-, 100-, and 500-year) flood events are determined. Finally, corresponding flood hydrographs are generated using the Snyder Method. These hydrographs are used as the primary inputs of the combined 1D/2D hydraulic model.

Climate change models are used to include the effect of CC on future floods. In this study, the potential impacts of CC are assessed through the analysis of 17 Coordinated Regional Climate Downscaling Experiment (CORDEX) – Regional

Climate Models (RCMs) for Representative Concentration Pathways (RCP) 8.5 scenario. These models are selected based on previous studies as in Kentel et al. (2021) and Aziz et al. (2020). CORDEX-RCMs are evaluated using the CORDEX Errata page (EURO-CORDEX, 2021), and the ones with potential problems that may affect flood risk analysis are eliminated from the final climate model list.

As can be seen in Table 1, **a flood simulation** has to be conducted for each year of the simulation period (i.e., 2025-2100). In this study, we only considered the possibility of occurrence of 2-, 5-, 10-, 25-, 50-, 100- and 500-year flood events. However, we do not know when a flood event will occur during the simulation period and its return period. The following approach is used to assign flood events to each year from 2025 to 2100: A random number between zero and one is generated for each year for each possible return period. For example, for 2025, seven random numbers representing 2-, 5-, 10-, 25-, 50-, 100-, and 500-year events are generated. If the generated number is less than the exceedance probability of the flood event, that event is presumed to happen in that year. For example, if the random number generated for the 2-year flood event for 2025 is 0.15, then the 2-year flood event is assigned to 2025 since 0.15 is less than 0.5 (i.e., the exceedance probability of the 2-year flood event). The occurrence of other flood events in 2025 is decided similarly. It is assumed that if multiple flood events are projected to occur in a year, the flood event with the highest return period will ocur in that year. An example is given in Table 1. This will result in one possible realization of flood events in the simulation period (hereafter will be referred to as “Realization”). To handle the uncertainties arising from the procedure of assigning flood events to the simulation period, 100 different Realizations are generated and used in flood risk analysis. After determining the flood events, the hydraulic model is run, and inundation maps are generated. Finally, total economic damage for the study area is calculated using depth-damage curves for Europe given by Huizinga et al. (2017).

Table 1. An example of realization generation

	Flood events							Selected
	2 (0.5)	5 (0.2)	10 (0.1)	25 (0.04)	50 (0.02)	100 (0.01)	500 (0.002)	Flood Event
2025	0.81	0.15	0.96	0.40	**0.01**	0.47	0.81	**50**
2026	0.59	0.49	0.29	0.39	0.94	0.85	0.59	No flood
.	.	.	.	.	.	.	.	.
.	.	.	.	.	.	.	.	.
2100	0.28	0.24	0.57	1.00	0.64	0.77	**0.001**	**500**

Values in parentheses are the exceedance probabilities of the flood events
Bold values show the selected floods for the corresponding year

The combined 1D/2D hydraulic model of the study area is developed using the Hydrologic Engineering Center's River Analysis System (HEC-RAS) of the US Army Corps of Engineers. The combined 1D/2D Hydraulic Model is preferred since the study area is highly urbanized. The 1D model is used to model flow inside the river, while the 2D model is run for the remaining area, which is prone to inundation. The total length of the modeled river reach is approximately 23.5 km, and 1.025 cross-sections are generated using the bathymetry data of Göksu River for the 1D hydraulic model.

Flood hydrographs (obtained by transferring the outputs of the hydrologic model at E17A014 with the drainage area-ratio method) are entered into the combined 1D/2D hydraulic model as the upstream boundary condition, while normal depth is entered into the model as the downstream boundary condition. Two mesh sizes are used for the 2D area: 6 m by 6 m mesh within the 100 m buffer zone of the river banks and the urbanized area, and 30 m by 30 m mesh for the rest of the model area. The Coordination of Information on the Environment (CORINE) dataset (Copernicus Land Monitoring Service, 2018) is used as the land cover data for the 2D study area. Corresponding Manning values are taken from the study of Papaioannou et al. (2018).

The agent-based model (ABM) is developed using NetLogo created by Uri Wilensky (1999). The flowchart of the ABM is given in Figure 4. The duration of

the simulation is 75 years, from 2025 to 2100, and yearly time steps are used. As explained earlier, the best-performing climate model's temperature and precipitation time series are inputs for the calibrated hydrological model to include CC impacts on flood risks. Mitigation and adaptation measures that can be taken by agents (the public, the government, or both) are included in the analysis through ABM.

The public (i.e., households living in the study area) and the government are the main agents in our study. The behavior of the public agent, which consists of 28,863 agents, is simulated using risk perception and coping perception and structured as in Tonn and Guikema (2018). The equations are provided below:

$$Risk\ Perception = \sum (Formula\ \times Beta) \quad (1)$$

$$Coping\ Perception = \sum Formula \quad (2)$$

The details of the calculations regarding risk perception and coping perception are given in the Appendix. The threshold values for risk and coping perceptions are determined as 30 based on a sensitivity analysis. The details of the sensitivity analysis are also given in the Appendix. The public agent is assumed to take action if risk and coping perceptions are greater than 30.

On the other hand, the government agent behavior is designed based on two management strategies: i) proactive management strategy and ii) reactive management strategy. The scenarios are generated based on the management strategies for the government agent.

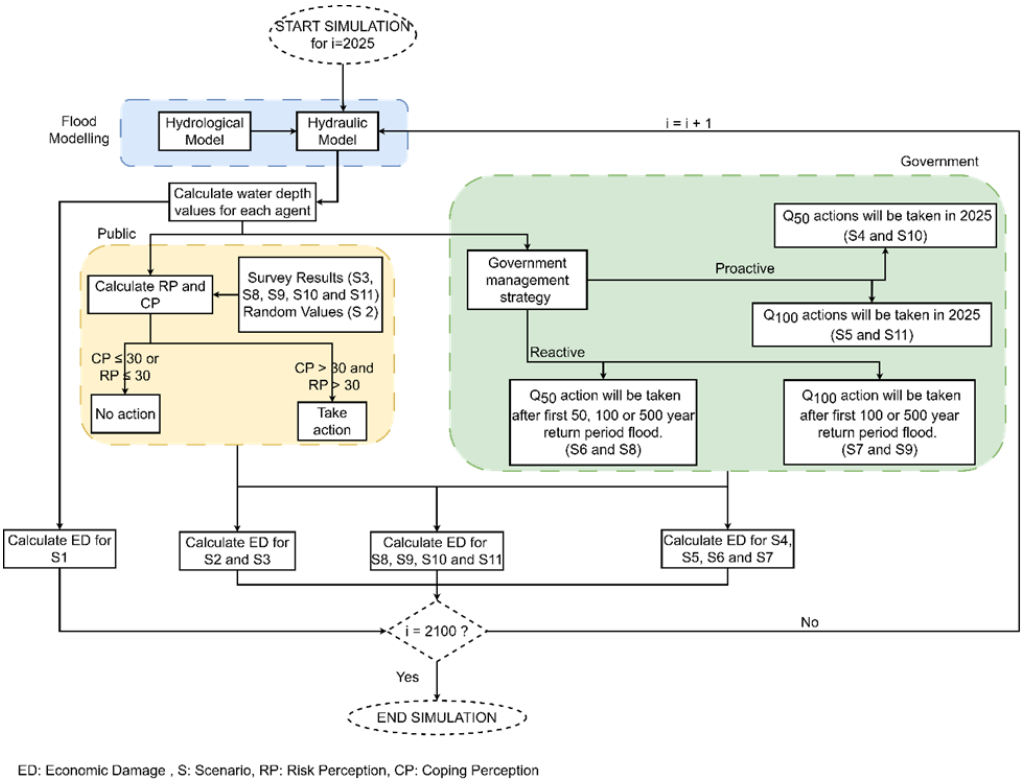

Figure 4. Flowchart of the model simulation

To realistically model the public's risk and coping perceptions of flood hazards in the ABM, a survey is prepared and conducted in the study area. The questions are selected based on the literature review. It consists of open-ended questions, multiple choice questions, and yes/no type questions. 180 surveys are conducted by selecting the respondents from various parts across the study area to reduce bias (see Figure 5). The survey results are distributed through the whole study area as follows: The study area is divided into two regions: the 500 meter-buffer zone around Göksu River and the remaining area. Survey results obtained in each region are then randomly assigned to the agents located in that particular region.

A scenario-based approach (see Table 2) is used to investigate the impacts of the agents on flood risks. In the model, the government is characterized as either reactive or proactive. A reactive government takes action only after a certain return period flood event is experienced, while a proactive government takes action immediately

without waiting for such an event. Actions by people and the government are modeled through a scenario-based analysis. A base scenario (S1) represents the traditional flood risk analysis. Thus, actions are completely ignored (i.e., no agents, thus no actions). In scenario 2, public actions are included, but random risk and coping perceptions are assigned to agents. This scenario represents the case where no survey is conducted (similar to Tonn and Guikema's (2018) study). In the third scenario, survey results are used to assign risk and coping perceptions to the agents. In scenarios 4, 5, 6, and 7, the government is the only agent that takes action, and details of these scenarios are explained in Table 2. Finally, both the government's and the public's actions are included in scenarios 8, 9, 10, and 11. Scenarios are shown in Table 2 as well.

Table 2. The scenarios designed to investigate the impact of agent's actions on flood risks

Scenario Number	**Scenario Name**	**Agent[1]**	**Survey[2]**	**Explanations**
S1	Base	None	No	No agents; thus, actions are not used.
S2	PubRand	Public	No	Risk and coping perceptions are randomly assigned to public agent.
S3	PubSur	Public	Yes	Risk and coping perceptions are assigned to the public agent according to the survey results.
S4	ProGo50	Government	-	The proactive government takes action to mitigate the consequences of a 50-year return period flood event.
S5	ProGo100	Government	-	The proactive government takes action to mitigate the consequences of a 100-year return period flood event.
S6	ReGo50	Government	-	The reactive government agent takes action to mitigate a 50-year return period flood event after a 50-, 100- or 500-year return period flood event is experienced.
S7	ReGo100	Government	-	The reactive government agent takes action to mitigate a 100-year return period flood event after a 100- or 500-year return period flood event is experienced.
S8	PubSur – ReGo50	Public & Government	Yes	PubSur and ReGo50 together.
S9	PubSur – ReGo100	Public & Government	Yes	PubSur and ReGo100 together.

Scenario Number	Scenario Name	Agent[1]	Survey[2]	Explanations
S10	PubSur – ProGo50	Public & Government	Yes	PubSur and ProGo50 together.
S11	PubSur – ProGo100	Public & Government	Yes	PubSur and ProGo100 together.

[1] The government, the public, or both are used as agents in this study.
[2] When survey results are used in assigning risk and coping perceptions to people, "Yes" is used in this column; when risk and coping perceptions are randomly assigned to people, "No" is used in this column. If the public agent is not included in the scenario, "-" is used.

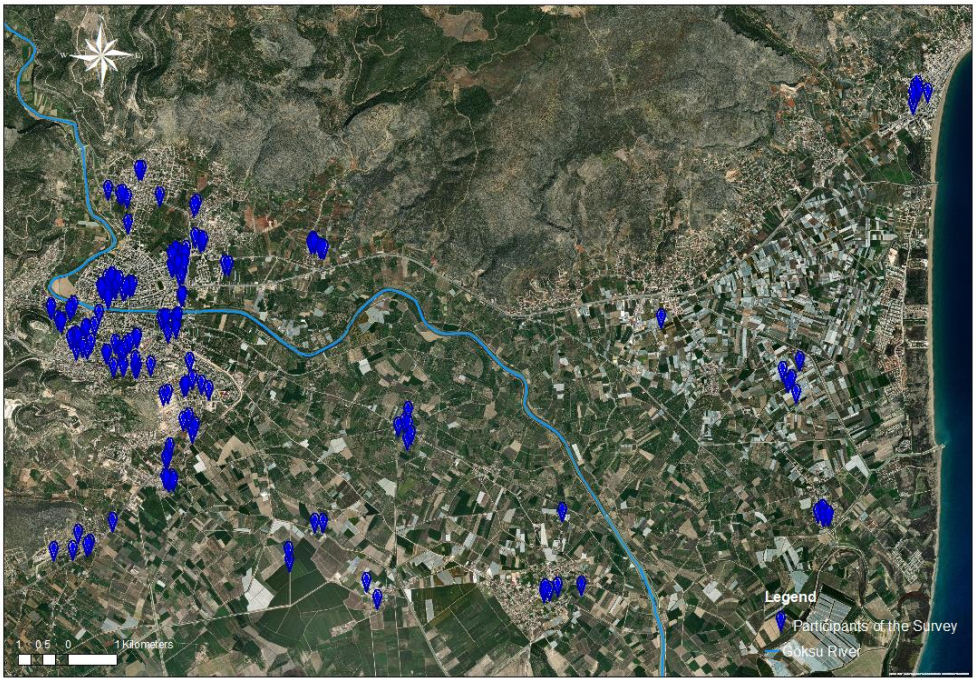

Figure 5. Locations of the participants of the survey (Basemap source: Esri, Maxar, Earthstar Geographics, and the GIS User Community)

As explained previously, 100 Realizations are generated for the 75-year simulation period. In other words, each scenario is replicated 100 times. Let $ED_{i,j,k}$ denotes economic damage in year i, for Realization j of scenario k. Then, the total economic damage for each Realization of each scenario, $TED_{j,k}$, is calculated by summing up yearly economic damages of 75 years of the simulation period:

$$TED_{j,k} = \sum_{i=2025}^{2100} ED_{i,j,k}\,, \forall j,k \qquad (3)$$

The average economic damage for each scenario k, AED_k, is calculated by taking the average of total economic damage obtained for 100 Realizations of that scenario:

$$AED_k = \frac{\sum_{j=1}^{100} TED_{j,k}}{100}, \forall, k \quad (4)$$

Depth-damage curves specific to Türkiye are not available. Therefore, the curves suggested by Huizinga et al. (2017) for Europe are utilized, and the costs of actions that can be taken by the public agent are ignored in this study.

The government's action is represented as the construction of a dike. The costs of the government's actions are calculated based on the study of Haer et al. (2020), where € is used as the currency unit. Thus, calculated economic damage values bear a certain degree of error. However, we believe that comparing scenarios relative to each other is still useful.

4. RESULTS

4.1. Results of the hydrological model

The hydrologic model is calibrated and validated for the periods of 1965-1978 and 1981-1986. The observed discharges and the outputs of the hydrological model are compared and performances of the statistical measures for the hydrological model are given in Table 3.

Table 3. Performances of the statistical measures

Measure	Performance Evaluation Criteria (Moriasi et al., 2015; HEC, 2020) Very Good	Good	Satisfactory	Calibration Period (1965-1978)	Validation Period (1981-1986)
The RMSE-observations standard deviation ratio (*RSR*)	[0.0,0.5]	(0.5,0.6]	(0.6,0.7]	0.53	0.54
Nash-sutcliffe efficiency (*NSE*)	(0.8,1.0]	(0.7,0.8]	(0.5,0.7]	0.72	0.71
Percent bias (*PBIAS*)	(-5,5)	(-10,-5] & [5,10)	(-15,-10] & [10,15)	-3.26	1.04
Coefficient of Determination (R^2)	(0.85,1.00]	(0.75,0.85]	(0.60,0.75]	0.74	0.72
Peak Discharge (m^3/s)	± 10% of observed value			*1074 – 782 (37.3%)	*1090 - 981 (11.1%)
Discharge Volume (mm)	± 10% of observed value			*5105.36 – 4939.39 (3.4%)	*1835.47 – 1854.52 (1.0%)
Date/Time of Peak Discharge	± 12 hours range of observed value			*22.01.1969 – 14.03.1968	*28.12.1981 – 10.11.1985

* The first value represents the observed value, while the second one represents the calculated value

Color code that shows the performance evaluation criteria

Very Good	Good	Satisfactory	Not Satisfactory

Although peak discharge and time of peak discharge values for both the calibration and validation periods do not fall within the 10% range of observed values, the overall performance of the hydrological model is very good and satisfactory based on the statistical measures (Moriasi et al., 2015; HEC, 2020). Thus, model calibration is assumed to be acceptable. After the calibration and validation, hydraulic structures are entered into the hydrological model.

4.2. Selection of the best RCM

The final climate model list that is used in the study is given in Table 4. As explained by Mesta et al. (2024), extreme events are poorly represented in the ensembled time series. Thus, instead of using ensemble precipitation and temperature time series, the best-performing climate model is identified using correlation coefficient, root mean square error, and percent bias, and projections of this model are used in this study. M5 is identified as the best RCM for the study area.

Table 4. The list of climate models

	Climate Model (RCM/GCM)			Climate Model (RCM/GCM)	
Model ID	**Driving GCM**	**RCM**	**Model ID**	**Driving GCM**	**RCM**
M1	CNRM-CM5	CCLM4-8-17	M10	CM5A-MR	RCA4
M2	CNRM-CM5	ALADIN63	M11	HadGEM2-ES	CCLM4-8-17
M3	CNRM-CM5	RCA4	M12	HadGEM2-ES	RACMO22E
M4	EC-EARTH	HIRHAM5	M13	HadGEM2-ES	RCA4
M5	EC-EARTH	CCLM4-8-17	M14	MPI-ESM-LR	CCLM4-8-17
M6	EC-EARTH	RACMO22E	M15	MPI-ESM-LR	REMO2009(r1i1p1)
M7	EC-EARTH	RCA4	M16	MPI-ESM-LR	REMO2009(r2i1p1)
M8	CM5A-MR	WRF331F	M17	NorESM1-M	HIRHAM5
M9	CM5A-MR	WRF381P			

4.3. The results of the combined 1D/2D hydraulic model

Using the outputs of M5 RCM, the hydrological model is run for the period 2025 – 2100. Discharges for different return periods are calculated using both recorded discharges and the outputs of the hydrological model with M5 RCM. The results are provided in Table 5. It can be seen that climate change causes a decrease in the peak discharges in the study area.

Table 5. Calculated discharges for different return periods

Return Period	**Q (m^3/s)**	
	Historical	**M5 RCM**
2	637.6	307.7
5	968.5	408.2
10	1181.9	490.4
25	1445.0	589.2
50	1636.6	760.4
100	1824.8	934.8
500	2256.2	1589.9

The outputs (daily average temperature and daily average rainfall) of M5 between 2025 and 2100 are entered into the calibrated hydrological model. The peak discharges for each year are obtained. Among gamma, Generalized Extreme Value, generalized logistic, generalized Pareto, Gumbel, log-Pearson III, log-normal, logistic, normal, and Pearson III, generalized logistic is identified as the best-fitting distribution to these values using HEC-SSP 2.3 (Hydrologic Engineering Center, 2023). Finally, discharges of flood events with different return periods (i.e., 2-, 5-, 10-, 25-, 50-, 100- and 500-year events) are calculated.

The combined 1D/2D coupled hydraulic model was validated based on the State Hydraulic Works staff meeting. Insight was provided regarding a massive flood event that occurred in Silifke between the 5th and 7th of March, 2004. They shared the details about the locations where the flood water enters and leaves Silifke from the left bank of Göksu River. The entering and leaving locations of the flood water are marked in Figure 6. These locations are validated with the combined 1D/2D coupled hydraulic model. Moreover, it was said that Göksu River can pass around 800 m^3/s safely; our model cannot handle 800 m^3/s safely, but 33 buildings are inundated because of this flood event. Our model cannot handle this amount because of the inexact bridge dimensions. This data could not be obtained from the related institution.

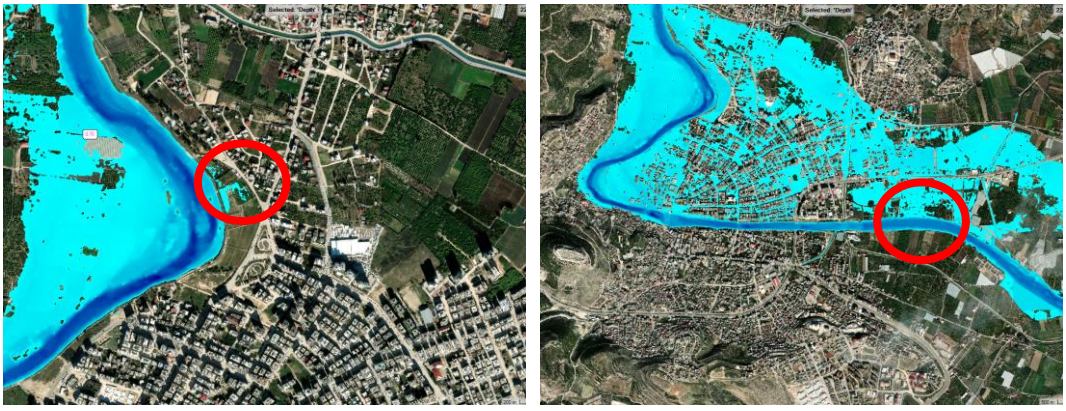

(a) (b)

Figure 6. The combined 1D/2D coupled hydraulic model results: (a) The entering location of flood water (b) The leaving location of flood water (Basemap source: Esri, Maxar, Earthstar Geographics, and the GIS User Community)

4.4. The results of ABM – economic damage

The box plots of average economic damages of 100 Realizations for each scenario are given in Figure 7. As shown in Figure 7, the average economic damage decreases as agents implement actions, and the government's actions are more effective than public actions. Public agent's actions resulted in a 35.4% and 19.7% decrease in the mean values for PubRand and PubSur compared to the Base scenario, respectively. These results show that assigning random behavior to public agents may result in overestimating the reduction in total economic damage. Thus, site-specific information is crucial in realistically evaluating flood consequences.

On the other hand, the government's actions result in larger reductions in economic damages. As expected, a proactive government decreases the economic damage more than a reactive government. It is also evident from the results that the economic damage is notably lower if the government has proactive management strategies and takes an action that prevents damages from a 100-year flood compared to an action that prevents damages from a 50-year flood. On the other hand, in the case of a reactive government, the average economic damage is higher for the ReGo100 scenario compared to the ReGo50 scenario. This may seem counterintuitive, but there are two main reasons for this result. The first one is that there are Realizations where a 100-year flood does not occur, but one or more 50-year flood occur. For such Realizations, the government takes action in the ReGo50 scenario, while no action is taken in the ReGo100 scenario. The second reason is that in some Realizations, a 100-year flood happens late and the government does not take any action until that time in the ReGo100 scenario. However, when a 50-year flood happens earlier in these Realizations, actions are taken early in the ReGo50 scenario, reducing economic damage. The final inference from Figure 7 is that the economic damage is the lowest when both the public and the proactive government take mitigation actions against floods.

One of the goals of this study is to investigate the added value of a survey that is used to collect information about public risk and coping perceptions instead of

randomly assigning them. To facilitate interpretation, the same flood event is assumed to occur during each year of the 75-year simulation period. Figure 8 illustrates the change in total economic damage over time for both the PubRand and PubSur scenarios for different return period flood events. As expected, the total economic damage initially decreases and stabilizes with time. The initial decrease is attributed to the increase in the individual's risk and coping perceptions as they take action when their perceptions are high (see Figure 4). Once all people who have experienced floods take action, the average economic damage stabilizes. As can be seen in Figure 8, the total economic damages for the PubRand scenario are less than those of the PubSur Scenario for all return periods. This supports the previous findings that the PubRand Scenario underestimates the economic damages within the study area. It indicates that people's flood risk and flood coping perceptions are skewed towards lower-than-average values, which is a realistic outcome for Türkiye. Thus, especially for regions where flood awareness is limited (Türkkan & Hırca, 2021), surveys are essential for accurately modeling the impact of public action on economic damage reduction.

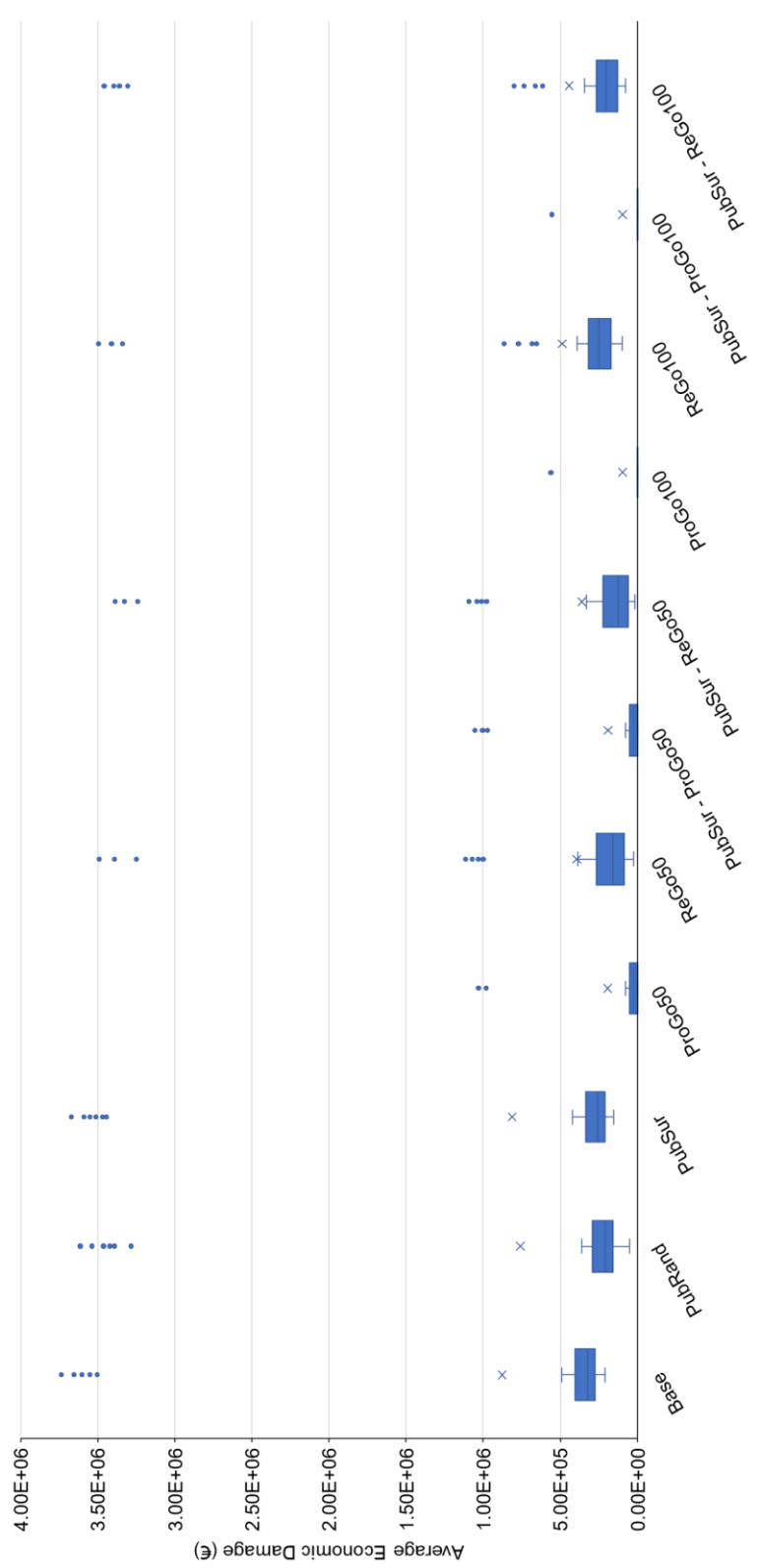

Figure 7. Average economic damage for each scenario

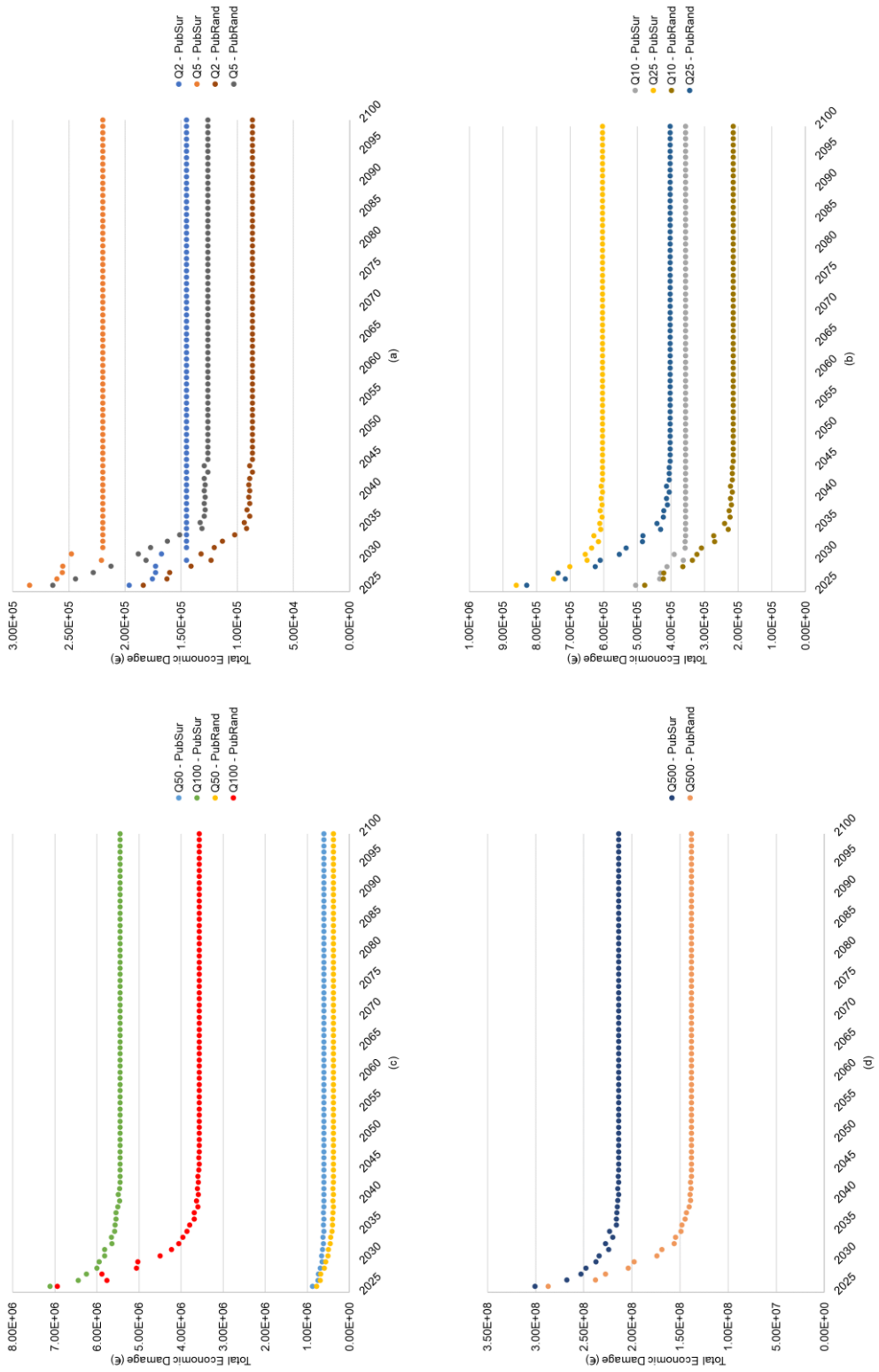

Figure 8. Total ED for PubSur and PubRand scenarios: (a) 2-year and 5-year events (b) 10-year and 25-year events (c) 50-year and 100-year events (d) 500-year event

The box plots B/C of 100 Realizations for scenarios 4 – 11 are given in Figure 9. The B/C of the scenarios with reactive government are lower than those with proactive government. It is also observed that the B/C of the scenarios with governments that take action against 50-year flood are higher than those of 100-year flood, regardless of whether the government is proactive or reactive.

When the other settings of the scenarios are the same, the mean values of the scenarios with proactive and reactive governments do not differ much. However, the variability is less in the scenarios with a proactive government. In addition, B/C values are less than 1.0 for some Realizations of the scenarios with a reactive government. Thus, the proactive behavior of the government is always feasible, while the reactive government's actions are not feasible for outlier Realizations, particularly when severe floods occur late in the simulation period. In these cases, the total economic damage is greater than the others. As explained earlier, the occurrence times of serious floods (50-year, 100-year, or 500-year floods) significantly affect economic damage. Moreover, it can be said that taking action against a 50-year flood is more beneficial for the study area. The rationale behind this can be attributed to the high cost of implementing a 100-year flood action plan and the likelihood of 50-year floods to occur earlier in the simulation period. It can also be concluded from Figure 9 that there is not a significant difference between the scenarios with only the government and with both the government and the public. As can be seen in Figure 9 that B/C values of the scenarios with both the government and the public are slightly greater than those with only the government. The main reason for this result is that the economic damage values are slightly lower in the scenarios in which both the government and the public agents are included.

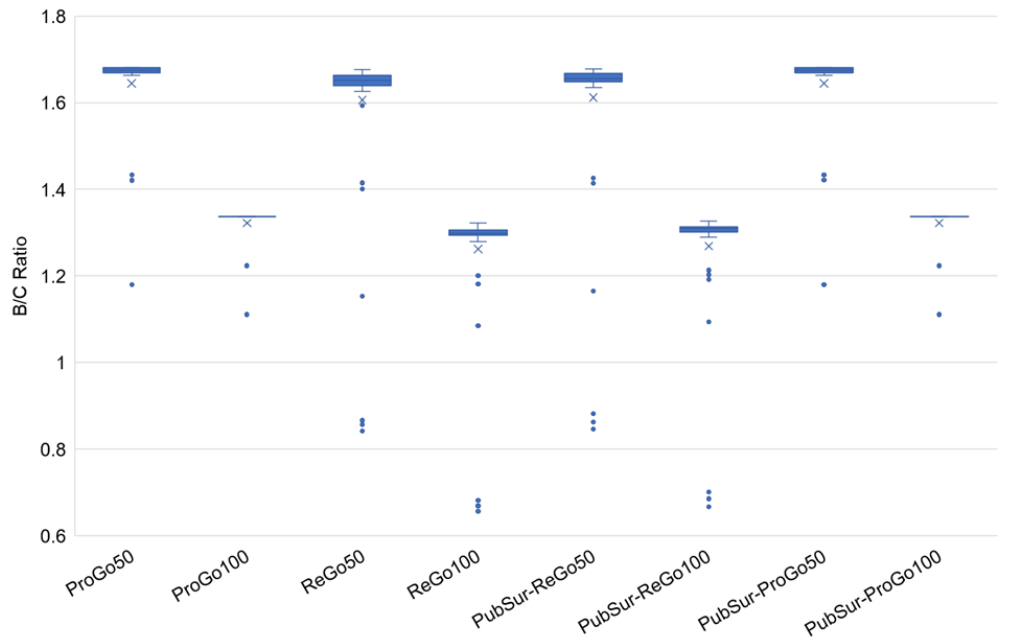

Figure 9. Box plots of B/C for scenarios 4 – 11

4.5. The results of ABM – the timing of a flood event

We observed that the timing of a severe flood (50-year, 100-year, or 500-year flood) affects total economic damage; thus, the following analysis is conducted to assess the significance of the timing of a severe flood. The Realizations are grouped into two: the first group includes the Realizations where a severe flood occurs within the initial 10 years of the simulation period (referred to as Early, denoted as E), while the second group has the rest of the Realizations (referred to as Late, denoted as L). The results of all scenarios except the base scenario are provided in Figure 10. It can be seen that the average damage of the scenarios with a reactive government in group E is less than the scenarios with a reactive government in group L. This is an expected result as an early occurrence of a severe flood prompts the reactive government to take action, resulting in decreased economic damage. On the other hand, scenarios with a proactive government that takes action against the 100-year flood exhibit very similar average economic damage values for both groups E and L. This is due to the fact that as the proactive government takes action at the very first stage, the timing of the flood event becomes unimportant.

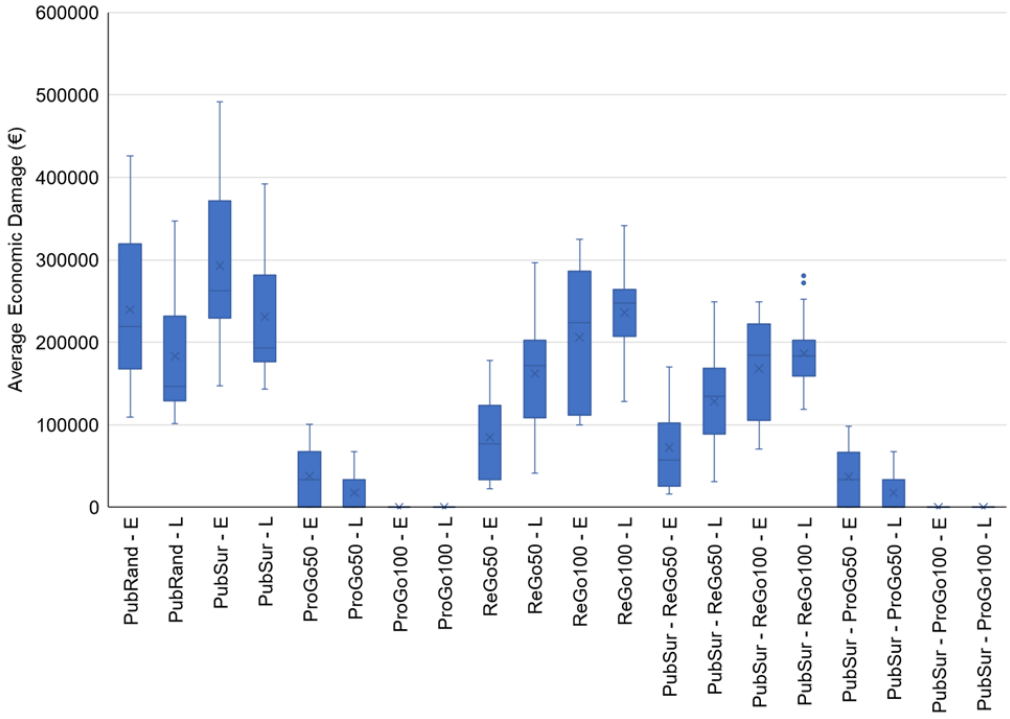

Figure 10. The impact of the timing of a severe flood. Here, "L" represents Realizations with a major flood event in the first 10 years, while "E" represents the rest.

Counterintuitive results are observed for PubRand and PubSur scenarios where the average economic damage for group E is greater than that of group L. Thus, following analysis is conducted for the PubSur scenario: i) A total of 30 Realizations are generated, ii) Each Realization consists of 30 time steps (i.e. 30 years), iii) In the 1st Realization, a 500-year flood occurs in the 1st year and in the rest of 29 years a 50-year flood occurs. In the next Realization, the 500-year flood occurs in the 2nd year while all other years have 50-year floods, and the location of the 500-year flood shifts to the next year for each Realization.

Figure 11 shows that average economic damage increases with the shifting of the 500-year flood through to the end of the simulation period. It is evident that the timing of a severe flood affects the public's decisions about flood mitigation measures. The public takes action earlier because of the earlier serious flood event. Thus, the average economic damage decreases. This behavior supports the validity

of the ABM used in this study. Figure 11 also demonstrates how important it is for the public to take action against floods. For this reason, it is important to educate people against floods and increase the awareness.

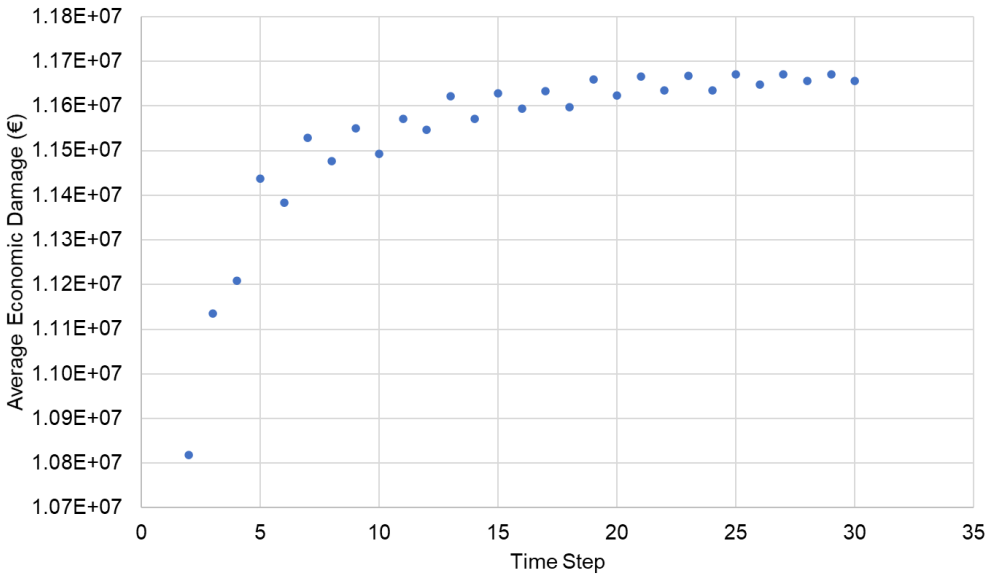

Figure 11. The impact of the timing of a severe flood for the PubSur Scenario

The duration between flood events causes significant changes in economic damages. Figure 12 shows the economic damage change between two 500-year flood events for the PubSur scenario. Different realizations are generated to see the effect of the duration between two flood events. 21 realizations are generated, and these realizations are designed as follows: i) there will be two 500-year flood events, and ii) It is assumed that there will be no flood event in other time steps. The duration between two flood events is calculated as the total number of years without flood events. On the other hand, change in the economic damage is calculated as the difference between the economic damage of the second flood event and the first flood event. Negative values show that economic damage decreases, while positive values show that economic damage increases. As seen from Figure 12, the rate of increase in economic damage is initially greater. After around nine years, the rate of increase decreases. This shows that flood risk perception and coping perception values of the people tend to be stable after some point. In our study, around nine

years, the change in the economic damage is becoming zero. This also supports the findings that are shown in Figure 8. It can be seen that economic damage is becoming stable around nine years (See Figure 8). Figure 12 also implies that economic damage change values stabilize after 25 years. This shows the effect of timing on flood risk and flood coping perception. People tend to forget the results of floods. Therefore, their flood risk perception and flood coping perception values decrease, and they do not take any action.

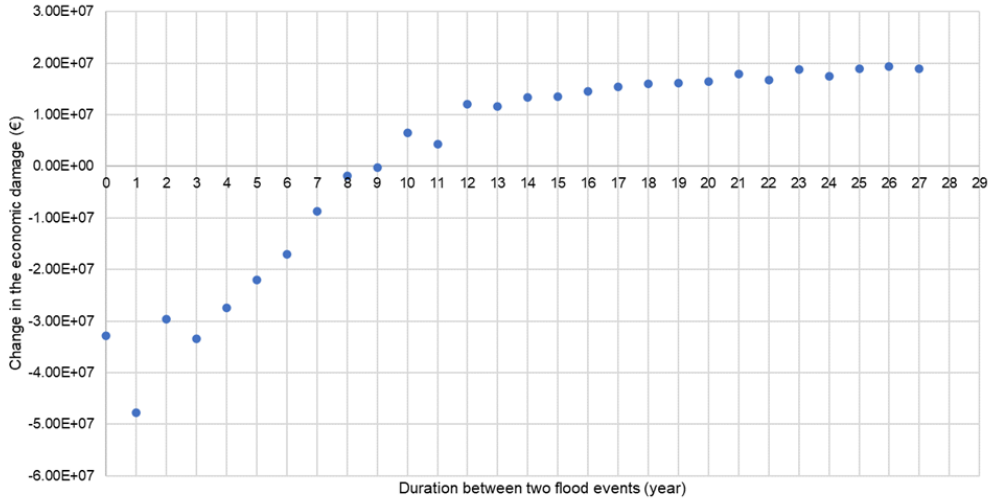

Figure 12. The effect of the duration between two flood events on economic damage change

5. CONCLUSION

FRM studies are more important than ever before due to CC impacts. In this study, the impacts of CC and the agents on flood risks were analyzed using a hydrological model, a combined 1D/2D hydraulic model, and ABM. For future FRM, integrating CC impacts into the hydrological model and the hydraulic model is crucial because the magnitude and frequency of flood events are changing. Moreover, the agents should be integrated into the FRM studies too.

The importance of the agents in FRM was shown by generating 11 different scenarios and 100 Realizations in our study. Firstly, the public agent should be included in FRM studies, and conducting a survey to evaluate the public's behavior

against flood events is important. In this study, the average economic damage of the scenario that the survey results are used is greater than the scenario with the random values. This shows the importance of the surveys. If a survey is not conducted in the study area, it is not possible to evaluate realistically the public's reactions to flood events. This is very important for the regions where the flood awareness is limited.

total economic damage is generally higher for scenarios with the reactive government than those with the proactive government. The total economic damage value is the lowest for the PubSur-ProGo100 Scenario. This result shows that including both the public and government agents in FRM is vital.

Another conclusion of this study is that the timing of a severe flood event is important. The economic damage value of the Realization that a serious flood event occurs earlier is less than the Realization that a serious flood event occurs late. The timing of a serious flood event is especially important for the reactive government. The timing is also important for the public agent. If the public experiences flood events earlier, they tend to take action earlier, and economic damage decreases. For this reason, educating the public about flood consequences and raising awareness about floods is really important.

B/C of the scenarios with the government, which takes action against 50-year flood events, is greater than those with the government, which takes action against 100-year flood events due to the high cost of the 100-year flood action. Another inference is that B/C is always greater than 1.0 in the scenarios with the proactive government, while it is less than 1.0 for some Realizations in the scenarios with the reactive government. This is an important conclusion because the consequences of the floods might be destructive for a reactive government.

The final conclusion is that the public tends to forget the consequences of floods for around nine years. Thus, this also supports the importance of educating the people about floods because the public should be aware of the consequences of floods. They should not underestimate the outcomes of the floods. This is especially important for the regions where flood events occur frequently.

The threshold values are important in the decision mechanism of the public agent. Thus, these values should be determined carefully. As a future study, these factors will be analyzed in more detail.

APPENDIX

RP and CP are calculated using the equation of perceived risk which is proposed by Tonn and Guikema (2018). The survey questions to calculate RP and CP are given in Table A1 and A2, respectively. The factors related to the neighbors are not included in our study. Furthermore, home value is calculated based on the methodology provided in the study by Tonn and Guikema (2018). However, in Silifke, it is not possible to obtain those values. For this reason, random values are assigned for this factor.

Table A1. Risk perception factors (Tonn & Guikema, 2018)

Factor	Description	Formula	Beta
Flood Experience	Has the agent experienced flooding in previous years?	Number of floods/ number of years	200
Near-miss Experience	Has the agent experienced flooding in previous years?	Number of near-miss events/number of years	-100
Community Mitigation	Has the community previously completed mitigation?	Yes (1) or No (0)	-20
Agent Mitigation	Has the agent previously completed mitigation?	Yes (1) or No (0)	-20
Information	Did the community disseminate information in the previous year?	Yes (1) or No (0)	20

Table A2. Coping perception factors (Tonn & Guikema, 2018)

Factor	Description	Formula
Base Coping Perception	Random value assigned to each agent	A random value between 0 and 20
Home Value	Value assigned based on property value	Random value: 5, 10, 15 or 20
Prior Agent Mitigation	Has the agent previously completed mitigation?	Yes (20) or No (0)
Information	Did the community disseminate information in the previous year?	Yes (20) or No (0)

Another difference between Tonn and Guikema's study and this study is the threshold values for RP and CP. RP and CP values are determined based on the sensitivity analysis. Figure A1 shows the economic damage change in 50 years with different CP and RP threshold values. The first value represents CP while the second one represents RP. It can be seen that if both CP and RP are below 30, economic damage rapidly decreases because most of the agents tend to take action in this situation. On the other hand, if both parameters are above 30, many agents do not want to take action. Hence, economic damage does not change much as time passes. For this reason, threshold values for CP and RP are selected as 30.

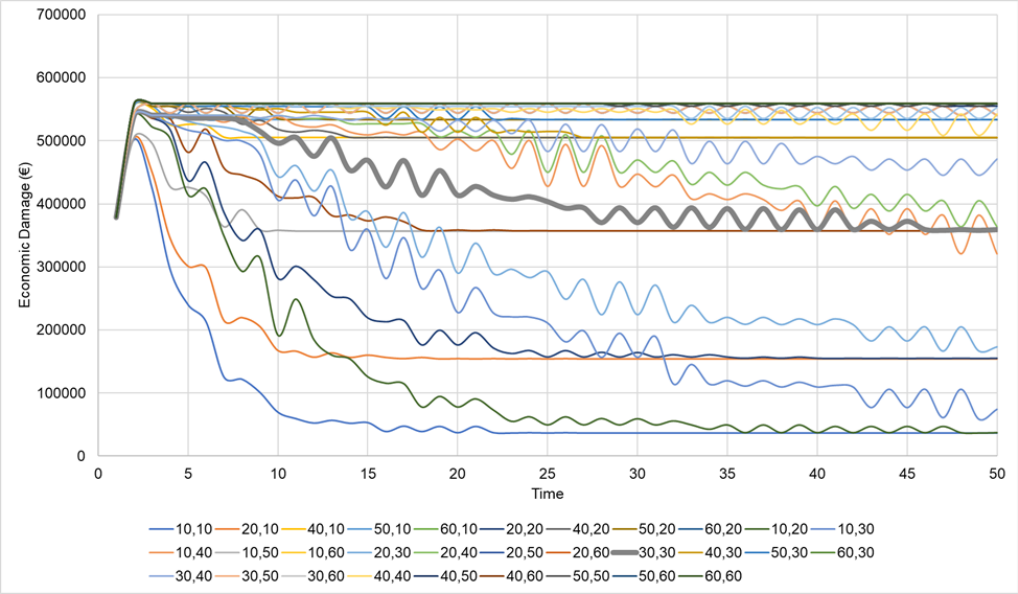

Figure A1. Economic damage change with changing CP and RP threshold values

REFERENCES

Arnell, N., & Gosling, S. (2016). The impacts of climate change on river flood risk at the global scale. Climatic Change, 134, 387-401.

Attems, M., Thaler, T., Genovese, E., & Fuchs, S. (2020). Implementation of property-level flood risk adaptation (PLFRA) measures: Choices and decisions. WIREs Water, 7(1).

Aziz, R., Yucel, I., & Yozgatligil, C. (2020). Nonstationarity impacts on frequency analysis of yearly and seasonal extreme temperature in Turkey. Atmospheric Research, 238, 1-13.

Bai, Y., Zhang, Z., & Zhao, W. (2019). Assessing the Impact of Climate Change on Flood Events Using HEC-HMS and CMIP5. Water, Air, & Soil Pollution, 230.

Bangalore, M., Smith, A., & Veldkamp, T. (2019). Exposure to Floods, Climate Change, and Poverty in Vietnam. Economics of Disasters and Climate Change, 3, 79-99.

Bayazıt, Y., Koç, C., & Bakış, R. (2021). Urbanization impacts on flash urban floods in Bodrum Province, Turkey. Hydrological Sciences Journal, 66(1).

Beden, N., & Keskin, A. (2021). Flood map production and evaluation of flood risks in situations of insufficient flow data. Natural Hazards, 2381-2408.

Bilici, Ö., & Everest, A. (2017). 29 ARALIK 2016 MERSİN SELİNİN METEOROLOJİK ANALİZİ VE İKLİM DEĞİŞİKLİĞİ BAĞLANTISI. Doğu Coğrafya Dergisi, 227-250.

Blöschl, G., Hall, J., Viglione, A. et al. (2019). Changing climate both increases and decreases European river floods. Nature, 573, 108-111.

Botzen, W., Aerts, J., & van den Bergh, J. (2009). Dependence of flood risk perceptions on socioeconomic and objective risk factors. Water Resources Research, 45(10).

Bronstert, A. (2003). Floods and Climate Change: Interactions and Impacts. Risk Analysis, 23(3), 545-557.

Bubeck, P., Botzen, W., Kreibich, H., & Aerts, J. (2013). Detailed insights into the influence of flood-coping appraisals on mitigation behaviour. Global Environmental Change, 23(5), 1327-1338.

Bubeck, P., Botzen, W., Laudan, J., Aerts, J., & Thieken, A. (2018). Insights into Flood-Coping Appraisals of Protection Motivation Theory: Empirical Evidence from Germany and France. Risk Analysis, 38(6), 1239-1257.

Bubeck, P., Botzen, W., Suu, L., & Aerts, J. (2012). Do flood risk perceptions provide useful insights for flood risk management? Findings from central Vietnam. Journal of Flood Risk Management, 5(4), 295-302.

Buldur, A., Pınar, A., & Başaran, A. (2007). 05-07 MART 2004 TARİHLİ GÖKSU NEHRİTAŞKINI VE SİLİFKE'YE ETKİSİ. Selçuk Üniversitesi Sosyal Bilimler Enstitüsü Dergisi, 139-160.

Coughlan, M., Cronin, P., & Ryan, F. (2013). Survey research: Process and limitations. International Journal of Therapy and Rehabilitation, 16(1).

CRED & UNDRR. (2020). Human cost of disasters: An overview of the last 20 years 200-2019.

Dawson, R., Peppe, R., & Wang, M. (2011). An agent-based model for risk-based flood incident management. Natural Hazards, 59, 167-189.

Dubbelboer, J., Nikolic, I., Jenkins, K., & Hall, J. (2017). An Agent-Based Model of Flood Risk and Insurance. Journal of Artificial Societies and Social Simulation, 20(1).

Easterling, D., Meehl, G., Parmesan, C., Changnon, S., Karl, T., & Mearns, L. (2000). Climate Extremes: Observations, Modeling, and Impacts. Science, 289(5487), 2068-2074.

Gilbert, N. (2008). Agent-Based Models. United States of America: Sage Publications.

Giorgi, F., & Lionello, P. (2008). Climate change projections for the Mediterranean region. Global and Planetary Change, 63, 90-104.

Gül, G., Rosbjerg, D., Gül, A., Ondracek, M., & Dikgola, K. (2010). Assessing climate change impacts on river flows and environmental flow requirements at catchment scale. Ecohydrology, 28-40.

Haer, T., Botzen, W., de Moel, H., & Aerts, J. (2017). Integrating Household Risk Mitigation Behavior in FloodRisk Analysis: An Agent-Based Model Approach. Risk Analysis, 37(10), 1977-1992.

Haer, T., Husby, T. G., Botzen, W. J., & Aerts, J. C. (2020). The safe development paradox: An agent-based model for flood risk under climate change in the European Union. Global Environmental Change, 60.

Hallegatte, S., Ranger, N., Bhattacharya, S., Bachu, M., Priya, S., Dhore, K., . . . Herweijer, C. (2010). Flood Risks, Climate Change Impacts and Adaptation Benefits in Mumbai: An Initial Assessment of Socio-Economic Consequences of Present and Climate Change Induced Flood Risks and of Possible Adaptation Options. Paris: Organization for Economic Co-operation and Development Publishing.

Hammond, R. (2015). Considerations and Best Practices in Agent-Based Modeling to Inform Policy. In Assessing the Use of Agent-Based Models for Tobacco Regulation (pp. 161-193). Washington DC: National Academies Press.

Hirabayashi, H., Mahendran, R., Koirala, S., Konoshima, L., Yamazaki, D., Watanabe, S., . . . Kanae, S. (2013). Global flood risk under climate change. Nature Climate Change, 3, 816-821.

Huizinga, J., De Moel, H., & Szewczyk, W. (2017). Global flood depth-damage functions: Methodology and the database with guidelines. Luxembourg: Publications Office of the European Union.

Hunter, D. (2002). Risk Perception and Risk Tolerance in Aircraft Pilots. Washington, DC: Office of Aerospace Medicine.

Hydrologic Engineering Center. (2023). HEC-SSP Version 2.3.

İhlas Haber Ajansı. (2017, March 15). Silifke'de Göksu ırmağının debisi yükseldi, bin 109 dekar alan zarar gördü. Retrieved from İHA: https://www.iha.com.tr/mersin-haberleri/-1648015

IPCC. (2014). Climate Change 2014 Synthesis Report. Geneva.

IPCC. (2018). An IPCC Special Report on the impacts of global warming of 1.5°C above pre-industrial levels and related global greenhouse gas emission pathways, in the context of strengthening the global response to the threat of climate change,... to eradicate poverty.

Jonkman, S., & Vrijling, J. (2008). Loss of life due to floods. Journal of Flood Risk Management, 43-56.

Kentel, E., Yücel, İ., Mesta, B., Akgün, Ö., Özcan, C., Ercan, E., . . . Matur, İ. (2021). TÜBİTAK Antalya Havzası'nda İklim Değişikliğinin Debi ve HES Enerji Üretimine Etkilerinin İncelenmesi Projesi (Pr No: 118Y365). Ankara: TÜBİTAK.

Kreibich, H., Bubeck, P., Van Vliet, M., & De Moel, H. (2015). A review of damage-reducing measures to manage fluvial flood risks in a changing climate. Mitigation and Adaptation Strategies for Global Change , 967-989.

Laudan, J. (2019). Changing Susceptibility of Flood-prone Residents in Germany: Mental Coping and Mitigation Behaviour in the Context of Different Flood Types. Potsdam: University of Potsdam.

Liu, D., Li, M., Li, Y., & Chen, H. (2022). Assessment of Public Flood Risk Perception and Influencing Factors: An Example of Jiaozuo City, China. Sustainability, 14(15).

Liu, W., Feng, Q., Engel, B., Yu, T., Zhang, X., & Qian, Y. (2023). A probabilistic assessment of urban flood risk and impacts of future climate change. Journal of Hydrology, 618.

Mahmood, R., Jia, S., & Zhu, W. (2019). Analysis of climate variability, trends, and prediction in the most active parts of the Lake Chad basin, Africa. Scientific Reports, 1-18.

Mariotti, L., Coppola, E., Sylla, M., Giorgi, F., & Piani, C. (2011). Regional climate model simulation of projected 21st century climate change over an all-Africa domain: Comparison analysis of nested and driving model results. Journal of Geophysical Research, 116(d15111), 1-22.

Merz, B., Blöschl, G., Vorogushyn, S., Dottori, F., Aerts, J., Bates, P., . . . Macdonald, E. (2021). Causes, impacts and patterns of disastrous river floods. Nature Reviews Earth & Environment, 592-609.

Mesta, B., Akgun, O., & Kentel, E. (2024). Improving precipitation estimates for Turkey with multimodel ensemble: a comparison of nonlinear artificial neural network method with linear methods. Neural Comput & Applic.

Netzel, L., Heldt, S., Engler, S., & Denecke, M. (2021). The importance of public risk perception for the effective management of pluvial floods in urban areas: A case study from Germany. Journal of Flood Risk Management, 14(2).

Nigussie, T., & Altunkaynak, A. (2019). Modeling the effect of urbanization on flood risk in Ayamama Watershed, Istanbul, Turkey, using the MIKE 21 FM model. Natural Hazards, 99, 1031-1047.

Ogras, S., & Onen, F. (2020). Flood Analysis with HEC-RAS: A Case Study of Tigris River. Hindawi Advances in Civil Engineering.

Oubennaceur, K., Chokmani, K., Gauthier, Y., Ratte-Fortin, C., Homayouni, S., & Toussaint, J. –P. (2021). Flood Risk Assessment under Climate Change: The Petite Nation River Watershed. Climate, 9(125), 1-23.

Ranger, N., Hallegatte, S., Bhattacharya, S., Bachu, M., Priya, S., Dhore, K., . . . Morlot, J. (2011). An assessment of the potential impact of climate change on flood risk in Mumbai. Climatic Change, 104, 139-167.

Rogers, R. (1975). A Protection Motivation Theory of Fear Appeals and Attitude Change. The Journal of Psychology, 91(1), 93-114.

Şen, O., & Kahya, E. (2017). Determination of flood risk: A case study in the rainiest city of Turkey. Environmental Modelling & Software, 93, 296-309.

Swain, D., Wing, O., Bates, P., Done, J., Johnson, K., & Cameron, D. (2020). Increased Flood Exposure Due to Climate Change and Population Growth in the United States. Earth's Future, 8(11).

Tabari, H. (2020). Climate change impact on flood and extreme precipitation increases with water availability. Scientific Reports, 10.

Tanaka, T., Kiyohara, K., & Tachikawa, Y. (2020). Comparison of fluvial and pluvial flood risk curves in urban cities derived from a large ensemble climate simulation dataset: A case study in Nagoya, Japan. Journal of Hydrology, 584.

Tonn, G., & Guikema, S. (2018). An Agent-Based Model of Evolving Community Flood Risk. Risk Analysis, 38(6), 1258-1278.

Turkish Statistical Institute. (2024). Adrese Dayalı Nüfus Kayıt Sistemi Sonuçları. Retrieved from Merkezi Dağıtım Sistemi.

Türkkan, G., & Hırca, T. (2021). The investigation of food risk perception as a quantitative analysis from socio-demographic perspective. Natural Hazards, 715-733.

WCRP CORDEX. (n.d.). What is regional downscaling? Retrieved from CORDEX: https://cordex.org/about/what-is-regional-downscaling/

Wing, O., Lehman, W., Bates, P., Sampson, C., Quinn, N., Smith, A., . . . Kousky, C. (2022). Inequitable patterns of US flood risk in the Anthropocene. Nature Climate Change, 156-162.

Xu, X., Wang, Y. C., Kalcic, M., Muenich, R. L., Yang, Y. C., & Scavia, D. (2019). Evaluating the impact of climate change on fluvial flood risk in a mixed-use watershed. Environmental Modeling & Software, 122.

Yalcin, E. (2019). Two-dimensional hydrodynamic modelling for urban flood risk assessment using unmanned aerial vehicle imagery: A case study of Kirsehir, Turkey. Journal of Flood Risk Management, 12(S1).

Yang, T., & Liu, W. (2020). A General Overview of the Risk-Reduction Strategies for Floods and Droughts. Sustainability, 12(7).

Yeğin, M. (2015). Master's Thesis: Flood risk mapping using economic, environmental and social dimensions. Ankara: Middle East Technical University.

Zaalberg, R., Midden, C., Meijnders, A., & McCalley, T. (2009). Prevention, Adaptation, and Threat Denial: Flooding Experiences in the Netherlands. Risk Analysis, 29(12), 1759-1778.

Zhai, G., Sato, T., Fukuzono, T., Ikeda, S., & Yoshida, K. (2006). WILLINGNESS TO PAY FOR FLOOD RISK REDUCTION AND ITS DETERMINANTS IN JAPAN. Journal of the American Water Resources Association, 42(4), 927-940.

Zhou, Q., Leng, G., Su, J., & Ren, Y. (2019). Comparison of urbanization and climate change impacts on urban flood volumes: Importance of urban planning and drainage adaptation. Science of The Total Environment, 24-33.

Zhuo, L., & Han, D. (2020). Agent-based modelling and flood risk management: A compendious literature review. Journal of Hydrology, 591.

CURRICULUM VITAE

Surname, Name: Yeğin, Murat

EDUCATION

Degree	Institution	Year of Graduation
MS	METU Civil Engineering	2015
BS	METU Civil Engineering	2012
High School	Fethiye Kemal Mumcu Anatolian High School, Ankara	2007

WORK EXPERIENCE

Year	Place	Enrollment
March 2020 - Current	METU	Research & Teaching Assistant
March 2018 – March 2020	Adimsu Construction Engineering Consulting Food Industry And Trade Ltd. Co.	Civil Engineer
June 2017 – March 2018	DHI Turkey	Civil Engineer
December 2014 – June 2017	Erges Engineering Consulting Ltd. Co.	Civil Engineer
April 2013 – December 2014	Eser Project And Engineering	Civil Engineer

CONSULTANCY PROJECTS

Year	Employer	Project
2022 - …	Turkish Electricity Transmission Corporation	Flood Assessment Report of Electricity Transmission Lines
2020	Egeplan Planlama Ltd. Şti	Development of Mitigation Measures and Risk Reduction Criteria in Spatial

2019	World Bank	Planning Project conducted for Republic of Turkey Ministry of Environment and Urbanization. "URP/RAJUK/S-05 Development of Risk Sensitive Land Use Planning Practice in Greater Dhaka" URP/RAJUK/S-05 Development of Risk Sensitive Land Use Planning Practice in Greater Dhaka PACKAGE NO: URP/RAJUK/S-05; Credit No: 55990. Preparation of "Flood Risk for Dhaka City, Bangladesh" report.

FOREIGN LANGUAGES

Advanced English

PUBLICATIONS

1. Flood Risk Mapping Using Economic, Environmental and Social Dimensions (Master Thesis)
2. Yegin, M. and Kentel, E. (2016, September 21-23). Flood Risk Mapping Using Economic, Environmental and Social Dimensions [Conference Presentation]. 12th International Congress on Advances in Civil Engineering, Boğaziçi University, Istanbul, Türkiye.
3. Flood resilience assessment and possible solutions to decrease flood vulnerability of a city (MCR 2030, UNDRR)
4. Yegin, M., Mesta, B. and Kentel, E. (2023, March 7-8). Impact of Climate Change on Flood Inundation Maps at Silifke, Goksu River Basin, Türkiye [Conference presentation]. German University of Technology in Oman, Muscat, Sultanate of Oman.
5. Korpinar, A., Demirer, F.E., Yegin, M., Karakaya, G. and Kentel, E. (2024). Assessing the stationarity assumption in frequency analysis of annual

maximum precipitation time series. [Submitted to Hydrological Sciences Journal]

6. Yegin, M., Karakaya, G., and Kentel, E. (2024). Nonstationary Frequency Analysis of Annual Maximum Flow Series: Climate Change versus Land Use / Land Cover Change. [Submitted to Water Resources Management]